NASA CR 72974
CW-WR-71-034.F

TIP-TURBINE LIFT PACKAGE DESIGN

by

R. Jaklitsch, A. Leto, W. Pratt, R. Schaefer

CURTISS-WRIGHT CORPORATION

Prepared For

NATIONAL AERONAUTICS AND SPACE ADMINISTRATION

NASA LEWIS RESEARCH CENTER

CONTRACT NAS 3-14327

Laurence W. Gertsma, Project Manager

1. Report No.	2. Government Accession No.	3. Recipient's Catalog No.
NASA CR-72974		

4. Title and Subtitle	5. Report Date
TIP-TURBINE LIFT PACKAGE DESIGN	July, 1971
	6. Performing Organization Code
7. Author(s)	8. Performing Organization Report No.
R. Jaklitsch, A. Leto, W. Pratt, R. Schaefer	CW-WR-71-034.F
9. Performing Organization Name and Address	10. Work Unit No.
Curtiss-Wright Corporation Wood-Ridge, New Jersey	11. Contract or Grant No. NAS 3-14327
12. Sponsoring Agency Name and Address	13. Type of Report and Period Covered
National Aeronautics and Space Administration Washington, D. C. 20546	Contractor Report
	14. Sponsoring Agency Code

15. Supplementary Notes

Project Manager, Laurence W. Gertsma, Fluid System Components Division, NASA Lewis Research Center, Cleveland, Ohio

16. Abstract

A layout design of a Lift Fan driven by a Two-Stage Hot Turbine at the Fan Blade Tips is reported. Layout drawings, a description of the Lift Package System and a discussion of the design analyses are presented. Areas of major design analyses included segmented and continuous turbine blade support rings, a hot-gas scroll, hot-gas seals during transient thermal and maneuver load conditions, main support bearings and system weight.

17. Key Words (Suggested by Author(s))	18. Distribution Statement
Tip-Turbine Lift Fan Lift Fan Design of Tip-Turbine Lift Fan	Unclassified - Unlimited

19. Security Classif. (of this report)	20. Security Classif. (of this page)	21. No. of Pages	22. Price*
Unclassified	Unclassified	194	$3.00

* For sale by the National Technical Information Service, Springfield, Virginia 22151

FOREWORD

The technical and administrative guidance contributed on this design task by personnel of the Lewis Research Center of the NASA, including Messrs. L. Gertsma, H. Rohlik, W. Rowe, B. Leonard and a number of aerodynamic and thermodynamic specialists is gratefully acknowledged.

In addition to the authors cited, numerous C-W personnel in the various technical disciplines of Stress, Vibrations, Heat Transfer, Aerodynamics, Metallurgy, Manufacturing Engineering, Bearings and Seals contributed to this program.

ABSTRACT

A layout design of a Lift Fan driven by a Two-Stage Hot Turbine at the Fan Blade Tips is reported. Layout drawings, a description of the Lift Package System and a discussion of the design analyses are presented. Areas of major design analyses included segmented and continuous turbine blade support rings, a hot-gas scroll, hot-gas seals during transient thermal and maneuver load conditions, main support bearings and system weight.

TABLE OF CONTENTS

TABLE OF CONTENTS - Continued

LIST OF FIGURES

LIST OF FIGURES - Continued

LIST OF FIGURES - Continued

I. SUMMARY

A final layout design of a Lift Fan driven by a Two-Stage Hot Turbine at the Fan Blade Tips was conducted by the Curtiss-Wright Corporation for the NASA Lewis Research Center, and the design accomplishments are reported herein. Areas of major design analysis include segmented and continuous turbine blade support rings, a hot-gas scroll, hot-gas seals during transient thermal and maneuver load conditions, main support bearings and system weight. The layout drawings, a description of the Lift Package System and a detailed discussion of the design analyses are presented in this report.

During the early part of the design, a major portion of the effort was directed toward studying two configurations of supporting the turbine blades at the fan blade tips, a continuous ring and a segmented ring. The segmented ring was selected on the basis of offering more favorable fan rotor dynamics, ease of manufacture, lower weight and simplicity of assembling and servicing the system.

The completed design is considered adequate for a continued effort consisting of the preparation of final shop-fabrication type drawings for procurement of test hardware. Adequate strength and vibratory margins were achieved in the design to satisfy the required 1000-hour operating life for the specified duty cycle conditions.

The labyrinth seals that were incorporated in the design to limit the leakage of hot-gas turbine flow are considered acceptable for initial test evaluation of the Fan Package. Although the use of cool buffer air was provided in the most critical front seal to improve performance, the seals must be made to close tolerances and should be investigated experimentally for thermal and maneuver load transient effects. Alternate sealing methods currently being studied by NASA may offer improved performance and could be applied to the design at a later time.

Grease-packed bearings are satisfactory for flight operation and appear to be also acceptable for longer test stand operation. Should additional bearing cooling be required for sustained test stand operation, an air or water cooling system can be used, and provisions of this method of cooling were included in the design.

I. SUMMARY (CONTINUED)

A final total weight of 680 pounds was calculated for the complete Fan Package. A weight-reduction review was made and potential weight savings were indicated in the areas of the hot-gas scroll, the fan rotor blade fir tree and tenon attachment, the disk, the spindle, and the fan stator vane and support assembly. Weight reductions in these areas are expected to result in the achievement of a target weight of 570 pounds.

To assure operational success of the Fan Package, further effort should be directed toward specific areas of the design. These would include the hot-gas seals, thermal gradients in the fan air shroud, cooling of the second stator housing, fatigue of the brazed turbine blade attachment and the aerodynamic performance of the hot-gas scroll.

II. INTRODUCTION

Interest in lift fan engines for Vertical and Short Take-Off and Landing (VSTOL) Aircraft for commercial applications has increased considerably during recent years. The NASA Lewis Research Center is currently studying VSTOL engines and endeavoring to establish technology goals toward achieving high performance, low weight, low noise and high reliability.

As a part of this effort, NASA has been studying a Tip-Turbine Lift Package concept. This concept is one that is applicable to a multi-engine aircraft in which a series of lift fans could be installed in the wings, wing pods or fuselage pods and be used solely for lift during the take-off and landing regimes of flight. More conventional type engines would be employed for forward flight.

To investigate the feasibility of various aspects of the Tip-Turbine Lift Package, NASA assigned Curtiss-Wright a task of jointly designing a complete system. This system consists of a lift fan driven by a tip turbine supplied with hot gas from a combustor through a hot-gas scroll and duct system. The aerodynamic designs of the fan, turbine, inlet passage, combustor and the recommended Rotating Gas Seal configurations were furnished by NASA. The design effort of Curtiss-Wright included sizing the hot-gas scroll, determining seal leakages and temperature distributions for steady-state and transient conditions, performing structural and vibratory analyses, establishing design criteria and maneuver loads, evaluating and reviewing component weights, selecting materials and fabrication methods and establishing a final overall mechanical design.

This Curtiss-Wright effort was performed under NASA Contracts NAS 3-12423 and NAS 3-14327, and this report presents and discusses the design features and design analyses performed on this task.

III. ENGINE DESCRIPTION

The basic Tip-Turbine Lift Package is shown in Figure 1. The design consists of a single fan rotor with an exit stator vane rear frame and mount assembly, a two-stage tip turbine, a hot-gas scroll and turbine inlet nozzle, a buffer air seal manifold, a bellmouth inlet, and an exhaust duct assembly.

The fan has 48 blades and is driven by an annular two-stage hot-gas impulse-type tip turbine. Twenty-four segmented turbine carriers with 21 turbine blades per row are pinned to the tip tangs of every pair of fan blades. The fan blades attach to the twin-webbed disk by a three-tooth fir tree and tenon arrangement. The fan rotor assembly is supported on grease-packed ball bearings to a stationary shaft that is cantilevered from the inner support ring structure of the exit stator vane frame and mount assembly. The fan exit stator vanes rigidly connect the inner support structure with the outer support structure, which is also the main engine mount ring. All lift (thrust) and maneuver loads transfer to the airframe through three equally-spaced trunnion support pads and pins which are provided on this outer support ring.

A 360-degree scroll supplies hot-gas at 1440°F to the annular tip turbine. The scroll consists of a single inlet pipe and two 180-degree branches with decreasing flow areas. Pressurized air is delivered to and burned in a combustor which is located upstream of the inlet to the scroll. This inlet air is supplied from an aircraft-mounted air generator.

The scroll support housing attaches to the second stage turbine stator ring which, in turn, attaches to the hot-gas exhaust housing. This entire assembly comprises the outer envelope of the fan and is cantilevered from the main engine mount ring by a series of radial pins. The exhaust housing fits over the main mount ring. Radial struts connect the inner and outer shells of the housing to form the annular exhaust gas passage. The exhaust gas discharges parallel to the fan flow and supplements the total lift load generated by the fan. Cutouts in the exhaust duct allow clearance for the three mount trunnions.

Labyrinth lip seals are used for sealing between the rotating turbine parts and the stationary structural members. The front labyrinth seal functions in

conjunction with a buffer air system to prevent the loss of high pressure hot turbine gas into the fan air stream and to cool the front face of the first turbine rotor carrier structure. The buffer air is supplied to the manifold from a low pressure bleed stage on the air generator compressor through eight equally spaced inlet tubes. These tubes reach over the upstream side of the hot gas scroll and just underneath the bellmouth inlet. The buffer air manifold is mounted to brackets on the inner wall of the scroll neck with radial pin bolts.

Spring loaded face seals located at the front and rear ends of the turbine section seal between the stationary members of the structure.

The fan airflow enters the fan passage through a bellmouth inlet structure which also mounts to the buffer air manifold. A rotating spinner is used at the hub section of the fan inlet in the flight configuration. A larger stationary hub, enclosing instrumentation and cooling equipment, was also designed for the test stand version and is shown in Figure 2.

Noise elimination features were incorporated into the lift fan design as requested by NASA. These include the exit stator to fan rotor blade spacing of 1.5 of the rotor blade axial chord at the tip, and silencing material on the outer wall of the fan passage downstream of the fan exit. The silencing material will consist of a tuned cellular honeycomb material to be defined by NASA.

Thermal insulation blankets will cover the entire outer hot structure which includes the scroll, stator ring and exhaust housing. A one-half inch foil covered blanket will be laced to the fan structure to protect the nearby airframe structure, the bellmouth and the buffer air manifold. A foil heat shield will be used between the buffer air manifold and the hot gas scroll where the clearances are small.

There were no controls or accessory drives included in this design, although a speed-sensing pick-up was provided.

A list of all of the design layout drawings is presented in Figure 3.

IV. ENGINE TECHNICAL DATA

The mechanical design of the Tip-Turbine Lift Package was prepared by Curtiss-Wright based on the aerodynamic and performance information supplied by NASA. The following is a list of data received from NASA or derived from NASA information. This was used for determining the design loads, temperatures, material selections and for performing aerodynamic, thermal, stress and vibratory analyses. The flight maneuver loads were established by Curtiss-Wright.

Figure 4 — OPERATING CHARACTERISTICS AND INTERNAL GAS CONDITIONS - A list of basic internal aerodynamic and performance data at the sea level static 90°F design point condition.

Figure 5 — FAN PASSAGE AND BLADE PROFILE - A tabulation of the fan air passage coordinates and the fan blade leading and trailing edge meridional profile coordinates.

Figure 6 — FAN PASSAGE AERODYNAMIC DATA - A summary of the aerodynamic station coordinates and passage aerodynamic boundary data at the outer and inner streamlines in the flow path.

Figures 7 and 8 — FAN ROTOR BLADE AND STATOR VANE AERODYNAMIC DATA - A summary of the aerodynamic data at the inlet and outlet of each blade row for the determination of gas bending moments and shear loads.

Figure 9 — TURBINE OPERATING CHARACTERISTICS - A listing of the turbine weight flow, pressure and temperature at stations in the gas passage including the burner, scroll and between the blade rows.

Figure 10 — TURBINE VECTOR TRIANGLES AND PASSAGE HEIGHTS - The relative and absolute values of the turbine entry and exit gas velocities given at the mean radius of the gas passage, and the gas passage heights, defined at the exit from the blade row.

IV. ENGINE TECHNICAL DATA (CONTINUED)

Figure 11 — FLIGHT MANEUVER LOADS AND DUTY CYCLE - Summarizes the inertia loads and angular velocities to be taken about the C.G. of the lift fan package. The values have been selected as representative on a commercial lift fan application and are used to determine maximum load conditions on the fan and stator support structure.

The duty cycle is defined as the design life, number of starts per flight and length of fan operation.

Figure 12 — OVERALL LOAD SUMMARY - A summary of the aerodynamic forces on the lift-fan package for the determination of bearing and mount reaction loads.

A summary of materials data is also presented in Figures 13 through 28.

The design criteria used throughout are shown in Figures 29 through 32.

V. FAN ROTOR

The fan rotor assembly is shown in Figure 33. There are 48 individual fan blades attached at the rim of the hollow disk. The blade has a three-tooth fir tree which is connected to the shelf and airfoil root by a tapered rectangular shank. Two tangs of rectangular cross-section are located at the tip of the blade and have large fillet-radius transitions into the airfoil. The turbine sector assemblies are pinned to the tangs, and each sector spans a pair of fan blades.

The disk is a one-piece machined and welded titanium structure utilizing a hollow trapezoidal section with conical sides for rigidity and lightness. The rim is broached for a three-tooth fir-tree attachment, and the hub is step-bored for the shaft bearing. One end of the bore is shouldered and the other is flanged for retaining and installing the two spaced angular-contact bearings. This method is feasible because of the short axial span and negligible temperature differential between the inner and outer bearing race spacers. A more detailed description of the bearings, loadings and lives is included in the Bearing section.

The rotor assembly is sized to carry the steady state loads combined with a gyroscopic couple resulting from an angular velocity in the pitch or roll direction. Steady state loads consist of the pressure, aerodynamic and centrifugal forces that act on the fan rotor and turbine carrier assembly.

The fan blade material is forged 6Al-4V titanium alloy and the disk is forged 5Al - 2.5Sn titanium alloy. The disk is machined as two halves and electron beam welded at the rim and bore, thus forming a hollow disk.

The fan blade aerodynamic design, number of blades and airfoil coordinates were provided by NASA. The fan passage for the hub and tip contours and the fan blade edge location in the passage are given in Figure 5.

A. Design Input Data and Analysis

The fan rotor blade is subject to the aerodynamic, centrifugal and gyroscopic maneuver loads that are developed during its operation.

V. FAN ROTOR (CONTINUED)

The aerodynamic loads on the fan blade and the turbine sector attached to the top of the blade were determined from the aerodynamic data provided in Figures 7, 9 and 10. The turbine carrier and tip tangs also produce a centrifugal load at the tip of the blade and an offset moment due to the unequal distribution of this load between the two tangs. During maneuvers, a gyroscopic couple can develop and produce still another bending moment on the blade. The gyroscopic couple is based on the turbine carrier weight and the upper one-third of the fan blade weight. A summary of the fan blade tip data is given below:

Fan Blade Tip CF Load, lbs/Blade 8600

Fan Blade Tip Offset Moments, lb-in/Blade

1. Axial (acting in downstream direction)..... 810
2. Tangential (in direction of rotation)..... 530

RPM 3030

Pitch or Roll Angular Velocity, radians/sec.....1.0

Tip Mass Moment of Inertia, lb-in^2 67,200

Gyroscopic Couple, lb-in 55,200

Maximum Gyro Shear Load, lb/Blade (Fan Axial direction)... $\pm$ 84

The maximum loading on the fan blade is the steady state condition combined with the gyroscopic couple resulting from the angular velocity about the pitch or roll axes. The applied bending moments due to the aerodynamic, centrifugal, and gyroscopic loads were combined to give the initial blade moments before restoring. These moments were used in the computer program together with the airfoil area, radii and an equivalent tip mass for the carrier. The program calculates the centrifugal restoring moments of each section and algebraically combines them with the input moments to give the net bending moment in the airfoil. Figures 34 and 35 summarize the input, restoring and net blade moments in the axial and tangential planes respectively for three basic design conditions:

1. Steady state
2. Steady state plus an upward axial force due to gyroscopic moment
3. Steady state plus a downward axial force due to gyroscopic moment.

These axial and tangential bending moments were resolved into components in the weak and strong bending axes of the blade as shown in Figure 36.

Properties of the airfoil section as determined from the blade coordinates are also presented. Figure 37 gives the chord, area, weak axis angle, thickness-chord ratio, and torsional spring constant. Figure 38 gives the reciprocal of the section modulii at the leading edge, trailing edge and back of the blade.

All parts of the rotor assembly operate at ambient temperatures except the tip tangs where heating occurs as given by the temperature history in Section XIII.

B. Stress Analysis

The results of a stress analysis of the fan rotor assembly is presented below. All margins of safety were determined to be satisfactory.

1. Fan Rotor Blade

The fan rotor blade was analyzed at 3030 RPM for the centrifugal, aerodynamic and gyroscopic loads presented in the preceding section. The blade was treated as a cantilever beam fixed at the rim of the disk. The combined stress in the airfoil is the total of the direct stress due to the centrifugal force and the bending stress due to the restoring moment and gas load.

The direct and combined stresses for the Steady State Condition (1) are plotted in Figure 39. The combined stresses for the two Gyroscopic Loading Conditions 2 and 3 are plotted in Figures 40 and 41. The maximum combined stresses for the Steady State and Gyroscopic loading conditions are summarized in the table below:

V. FAN ROTOR (CONTINUED)

Condition	1 Steady State	3 Steady State plus Gyro Moment
Radius	10.3	10.3
Stress Location	TE	LE
Maximum Combined Stress, psi	37,400	46,900
Material 6Al-4V Titanium		
Allowable Strength .2% Yield Strength (psi)	120,000	120,000
Margin-of-Safety	+ 2.2	+ 1.6
Vibratory Margin	12.0	3.3

The vibratory margins were taken from the modified Goodman diagram of Figure 42. This blade is not critical for static or fatigue loading. The heavier sections are necessary in obtaining small deflections due to the gyroscopic loading.

2. Fir tree and Tenon

The fir tree and tenon stress analyses were simultaneously performed by the computer program. The program input requires the dimensions defining the geometry of the fir tree and tenon, the stress concentration factor for notched beams, the Heywood factor constants, material properties, centrifugal loads, bending moments due to gas loading and offset centroids.

The analysis is shown only for the upper and lower fir tree and tenon necks, which are more highly stressed than the middle neck. Centrifugal loads are shared about equally by all the teeth. Bending moments are distributed on a 50, 30, 20 percent basis about the weak axis and are distributed equally about the strong axis between the upper and lower fir tree and tenon teeth. This method of load and

moment distribution is a reliable criterion based on test data and actual engine hardware.

A summary of the fir tree-tenon analysis load and moment inputs and stress outputs are shown in Figure 43 for the two controlling design conditions. The computer output lists the steady state stress, gas bending stress, allowable vibratory stress per a Modified Goodman Diagram, and vibratory margins for each corner of the upper and lower neck of both the fir tree and tenon. All allowable vibratory stresses are greater than the minimum of two gas bending stresses, and the critical neck steady state stress is well below the 6Al-4V titanium alloy material 0.2% yield strength of 120,000 psi. The attachments therefore have satisfactory margins of safety.

This fir tree and tenon configuration is a reliable and structurally sound design. Further reduction in weight is possible by increasing the width of the V-notch in the rim where the two disk halves are welded. This would insure low weight with no additional offset stresses. A two-tooth fir tree attachment could also have been designed to work within the available space but was discarded in favor of an overall stronger three-tooth arrangement. A dovetail design was found to be structurally weaker and was therefore not acceptable.

3. Fan Blade Tip Tangs

The 24 turbine carrier assemblies are pin connected to the tip tangs on the fan blade. There are two tangs on each fan blade. The tang load consists of the radial reactions at the turbine carrier support, the radial and tangential load components of turbine torque, the axial load due to gyromoments, the tangential load due to fan blade untwist, the carrier thrust load, the middle seal arm bending moment and the centrifugal force of the tang itself. Maximum loads develop at the forward tang because of the geometry of the

turbine carrier assembly. The forward tang was analyzed as a cantilever beam for the combined tension, bending and shear loads acting at the pin hole, the shank, and in the fan airfoil attachment.

A stress summary of the forward tang is given in Figure 44. Both steady state and gyroscopic load conditions are shown. All margins of safety are satisfactory. The aft tang loads and stresses are lower and are not governing in the design, even at the slightly higher operating temperature.

4. Fan Rotor Disk

The fan rotor disk analysis was performed at 3030 RPM for the steady-state and gyroscopic loading conditions, and a 15 percent overspeed condition was examined. Steady state loads include the centrifugal and aerodynamic loads acting on the rim of the disk. The gyroscopic moment loads developed during a one radian per second angular maneuver were superimposed on the steady state loads. Although the gyro-moment varies around the rim of the disk, this analysis considers the maximum moment from the fan blade to be a uniform one on the disk.

A summary of the steady-state and gyro-moment disk rim loads is shown in Figure 45. The disk rim loads at a radius of 8.0 inches were obtained from the direct, bending and shear loads at the upper fir tree neck at a radius of 8.97 inches and from the centrifugal load of the fir tree and tenon attachment. All loads were transferred into the rim of the disk as uniform radial and axial shear line loads. A comparison of the loads for both the steady state and gyro conditions shows that their differences are small. Therefore, the stress results are shown only for the maximum loading condition, which includes steady state and gyro loads.

The trapezoidal section rotor disk was analyzed as a combination of shells and rings by means of the General Shell computer program. Zero

shear and rotation was assumed at the middle of the hub section because of disk symmetry and nearly symmetrical loading. Zero shear and rotation was also assumed at the outboard ends of the hub over each bearing since the radial input loads are self-balanced and the extensions are long cylinders. The long cylinder does not loosen significantly over the bearings, thereby keeping the diametral fit with the outer race constant and minimizing radial looseness of the fan rotor assembly during running. Axial pressure loads across the disk are low and were ignored. However, the rotating centerbody loads acting through the disk hub were added to the results from the computer output.

The disk stresses are presented in Figure 46 for the gyroscopic loading condition. The maximum radial stresses on the inner and outer disk surfaces and the average radial and tangential mean line stresses are plotted. The disk is a 5Al-2.5SN titanium alloy with a 110,000 psi 0.2 percent yield strenth and 115,000 psi ultimate tensile strength, and operates at ambient temperature. A summary of the critical disk stresses is given below for the steady state design speed and overspeed conditions.

Speed	Location	Stress psi	Allowable Stress, psi	MS
100% 3030 RPM	Bore	27,000	120% of 0.2% yield=132,000	+ 3.9
	Neck	93,000	2% yield = 110,000	+ .18
	Rim	24,000	80% of 0.2% yield= 88,000	+ 2.66
115% 3480 RPM	Avg.Tang	44,200	90% of UTS = 103,500	+ 1.35

All margins of safety are satisfactory.

A study of Figure 46 reveals significant bending stresses in the conical webs. This is a consequence of the hoop stress in the webs requiring a radial reaction for equilibrium. Since the webs are conical, the radial reaction for equilibrium requires force components normal

to the web, and this results in web bending. The webs were made thick enough to limit the stress to acceptable values. Reducing the conical angle of the webs would diminish this bending with a subsequent weight savings. No further optimization of the disk design was pursued. An interesting possibility would be to curve the webs slightly inward and let the web tension balance the bending forces.

Radial displacement of the disk is 0.0118 inches at the rim and 0.0055 inches at the bore. A thermal growth of 0.00091 inches at the rim results from a temperature increase from 70°F to 90°F.

C. Vibration Analysis

The principle natural frequency modes in torsion and bending were calculated for the fan rotor blades, and an interference diagram was constructed as shown in Figure 47. The critical excitation frequency orders are:

1 & 2 - excitation frequencies normally generated by the engine or fan rotor.

36 - number of exit stator vanes.

The blade was considered to be fixed in torsion and bending at the firtree attachment and at the tip tangs which carry the interlocking turbine carrier assemblies (2nd mode, fixed-fixed). The analysis results show that the fan rotor blade will have satisfactory vibratory characteristics throughout the engine operating range. The blade resonant natural frequencies are well over the second engine order and well below the 36th engine order at the design speed of 3030 RPM. The interferences indicated at about 550 RPM are at low fan and turbine weight flows and can be neglected.

V. FAN ROTOR (CONTINUED)

The flutter analysis values (V/bw) in torsion and bending are shown below:

Type	Air Velocity (ft/sec)	Reduced Velocity (V/bw)	Maximum Acceptable Reduced Velocity (V/bw)
Torsion	1008	1.9	2.0
Bending	1008	1.9	6.66

The air velocity represents 115 percent of the design inlet velocity at the three-quarter span of the blade. This is considered the maximum expected velocity for a fan-in-wing installation. The fan rotor blade is therefore satisfactory in flutter.

The natural frequency of the fan blade vibrating as a cantilever beam with a tip mass was also analyzed (1st mode, fixed-free). Due to the interlocking arrangement of the turbine carriers, all the fan blades would have to vibrate in unison for this mode. The bending natural frequency and 1st engine order excitation frequency are plotted in Figure 48. Although this blade mode could be excited at 1775 RPM, the excitation forces available are not believed strong enough to cause any serious vibration. In addition, the interlocking carrier assemblies would offer considerable damping. Similarly, the flutter excitation of this mode is not considered probable due to the damping and excitation requirement that all blades vibrate in phase. Because of this and the phase requirements for the first mode of vibration, the blade will respond primarily in the second mode of vibration during fan operation.

VI. TURBINE ROTOR

The tip turbine rotor blade and carrier assembly is shown in Figure 49. Twenty-four (24) of these carrier assemblies form an annular two-stage impulse turbine. Each carrier assembly is supported across a pair of fan blades which are directly driven by the turbine.

Each assembly consists of two rows of turbine rotor blades having 21 blades per row. Hollow turbine rotor blades with tip shrouds are used. The inner ends of the blades are brazed into circumferentially-segmented hat section railings which provide the beam support across the fan rotor blade tips. A fan air shroud riveted to the bottom of the railings separates the turbine gas from the fan airflow. The railings are pinned directly to the tip tangs on the fan rotor blades.

Three circumferential labyrinth gas seals are used on the turbine carrier. The front and rear sealing lips are an integral part of the fan air shroud. The middle seal is an overhung arm from the first turbine rotor support rail.

A ribbed waffle plate design was used for the fan air shroud and incorporates integral axial and circumferential ribs on a curved plate as shown in Figure 50. The plate is adjacent to the fan flow annulus while the ribs are on the turbine cavity side. The windage loss due to the ribs rotating at rated speed has been estimated to be approximately sixteen horsepower. The waffle plate design was used to minimize thermal distortion, increase stiffness and rigidity, and to obtain an optimum lightweight design. The axial ribs which intersect the circumferential rails are heavier than the circumferential ribs to support the overhung shroud loads with minimum deflection. A circumferential rib is located under each leg of the railing to seal across the blade rows. The axial joint between adjacent sectors is sealed with an overlapping lip. The panel has four cutouts for the fan blade tangs. The carrier rails have deep sections which must support the carrier assembly across the fan blade tangs. The front rail also supports the middle seal arm and bracket assembly. The carrier is internally reinforced by circumferential and radial stiffeners. The radial end stiffeners also ke_ the adjacent sectors together on the rotor assembly for tracking purposes and serve as axial gas seals for the blade row.

VI. TURBINE ROTOR (CONTINUED)

Heavy pin bosses are brazed into the side walls of the railing for the transfer of load into the tangs. Externally the middle seal support arm is attached to the sidewall of the first turbine carrier railing. A more detailed cross-section of the arm is shown in Figure 51. Also shown is the obsolete honeycomb fan air shroud which was found to be structurally unacceptable due to extreme thermal stress gradients.

Hollow brazed metal construction was used almost exclusively to minimize the centrifugal force loads on the structure. The railing and its internal reinforcement is fabricated from 0.020 inch Inconel X sheet stock, and the turbine blades, tip shrouds and middle seal arm face sheets are made from 0.010 inch Hastelloy X sheet stock. The fan air shroud is made of René 41 alloy, and its ribbed construction requires both electro-chemical machining and chemical milling operations. The high temperature alloys were selected for their strength at temperature, their fabrication qualities and joining compatibility. The fan air shroud was made as a separate piece to permit: (1) machining the inner faces on the pin bosses in the railing; (2) replacement of damaged turbine blades; and (3) expansion features between the mated members.

A. Design Input Data and Analysis

The turbine rotor assembly was analyzed for the pressure, aerodynamic and centrifugal loads that develop during its operation. The basic aerodynamic data for the turbine section are presented in Figures 9 and 10. The load data are presented along with the stress analysis summary. Airfoil coordinates for the turbine blades as defined by NASA were converted into detailed section properties required for the analysis. Constant cross-section blades were used because of the small blade height-to-mean radius ratio. A comprehensive thermal analysis of the hot turbine section components is presented in the Heat Transfer section.

VI. TURBINE ROTOR (CONTINUED)

B. Stress Analysis

The stress analysis of the turbine rotor assembly was divided into three groups:

1. Turbine Rotor Blades
2. Fan Air Shroud
3. Turbine Carrier Rails

Each group consists of detailed analyses of the critical sections of the structure. A discussion and summary of the analysis are presented in the following sections. All margins of safety are satisfactory.

1. Turbine Rotor Blade

The turbine analysis includes the turbine blade, attachment, shelf, and tip shroud. The blade is a constant cross-section hollow airfoil with individual tip shrouds. It is brazed into radial slots in the carrier rail at its root section and was analyzed as a cantilever beam. The loads will result from centrifugal force, and aerodynamic and offset bending moments. The offset moments are included in the analyses at the root section and in the brazed attachment because of the center-of-gravity position of the blade elements. A summary of the first and second stage turbine rotor blade loads and stresses is shown in Figures 52 and 53, respectively. Included in the figures are the CF loads, bending moments, blade section properties, material properties and temperature. Maximum stress in the airfoil is a combination of direct stress due to radial centrifugal load and bending stress due to lateral aerodynamic loads and offset moments. Combined stresses are given at the leading edge, trailing edge and convex side of the blade. Thermal stresses were neglected because thermal gradients are expected to be small. From the Modified Goodman diagrams of Figure 54, the turbine blade stresses are safe with respect to the endurance limit of the material.

The stress analysis summary for the brazed attachment, shelf and tip shroud is also presented in Figures 52 and 53. The brazed joint strength of the blade attachment in the rail includes the CF loads and moments at the root section of the airfoil plus the CF loads due to the slotted sections of the rail and shelf as well as the portion of the airfoil that is below the shelf. The slotted sections of the rail and shelf are brazed to the airfoil and it is assumed that their loads are also transmitted by the airfoil into the brazed joint. The joint carries all blade loads in shear. Only the vertical slots are considered to carry load. All braze strengths are based on a 50 percent coverage factor.

The shelf was analyzed for bending due to centrifugal loads at the front and rear overhangs. The tip shrouds were analyzed for bending due to centrifugal loads. The shroud is 0.010 inches thick and has an 0.04 inch high lip around the edge. The lip stiffens the shroud against vibrations and reduces the stresses and deflections. The brazed joint between the shroud and blade was also checked for shear strength.

The stresses evaluated in the brazed attachment, the shelf and the tip shroud were all determined to be acceptable.

2. Fan Air Shroud

The fan air shroud was analyzed as a simply supported beam with overhung ends. Centrifugal force presses the shroud against the underside of the two circumferential carrier rails. The rails were assumed to be rigid supports and the reaction load at each rail is shared equally by each of the legs. Bending stresses were checked in two locations at sections taken normal to the axial ribs on the shroud. The first location (Section X-X) is in the middle of the shroud between tang holes; the second location (Section Y-Y) is at a rib which passes alongside a tang hole. A closer rib spacing was used at the tang holes to stiffen

the weakened area and provide a load path around the holes. Because of the shear stress distribution resulting from widely spaced ribs supporting the thin shroud skin, reduced section properties have been used. The ribs are also thickened to reduce stresses where the higher operating temperatures occur.

The panels formed by the intersecting ribs were treated as flat plates with a uniform normal load. Maximum stress occurs in the largest panel which was analyzed as having both supported and fixed edges. In the case with supported edges, large deflections occur and diaphragm stresses, which help to carry the plate load in direct tension, were calculated. The additional stiffness due to curvature of the panel was not considered because of the large radius of curvature.

A summary of the fan air shroud stresses, deflections, temperatures and material properties is shown in Figure 55, and there are satisfactory margins of safety.

The fan air shroud was designed as a thin ribbed skin open to turbine gas on one side and fan air flow on the other. Cooling by this method results in a maximum skin temperature between 600 and 675°F. The stress analysis of the shroud was based on maintaining a uniform temperature throughout the structure with the effects of thermal gradients being largely minimized by the cooling action produced by the fan air flow scrubbing the inner wall of the fan air shroud. Any temperature gradients in the shroud could produce warpage and if restrained, could cause stresses in the shroud and its adjoining structure. The extent to which any thermal gradients develop can best be determined experimentally where the same heating and cooling influences are duplicated. Corrections to remove the gradients or their effects can then be dealt with selectively by slotting, scalloping or re-proportioning the ribs to optimize the heat flow paths and the strength of the structure.

VI. TURBINE ROTOR (CONTINUED)

3. Turbine Carrier

The turbine carrier assembly operates in a centrifugal field at 3030 RPM. All carrier loads are reacted at the fan blade tip tangs that are pin-connected to the bosses in each carrier railing. The loads are due to rotating inertia, aerodynamic and pressure forces, blade untwist and gyroscopic moments. Maximum loads occur on the first turbine rotor carrier due to the middle seal support arm weight and load distribution from the fan air shroud. The fan air shroud was assumed to be simply supported under each carrier railing and the reactions were applied uniformly to the railing. Each leg on each rail was assumed to share each reaction load equally. The untwist moments are reacted by a force couple both at each end of the carrier and in the fan air shroud. Gyroscopic moment loads go directly into the tip tangs and were assumed to cause no bending in the carrier assembly. The turbine blade aero loads at the rim of the carrier and the pressure load across the carrier were omitted from the carrier analysis because they were small. However, the pin and pin boss analyses include turbine torque and untwist moments in addition to the radial carrier load reactions and seal arm moments. A schematic free-body diagram of the carrier is shown for the radial loads applied at a radius through the pin centers.

Thermal stresses were not considered in the carrier analysis since provisions were made to allow for differential thermal growth between the rail and the fan air shroud. The differential temperatures between the rail side walls are expected to cause some negligible rotation or lean. This condition will be greater in the first turbine carrier than in the second because of the additional cooling from the buffer air manifold.

The first stage turbine carrier rail was analyzed as a simply-supported beam with overhanging ends and subject to both a uniform and concentrated distribution of loads in the circumferential direction. The

carrier was considered a free body having no interaction with the second turbine carrier rail through the fan air shroud. Steady state temperatures were assumed. A summary of the carrier stresses is presented in Figure 55. Stresses are included for the railing cross-section, flanges, internal stiffeners and seal support arm. The results of the support pin and shroud attaching rivet analyses are also shown.

C. Vibration Analysis

The fundamental natural frequency modes in bending and torsion were calculated for the two rows of turbine rotor blades, and interference diagrams were constructed as shown in Figures 57 and 58. Due to the small physical size of the turbine blades, high natural frequencies were obtained. The major excitations are the stator vane passing frequencies.

The turbine blades were analyzed for the bending and torsional natural frequencies as cantilever beams with fixed tip masses. The tip mass consists of individual blade shrouds that are separated from one another by a clearance. The effect of the tip shrouds is to lower the natural frequencies. The fall-off in frequency near design speed is due to the decrease in Young's Modulas with temperature. Constant cross-section hollow blade airfoils were used. Because of the potential flexibility at the brazed root attachment configuration, the bending frequencies were reduced by 10 percent.

The following table summarizes the potential blade resonant speeds and reduced velocity flutter values.

VI. TURBINE ROTOR (CONTINUED)

Turbine Rotor	Mode	Natural Freq. @ 3030 RPM & Oper. Temp.	Interference			Reduced Velocity V/bw	Maximum Acceptable Reduced Velocity
			EO	Source	RPM		
1	Bending	9,360	286 274	2nd Stator 1st Stator	2180 2250	1.27	6.66
	Torsion	39,800	-	-	None	0.30	2.00
2	Bending	2,390	286	2nd Stator	540	2.96	6.66
	Torsion	9,750	286	2nd Stator	2250	0.72	2.00

The first turbine rotor has possible bending resonances at 2180 and 2250 RPM, and no torsional resonances. The second turbine rotor has a possible bending resonance at 540 RPM and a torsional resonance at 2250 RPM. Although it would be desirable to have no potential blade resonances above 50 percent of the design speed, the following exceptions are applicable to the present design:

1. The sources of excitation are almost a chord length away from the turbine blades and may be sufficiently diminished in strength.

2. The turbine will accelerate through the potential resonance points.

3. The potential resonance points occur below the light-off speed and at lower temperatures than those at the design condition. However, the airflow through the turbine at 2250 RPM is approximately the same as the gas flow at design speed.

A possible means of increasing the natural frequency sufficiently was investigated so that the interference will occur above 100% speed. The method was to tie the shrouds of two adjacent blades together. An experimental test tieing two solid turbine blade shrouds together showed an increase in the bending natural frequency by about 25 percent. Applying this result to the tip turbine design, the 1st stage bending interference was brought closer to the steady state design speed which was undesirable.

A three-shroud test should be made to more closely represent the configuration required for the carrier with 21 blades per row. Tying more than three shrouds will cause unfavorable thermal growth problems.

In addition, an investigation to lower the natural frequencies was undertaken. An increased tip mass was checked analytically and showed that a 10 percent reduction in natural frequencies could be obtained. The results were within the degree of calculation accuracy, and the small improvement did not justify making the changes at this time.

Experimental evaluation of the vibratory characteristics of the turbine rotor blade will be required to verify the durability of the design. Two areas of particular concern are the fatigue life characteristics of the brazed root attachment of the turbine blade at the carrier rim and achieving the best practical blade spacing between rotors and stators to assure adequate dissipation of the excitation energy for both steady state and gyromoment blade positions.

D. Continuous Ring Design

Two methods of supporting the tip turbine drive system on the fan rotor blades were investigated, One method used a segmented turbine carrier attached to the fan blade tip by means of pins; the other method utilized a free mounted continuous ring which supports the turbine blades and related hardware. This latter system is self-supporting, and only the driving torque is transmitted to the fan blades. It was concluded that the more conventional segmented turbine carrier was a better design than the continuous ring from both a standpoint of fan rotor dynamics and manufacturing feasibility.

In the continuous ring design, an annular 2-stage turbine was attached to the ring, and this assembly was concentrically mounted on the fan rotor blade tips. The ring was free radially and supported in the axial and tangential directions. During operation a large radial movement of the ring occurs with respect to the fan blade support as the result of thermal

and elastic growths. Because of this growth an air shroud is needed at the fan blade tips to maintain a smooth fan air passage throughout the operation. In order to raise the natural frequency of the fan rotor assembly above the operating speed, the fan blades must be connected by an intermediate stiffening ring at about two-thirds blade height.

The design of a continuous ring is a function of its inertia stress and deadweight stress. The inertia stress in a large diameter ring with a small cross-section depth can be considered as constant. The deadweight stress covers the centrifugal load of all items attached to the ring including the turbine blades. The deadweight stress varies as the cross-section area of the ring and hence its weight. An optimum ring design can therefore be determined consistent with the allowable material properties at the operating temperature.

The first order natural frequency of the carrier ring assembly is characterized by a simple spring system in which an effective mass is supported by the fan blades that act as cantilever springs capable of transverse in-place displacements. The effective mass acting at the blade tip consists of the total carrier ring weight plus 50 percent of the blade tip mass, which includes the radial tip supports and the upper third of the blade airfoils.

The critical speed of the fan rotor assembly with continuous ring and unsupported fan blades was approximately 40 percent of the operating speed. In order to raise the critical speed of the system to 30 percent above the operating speed, only the spring rate of the system can be increased since the minimum design weight of the ring was already established by the allowable strength of the material. Several approaches were taken to increase the system spring rate from the initial estimated 5000 lbs per inch of the cantilevered blades to the required 22,000 lbs per inch total. Parallel springs added at the blade tips were too bulky and weak under their own inertia loads. Increased fan blade chords raised the weight by greatly increasing the overall length of the package by virtue of the

1.5 axial fan blade tip chord stator spacing rule. Rigidly securing the continuous turbine ring to the fan blade tip was not elastically compatible with the blades. The solution decided upon that gave the least weight increase was tying the blades together with an integral ring in the fan air passage to effectively reduce the length of the cantilever spring support and thereby increase the spring rate.

Some of the manufacturing and operating problems that were responsible for the rejection of the continuous ring are presented below.

Analyses show that the total weight of a continuous ring including turbine blades, mounting attachments, and seals is higher with the currently available high temperature material choice than its segmented counterpart.

The 64-inch diameter ring would be flexible in handling due to its lightness with the risk of damage to the turbine blades. Close manufacturing controls on tolerances and roundness would be necessary to assure dynamic balancing. The less predictable spring back after machining would always be present, and along with looseness in the radial supports, a prevailing eccentricity would produce unbalance. The accuracy to which the blades can hold the ring round is uncertain and not dependable. Distortion from the high operating temperature and thermal gradients will produce additional changes that might disturb the balance of the fan rotor assembly particularly on restarts. Turbine gas seal clearances would involve matching the large radial thermal growths of both the ring and stationary structures, in addition to a rotation produced in the ring by the axial thermal gradient. The above items represent areas of detailed risk related to the use of a continuous ring which must be manufactured and operated in a realistic manner. Since no weight saving is involved, a thorough mechanical evaluation required of these critical areas would only detract from the performance development of the overall lift fan package. The continuous ring may still merit support, however, in the development of advanced hot gas sealing techniques.

The integral fan blade stiffening ring would be formed by welding together the extensions forged on the fan blade airfoil. Weld shrinkage, heat treatment and roundness of the finished ring, pre-machining and holding alignment of the fir tree attachments, and fan blade replacement all reflect on the costly production methods and difficult salvage potential of a one-piece fan blade assembly. Aerodynamic performance is also penalized by the restriction in the fan airstream passage.

Although manufacturing problems are not wholly eliminated with the segmented turbine carrier assembly, the total weight is less and each unit is smaller and easier to manufacture, handle, heat treat, install, replace and balance. In operation the segmented carrier produces a radial pull, which increases the centrifugal restoration force on the fan blade and reduces bending deflections.

VII. FAN STATOR VANE AND SUPPORT ASSEMBLY

The complete titanium fan stator vane and support assembly consists of 36 vanes welded to an outer support ring and an inner torus and ring assembly and bolted to a stationary rotor shaft spindle as shown in Figures 59 and 60. The entire bolted and fabricated assembly combines the requirements of the fan exit stator vanes, the main rotor support assembly and the three-point engine mount assembly.

Two arrangements were initially considered in the original design of the rotor shaft assembly. They are a rotating fan rotor spindle and a stationary spindle attached to the vane and support assembly. The stationary spindle arrangement was selected because of its overall simplicity and added rotor stiffness. Two systems for the support assembly were also initially considered. They are two fixed-strut supports at right angles and stiffened fan stator vanes. After some preliminary gyroscopic deflection checks, it was decided that a support system utilizing the fan stator vanes is structurally feasible and potentially lighter providing these vanes are sufficiently rigid and provisions are incorporated for thermal expansion between this housing and the turbine exhaust and scroll housing assembly.

The initial fan stator vane and support assembly design incorporated a system in which the original 54 individual fan stator vanes were positioned accurately, bolted at the inner annulus and pinned at the outer ring. This system, although acceptable, had three main disadvantages, namely, the location of vanes became critical and required close tolerances, the relative looseness of the outside ring could cause severe wear problems, and the stator vanes were not sufficiently rigid to take the assumed gyroscopic loads. In view of this, it was concluded that a structure could be welded similarly to a spoked housing and would offer a more stable system. It was also agreed to increase the chord length 50% with a corresponding decrease of the number of vanes from 54 to 36 so as to keep the same aerodynamic solidity. These longer chord vanes had the overall effect of increasing the stiffness of the support system by a factor of approximately 3.4. The final design incorporates all these features and is briefly described below.

VII. FAN STATOR VANE AND SUPPORT ASSEMBLY (CONTINUED)

The 36 solid titanium vanes are welded to an outer support ring and inner torus ring assembly. The outer ring assembly incorporates thermal expansion provisions in the form of 12 pins that attach to the turbine exhaust and scroll assembly. In addition, provisions for three 120° apart engine mount pads are incorporated as well as attached honeycomb structures for noise suppression. On the inside the stator vanes are welded to a ring and torus assembly similar to the outer ring. Maximum stiffness is attained by "tying-in" the walls of the inner torus support by using 18 one-piece ribs which extend to the outer aerodynamic wall of this support. The rib is welded along the front and rear flanges making it an extremely rigid box-like structure. The entire fabricated structure is then bolted to the stationary titanium shaft spindle which, in turn, supports the fan rotor assembly through two grease packed angular contact bearings.

The complete support assembly is sized to carry the engine mount loads and steady state loads combined with a gyroscopic couple resulting from an angular velocity in the pitch or roll direction. Steady state loads include the normal pressure and aerodynamic forces at design speed and thrust. Solid vanes are only structurally required at the engine mount location in the form of two vanes straddling each mount. This will allow 30 vanes to be made hollow with a resulting sizable weight saving.

A. Design Input Data and Analysis

The maximum fan stator vane and support assembly loads are a combination of the aerodynamic, gyroscopic and mount reactions which develop during steady-state operation. The loads act on the structure through the stator vanes, spindle and outer housing connections.

The fan stator vane loads are determined from the aerodynamic data in Figure 8; the maneuver loads are determined from the data in Figure 11; and the lift loads are based on the summary in Figure 12. All inertia loads in Figure 11 are small and were neglected. A gyroscopic moment of 72,000 lb-in. in pitch is developed, however, by the full rotor system due to a roll rate of one radian per second.

VII. FAN STATOR VANE AND SUPPORT ASSEMBLY (CONTINUED)

Figure 61 summarizes the fan stator support axial mount loads due to a total lift load of 10,758 lbs. and a gyroscopic moment of 72,000 lb-in. Four loading combinations were checked on the three point mount system to cover positive and negative gyromoments in the pitch and roll axes. The maximum mount reaction occurs for condition 3 with a gyromoment in pitch.

Figure 62 presents the condition 3 maximum applied loads and moments on an isometric view of the stator vane support assembly. The full fan rotor system lift load of 2,953 pounds and pitch gyromoment of 72,000 lb-in. acts through the spindle which is supported by the hub section. The hub, stator vane and outer ring lift loads total 3,517 pounds. An additional 4,288 pound outer housing load enters the outer ring through 12 radial support pins in the exhaust housing. The maximum mount reaction load of 5,073 pounds is shown. All three mounts are straddled by a pair of stator vanes, and typically illustrated in the sketch as vane numbers 1 and 36. The vanes are numbered clockwise looking downstream.

All loads are completely reacted at the stator support outer ring. Since the outer ring is assumed to have no rolling stiffness, the applied axial loads are reacted as axial shear loads at the outer ends of the stator vanes, except in the vicinity of the three aircraft mounts. For tangential loading, the outer ring is capable of giving full fixity to the ends of the stator vanes.

At each of the three main mount points the two stator vanes that straddle the mount are used to react the offset moments due to the axial mount loads. These moments are reacted as shear loads at the outer and inner rings of the stator vane support and produce maximum axial plane bending moments at the outer ends of these mount location stator vanes.

The additional axial shear load at the outer ring from the three mount points is reacted by ten adjacent stator vanes (five per side). For stressing of these ten vanes adjacent to the two vanes straddling each mount, only six are considered effective in transferring the shear load.

When the effect of this shear is added to the existing loading on these adjacent blades, the blades closest to the ones straddling the lift fan mounts have their highest axial plane bending moment at the inner ring location.

The axial loads transmitted to the stator support by the 12 equally spaced exhaust housing mount pins are reacted at the three main mount pads. Since the pins are loaded by the outer shell of the exhaust housing, a moment is transmitted to the stator support outer ring. Some of this moment is transmitted to adjacent blades in the same manner as for the main mount overhung moment. The rest of the moment is transmitted as torsion in the outer ring. The analysis shown does not account for these moment effects in the stator vane but does show an adequate margin-of-safety to allow for them.

The total axial and tangential shear load and bending moments distribution along the length of the fan stator vane is given in Figures 63 and 64 respectively. Shears and moments in the axial plane are given for vanes 1 and 36 which straddle the mount pin, and for vanes 2 and 35 which are adjacent to vanes 1 and 36. Shears and moments in the tangential plane are given for vanes 1 and 36 and are approximately the same for vanes 2 and 35. The shears and moments are based on the steady state aero loads on the vanes, the fan rotor and hub lift loads, the gyrocouple loads and the mount reaction loads. Since the hub is free to rotate, the symmetric axial loads do not result in tangential shear reactions at the vane tips (outer diameter). However, for the gyroscopic loading, no rotation of the hub relative to the outer ring takes place. Thus for this case, the blade tip deflection is axial only and a tangential load is generated by the gyromoment in the outer ring.

Section properties for the fan stator vane are given in Figure 65. Calculated data is shown for the areas, moments-of-inertia and extreme fiber distances from the 12.15 to 27.10 inch radii. Data to the innermost and outermost radii are assumed equal to the values at 12.15 and 27.10 inches

radii respectively. Constant values are used for the maximum airfoil thickness, chord length and torsional spring constant because of their negligible differences along the length of the vane.

The axial (parallel to fan axis) load distribution in the outer ring is determined from the load transferred to it through the 36 stator vanes, 12 exhaust housing pins, and 3 mount trunnions. All loads are assumed to act at the centroid of the ring which is symmetrically loaded about the axis of one of the three main mounts. As the ring is continuously supported by the stator vanes, none of the load is reacted as torsion and each half ring is treated as a straight beam for obtaining the bending moment distribution. A summary of the circumferential bending moment and axial shear load distribution in the outer ring is given in Figure 66.

B. Stress Analysis

The results of the stress analysis of the fan stator vane and support assembly is presented in Figure 67. In general, the various components of the assembly have been designed for rigidity to provide acceptable deflections at the tip of the fan rotor under gyroscopic conditions. Therefore the structure has ample margin-of-safety and vibratory margin levels.

1. Fan Stator Vanes

The fan stator vanes are used as structural spokes to connect the inner and outer rings of the support assembly. The vanes are considered as guided axially and tangentially at the inner ring and pinned axially and fixed tangentially at the outer ring. Maximum bending stresses develop in the trailing edge at the outer end of the two vanes which straddle the main mount (Vane Nos. 1 and 36). Maximim bending stresses also develop in the trailing edge at the inner end of the two vanes (Nos. 2 and 35) adjacent to Vanes 1 and 36.

VII. FAN STATOR VANE AND SUPPORT ASSEMBLY (CONTINUED)

2. Outer Ring

Maximum loads and moments develop on either side of the mount pin located on the axis of symmetry. Peak values at the mount were disregarded because of the distribution provided by the bolting pad in the mount ring. The outer ring was checked for bolt tension and bending moments in the pad, and bending, shear and buckling in the critical sections of the ring.

3. Inner Support and Spindle

Maximum loads and moments in the support develop on either side of the mount pin location on the axis of symmetry. The support structure was analyzed for direct, bending and shear stresses and checked for stability. An analysis of the spindle is included.

C. Vibration Analysis

The principle natural frequency modes in torsion and bending were calculated for the fan stator vanes and an interference diagram was constructed as shown on Figure 68. The critical excitation frequency orders are:

1 & 2 - excitation frequencies normally generated by the engine or fan rotor

48 - number of fan rotor blades

The vanes were considered as fixed in torsion and bending at their inner and outer ends where they are welded into the supporting structure. Both solid and hollow vanes were checked to substantiate the flight weight configuration. The test stand configuration, however, will have only solid stator vanes. The analysis results show that the stator vanes will have satisfactory vibratory characteristics throughout the engine operating range. The vane resonant natural frequencies are well over the second engine order and well below the 36th engine order at a design speed of 3030 RPM. The torsional interferences indicated at 1200 and 1480 RPM are at low weight flows and can be neglected.

VII. FAN STATOR VANE AND SUPPORT ASSEMBLY (CONTINUED)

The flutter analysis values, V/bw, in torsion and bending are shown below:

Type	Air Velocity (ft/sec)	Airfoil	Reduced Velocity (V/bw)	Maximum Acceptable Reduced Velocity (V/bw)
Torsion	845	Solid	.66	2.00
		Hollow	.54	2.00
Bending	845	Solid	2.70	6.66
		Hollow	2.17	6.66

The above air velocity represents 115% of the design inlet air velocity at the mid-span of the vane. This is considered the maximum expected velocity for a fan-in-wing installation. The stator vane is therefore satisfactory in flutter.

VIII. SCROLL HOUSING AND TURBINE FIRST STATOR

The hot gas scroll assembly is an all welded Rene'41 annular structure as illustrated in Figure 69. It was designed with circular sections to minimize internal pressure stresses, and it has mechanical ties in the form of airfoil-shaped struts which are aligned with the flow at the entrance to the outlet neck upstream of the turbine nozzles. In addition to the pressure load, the scroll was sized to carry the nozzle reactions and the buffer air manifold and bellmouth inlet loads. The inlet reaction load will be carried by the connecting air supply ducting which will include a flexible line with a bend and will be capable of taking tensile loads per agreement with NASA.

The circular scroll sections are constructed of 0.040 inch thick formed sheet material and joined circumferentially to tapered arms on the scroll neck inlet. The neck is an annular passage which turns the gas flow from radially inward to axial (parallel to the fan axis) for entering the turbine. The inner and outer walls of the neck are fabricated from 0.065 and 0.080 inch thick sheet material and a machined flange. The ties and turbine nozzles are welded into eloxed slots at the entrance and exit ends of the neck. The ties in each 180 degree half of the neck are a mirror image orientation of each other to conform with the two-directional flow split at the scroll inlet. The turbine nozzles are oriented to the flow with a zero degree entrance angle. The annular passage walls are circumferentially contoured to form a divergent nozzle for supersonic flow. Figure 70 shows the fabricated scroll neck with solid turning vanes and turbine nozzles. Figure 71 shows a cast scroll neck with solid turning vanes and hollow sheet metal turbine nozzles. Because of the uncertainty of welding to the René 41 casting, this design was superseded by the fabricated sheet metal configuration in which the processing methods are well established and a lower risk is involved. The turning vane coordinates are the same for both configurations.

Equally spaced brackets are welded to the curved inner wall of the scroll neck for supporting the buffer air manifold and bellmouth inlet duct. The scroll support housing extends from the outer wall of the scroll neck at the turning vanes (ties) to a flanged end which attaches to the stator support at assembly.

VIII. SCROLL HOUSING AND TURBINE FIRST STATOR (CONTINUED)

The inlet duct makes a radial tee connection with the scroll duct (see Figure 72). Its plane is displaced parallel to the scroll in order to clear the bellmouth inlet duct. The structure is reinforced at this intersection by the turning vanes and splitter plate. An 0.071 inch thick material is used in this area.

The combustor housing is 24 inches long and is welded directly to the inlet duct. The material thickness is 0.050 inches and a flange is provided at the burner headplate end for assembly of the combustor basket. The short distance from the combustor to the scroll provides ample mixing distance to flatten the temperature profile and virtually eliminates the need for hot gas ducting in the airframe.

The mechanical properties of the Rene 41 scroll material are well suited to the structural requirements dictated by the elevated pressures and temperatures for operating the turbine. Careful welding and heat treat procedures have been prepared to accommodate the forming, welding, hardening and stress relief processes necessary to fabrication and attaining the maximum mechanical properties of the material.

A. Design Input Data and Analysis

The scroll aerodynamic data, turbine nozzle coordinates and combustor housing dimensions were supplied by NASA. Curtiss-Wright sized the scroll inlet, gas passages and outlet neck from the information in Figure 9. The aerodynamic loads, pressure loads, and bellmouth inlet and buffer air manifold loads were obtained from the information shown in Figures 4, 6, 9 and 10. Maneuver loads and the nozzle torque loads were small and were therefore omitted. The scroll was designed for maximum loads at the steady-state and critical transient operating conditions. Heat transfer data summarizing the temperature-time history of the hot section components is presented in Section XIII.

VIII. SCROLL HOUSING AND TURBINE FIRST STATOR (CONTINUED)

B. Aerodynamic Design

1. Scroll Configuration and Turning Vanes

A turbine inlet hot gas scroll was designed to provide uniform circumferential pressure and flow into the full admission two-stage axial tip turbine with an overall total pressure loss of 4.38 percent. The inlet supply pipe was defined as having a 10.75 inch diameter (A = 90.76 sq. in.) at the combustor outlet and the aerodynamic data for the scroll are given in Figure 9.

The tee connection where the gas supply pipe from the combustor joins the scroll incorporates turning vanes and a splitter plate to divide the gas flow and turn it approximately 90 degrees into each half of the 360 degree scroll while maintaining a low turning loss. The inlet pipe size at the entrance to the scroll was tapered to 9.625 in. diameter, area = 72.76 sq. in. at Section BY-BY in Figure 72. The gas flow Mach number at this location is 0.190, giving a turning loss of 0.6 percent and establishing a pressure level for sizing the remainder of the scroll. Because the flow divides equally into each half of the scroll, the entrance flow area of each half of the scroll was set at one-half the total inlet area, or at 36 sq. in. at the zero degree intersection with the tee. This area rapidly converges to the scroll design flow area of 25 sq. in. within approximately 15 degrees. The inlet pipe was sized to provide constant area into and out of the inlet turning vanes. In shaping the inlet tee (Section BK-BK) circular sections were used and the slope of the converging rear wall was limited to allow sufficient clearance for machining the back of the circumferential bolting flange. The resulting sections at BP-BP and BQ-BQ result in a constant projected area into and out of the turning vanes of slightly less than 36 sq. in. which is satisfactory and softens the transition back into the scroll design flow area of 25 sq. in. The area schedule through the tee is as follows:

VIII. SCROLL HOUSING AND TURBINE FIRST STATOR (CONTINUED)

AREA SCHEDULE THROUGH INLET TEE

HOT GAS SCROLL

Location on Figure 72	Section	Area - sq. in.
1. Inlet to scroll, D = 9.625 in.	BY-BY	72.76
2. Entrance to Turning Vanes (projected area)	BQ-BQ	33.62
3. Exit from Turning Vanes (projected area)	———	33.51
4. Scroll Passage, θ = 10°	BM-BM	29.5
5. Scroll Passage, θ = 15°	BN-BN	25.8

To save axial length, the scroll duct was placed over the turbine and a 90 degree annular neck was provided to turn the flow from radially inward to axial (parallel to the fan axis) for entering the turbine. A cascade of turning vanes was located around the inside diameter of the scroll passage at the entrance to the scroll neck to remove the tangential component of scroll gas velocity and direct the flow radially inward. The leading edges of the turning vanes are oriented 30 degrees into the flow to induce turning, with the remaining 60 degrees of turning occurring in the vane cascade.

A NACA 65 series airfoil with a maximum thickness ratio of 8 percent, a circular arc mean line with 60 degrees of camber and a solidity of 1.5 was used for the turning vane. The 60 degree turn required a sidewall flare of 2:1 to provide a constant flow area through the vanes as shown in Figure 73 and this resulted in a reasonable mechanical design and flow passage aspect ratio. Account was also taken of the vane thickness so as to provide for uniform gas velocity through the vanes and into the turbine nozzles. A low back-pressure cascade resulted.

VIII. SCROLL HOUSING AND TURBINE FIRST STATOR (CONTINUED)

The cascade "diffusion factor" in this design, is about 0.18. The neck provides for circumferential static pressure communication just up stream of the turbine nozzles, and assists in obtaining uniform circumferential flow.

The calculated scroll flow area schedule, Mach number, and pressure distribution are shown in Figure 74. The scroll is designed for a constant circumferential static pressure around the I.D. and into the turbine. The constant scroll I.D. static pressure is maintained by reducing scroll sectional area both in proportion to the flow leaving the scroll and the drop in total pressure due to friction and bend effects. The radial gradient in static pressure across the scroll at any location was also considered in that a mean scroll Mach number was selected at all locations so that the I.D. static pressure will remain constant.

The actual scroll area closely follows the calculated area schedule except at the intersection with the inlet and at the 180 degree position where an area greater than zero was allowed for pressure balancing each half of the scroll. The 4.83 sq. in. area at 180 degrees is smoothly blended with the scroll duct.

Delivering circumferentially uniform flow and pressure to the turbine depends largely on the ability to predict the slope of the scroll total pressure loss along the scroll curve. The overall level of system total pressure loss is dependent both on scroll loss and the losses of the scroll inlet and I.D. turning cascades.

The scroll total pressure loss was obtained from bend loss correlations and frictional loss data. Losses occur in pipe bends with secondary flow patterns. When air is continuously bled from the pipe I.D., as in this scroll design, the secondary flow pattern and the resulting losses can be altered. For these reasons, a development program is recommended in order to produce a scroll design with the desired characteristics.

VIII. SCROLL HOUSING AND TURBINE FIRST STATOR (CONTINUED)

2. First Stage Turbine Nozzle

The first stage turbine nozzles are located at the exit of the scroll neck. They were designed by NASA per the aerodynamic data in Figures 9 and 10. The nozzles were designed for supersonic flow and have a convergent-divergent passage. The throat is formed by the contoured inner and outer walls of the scroll neck outlet. Coordinates for the airfoil and wall shape are given in Figure 70.

C. Stress Analysis

1. Scroll and Inlet

This portion of the hot gas scroll consists of a toroidal gas duct and an inlet pipe. The gas duct is symmetrical about the inlet pipe axis and its cross-sectional area decreases as it recedes from the inlet. The gas scroll and inlet duct were designed for 1000 hours life at the steady-state design condition which includes an operating temperature of 1440°F and a pressure differential of 90 psi. The results of the scroll and inlet stress analysis are summarized in Figure 75. All margins of safety are satisfactory.

The mechanical and thermal stresses for the torus were derived for a basic sheet metal thickness of 0.04 inches with tapered arms to 0.08 inches utilizing the shell computer program. Segment 1-2 was analyzed as a constant cross-section torus equal to Section A-A, and segment 2-3 was analyzed as a constant cross-section torus equal to Section B-B.

The meridional and tangential total stress results are summarized around the cross-sectional perimeter of the torus shell. The meridional stresses exceed the hoop stresses and the higher stress occurs in the larger Section A-A. Both the operating temperature and room temperature conditions were considered to determine the influence of thermal stresses. The two-dimensional effect of thermal displacements at

the fixed ends of the shell support at the entrance to the scroll neck was also included in the analysis. A 1.5 factor was used to account for any stress discrepancy due to the assumptions of a constant cross-section torus and a uniform support at the inner edge of the cross-section. A breakdown of the maximum stresses into their membrane and bending components is given at location, c in Section A-A and location a in Section B-B.

The mechanical and thermal stresses for the inlet duct were derived for a basic sheet metal thickness of 0.065 inch. This thickness covers the local bending condition in the duct skin between the turning vanes and allows for a stress intensification factor for tee sections of 2.5 (i.e., 2.5 x hoop stress in the inlet pipe).

2. Scroll Neck and Support Housing

The vanes and nozzles in the annular scroll neck serve as mechanical ties between the inner and outer walls of the passage. Both the steady state and transient operating conditions were analyzed. The pressure, aerodynamic loads and stress results are summarized in Figure 76. All margins of safety are satisfactory.

The mechanical and thermal stresses in the scroll neck were determined for basic sheet metal thicknesses of 0.065 and 0.080 inches, utilizing the shell computer program. Fixity against rotation was assumed at points a, b, c and d. To ensure stiffness in the area between a and b, the nozzles connecting the inner and outer walls were conservatively sized for the maximum bending moment at point a. No radial restraint of the circumferential sealing face on the inner wall was assumed since this sealing face was slotted radially to relieve thermal loads.

The support housing shell was also checked for mechanical and thermal stresses using the shell computer program which included inputs for the second stage turbine stator and exhaust housing assemblies. The

second stage turbine stator and exhaust housing results are summarized in separate sections of this report. The basic shell thickness of the scroll support housing is 0.050 inches. Tapered ends were used at the junction with the scroll neck and at the bolting flange to relieve the resulting discontinuity stresses. The low cycle fatigue life data for the material used was taken from Figure 20.

D. Vibration Analysis

The shorter length first stage turbine stator vane will have higher natural frequencies than the second stage turbine stator vanes. Since the first stage vanes will see the same excitation frequency as the second stage (504th engine order), no resonant excitation is expected.

Similarly, no resonant excitation is expected with the upstream scroll neck inlet vanes.

IX. TURBINE SECOND STATOR

The Hastelloy X second stage turbine stator vane assembly is shown in Figure 77. The assembly consists of two 180-degree half outer and inner rings which are bolted together at their parting line. The hollow sheet metal blades (286) are brazed into the triangular sectioned 180° outer ring that incorporates scalloped front and rear flanges for bolting to the scroll and exhaust housing assembly. These blades are also brazed into a segmented inner shroud ring which supports the stationary element of the middle labyrinth seal. The inner shroud ring is made of eight sectors for each half to relieve the differential thermal growth caused by the rapid heating of this end with relation to the outer ring. Gas leakage across the inner shroud is minimized by lapping the slots with a sheetmetal tab. The sealing element is riveted to the inner shroud for ease of repair or servicing.

The stator assembly is fabricated in two halves to facilitate installation between the two rows of turbine rotor blades. The split line flange of the assembly is oriented 90 degrees to the scroll inlet pipe for easier access to the parting line bolts. The rear flange of the stator is indexed to the exhaust housing flange to permit positioning increments of 90 and 120 degrees. Thus, the scroll inlet can be oriented in any of seven positions with respect to the mount ring (exclusive of the exhaust housing support pins) by indexing the rear stator flange. Both stator flanges are doweled to hold concentricity with the mated parts. In addition, an axial adjusting shim is placed at the front flange to adjust for tolerance accumulation.

The outer formed sheet metal ring of the stator assembly is welded to forged and machined flanges. The hollow sheet metal blades which are brazed into the inner and outer walls of the ring form a truss which connects the blade to each flange. Consequ ntly, the axial plane bending moments produced by the pressure forces on the blades appear as radial loads on the bolted flanges in the overall assembly. The hoop stresses in these flanges resist the radial load and stabilize the stator support structure.

The Hastelloy X alloy is easily formed, brazed and welded, and requires no subsequent heat treatment for a minimum of distortion during manufacture. It

possesses a high degree of ductility and is well suited to the structural requirements of the design.

A. Design Input Data and Analysis

The stator vane assembly is subjected to the pressure, aerodynamic, thermal and maneuver loads during operation. The maneuver loads were determined to be small and were therefore neglected. Figures 9 and 10 show the basic aerodynamic data for determining the stator loads. In addition, loads from the gas scroll are transmitted through the outer support ring and flanges. Constant cross section airfoils are used because of the large mean radius of the annular gas passage. Section properties for the blades were determined from coordinates supplied by NASA. The stator design loads and properties are presented with the stress analysis summary. Stator temperatures are given in the heat transfer section which includes a discussion of the special provisions for increasing the heating rate of the outer stator structure to permit a quicker closing of the middle turbine seal.

B. Stress Analysis

The stator vane assembly stress analysis of the outer support ring, airfoil and inner shroud ring was performed for both steady state and transient operating conditions. A summary of the maximum stresses on the critical sections of the structure is presented in Figure 78, which also includes the basic loads, airfoil section properties and modified Goodman diagram. All design margins of safety, vibratory margins and low cycle fatigue life are considered satisfactory.

However, points a, b and c have negative margins of safety against the 0.2% creep in 1000 hours criteria. The high stresses are circumferential, compressive, and located close to the upstream flange. The flange develops a 7000 psi compressive hoop stress from the stator moment and somewhat less if the pressure stresses are included. Accordingly, the stresses that produce the negative margins are thermal in origin and are

considered secondary stresses since creep deflection will relieve them; i.e., they are self limiting. When viewed in this manner, all of the tabulated stresses are considered acceptable.

1. Stator Housing

The stator housing or outer support ring was analyzed as being a complete assembly with the gas scroll and exhaust housing. The structure was treated as a continuous shell with a pair of intermediate bolting flanges. Pressure and aerodynamic loads were assumed to act continuously while thermal loads vary with time. Both the steady state and transient phases of operation were checked. Steady state occurs after 340 seconds of operation. Maximum transient loads occur at 100 seconds from startup or 45 seconds after lightoff. Only the axial pressure loads were included on the housing. Tangential aero loads from the scroll and stator vanes were small and omitted. The axial moments from the stator were input as radial, circumferential line loads at the bolting flanges. The stress results are presented in Figure 78 with an explanation for accepting the negative margins of safety in creep discussed in the introductory paragraph at the beginning of this sub-section. The low cycle fatigue life for the outer housing, based on an equivalent stress at the transient condition and the lower bound of Manson's Curve in Figure 16, is over 50,000 cycles which is more than double the minimum required 24,000 cycles.

2. Stator Vanes

The stator vanes were analyzed as cantilever beams fixed at their root section or outer radius. Since the inner shroud ring is segmented it was not considered to be an effective restraint on the inner end of the airfoil for purposes of stress analysis. The gas loads acting on the blade are due to the pressure differential across the inner shrouds and the aerodynamic load across the vanes. Maximum axial and tangential gas bending moments were calculated at the root section of

the blade and resolved into the strong and weak bending axes of the airfoil section. The bending stresses at the leading edge, trailing edge and back of the blade, as well as the blade vibratory margin are also summarized in Figure 78.

The blade is also subject to low cycle fatigue during the transient condition due to the rapid heating of the inner shroud during heat-up. Although the axial slots relieve the radial thermal growth of the inner shroud and seal, circumferential growth still occurs and results in a tangential deflection which is a maximum in the blades at the ends of the segment. The maximum blade stress due to this deflection was determined and converted to an equivalent stress that was used to establish the low cycle fatigue life from the lower bound values of Manson's Curve. The allowable number of cycles is 25,000 which is above the minimum number of cycles. The allowable number of cycles may be raised by increasing the number of inner shroud ring segments, thus reducing the maximum blade deflection. Since axial slots represent additional leak paths across the stator, it is not recommended until engine development dictates this requirement.

3. Inner Shroud

The inner shroud is cantilevered from the inner end of the stator vanes and supports the stationary member of the middle labyrinth sealing element. Maximum bending stresses due to the axial pressure differential occurs in the shroud just above the riveted lap joint. A corrugation between the blades in the bend at the shelf stiffens the upper end of the shroud considerably. The steady state stress is summarized also in the above Figure.

C. Vibration Analysis

A vibration analysis was also performed for the second stage stator vane which was considered to have some support at both ends.

IX. TURBINE SECOND STATOR (CONTINUED)

Due to the flexibility of the attachment configuration, the bending natural frequency of the vane will be somewhere between the hinged-hinged and fixed-fixed end condition frequencies. As a conservative estimate, it was assumed that the fundamental bending mode would be 25% above the hinged-hinged condition. This corresponds to a frequency of 30,000 CPS at design conditions. The natural frequency is well above the major excitation source, which is the rotating blade passing frequency equal to the 504th engine order or 25,450 CPS at design speed. The torsional resonant frequency will be much higher than the bending frequency and should present no problems.

X. EXHAUST HOUSING

The exhaust housing is an all-welded Inconel 600 and Hastelloy X alloy annular structure as shown in Figure 79. The inner and outer shells have flanges at their forward end and are connected by twelve equally-spaced radial struts. Besides providing a passage for the turbine exhaust gas, this housing also serves to structurally connect the hot gas scroll and second stage turbine stator assembly to the outer ring of the fan stator vane and support assembly. The exhaust housing is assembled to this support with twelve radial pins which permit differential radial growth between the hot turbine exhaust housing duct and the cold fan air duct. The pins are secured to bosses in the exhaust duct struts and are free to slide in the outer ring of the stator vane and support assembly.

Nine of the struts are airfoil shaped and hollow. Three of the struts are triangular shaped with rounded side walls in the gas passage and large hollow openings for installing the trunnions on the fan stator vane and support assembly outer ring pads. At assembly, the exhaust housing and outer ring are concentrically fixtured as an assembly, and the pin holes are line-reamed to eliminate the true position tolerance requirements and enable the use of close pin clearances to minimize the displacement of the stationary element of the front labyrinth seal. It may be possible to eliminate this requirement later when high volume production becomes a reality and accurate fixturing can be used. The outer shell of the exhaust housing duct is stiffened with a circumferential ring in the plane of the mount pins, and both shells have circumferential stiffeners at their outlet.

Inconel 600 alloy was used for the sheet metal shells, stiffening rings and forward flanges. Hastelloy X material was used for the radial pins and the cast struts. Since the shells are sized for elastic stability, the mechanical properties of the Inconel 600 alloy are adequate, as well as being thermally compatible with the Hastelloy X struts and the second turbine stator vane assembly.

X. EXHAUST HOUSING (CONTINUED)

A. Design Input Data and Analysis

The exhaust housing supports the hot gas scroll and turbine stator assemblies from the plane of the radial support pins. Loads from the scroll and turbine stators are transferred through the exhaust housing and pins into the fan stator vane and support assembly outer ring rim. The axial shell load transferred from the second stage turbine stator assembly is given in Figure 78. The aerodynamic and pressure loads on the exhaust housing were small and omitted since the annular housing is at ambient pressure and has an almost constant area flow passage. Although the annulus pressure was designed to be atmospheric, a small deviation could result in a buckling differential on the shells. A pressure variation of $\pm$ 1 psi was assumed for the purpose of checking elastic stability.

Both the maneuver loads and tangential (torque) loads from the gas scroll and turbine stator assemblies were considered small and omitted from the shell analysis. These values are used however for the pin analysis. Maneuver load factors are given in Figure 11 and the tangential gas loads on the turbine stator vanes are given in Figures 76 and 78. Temperature data for the exhaust housing is given in Section XIII. Both the inner and outer shells are nearly at the same operating temperature.

B. Aerodynamic Design

The exhaust housing duct gas passage was aerodynamically designed to satisfy the following turbine exit conditions at an optimum total pressure loss:

P_{T8} = 15.67 psia
P_{S8} = 14.70 psia
T_{T8} = 1338°R
T_{S8} = 1316°R
W_8 = 29.9 lbs/sec
A_8 = 265 in^2
M_8 Axial = 0.31

X. EXHAUST HOUSING (CONTINUED)

Since the exhaust duct discharges to atmosphere, the back pressure is the same as the turbine exit static pressure; i.e., 14.7 psia. To meet this static pressure requirement it was necessary to size the exhaust duct exit area in such a manner as to compensate for the total pressure loss in the duct. On this basis the required exhaust duct exit area is 302 square inches.

The overall pressure loss in the exhaust duct consists of the following: a sudden expansion at the turbine exit, two gentle turns of approximately 17 degrees each, the friction loss on the annulus walls, the friction loss on the three wide struts, and the profile loss of the nine narrow aerodynamic struts. The overall pressure loss was estimated to be 1.47% of the turbine exit total pressure.

To obtain a smooth flow area variation along the duct, the outer and inner annulus walls were properly shaped to compensate for the blockage of the struts. At the turbine exit, the outside diameter of the annular passage was dictated by the physical requirement of having a radial gap between the outer annulus wall and the turbine rotor shroud in the cold assembly condition. The inside diameter of the duct was selected to avoid an undesirable step in the flow passage in the hot running condition. At the exhaust duct exit, the inside diameter was again predetermined by the physical requirements of assembly and thermal growth, whereas the outside diameter was sized to meet the flow area requirement after subtracting the area blocked by the struts.

The hot gas flow path area schedule and duct geometry is given in Figure 79.

C. Stress Analysis

The stress analysis summary and basic load data for the exhaust housing and support pins is presented in Figures 80 and 81 respectively. The duct was analyzed for both the steady state and transient operating conditions which covers the full range of temperature gradients. The

X. EXHAUST HOUSING (CONTINUED)

pin analysis includes only steady-state gas loads and flight maneuver loads. All margins of safety are satisfactory.

1. Exhaust Housing

The analysis of the exhaust housing duct outer shell considered the gas scroll housing and turbine second stator housing as part of the complete assembly. The outer shell is bolted to the stator housing at its forward end and supported by the radial pins at its aft end. The supported end of the outer shell is reinforced by the 12 struts, circumferential stiffener ring and the inner shell. In this analysis the supported end was conservatively assumed to be guided; i.e., free to displace radially but not rotate. The inner shell was not directly considered in deriving the stress distribution in the outer shell. A summary of the maximum shell stresses is presented in Figure 80 for the steady-state (t = 340 sec) and transient state (t = 100 sec) conditions. Since the exhaust duct temperatures are low, the material yield strength is governing.

The exhaust housing duct was aerodynamically designed to be at atmospheric pressure, i.e., 14.7 psia. A pressure tolerance of ± 1 psia was assumed for the purpose of assuring elastic stability in the shell structure. Only the cylindrical aft section of the exhaust duct was analyzed. The ducting upstream of the radial support pins is considerably stiffer by virtue of its compound curvature and end flanges.

The outer shell extends between the radial pins and exhaust duct exit and was treated as a symmetrically stiffened cylinder of twice its actual length to account for the unsupported exit end. The distance between stiffeners is also important and in order to be effective the stiffener must have a certain amount of rigidity. The stiffening ring is located in the plane of the radial support pins. The inner shell was treated as a curved cylindrical arch

X. EXHAUST HOUSING (CONTINUED)

supported between adjacent struts and having free curved edges. The results of the buckling analysis are given in Figure 80.

2. Radial Support Pin

Pin loads from the gas scroll and turbine stators are transferred through the exhaust housing and radial pins into the fan stator support outer ring. Since the exhaust housing duct is a relatively flexible structure, the pins were designed as cantilevers built in at the rigid outer ring of the fan stator support assembly and shear loaded at the junction with the outer exhaust shell only. The pin was checked for both the flight and landing condition maneuver load factors in combination with the lift load. Maximum stress in the pin will occur during the landing maneuver conditions and is summarized in Figure 81.

XI. TURBINE LABYRINTH SEALS

There are three dynamic hot gas seals in the tip turbine area as shown on the engine basic assembly in Figure 1. The rotating seal elements are thin metal circumferential fins that are suitably fastened to their support arms. As part of the turbine carrier assembly, they are also segmented in twenty-four places. The front and rear lip seals are part of the René 41 fan air shroud. The middle seal is supported from the side wall of the 1st turbine rotor carrier rail. Both the arm and seal lips are fabricated from Hastelloy X and Inconel X material respectively.

The stationary shroud seal elements are made of a Hastelloy X backing sheet and an Inconel 600 alloy brazed honeycomb core, and are filled with a soft high-temperature sealing material called Nicroseal. The Nicroseal will allow limited local gouging of the shrouds without damage to the sealing lips or an effect on the functioning of the seal. The rotor seal lips will be given a hard coating to resist wear if development testing indicates that this is required.

The upstream labyrinth seals the 1st turbine nozzle from the fan rotor shroud. Because of the high first stage turbine gas pressure, which is the result of a two-stage turbine design, a pressurized buffer air seal was used to prevent a large loss of turbine gas into the fan air stream. The use of a buffer air system also provides cooling of the front seal arm, tang, pin and upstream face of the first turbine rotor carrier rail, which would otherwise be at too high an operating temperature.

The buffer air will be distributed to the seal through an annular manifold that is fed from a low pressure bleed point on the air generator compressor. The front seal shroud is attached to the manifold which is held round and is supported by radial pins and brackets on the hot gas scroll.

The middle labyrinth separates the two turbine stages and seals against the pressure drop across the second stage nozzle. The downstream labyrinth restricts the hot exhaust gas from mixing in the fan air stream. Both rotating members of the outboard seals are underslung (radially inside the stationary

seal) to permit relative radial displacements due to thermal and elastic growths without interference. On the middle seal the stationary shroud is the underslung member because of its large thermal growth. The middle seal is part of the stator assembly which was made in two halves to permit its installation between the turbine rows.

A. Seal Displacements and Leakage

The choice of a labyrinth type seal was made because of a lack of successfully developed and tested alternate sealing methods. Labyrinth seals are a state-of-the-art application, but in a large diameter tip turbine with pressurized gas several additional design factors must be considered, among which are:

1. Seal leakage rate.
2. Manufacturing tolerances.
3. Radial and axial displacements.
4. Temperature-time transients.

For this design a steady state mean sealing gap of 0.020 inch was used to minimize the seal leakages and the buffer air consumption. A gap of this size at a 62-inch diameter will require extremely close dimensional control. This can be accomplished by holding close manufacturing tolerances, line reaming the radial support pin holes in the exhaust housing and gas scroll neck brackets, doweling the housing flanges and finish machining all sealing diameters at assembly. Distortions due to hot operation and restarts were not considered and must be separately dealt with during development.

Apart from the manufacturing aspects of sealing are the running factors which are broadly described as mechanical and thermal steady state displacements, and temperature transient displacements. Mechanical displacements occur as the result of loads acting on the fan rotor assembly and stator vane support structure and are due to direct strain or flexi-

bility in the support system. Considerable axial displacements occur at the fan blade tip from the steady state lift loads. Additional axial and radial displacements occur from the gyroscopic moments. A summary of the radial and axial displacements at the tip turbine lip seals is given in Figure 82 for the steady state and gyroscopic loading conditions. The displacements are comprised of the fan blade and disk elastic strain, fan blade deflection, rotation and axial translation of the inner support of the fan stator assembly and deflection of the fan rotor spindle. Both bending moment and shear deflections were included in the analyses.

From the steady state axial displacement position, the fan blade tip can make an excursion of $\pm$0.284 inch during a pitch or roll maneuver of one radian per second. The turbine and stator blade rows, tip tangs and seals have been positioned in the design in consideration of this maximum excursion, as illustrated in Figure 77. To hold this limit, the fan stator support structure was stiffened by increasing the blade chords and adding shear plates to the inner and outer structures.

Since the pivot or center-of-rotation of the fan rotor assembly is in the plane of the stator vanes due to the support structure geometry, axial deflections also produce small radial deflection components which are most pronounced during a pitch or roll maneuver. Seal gouging due to radial displacements could be eliminated by using a conical shroud instead of a cylindrical one, but assembly clearances and thermal problems appear to outweigh the advantages. Therefore, with a 0.020 inch seal gap a one radian per second spin will produce a maximum gouge in the cylindrical seal shroud to a depth of 0.043 inch as shown in Figure 83. Since the gouging occurs at a position axially displaced from the normal running location, a return to the steady state position operating point re-establishes the 0.020 clearance and the design flow conditions. Changes in the seal gap due to rub can be tolerated in the front seal to an extent of 0.056 inch at a 33.8 psia buffer air supply pressure and to 0.090 inch at a 47.3 psia supply pressure without impairing the function

of the seal but with an increase in buffer air flow. A similar increase in the clearance of the middle and rear seals will increase the leakage flow.

Thermal displacements result from the heating of the structural components by the turbine gases. They are largely radial in direction and variable in time. Both transient and steady state temperatures must be considered in setting the hot and cold seal clearances and predicting their variation with time, especially for this lift fan package where the nominal operating time is 2.5 minutes.

The steady state running clearance for the three tip turbine labyrinth seals was based on the radial elastic and thermal growths of the fan rotor and turbine structure under nominal operating conditions. Any gyroscopic effects are of short term duration and were not included. The elastic growth is based on the strain of the disk and fan blade under centrifugal load. Thermal growths are largest in the stationary structures, but occur in the fan rotor assembly to a small extent. Figures 84, 85, and 86 show the displacements of the rotating and stationary labyrinth seal members and the relative seal gas as a function of time. A second set of curves on the above figures discloses the amount of gas leakage through the seal gap given as a percentage of total turbine inlet weight flow. The leakage rates were based on proportioning the gas flows according to the flow or leakage areas and assuming that all pressure ratios remain the same. Losses through the segmented joints were found to be negligible as compared to the overall flow and were therefore neglected. In addition, no turbine power loss was assumed due to leakage around the seals during the transient. Data are given in Figure 84 for the front seal system with and without buffer air.

In the above figures the clearance given at t = 0 represent the cold seal gap at the time of assembly and correspond to the dimensions given on the layout drawings. The time scale extends up to the steady state temperature condition which is about 340 seconds. Although cool-down clearances are not included in the figures, when the turbine combustor is turned off,

the air generator must continue operating to supply cooling air through the turbine section. The air will cool the second stator outer housing sufficiently so that when the fan rotor runs down it does not seize on the middle seal shroud. The outboard seal shrouds are already fairly cool and the rotor wheel will not rub during shutdown.

With buffer air, the hot gas leakage into the fan air stream is zero at the front seal since the buffer air seal pressure is higher than the upstream turbine cavity pressure. Some of this buffer air is lost through the segmented carrier gaps and the remainder mixes with the hot gas stream. When buffer air is used, the front seal gap closes quickly during the warm-up period. Without buffer air there is an initial 35 percent loss of high pressure turbine gas into the fan air stream which overheats the carrier structure and fan rotor blade tips. In addition, there will be a considerable drop in turbine performance.

The middle seal closes very slowly and results in a large bypass of hot gasses around the second turbine stator vane. The slow closing is due to the time lag in the heating of the outer turbine stator support structure. Provisions to increase the radial growth rate are discussed in the Heat Transfer Section and the effects are included in Figure 85. The middle seal is last to close and represents a potential loss of power during the early part of flight. Full closure does not occur unless the flight duration exceeds 340 seconds.

The rear seal closes quickly during running due to the elastic growth of the fan rotor assembly, which is a function of wheel speed. The rear-seal-supporting bracket is insulated and aircooled and has a small thermal growth. Seal leakage due to pressure differential will be small and its effect on the fan air stream should be minor.

Mismatch of the turbine gas passage is given as a function of time in Figure 87. During the transient phase of operation, the passages will not be aligned. The second stator vane will take the longest to align with the turbine blades. To compensate for these offsets while the

turbine section is heating, the shelves and shrouds on the turbine rotors and stators were flared to aid in receiving the gas flow. Full alignment of the passage will occur when steady state temperatures are reached.

The use of labyrinth-type seals for the tip turbine will permit test stand evaluation of the lift fan package. Manufacturing controls must be strictly held and will require special fixturing equipment, set-ups and procedures to eliminate the tolerance accumulation. Under test stand conditions the seal clearances are affected only by centrifugal loads and thermal growths. Fan performance may lag slightly until the structure heats and the seal clearances close. As a flight package, however, angular pitching and rolling velocities will cause gyroscopic moments and radial and axial excursions of the fan blade tip, which would result in a seal rub and possible reduction in flight performance.

In conclusion, the use of labyrinth seals in this application is acceptable for test stand operation, but additional seal investigation may be necessary before suitable flight operation can be achieved.

In recognition of these limitations, labyrinth type seals and alternate methods of sealing are under study at NASA to allow the use of a two-stage high pressure turbine and these improved sealing methods could be eventually substituted. One of these methods is an air film device with flexible fingers to follow the runner through all blade tip excursions.

B. Buffer Air Aerodynamic Design

The buffer air flow system is depicted in the schematic of Figure 88. The accompanying table summarizes the flow parameters and recommended dimensions of the various manifold components for a 0.020 inch seal running clearance and a 1.05 lb. per sec. airflow into the turbine cavity. The air supply at the bleed point on the air generator has a pressure of 33.8 psia and a temperature of 250°F based on a 1.4375 inside diameter manifold and feeder tube size. The seal air is metered through orifices in the stationary seal shroud which are sized to a length-to-diameter ratio of approximately one and have a total area of 11.3 square inches.

Figure 89 is a plot of the buffer system plenum pressure and air flow rate against the seal running clearance. Plenum pressure is the pressure in the labyrinth cavity at station 19. Plenum pressure satisfies the continuity requirements between the upstream delivery and downstream discharge air flow rates. The air flow rate curves are given for the total flow delivered to the seal and the bleed flow discharged into the turbine cavity. The difference in these rates is the buffer air which spills into the fan air stream.

Three lip seals are used in the front labyrinth seal as a compromise between sealing effectiveness and fan air shroud weight control to minimize the centrifugal loads. A single lip is used between the plenum and the turbine cavity because of the low pressure ratio that exists. Two lip seals are used between the plenum and fan air stream because of the higher pressure ratio.

As the seal clearance increases above 0.020 inch, the plenum pressure decreases, and the buffer air flow into the turbine cavity increases slightly at first and then also decreases. The critical clearance is 0.056 inch, when the buffer airflow into the turbine cavity stops. Any further increase in the clearance would allow the hot gas to flow in the opposite direction and mix with the spillage into the fan air stream. The maximum practical seal clearance value for an effective buffer air system at a 33.8 psia air generator bleed pressure is somewhat lower than 0.056 inch or about 0.050 inch. Therefore with a seal design clearance set at 0.020 inch, approximately 0.030 inch of the shroud material may be removed for 360 degrees by rubs or gouges caused by excursions of the fan blade tip. Depths greater than 0.030 inch are permitted where the rub is local, but the effect on plenum pressure and starvation in the buffer manifold and turbine cavity should be experimentally evaluated.

Figure 90 is similar to the above figure except the air supply bleed point pressure is increased to 47.3 psia at 300°F. All pipe and tube sizes remain unchanged. The critical clearance is however increased to 0.090

inch which leaves about 0.064 inch for contingencies. The higher pressure system was not used in the flight design because the higher air flows increase the size of the air generator. However, the higher pressure system may easily be used during development testing.

XII. BUFFER AIR MANIFOLD AND BELLMOUTH INLET

The buffer air manifold is a torus with eight feeder tubes and a hollow rectangular support arm as shown in Figure 91. The support arm extends over the rotating element of the front labyrinth seal. The stationary shroud attaches to the support arm and has a series of closely spaced circumferential metering holes to evenly distribute the buffer air to the seal. The support arm is internally connected to the torus by large diameter holes. The eight feeder tubes equally spaced around the torus are connected by flexible hoses to the delivery pipe from the air generator. These hoses must be capable of sustaining axial tension so as not to impose additional pressure loads on the manifold. Twenty-four evenly spaced brackets are used on the torus for mounting to the hot gas scroll. The brackets provide radial freedom to permit relative thermal expansion of the scroll and manifold.

The buffer manifold is a machined and welded titanium 5Al-2.5Sn alloy assembly. The seal shroud is Hastelloy X material and is segmented in eight places to allow for the difference in thermal expansion between the seal and manifold. An Inconel 600 heat shield was also added to the manifold as a barrier to radiation from the turbine gases.

The bellmouth inlet is a curved cylindrical shell at the entrance to the fan air passage which encloses the hot gas scroll and buffer air manifold. This shell is directly mounted to the buffer air manifold. A rigid lightweight structure was obtained by using an adhesive bonded sandwich construction. The face sheets and core are of 5052 aluminum alloy sheet and the closures and inner shell extension are of 6061-T6 aluminum alloy.

An alternate design of bellmouth mounting is shown in Figure 92. It incorporates a separate mounting of the bellmouth directly to the hot gas scroll by means of radial expansion pins. However, mounting the bellmouth directly on the manifold has been selected as the best compromise between design simplicity, thermal compatibility, weight and dimensional stability.

XII. BUFFER AIR MANIFOLD AND BELLMOUTH INLET (CONTINUED)

A. Design Input Data and Analysis

1. Buffer Air Manifold

The buffer air manifold operates at an internal pressure of 33.8 psia. Externally it is subject to a pressure of 24.7 psia on the turbine cavity side and 14.7 psia on the support bracket side. This pressure differential produces an axially forward load of 2264 pounds that is reacted equally at the twenty-four support brackets. The manifold is at the internal air temperature of 250°F everywhere except at the stationary seal holder where the temperature is higher due to heat from the hot gas scroll. Inertia loads due to maneuvers were considered small and were omitted.

2. Bellmouth Inlet

The bellmouth inlet is subject to ambient pressure conditions on its inner surface and a static pressure gradient due to the entrance air velocity on its external flow surface. The pressure differential produces an axial forward load of 2100 lbs. that is reacted equally at the twenty-four support brackets. The inlet is always at ambient temperature. Inertia loads due to maneuvers were considered small and were omitted.

B. Stress Analysis

A stress analysis summary and the basic load data for the buffer air manifold and bellmouth inlet are presented in Figure 93 and indicate that all margins of safety are satisfactory.

1. Buffer Air Manifold

Maximum stresses develop in the torus in the region of the holes that lead to the support arm and in the inner wall of the support arm. Basic hoop stresses in the toroidal element are negligible since

minimum thicknesses are dictated by fabrication considerations rather than for strength. The combined stress effects due to beam bending between the support brackets and rolling due to the out-of-plane moments are also small.

2. Bellmouth Inlet

The bellmouth inlet was analyzed for stresses and deflections using the Shell comp··ter program. Equivalent thicknesses and elastic modulii were used to generate the correct deflection and loads on the sandwich type structure. The bending and direct stresses were calculated from the output bending moments, and shear and membrane forces.

The stress results are for the independently mounted bellmouth shown in Figure 92. Maximum moments and shear loads occur at the attachment to the support arm. The consequent stresses and deflections are low. Comparison calculations indicate that the direct-connected bellmouth design of Figure 91 will have similarly low values.

XIII. HEAT TRANSFER ANALYSIS

The interstage aerodynamic data presented in Figure 94 expands the turbine data given in Figure 9 to include two off-design transient conditions. It was prepared in order to furnish a basis for the transient heat transfer calculations of the turbine section components. The off-design data in the above figure represents the first approximation of the flow condition based primarily on energy considerations and does not reflect consideration of the velocity diagrams.

The off-design data were based on the turbine transient inlet operating conditions shown in Figure 95 and were established according to the following assumptions:

1. The air generator is first accelerated to full speed and then the axiliary combustor is lighted to provide the design turbine inlet conditions. There are no valves in the air ducting between the air generator and the fan tip turbine, therefore the tip turbine and fan are also accelerated by the air generator bleed air prior to light-off.

2. The air generator was assumed to have operating characteristics similar to those of the Curtiss-Wright CW657F jet air compressor which reaches idle speed in 40 seconds after light-off and full speed in 55 seconds. The data in the above figure are also based on the CW657F compressor map up to 55 seconds.

3. The RPM vs time relationship for the tip turbine was established by assuming that the power developed by the turbine is proportional to the cube of the RPM.

4. Design point conditions are established within 5 seconds after light-off. This is a reasonable assumption in view of the fact that the acceleration time from pre-light-off speed to 99% full speed was estimated to be 1.5 seconds when the design point condition is instantaneously imposed on this turbine.

5. The flow, temperature, and pressure conditions were assumed to change linearly with time between 55 and 60 seconds. For the purpose of heat transfer analysis, the changes could have been applied instantaneously as well with negligible change in computed temperatures.

A transient heat transfer analysis temperature summary of the turbine section components is shown in Figures 96 to 103. In this analysis the starting temperatures were stabilized at the air generator idle condition at t = 40 seconds before being brought up to power. The results show that most of the thin-walled structures reach a steady-state temperature in about 100 seconds. Thicker sections having more heat storage capacity reach steady-state temperatures in a somewhat longer period of time. The skin temperature of the fan air shroud was estimated as the average value of the carrier rail leg and fan air temperatures. The rear seal bracket was assumed to be fully cooled by the nacelle air through the exhaust duct struts. The heat transfer analysis was performed for a clearance gap of 0.020 inch on all rotating seals and includes the whirling effect imparted to the gas in close proximity to the rotating members. The front buffer seal air leakage into the turbine cavity is 1.05 lbs. per second as previously mentioned in Section XI.

Although an 0.020 inch seal gap was used in the analysis, the rotating seals start out initially with larger clearances that grow smaller as the fan rotor approaches operating speed and the stationary parts approach equilibrium temperatures. The effect of seal clearance transients on turbine performance and heat transfer was not considered analytically. For structural purposes, however, thin metal wall temperatures in the middle seal region were assumed to reach 1200°F while the seal is closing. This temperature is based on the mixing of equal amounts of turbine gas before going through the middle seal gap. The gas comes from (a) the weight flow that has done work going through the first stage turbine rotor, and (b) the supply gas which by-passes the first rotor and goes through the hollow 2nd stage stator vane as part of the stator housing accelerated heat-up provisions.

XIII. HEAT TRANSFER ANALYSIS (CONTINUED)

The second stage turbine stator design represents a compromise between mechanical considerations and thermal response for the closing of the middle labyrinth seal. Direct connection of the stator to the shell eliminates sliding fits and radial splines, but slows the radial growth of the middle seal stationary shroud. In order to close the interstage seal gap to operating clearance, the flange and outer shell must heat as rapidly as possible. This situation is favored in two ways in the design. First, the flanges are located near the rotor blade tips where the high swirl velocity of the hot gas scrubbing the flanges will maximize heating rates. Second, the shell is heated between flanges by providing holes in the forward support cone and in the hollow turbine stator vanes so that hot gas can flow from the high pressure region outboard of the first stage turbine rotor through the hollow vanes into the low pressure region that exists when the middle seal clearance is large. The hot gas circulating through the stator structure will heat the shell during the initial period of operation. When the seal clearance closes, the pressure differential and the bypass flow through the hollow vanes are diminished. Thereafter, steady-state housing temperatures are maintained by introducing some buffer cooling air at the first stage turbine rotor shelf and pumping it through the hollow rotor blades into the area of the front bolting flange on the second stage stator assembly. This method of controlling the steady-state temperatures requires experimental evaluation for verification. The heat transfer analysis did not include this effect but the temperature data presented reflects estimated reductions in the outer housing temperatures in the vicinity of the 2nd stage turbine stator assembly.

The outer housings and scroll are covered with a one-half inch insulating blanket which holds in the turbine heat and protects the surrounding bellmouth inlet, airframe and mounting structure. The blanket tapers to a double foil thickness heat shield between the inner scroll neck and buffer air manifold because the cold assembly clearance is limited. The seal support arm on the buffer air manifold is also protected from turbine gas radiation by a metal heat shield. The rear labyrinth seal and face seal support bracket is protected by a three-sixteenth inch insulating blanket on the turbine cavity side

and between the exhaust duct and mount ring clearance annulus. Ambient temperature nacelle air is used to purge this annulus and cool the rear seal support bracket. The air is drawn from the nacelle through hollow struts in the exhaust housing, openings in the insulating blanket, and holes in the silencing material upstream of the stator vanes where a lower than ambient pressure condition exists.

XIV. BEARINGS

The fan rotor assembly rotates on two grease-packed deep-groove angular contact ball bearings with integral seals that are mounted on a stationary spindle. This spindle is bolted to the hub of the fan stator vane and support assembly as shown in Figure 2. The outer bearing races are secured in the bore of the fan rotor disk while the inner bearing races are clamped to the stationary spindle. Both bearings are clamped and therefore preloaded at assembly but kept axially apart for rotor rigidity by utilizing a pair of accurately machined sleeves. These sleeves essentially act as axial extensions of the inner and outer races of the angular contact bearings. The axial preload reduces the probability of unloading one of the bearings when operating in the pure lift mode.

The bearing arrangement was selected on the basis of satisfying the load and life requirements of the fan rotor system and has the advantages of minimum fan rotor axial float, a self contained lubrication system (grease packed) and a minimum bearing width to give the maximum possible axial bearing spacing for fan rotor assembly rigidity.

Figure 2 shows a test stand spindle configuration for:

1. Mounting a stationary nosepiece and instrumentation pack
2. Providing cooling for the bearings
3. Protecting the fan rotor instrumentation wires and tubes.

An almost identical spindle is used on the flight configuration of the lift fan package, except that it is shortened. Its length is sufficient to satisfy bearing locking requirements and for installing a speed sensor.

A self contained lubrication system (grease-packed) was employed to simplify the design of the flight fan configuration and to keep the weight to a minimum. The same lubrication system is suitable for test stand operation. The significant difference between flight and test stand operation is the operating cycle duration, five minutes for flight and thirty minutes for test stand. Preliminary bearing sizing showed that the operating speed of 3030 RPM was within the acceptable range for grease lubrication of the sizes considered.

XIV. BEARINGS (CONTINUED)

The air cooling or air-and-water cooling provisions in the test stand spindle design can be used, if necessary, to lower the bearing temperatures during prolonged test stand running. Air external circulating oil bearing lubrication system could also be used for test stand operation.

In so far as the integral seals are concerned these bearings are operating in the acceptable speed range for grease lubrication but above the normal speed recommended by the bearing manufacturers for a sealed bearing. The approximate seal contact sliding velocity is 2800 feet per minute for the 315 size bearing and 3250 feet per minute for the 218 size. This condition requires attention to the seal contact pressure. Since these bearings have outer race rotation, during operation the grease will be displaced outward by centrifugal force and away from the dynamic contact surface. This will minimize the tendency for leakage. It is believed that the following factors will also contribute to favorable seal operation.

1. A controlled limited amount of grease will be packed in the bearings.

2. The primary requirement for the seal is to retain the grease when the fan is stationary, centrifugal force tending to carry the grease outward away from the sealing area when the fan is operating.

3. The seal configuration is so designed or can be modified so that during higher speed operation the centrifugal force acting on the seal will tend to reduce the contact pressure but when at rest will provide normal sealing contact.

Several bearing arrangements for the fan rotor system were considered before the previously discussed bearings were selected. Those arrangements are as follows:

1. Split inner race angular contact ball bearing with a cylindrical roller bearing.
2. Duplex angular contact ball bearing with a cylindrical roller bearing.

3. Deep-groove radial ball bearing with a cylindrical roller bearing.
4. Two opposed angular contact ball bearings.
5. Two deep-groove radial ball bearings.
6. Two deep-groove radial ball bearings with axial preload.

Also considered were variations in the location of the thrust bearing, a circulating oil system and the use of a rotating shaft versus a stationary spindle. NASA expressed a preference for the overall simpler stationary spindle configuration which was then used in the final design. The circulating oil system was discarded because of the unnecessary complexity and added weight. The thrust bearing was placed at the front of the fan rotor assembly to facilitate the design of a constant disk bore and a tapered spindle for strength and ease of assembly.

A. Design Input Data and Analysis

The fan rotor bearings are subject to the fan rotor assembly axial lift load and the radial loads that develop from the gyroscopic moments due to roll and pitch manuevers. The lift load was derived from the data in Figures 6, 7, 9 and 10 and is shown in Figure 12. As indicated in Figure 11, a maximum gyromoment of 72,000 lb-in occurs due to a 1 radian per second pitch or roll angular velocity. Other inertia loads and the rotor assembly unbalance are small and were omitted. Unbalance loads due to a missing fan blade or turbine carrier segment were not included in the analysis.

The bearing descriptions and design input loads are shown in Figure 104. The bearings are installed with an axial preload of 800 lbs to reduce the probability of unloading one bearing when operating in the lift mode. Figure 105 shows the net axial bearing loads at 3030 rpm and a steady state condition as a function of various assembly preloads for a 2953 pound fan lift load. At an 800 pound assembly preload, the net axial load at 3030 rpm is 2970 pounds for the thrust bearing and 18 pounds for the aft bearing

Figure 106 shows the resultant operating loads on each bearing for various assembly preloads when both the fan lift and gyrocouple loads are acting. At an 800 pound preload, the resultant axial load on the thrust bearing is 5060 pounds and 2110 pounds on the aft bearing. The resultant radial load is 8040 pounds in each bearing.

Preloads of much less than 800 pounds will result in unloading of the aft bearing and permit it to float. Although looseness is not expected to be detrimental to the bearing operation, some axial preload is preferred to provide angular stability for the fan rotor assembly. Preloads above 800 pounds increase the axial load on the thrust bearing and would lower its life.

B. Bearing Life Analysis

The table below shows the B-10 lives for the individual bearing under continuous operation at each of the two load conditions and the prorated lives under the combined loading for the percentages of time indicated in Figure 104. Also shown is the system life for each of the load conditions.

BEARING B-10 FATIGUE LIFE

Bearing No.	Continuous Operation		Pro-rated Life Under Combined Loading
	Steady State	Steady State Plus Gyromoment	
315 (thrust)	2466 hours	227 hours	2247 hours
218	4.2×10^7 hours	94 hours	9351 hours
System Life, hrs	2466 hours	70 hours	1899 hours

These life calculations are based on standard AFBMA constants, and include a life multiplication factor of 3.0. Bearing manufacturers' experience has shown that with current standard bearing materials and manufacturing processes, the actual B-10 life (the life that will be exceeded by at least 90 percent of a lot of identical bearings operating under identical conditions) is at

least three times the standard AFBMA calculated life. Further, the average life for a group of similar bearings is five times the B-10 life. Analysis of service experience and bearing test data has shown that no failures are anticipated during approximately the first 5 percent of the B-10 life for a bearing.

The bearing life analysis results show that the combined life of the thrust bearing (No. 315), the aft bearing (No. 218), and the system satisfactorily meets the minimum operating life requirement of 1000 hours.

XV. CRITICAL SPEED

The critical speed of the fan rotor assembly was calculated to be 4600 rpm based on a rotating weight of 204 pounds and a net support structure stiffness of 1.24×10^5 lbs per inch. The support structure stiffness includes deformation of the bearings, deflection of the spindle, and displacement of the fan stator vane and support assembly. At 4600 rpm, the critical speed is over 40 percent above the steady state speed of 3030 rpm and is therefore satisfactory.

A dynamic analysis of the fan rotor system was performed in order to estimate the maximum relative amplitudes of the blade tips when maneuvering of the aircraft imposes various angular input rates on the spinning rotor. The analysis was based on a step input rate of one radian per second to an undamped rotating system. The peak undamped response produced an axial relative deflection of 0.399 inch at the rotor blade tip. This peak will be attenuated by the presence of system damping in the bearings and the less severe nature of the actual input rate.

The precession frequency (approximately 25 cps) is at least five times greater than the dominant frequency characteristics of the input rate. This factor and the damping in the bearing will provide sufficient time for the transient gyroscopic response to be substantially attenuated before the maximum steady state deflection is reached. In addition, the build-up to a peak input rate of one radian per second is not instantaneous as assumed in the step input but rather a more gradual nature. For these reasons the final design was based on the results of a gyroscopic loading analysis which results in a relative axial tip deflection of 0.284 inch per radian per second.

XVI. WEIGHT SUMMARY

The weight summary of the flight configuration Tip Turbine Lift Package is presented in Figure 107. Two weight summaries are shown, initial estimated weights and final weights. The initial weights were based on preliminary estimates that were released in June 1970. The final weights were based on the latest configuration as represented on the basic assembly and the related layout drawings. The major change in weight occurred in the fan stator vane and support assembly which supports the fan rotor assembly. Additional stiffening was required in the stator vane structure to limit the resulting deflection at the fan rotor blade tips. This was done to prevent interference with the non-rotating components and to preserve the turbine seal integrity. Maximum deflections occur from a gyroscopic moment produced by an angular pitch or roll velocity of one radian per second.

The initial weight estimate was made assuming that all of the fan stator vanes were hollow. A subsequent analysis indicated that all hollow fan stator vanes were structurally inadequate. The design was therefore drawn as all solid vanes on the layout. A later and more extensive analysis indicated, however, that with six of the fan stator vanes solid and the rest hollow the structure would be satisfactory. The final weight estimates were therefore made for that vane configuration. It should be noted though, that all of the deflection values calculated were based on the use of all hollow fan stator vanes, making these values conservative.

The final total weight of 680 pounds was arrived at to meet the structural requirement for adequate strength and rigidity of the individual lift fan components. The desired target weight to meet the flight performance requirements is 570 pounds. In order to achieve this weight as closely as possible, light-weight high-strength alloys were used in all cool running components and high strength and temperature alloys were used on all hot-running components.

A review of the structural analyses was made in order to determine those areas where significant weight reductions might be obtained. These areas are the hot gas scroll, the fan rotor blade firtree and tenon attachment, the disk

and the spindle. In the above areas the design changes that would be made to reduce weight would not significantly reduce the rigidity of the components and affect the running clearances at the fan blade tip.

An improvement to the angular and linear displacement characteristics of the fan stator vane and support assembly will also result in structural changes to reduce its weight. The effect of the support assembly on the fan rotor blade tip deflections can be lessened by moving the center-of-rotation in the hub structure closer to the plane of the fan rotor and coning the stator vanes so they will carry tension loads as well as bending. Since the 1.5 axial fan chord spacing for the stator vane blade row location applies more at the outside diameter for noise abatement, a revision to the configuration could be made. The angular and linear displacement of the support assembly can then be adjusted by lightening the structure.

A conscientious follow-on effort in the above areas should product weight reductions that will contribute significantly toward reaching the target weight objective.

Another approach to weight reduction for consideration would be to lower the angular pitch and roll rate requirements so as to reduce the gyromoment that produces a major part of the fan blade tip deflection. This would become part of a coordination with the airframe manufacturer and regulatory agencies to establish the flight design criteria for a multi-fan Tip Turbine Lift Package installation in large commercial aircraft.

XVII. CONCLUSIONS

1. The completed design has adequate strength and vibratory margins to satisfy the 1000-hour life requirement and is therefore suitable for preparation of final shop-fabrication type of drawings for procurement of test hardware.

2. A segmented rather than a continuous ring for supporting the turbine rotor blades at the tips of the fan rotor blades is favored on the basis of more favorable fan rotor dynamics, ease of manufacture, lower weight and simplicity of assembling and servicing the system.

3. Although the labyrinth seals employed to limit the leakage of hot-gas turbine flow are acceptable for initial testing, they must be held to close tolerances and should be experimentally investigated for verification of transient thermal and maneuver load effects.

4. Alternate sealing methods being studied by NASA may offer improved performance and could be incorporated at a later time.

5. Grease-packed bearings are satisfactory for flight operation and appear to be acceptable for longer test stand operation.

6. Although the estimated weight is 680 pounds for the complete fan package, a target weight of 570 pounds is believed achievable by means of potential reductions in the areas of the hot-gas scroll, the fan rotor blade fir tree and tenon attachment, the disk, the spindle, and the fan stator vane and support assembly.

7. Further assurance of successful operation can be afforded by additional design effort in the areas of the hot-gas seals, thermal gradients in the fan air shroud, cooling of the second stator housing, fatigue of the brazed turbine blade attachment, and the aerodynamic performance of the hot-gas scroll.

TIP-TURBINE LIFT PACKAGE BASIC ASS

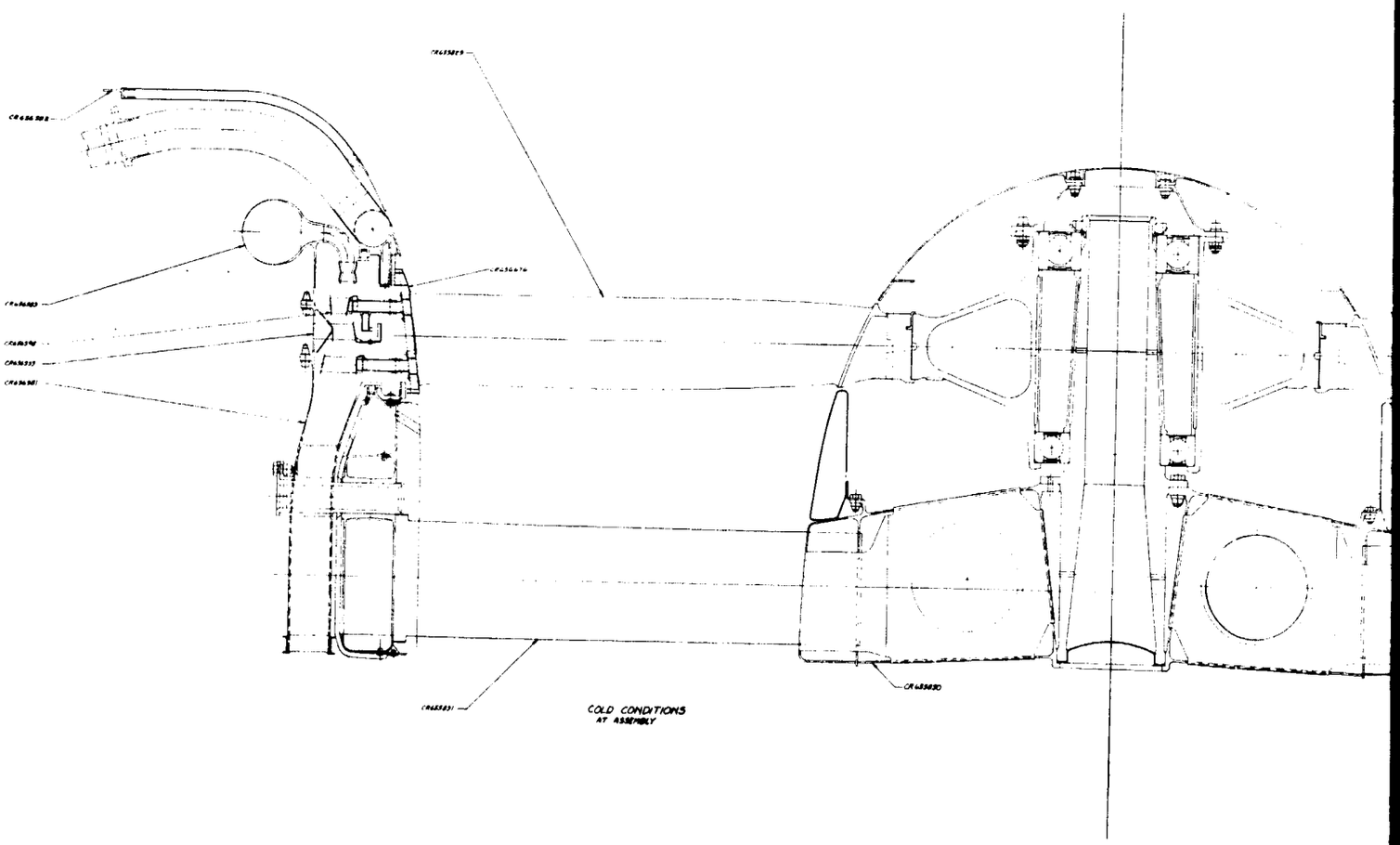

FOLDOUT FRAME 1

PACKAGE BASIC ASSEMBLY

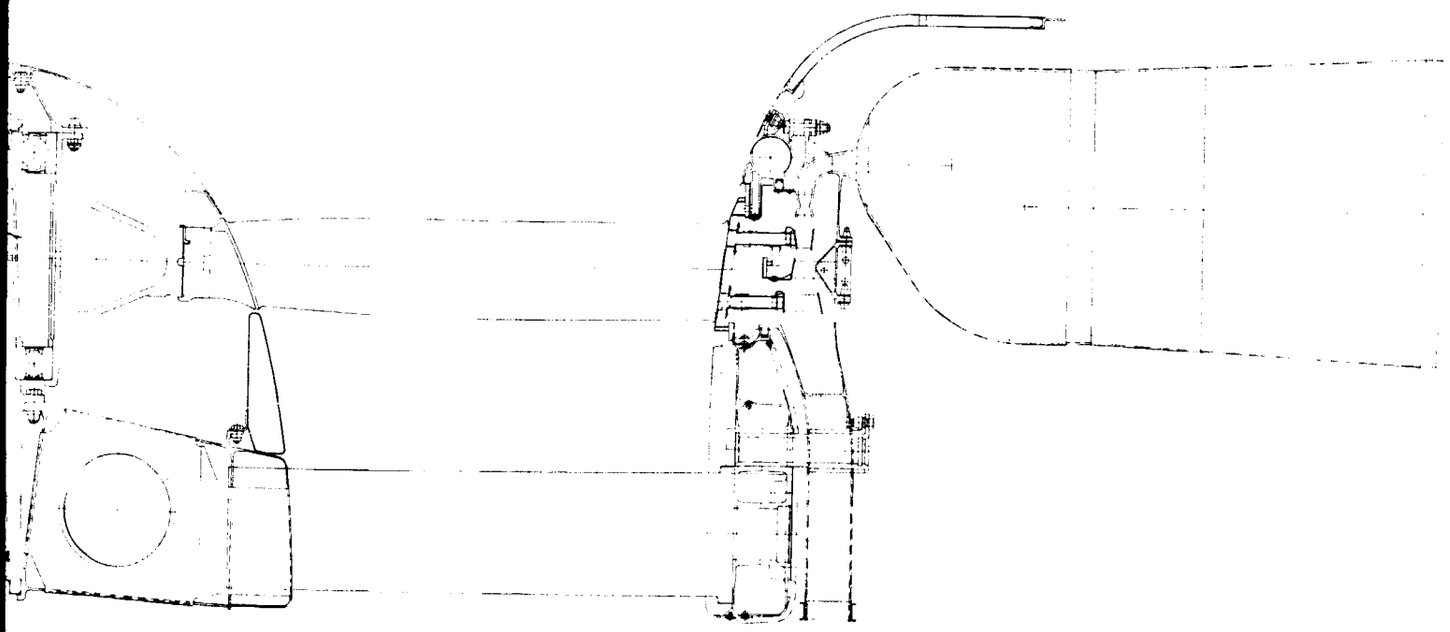

HOT CONDITIONS
OPERATING LOAD AND SPEED

FOLDOUT FRAME 2

Figure 1

FAN ROTOR ASSEMBLY INSTRUMENTA

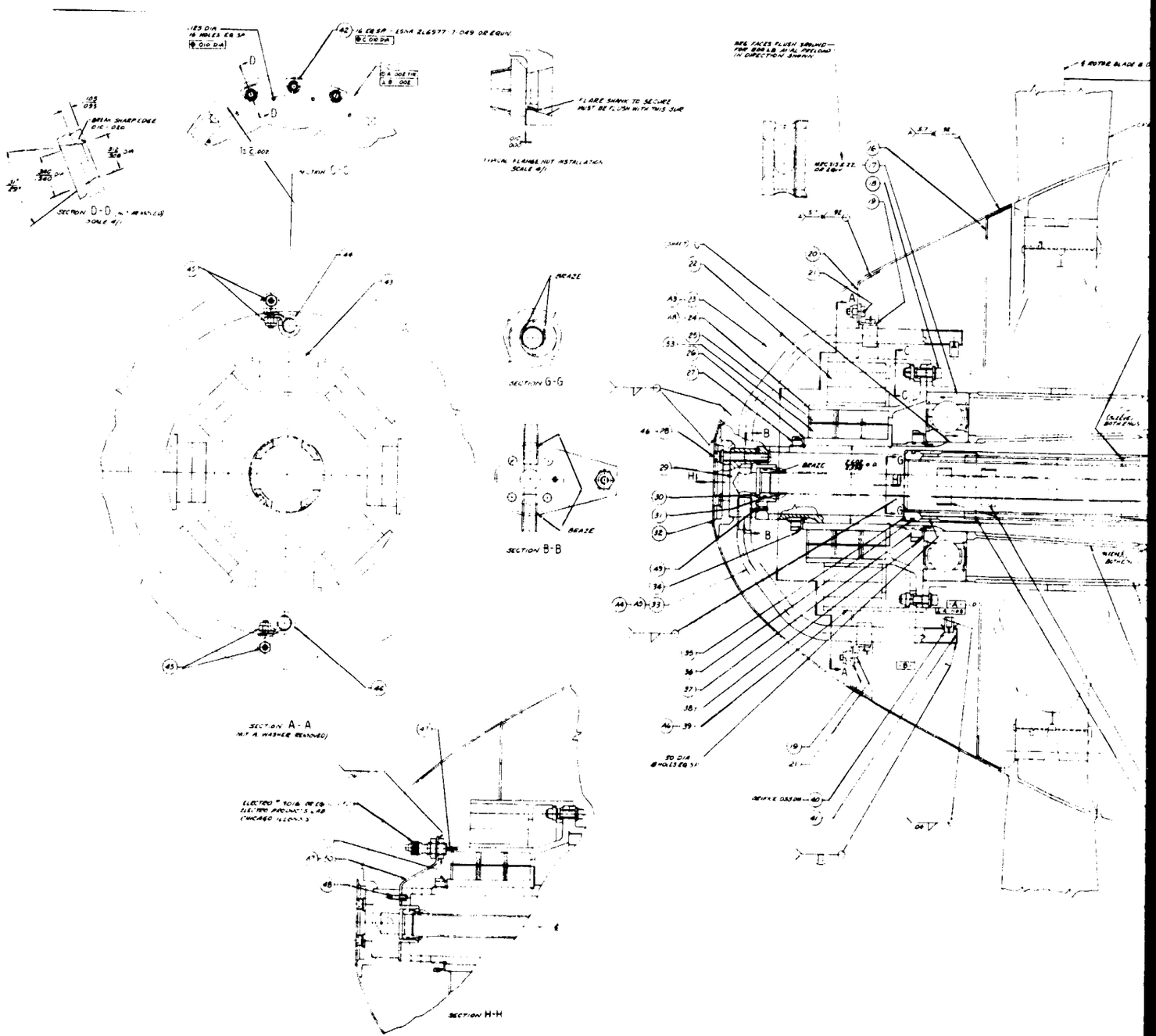

FOLDOUT FRAME 1

BLY INSTRUMENTATION PACKAGE

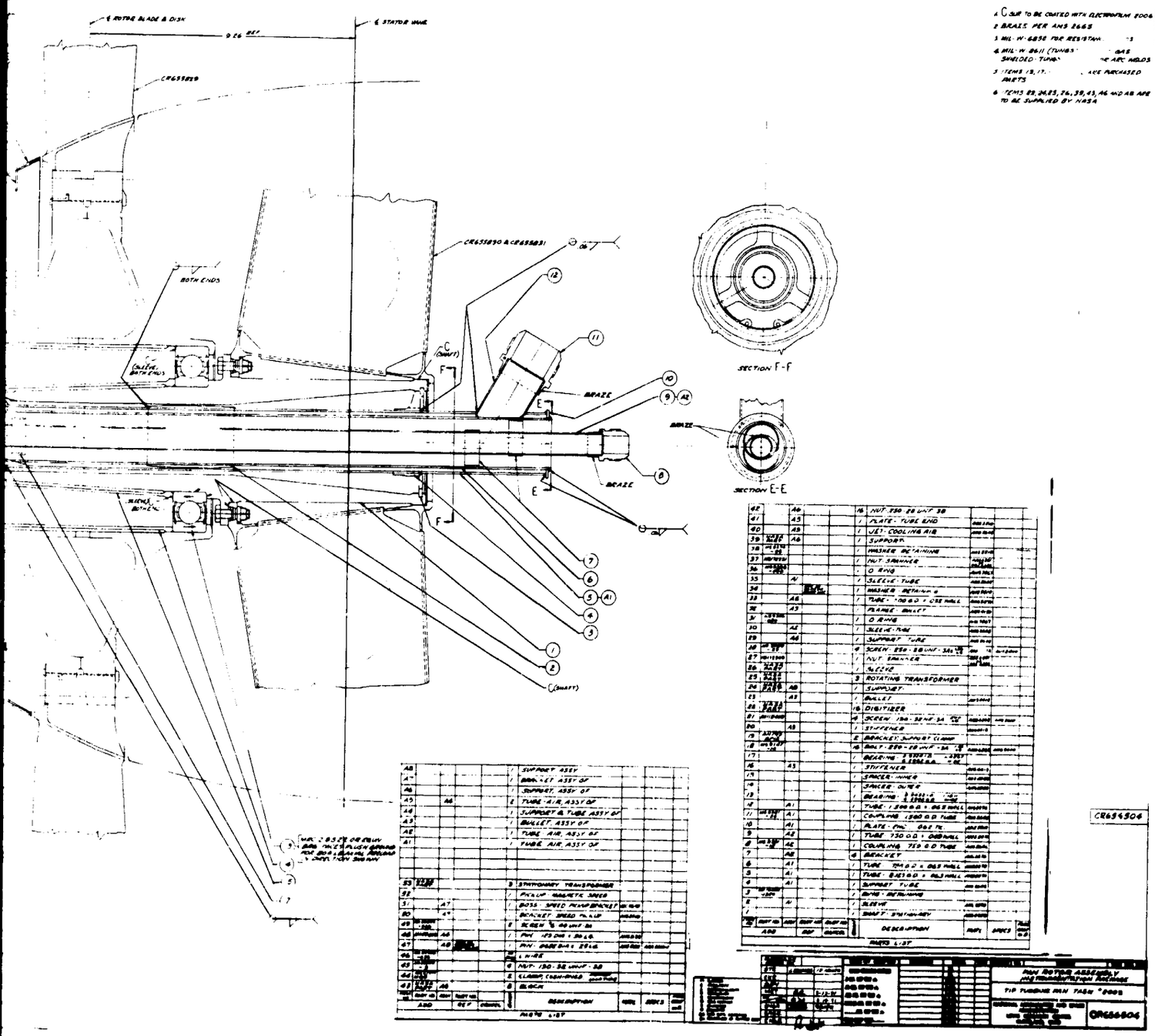

FOLDOUT FRAME 2

Figure 2

LIST OF LAYOUT DRAWINGS

CR655807	ENGINE BASIC ASSY
CR655808	HOT GAS SCROLL ASSY
CR655809	HOT GAS SCROLL - INLET
CR655810	HOT GAS SCROLL - EXIT
CR655811	BUFFER GAS MANIFOLD
CR655829	FAN ROTOR ASSY
CR655830	STATOR VANE & BEARING SUPPORT - (INNER)
CR655831	STATOR VANE & BEARING SUPPORT - (OUTER)
CR656504	FAN ROTOR ASSY INSTRUMENTATION PACKAGE
CR656553	STATOR ASSY - SECOND STAGE
CR656581	EXHAUST HOUSING ASSY
CR656582	BUFFER GAS MANIFOLD DIRECT CONNECTED BELLMOUTH
CR656583	HOT GAS SCROLL ASSY (WELDED SHEET METAL EXIT)
CR656598	TURBINE ROTOR ASSY
CR656599	FAN ROTOR SHROUD & FIRST STAGE TURBINE ROTOR SEAL SHROUD ASSEMBLIES
CR656676	FAN SHROUD ASSY

Figure 3

OPERATING CHARACTERISTICS AND INTERNAL GAS CONDITIONS

Condition

Altitude (ft)	0
Mach	0
Ambient T (^{o}R)	550
Ambient Pressure (psia)	14.70
Speed (RPM)	3033
Power Setting	Max.

Compressor (Air Generator Type A-3)

Inlet Temperature (^{o}R)	550
Outlet Temperature (^{o}R)	980
Inlet Pressure (psia)	14.70
Pressure ratio	8.0
Outlet Pressure (psia)	117.5

Ducting

Outlet Pressure (psia)	112.2
Outlet Temperature (^{o}R)	980

Combustor

Adiabatic Efficiency	0.98
Outlet Temperature (^{o}R)	1900
Outlet Pressure (psia)	105.0
Heating Value (Btu/lb)	18,640
Burner Pressure Ratio	0.944
Fuel Air Ratio	.0121

Scroll

Outlet Pressure (psia)	100.4
Outlet Temperature (^{o}R)	1900

Turbine

Adiabatic Efficiency	0.773
Pressure Ratio	6.41
Outlet Pressure (psia)	15.67
Mass Flow (lb m/sec)	29.25
Total Mass Flow (lb m/sec)	30.20
Outlet Temperature (^{o}R)	1338
Outlet Area (ft^2)	1.84

Nozzle (Turbine Exhaust)

Pressure Ratio	1.065
Pressure Loss (%)	1.47
Mass Flow (lb m/sec)	29.90
Nozzle Area (ft^2)	2.10

Fan

Airflow (lb m/sec)	541.0
Inlet Temperature (^{o}R)	550
Outlet Temperature (^{o}R)	579
Inlet Pressure (psia)	14.70
Pressure Ratio	1.20
Outlet Pressure (psia)	17.6
Adiabatic Efficiency (%)	0.86

Performance

Net System Thrust (lbs)	
(a) Fan & Turbine (lbs)	10,000
(b) Air Gen. (remote) lbs	895
(c) Total (lbs)	10,895
SFC (lb_m/lb_f - hr)	0.351

Figure 4

FAN PASSAGE AND BLADE PROFILE

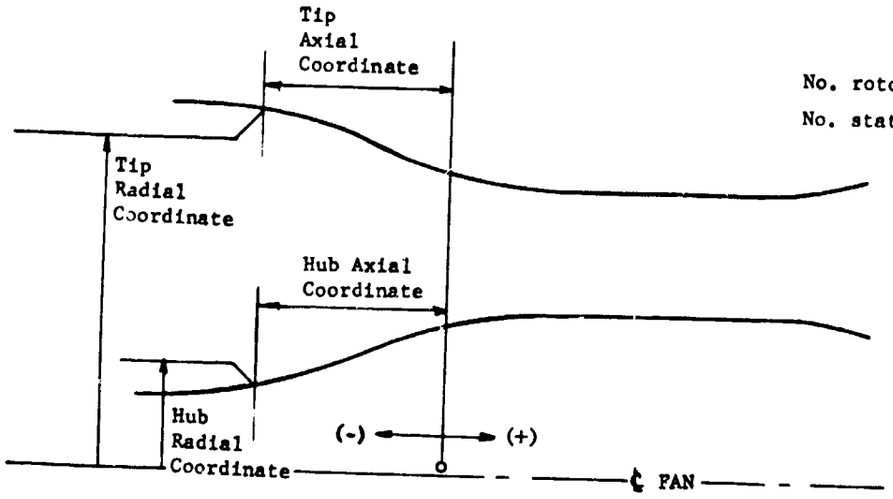

No. rotor blades 48

No. stator vanes 36

A. Fan Passage Coordinates for Tip & Hub Contours

Tip Axial Coordinate (inches)	Tip Radius. (inches)	Hub Axial Coordinate (inches)	Hub Radius (inches)
-26.000	36.500	-26.000	2.000
-20.000	36.500	-20.000	2.000
-17.500	36.460	-15.000	2.100
-15.000	36.300	-10.000	3.050
-12.500	35.800	-5.000	5.800
-10.000	34.500	0.	9.500
-7.500	32.120	5.000	11.406
-5.000	29.900	10.000	12.160
-2.500	28.600	15.000	12.260
0.	27.850	20.000	12.180
2.500	27.460	25.000	11.900
5.000	27.320	30.000	11.500
10.000	27.260		
15.000	27.260		
20.000	27.260		
25.000	27.260		
30.000	27.260		

B. Blade Edge Meridional Profile Coordinate

Fan Blade Inlet Coordinates		Fan Blade Outlet Coordinates	
Axial, in	Radial, in	Axial, in	Radial, in
0	27.6	3.48	27.3
-0.01	24.0	3.49	23.0
-0.02	19.0	3.50	19.0
0.02	14.0	3.46	15.0
0.25	9.6	3.20	11.0

Figure 5

Figure 6

FAN PASSAGE AERODYNAMIC DATA

Station	1	2	3	4	Fan Inlet 5	Fan Outlet 6	7	Stator Inlet 8	Stator Outlet 9	10	11	12
Axial Location - In.	-26.0	-16.0	-9.0	-4.0	1.55	6.8	11.785	17.0	22.0	29.0		
Outer Streamline No. 1												
Radius - In.	36.50	36.40	33.63	29.20	27.736	27.206	27.090	27.055	26.987	26.93	26.99	26.99
P_t - Psia	14.70	14.70	14.70	14.70	14.700	18.156	18.156	18.156	18.060	18.06	18.06	18.06
T_t - °R	550.0	550.00	550.00	550.00	550.00	588.770	588.770	588.770	588.770	588.77	588.77	588.77
P_s - Psia	14.31	14.43	14.30	11.73	11.404	13.777	13.950	14.010	14.688	14.78	14.77	14.89
T_s - °R	545.79	547.05	545.66	515.59	511.480	544.140	546.080	546.750	555.020	555.96	555.94	557.16
Inner Streamline No. 11												
Radius - In.	2.00	2.05	3.45	6.92	9.917	11.234	12.053	12.479	12.740	12.72	12.58	12.10
P_t - Psia	14.7	14.70	14.70	14.70	14.700	17.518	17.518	17.518	16.995	17.000	17.000	17.000
T_t - °R	550.00	550.00	550.00	550.00	550.00	580.410	580.410	580.410	580.410	580.41	580.41	580.41
P_s	14.114	14.04	11.73	13.13	11.920	11.105	11.554	11.893	14.028	14.52	14.56	14.79
T_s	543.64	542.79	515.59	532.55	518.010	509.510	535.310	519.590	549.460	554.93	555.31	557.82

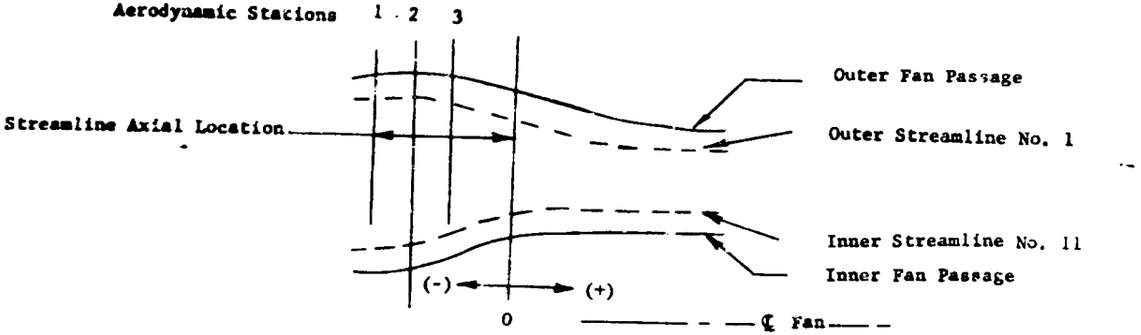

FAN ROTOR BLADE AERODYNAMIC DATA

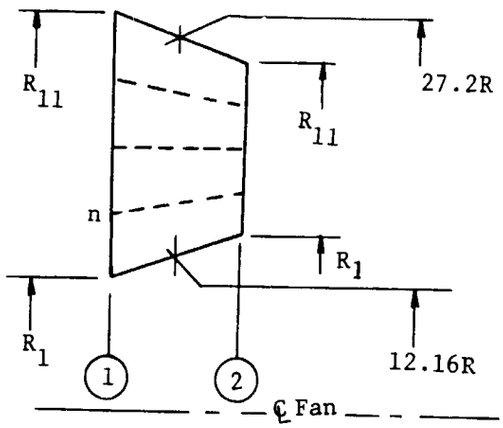

R = Radius to Streamline, ft

P_s = Static Pressure, psfa

T_s = Static Temperature, °R

C = Relative Velocity, fps

RAA = Relative Air Angle, Deg.

n = Streamline Nos 1-11

(1) = Inlet to Row

(2) = Outlet from Row

n	R1	PS1	TS1	C1	RAA-1
11	2.31160	1642.	511.5	1000.1	47.16
10	2.21680	1652.	512.3	973.0	46.30
9	2.11770	1673.	514.2	938.8	45.70
8	2.01220	1694.	516.1	902.8	45.01
7	1.89920	1713.	517.7	866.3	44.08
6	1.77650	1731.	519.2	829.0	42.84
5	1.64150	1748.	520.7	789.4	41.28
4	1.48920	1767.	522.3	745.4	39.44
3	1.31200	1788.	524.1	695.8	36.75
2	1.09670	1801.	525.1	647.7	32.50
1	0.82640	1716.	518.0	672.9	22.93

n	R2	PS2	C2	RAA-2
11	2.26720	1984.	766.7	31.06
10	2.17960	2007.	730.6	29.57
9	2.08660	2020.	700.2	27.54
8	1.98760	2025.	669.7	24.69
7	1.88140	2025.	640.4	21.15
6	1.76660	2018.	613.3	16.75
5	1.64070	2004.	589.0	11.14
4	1.50070	1978.	572.8	4.06
3	1.34190	1930.	575.9	-4.39
2	1.15760	1834.	618.3	-14.16
1	0.93620	1599.	757.8	-24.81

Figure 7

FAN STATOR VANE AERODYNAMIC DATA

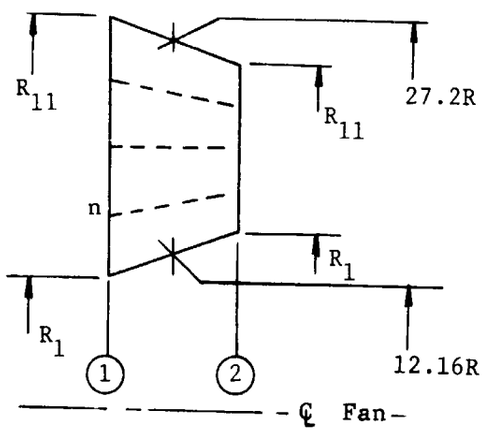

R = Radius to Streamline, ft

P_s = Static Pressure, psfa

T_s = Static Temperature, °R

C = Absolute Velocity, fps

AAA = Absolute Air Angle, Deg.

n = Streamline Nos. 1-11

(1) = Inlet to Row

(2) = Outlet from Row

n	R1	PS1	TS1	C1	AAA-1
11	2.25460	2017.	546.7	710.6	27.27
10	2.16570	2001.	544.9	720.5	27.54
9	2.07360	1989.	543.2	727.3	27.91
8	1.97710	1977.	542.0	733.8	28.73
7	1.87520	1964.	540.8	740.1	29.74
6	1.76670	1947.	539.3	747.5	30.89
5	1.65000	1926.	537.5	757.4	32.29
4	1.52290	1896.	535.0	771.1	33.83
3	1.38270	1854.	531.4	789.9	35.27
2	1.22520	1796.	526.2	816.4	36.88
1	1.03990	1713.	519.6	854.7	40.38

n	R2	PS2	C2	AAA-2
11	2.24890	2115.	636.9	0.0
10	2.16270	2125.	628.4	0.0
9	2.07220	2129.	623.1	0.0
8	1.97700	2130.	619.3	0.0
7	1.87650	2130.	616.1	0.0
6	1.76970	2128.	612.9	0.0
5	1.65520	2123.	609.4	0.0
4	1.53110	2115.	605.4	0.0
3	1.39420	2101.	601.1	0.0
2	1.24020	2077.	597.3	0.0
1	1.06170	2020.	609.8	0.0

Figure 8

TURBINE OPERATING CHARACTERISTICS

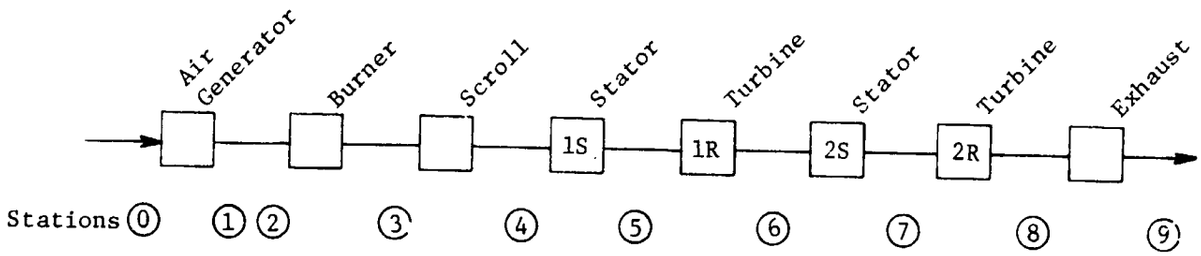

Station	P_{Static} psia	P_{Total} psia	T_{Static} °R	T_{Total} °R	Weight Flow lbs/sec
0		14.7		550	
1		118.0		980	28.9
2		111.2		980	
3		105.0		1900	29.25
4		100.4		1900	
5	24.7	84.79	1380	1900	29.90
6	24.7	30.79	1449	1534	
7	14.7	28.64	1290	1534	
8	14.7	15.67	1316	1338	
9		14.70			

Figure 9

TURBINE VECTOR TRIANGLES AND PASSAGE HEIGHTS

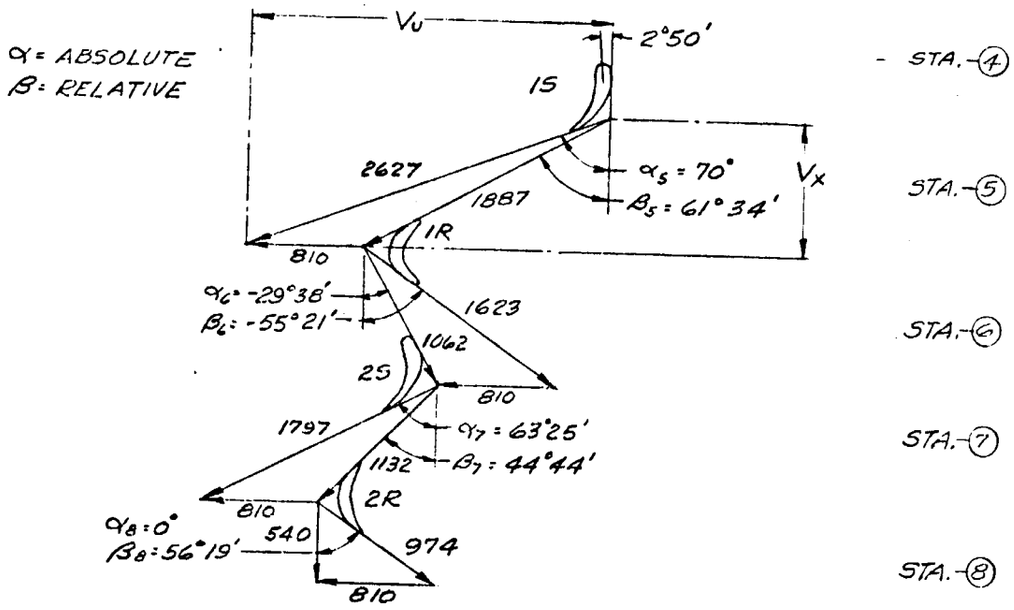

TURBINE HOT GAS PASSAGE

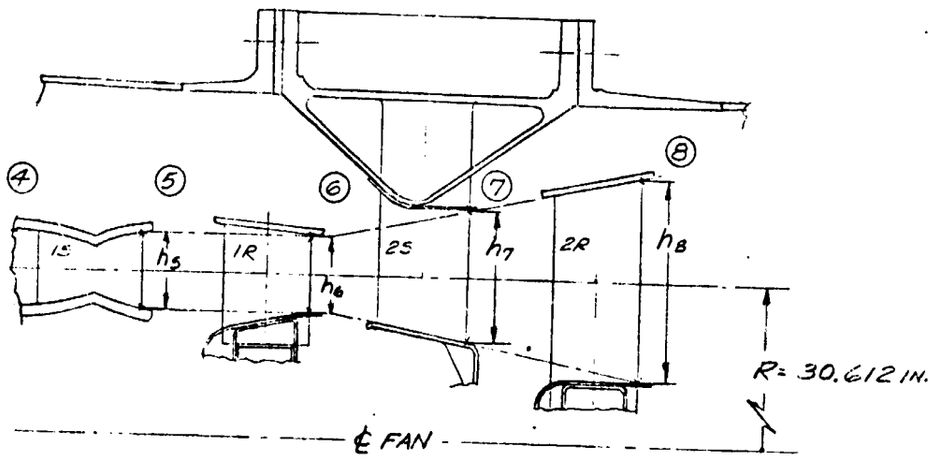

STATION NO.	5	6	7	8
Vu FT/SEC	2469	-525	1607	540
Vx FT/SEC	898	923	804	974
PASSAGE HEIGHT h IN.	.510	.528	.906	1.376
BLADE OR VANE AXIAL CHORD IN.	1S = .72	1R = .60	2S = .60	2R = .60

Figure 10

FLIGHT MANEUVER LOADS AND DUTY CYCLE

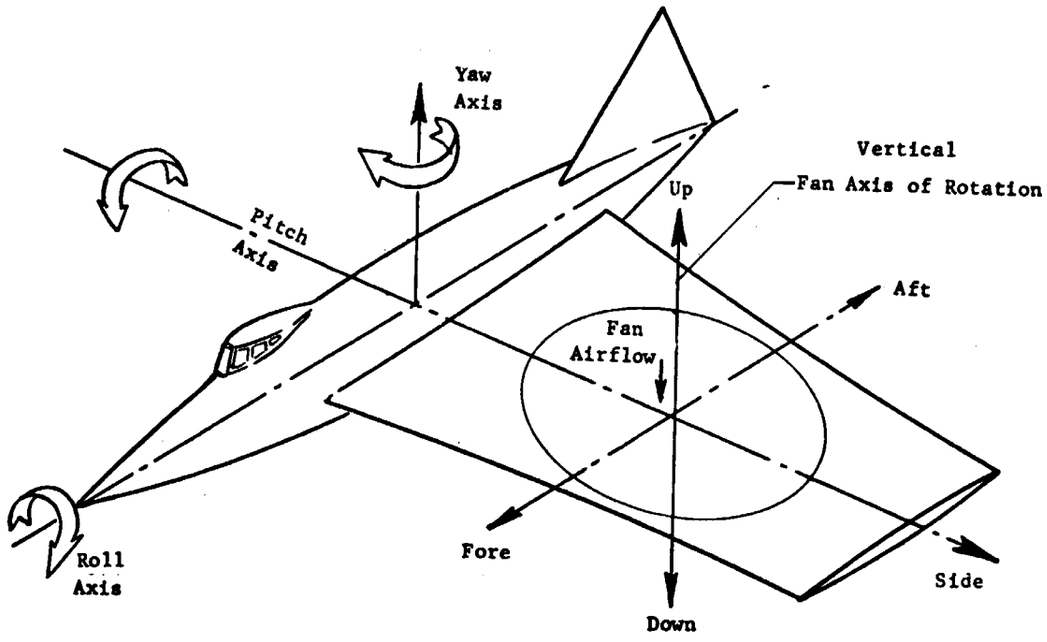

A. Load Factors	Flight	Touch Down (Landing)
1. g factors (g's)		
vertical	3.0 up or 7.5 down	2.0 up or 4.5 down
side	2.0	1.5
fore and aft	1.0	8.0
2. angular velocities (rad/sec)		
pitch	1.0	0
roll	1.0	0

B. Duty Cycle

design life (hours)	1000
No. of starts (cycles) per flight	2
length of operation per flight (min.)	5.0
(a) take-off 2.5 min.	
(b) landing 2.5 min.	
No. of flights per 1000 hours	12,000
No. of cycles per 1000 hours	24,000

Figure 11

OVERALL LOAD SUMMARY

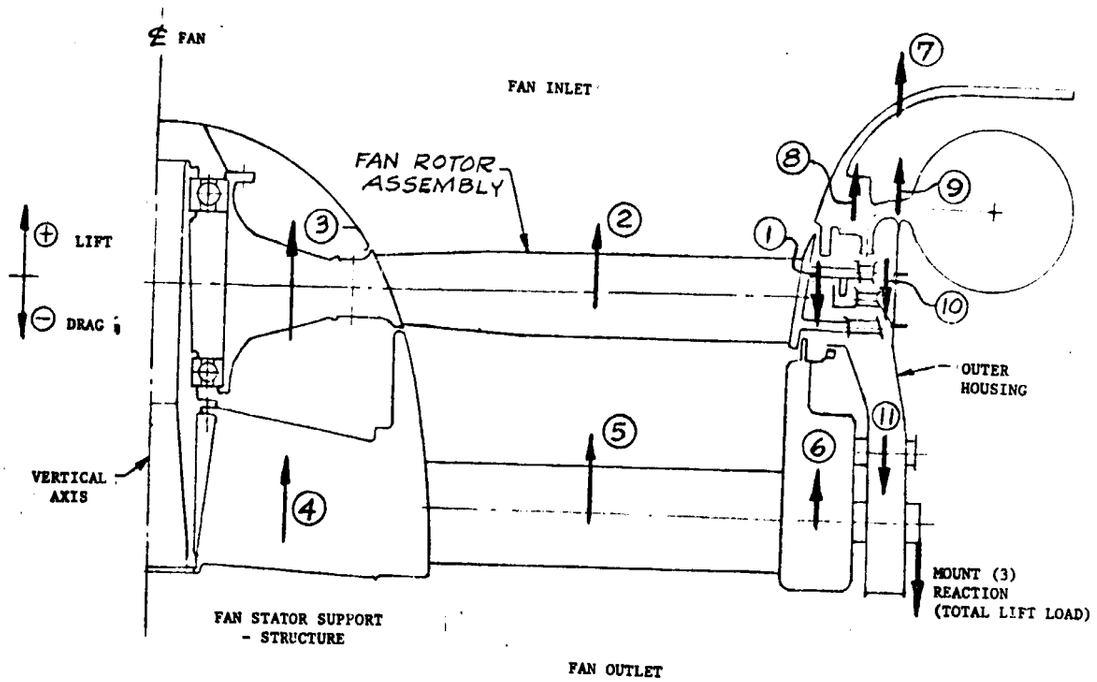

LOAD SUMMARY

	Total Load - lbs	
Fan Rotor		
1 Tip Turbine	- 426	
2 Fan	+ 3129	
3 Disk	+ 250	
	2953 lbs	(Bearing Thrust Load)
Fan Stator Support Structure		
4 Hub	+ 1514	
5 Vanes	+ 1905	
6 Outer Ring	+ 98	
	3517 lbs	
Outer Housing		
7 Bellmouth	+ 2100	
8 Buffer Manifold	+ 2264	
9 Hot Gas Scroll	+ 4735	
10 Second Turbine Stator	- 4751	
11 Exhaust Housing	- 60	
	4288 lbs	

Total Lift Load =10,758 lbs

Figure 12

HASTELLOY X (AMS 5536) SHEET - MINIMUM TENSILE PROPERTIES

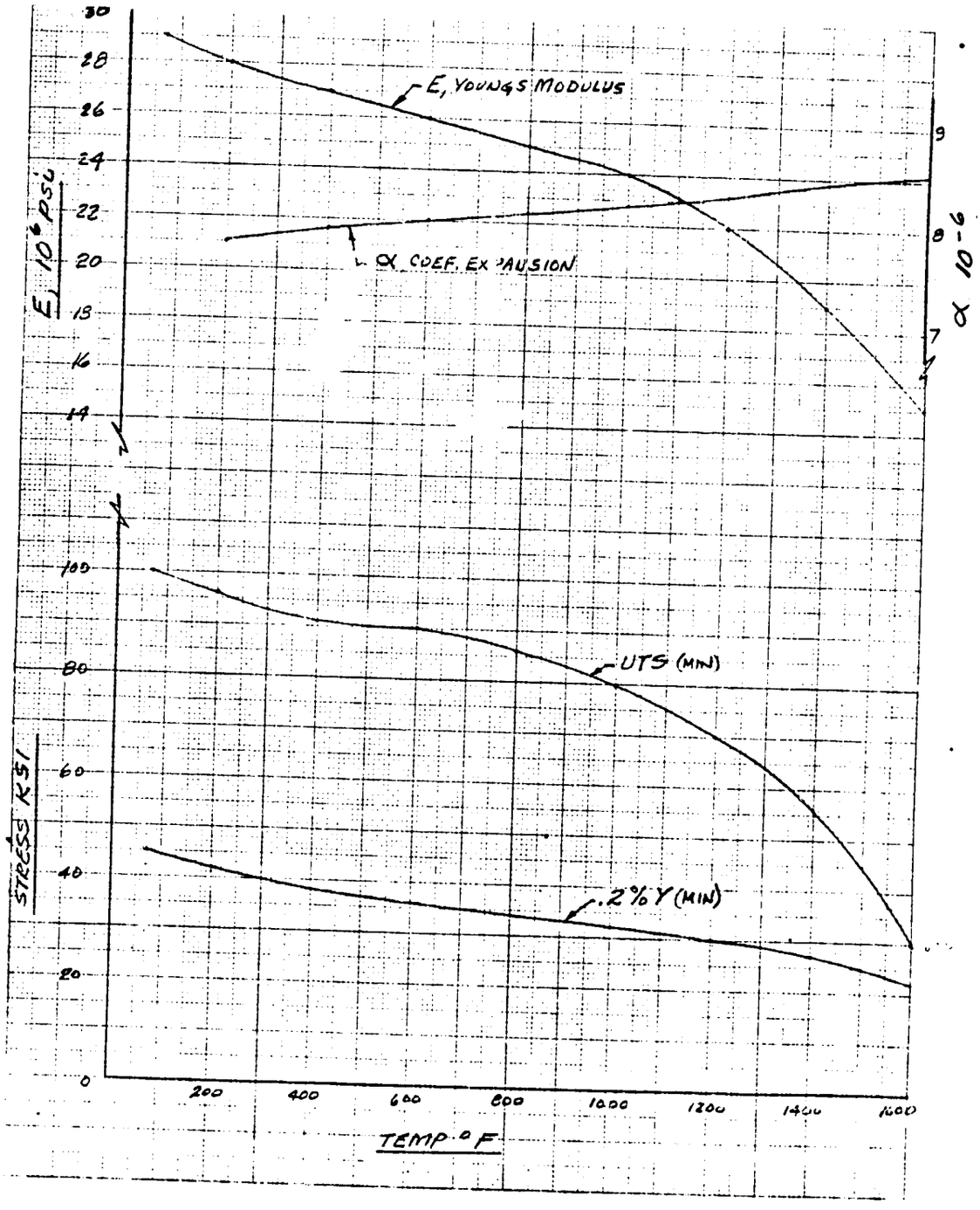

Figure 13

HASTELLOY X (AMS 5536) SHEET - 0.2% CREEP STRENGTH

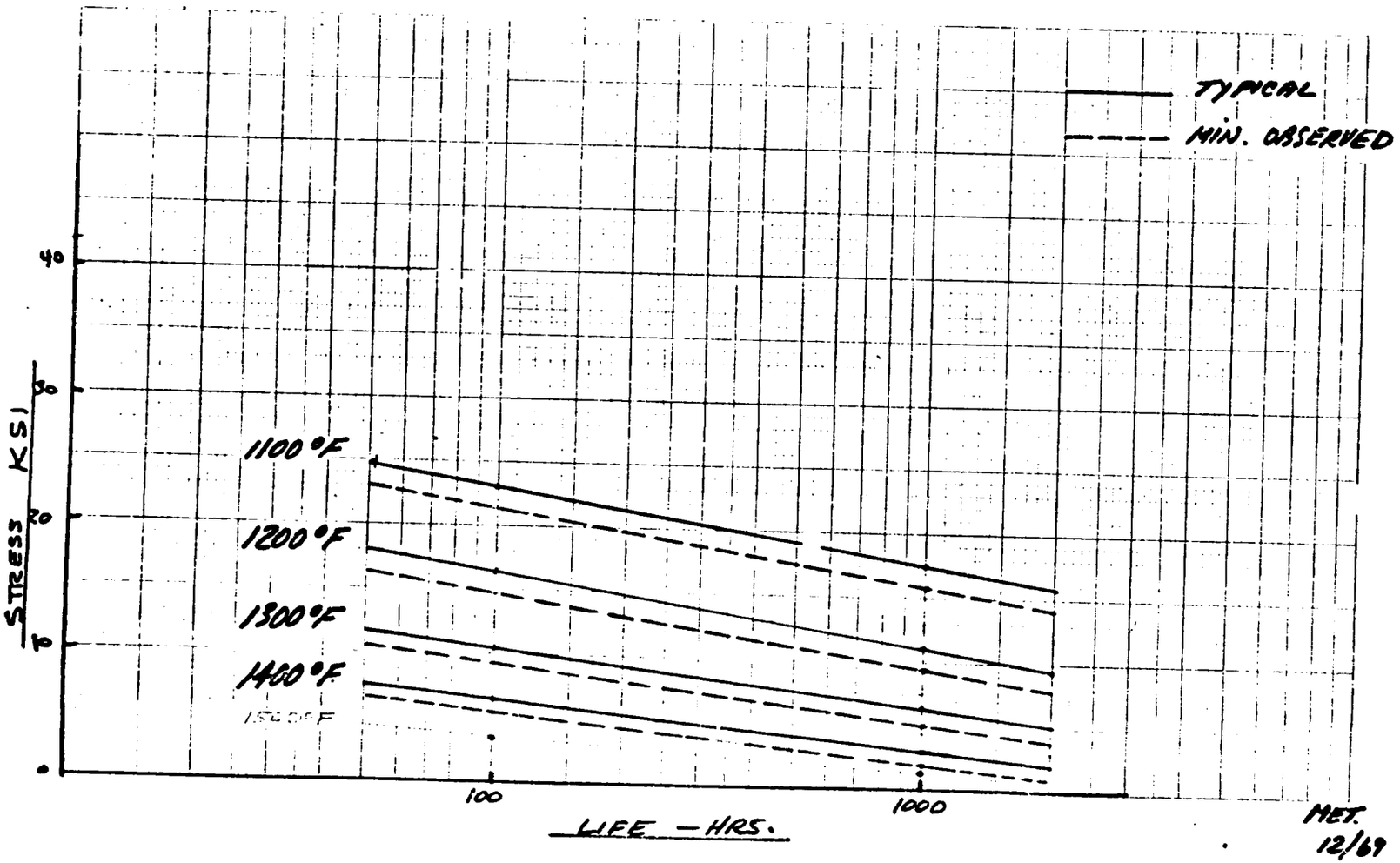

Figure 14

HASTELLOY X (AMS 5536) SHEET - STRESS RUPTURE STRENGTH

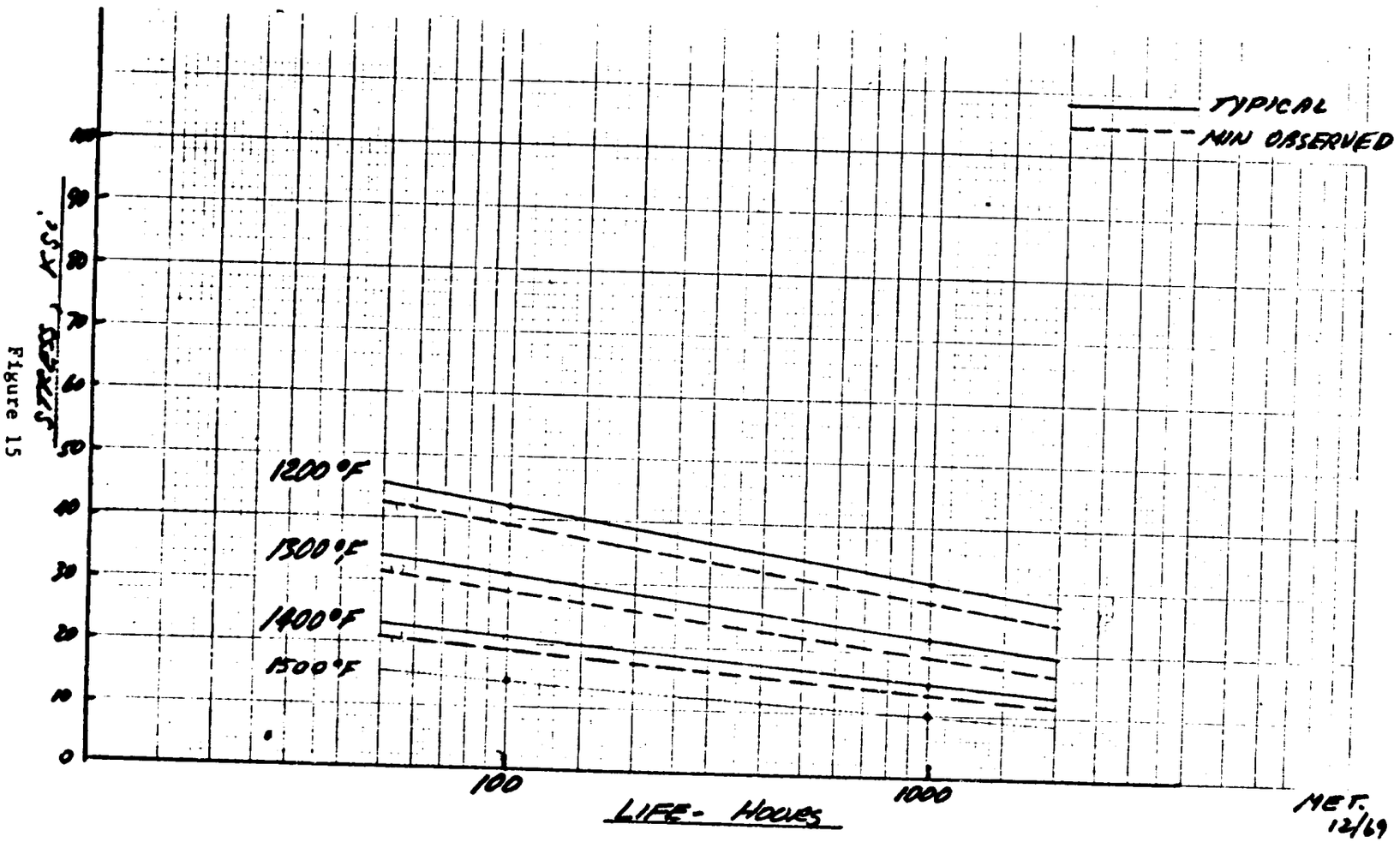

Figure 15

HASTELLOY X (AMS 5536) SHEET - LOW CYCLE FATIGUE STRENGTH

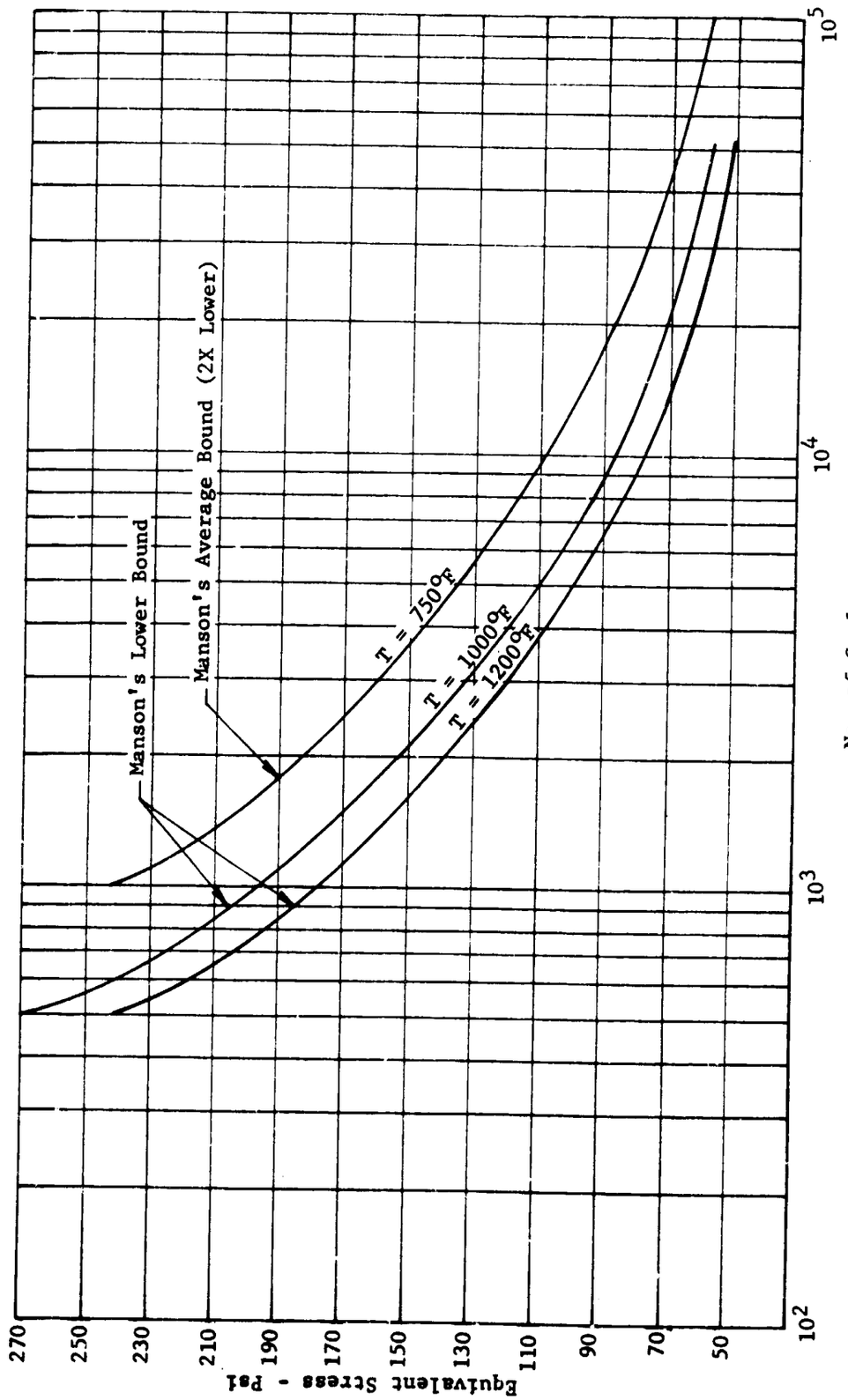

Figure 16

RENÉ 41 (AMS 5545) SHEET - MINIMUM TENSILE PROPERTIES

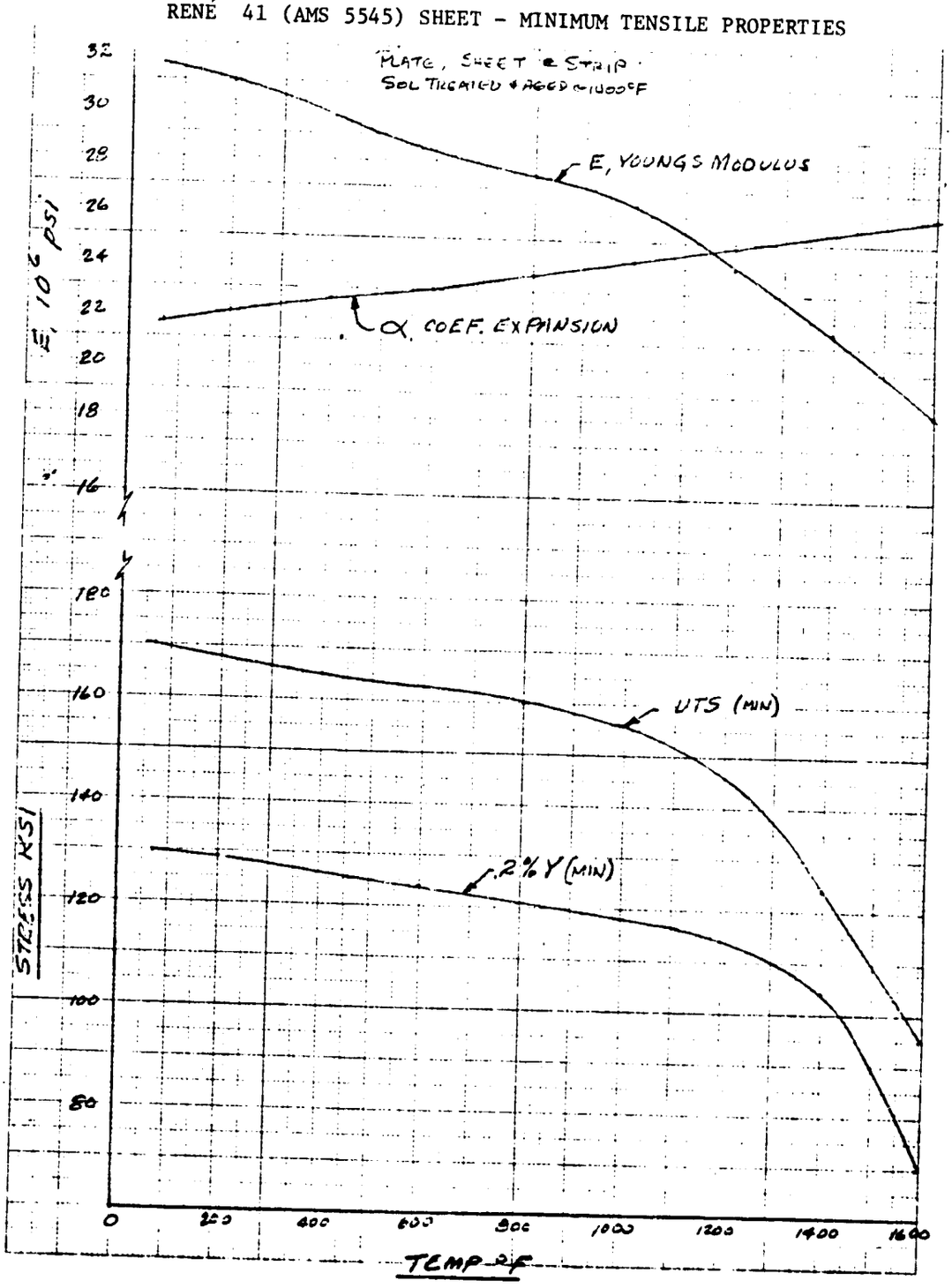

Figure 17

RENÉ 41 (AMS 5545) SHEET - 0.2% CREEP STRENGTH

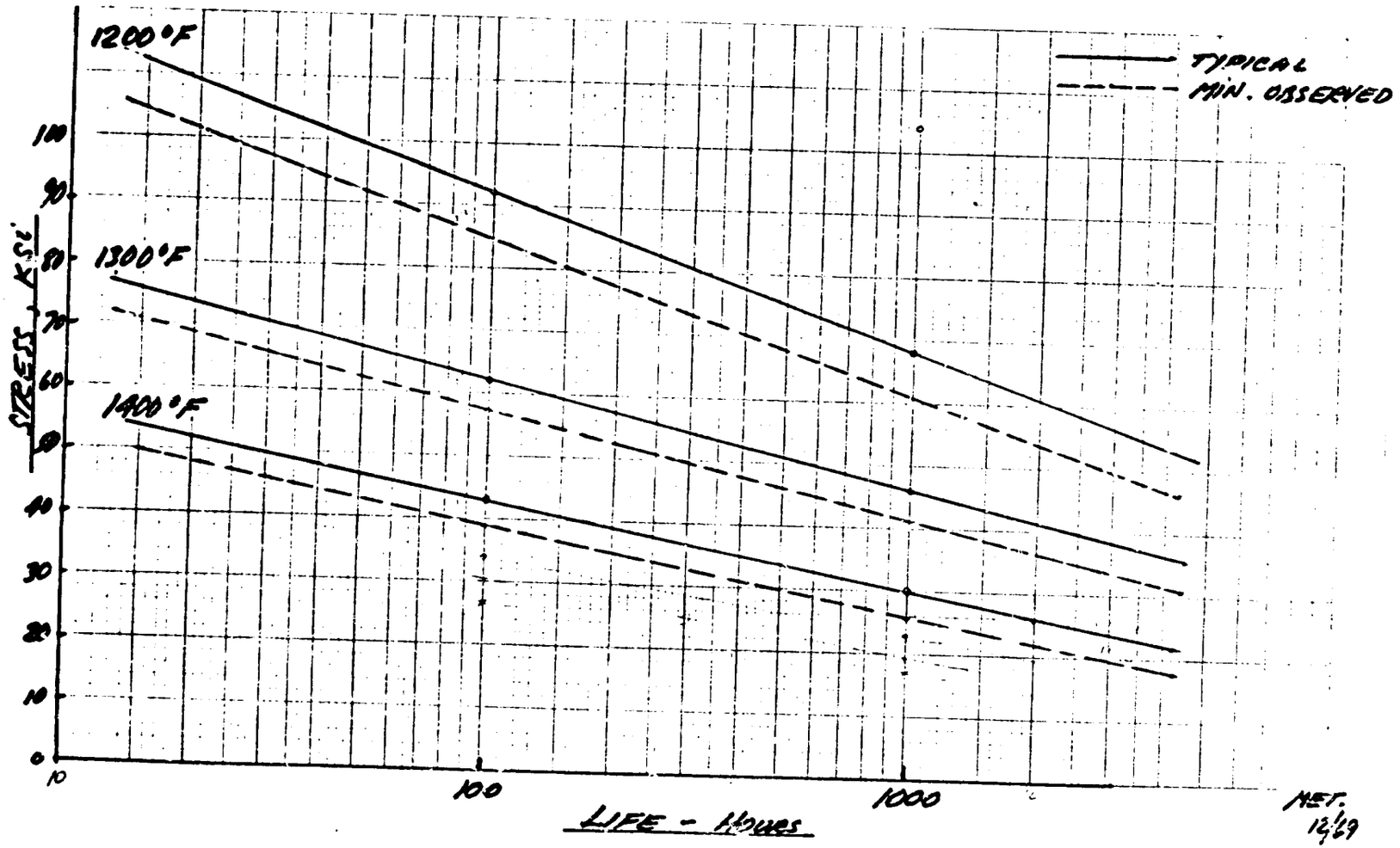

Figure 18

RENÉ 41 (AMS 5545) SHEET - STRESS RUPTURE STRENGTH

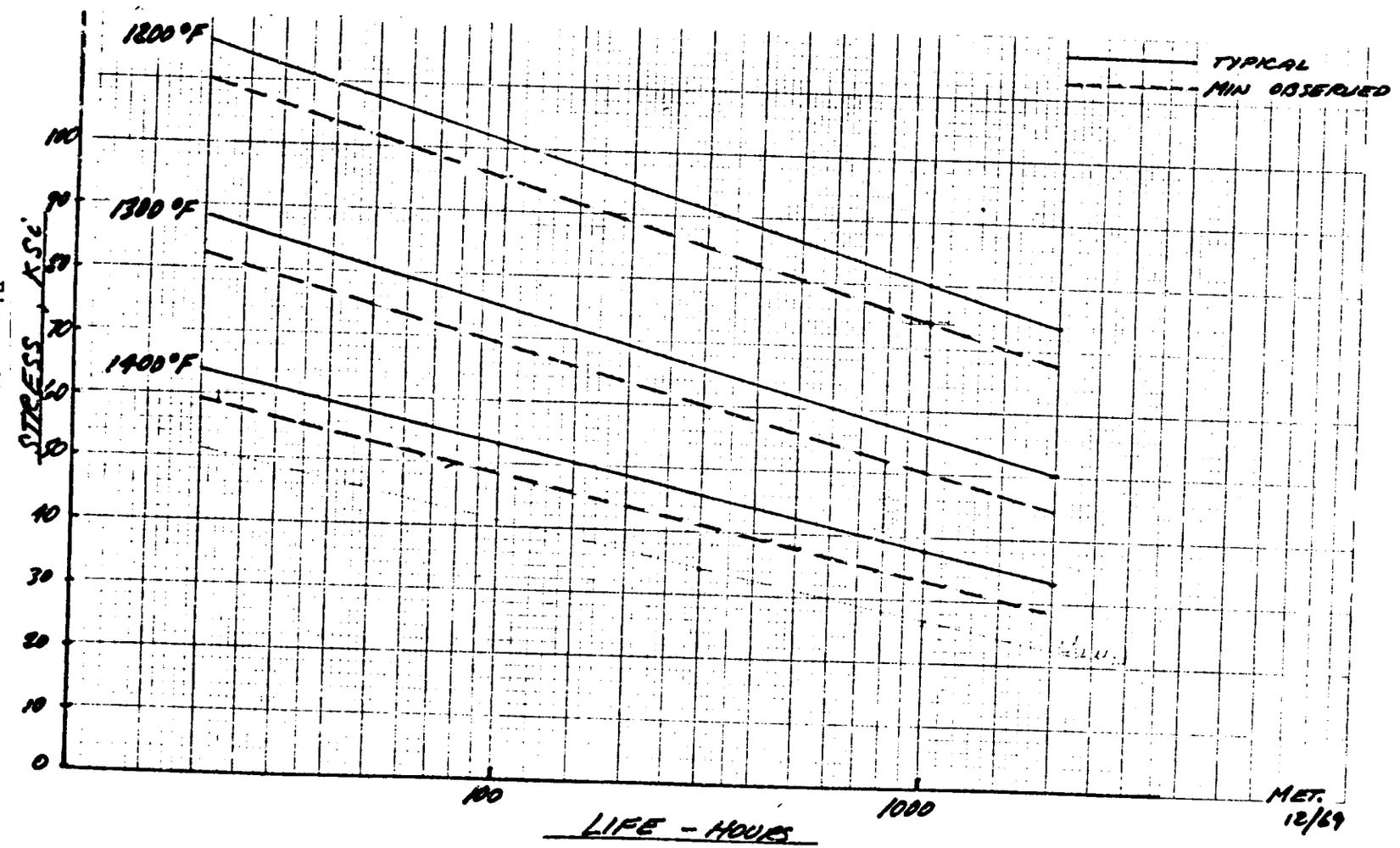

Figure 19

RENE' 41 (AMS 5545) SHEET - LOW CYCLE FATIGUE STRENGTH

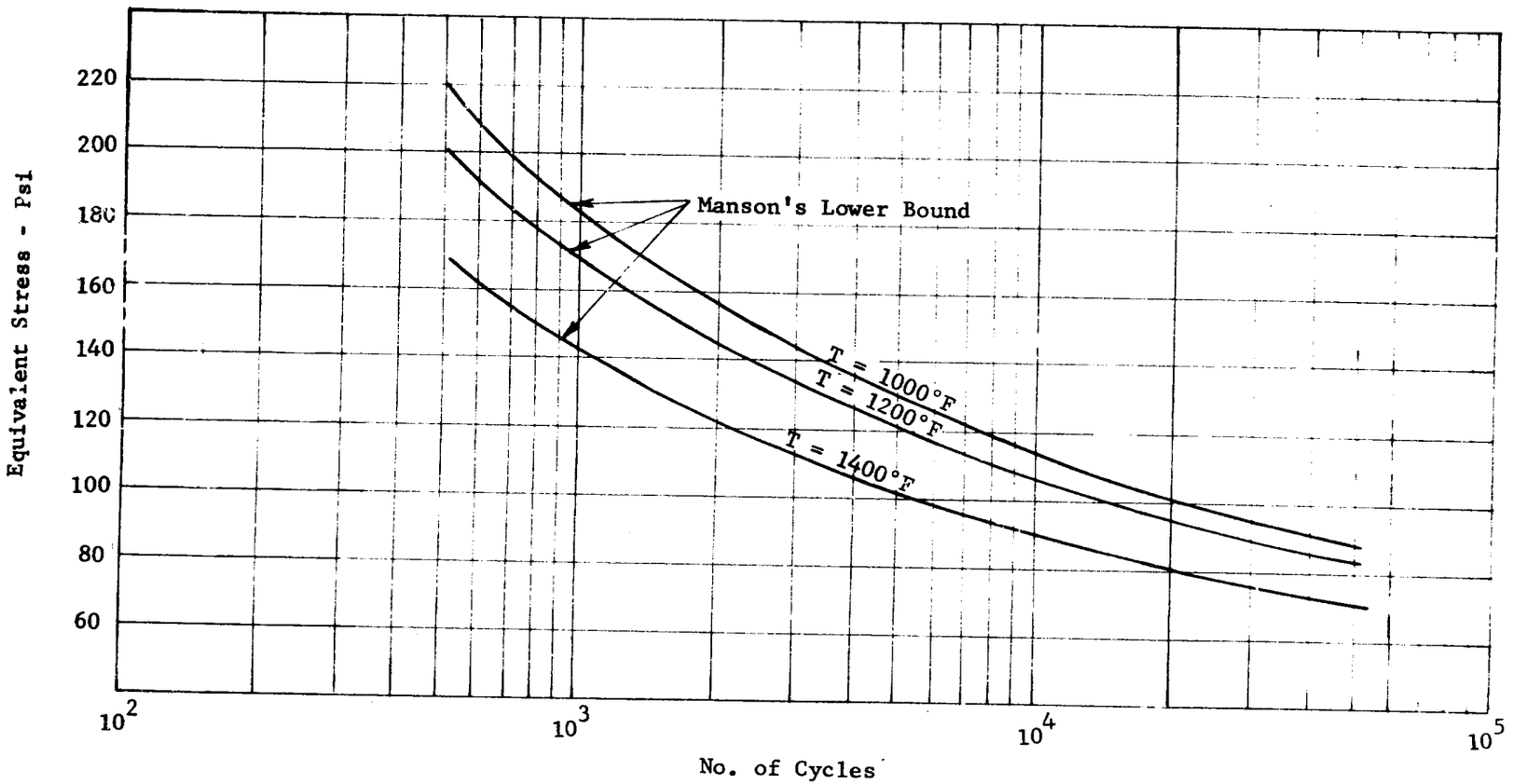

Figure 20

INCONEL X-750 (AMS 5542) SHEET - MINIMUM TENSILE PROPERTIES

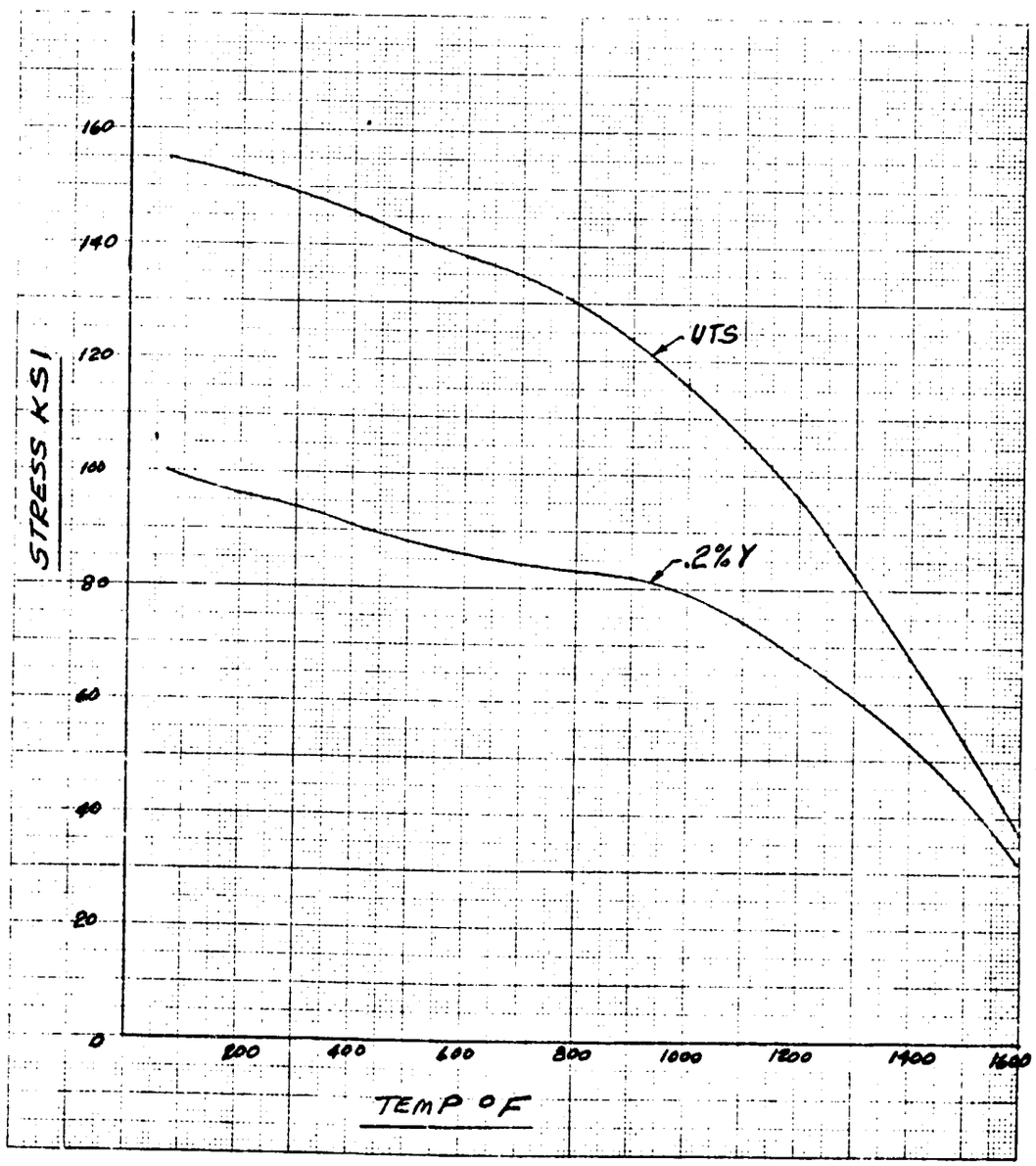

Figure 21

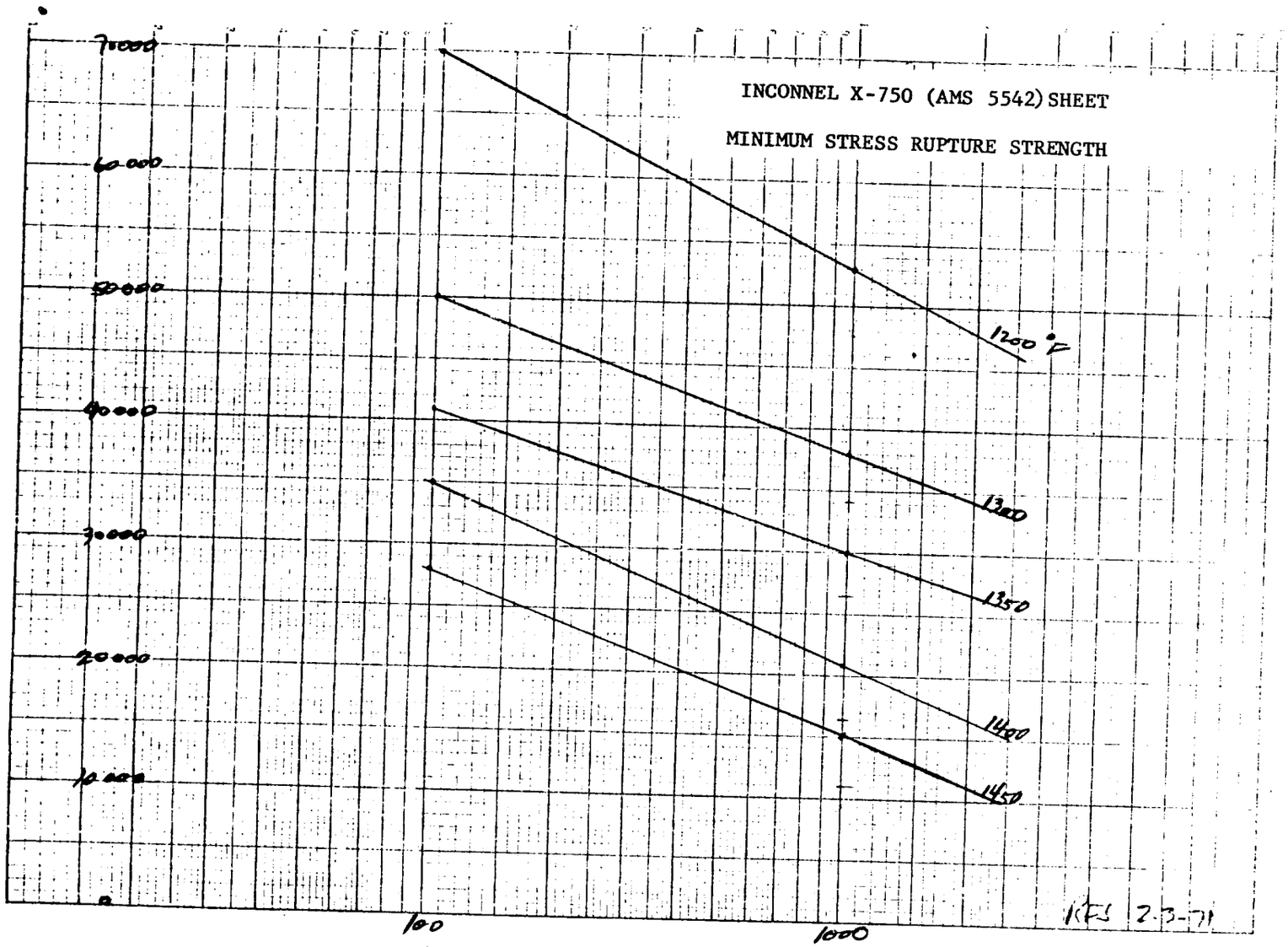
INCONNEL X-750 (AMS 5542) SHEET
MINIMUM STRESS RUPTURE STRENGTH
70000
60000
50000
40000
30000
20000
10000
0
100
1000
1200 °F
1300
1350
1400
1450
KFS 2-3-71

Figure 22

INCONEL 718 (AMS 5662) BAR - MINIMUM TENSILE PROPERTIES

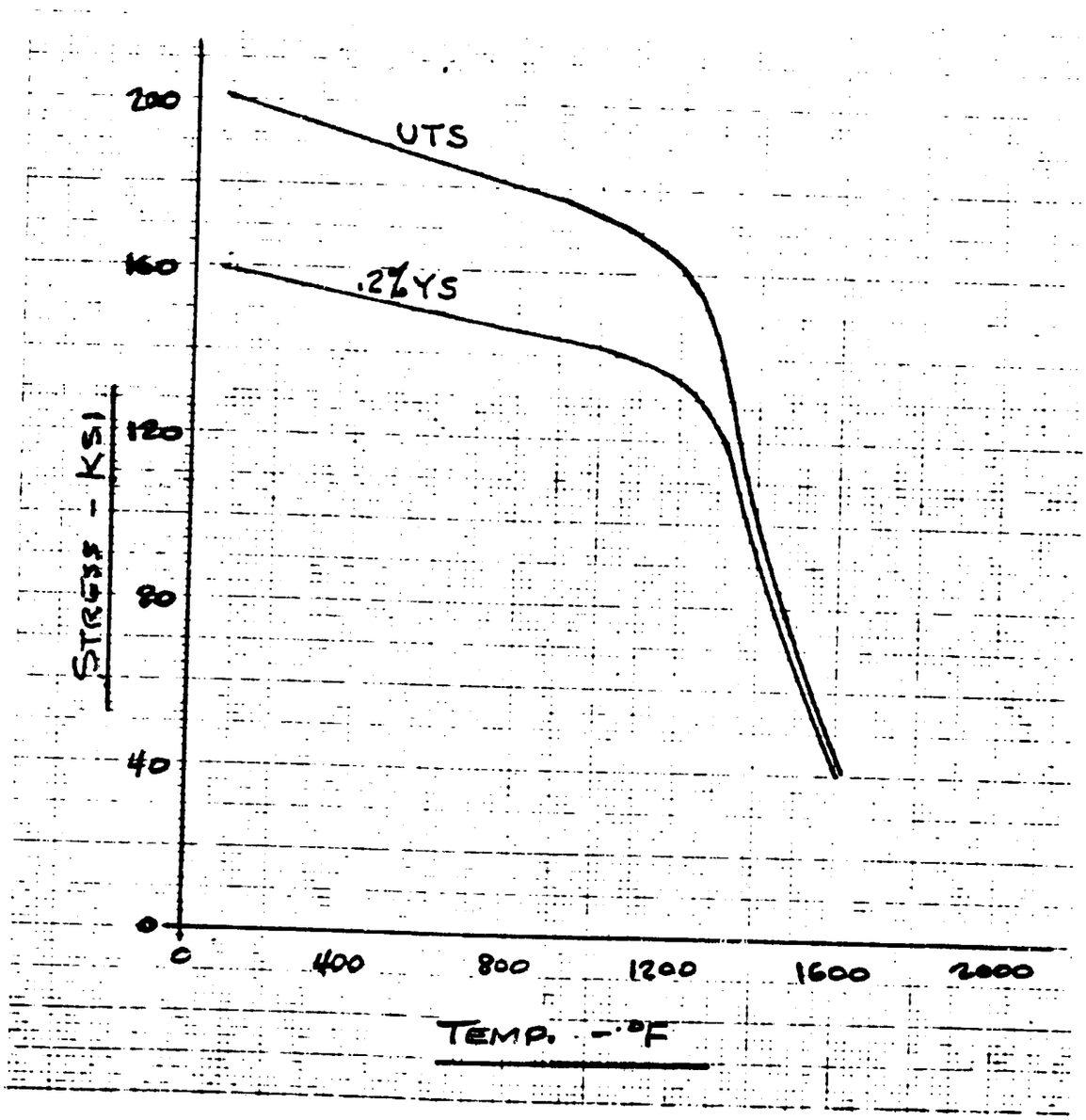

Figure 23

INCONEL 600 (AMS 5540) SHEET - MINIMUM TENSILE PROPERTIES

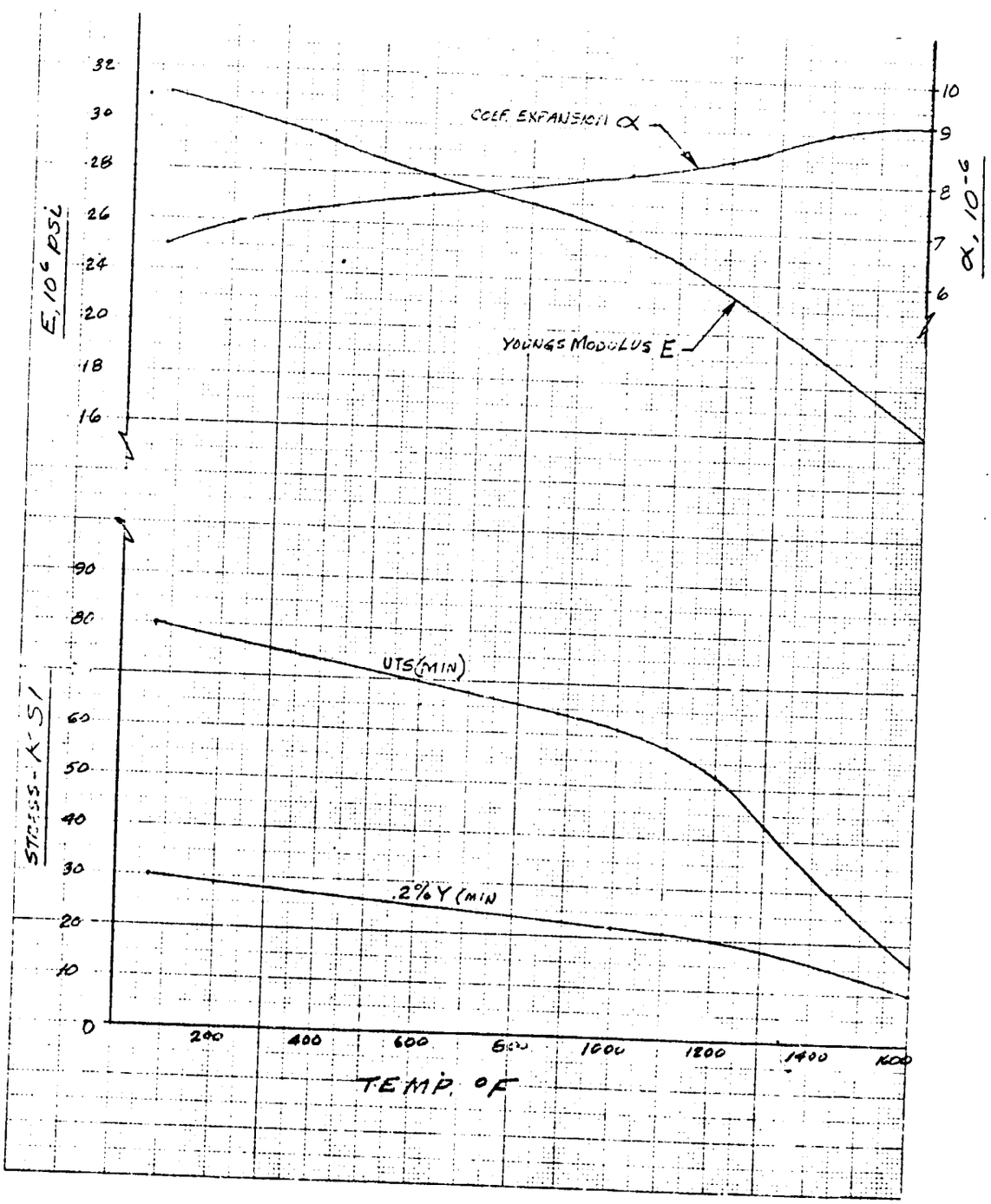

Figure 24

TITANIUM 6Al-4Va (AMS 4928) FORGING - MINIMUM TENSILE PROPERTIES

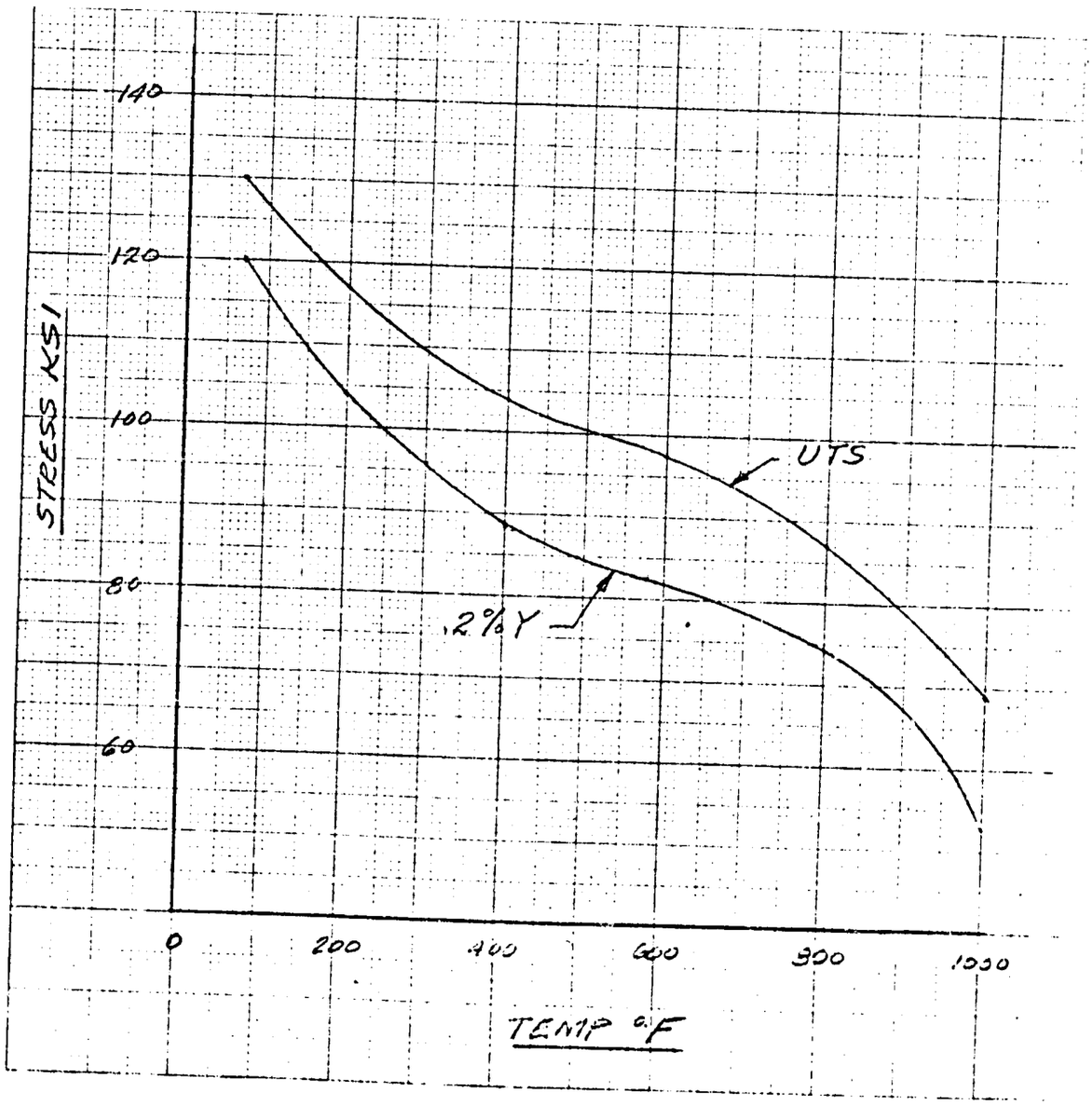

Figure 25

TITANIUM 5Al-2.5Sn (AMS 4966) FORGINC - MINIMUM TENSILE PROPERTIES

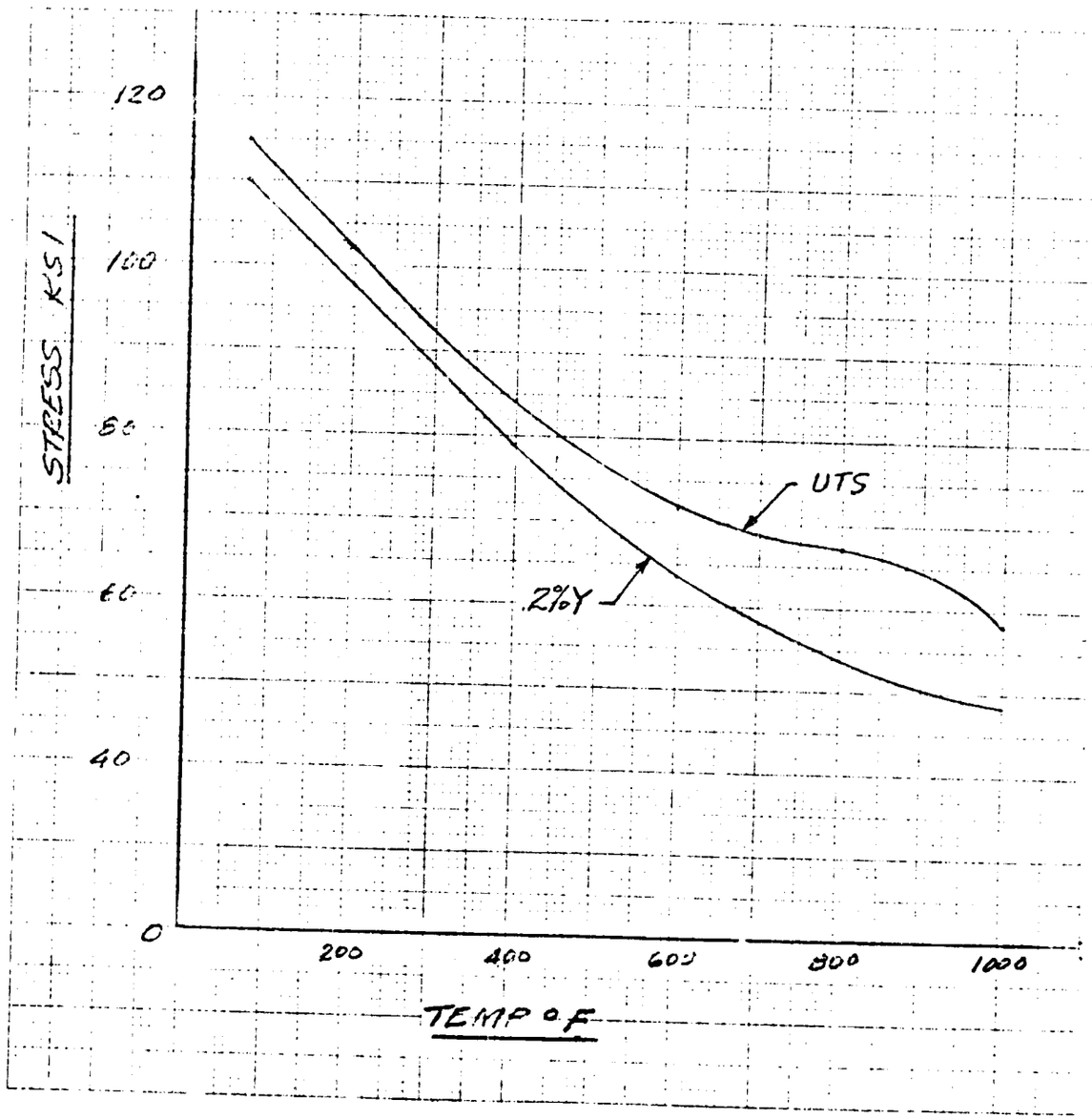

Figure 26

ALUMINUM 5052-0 (AM 4015) SHEET - TYPICAL TENSILE PROPERTIES

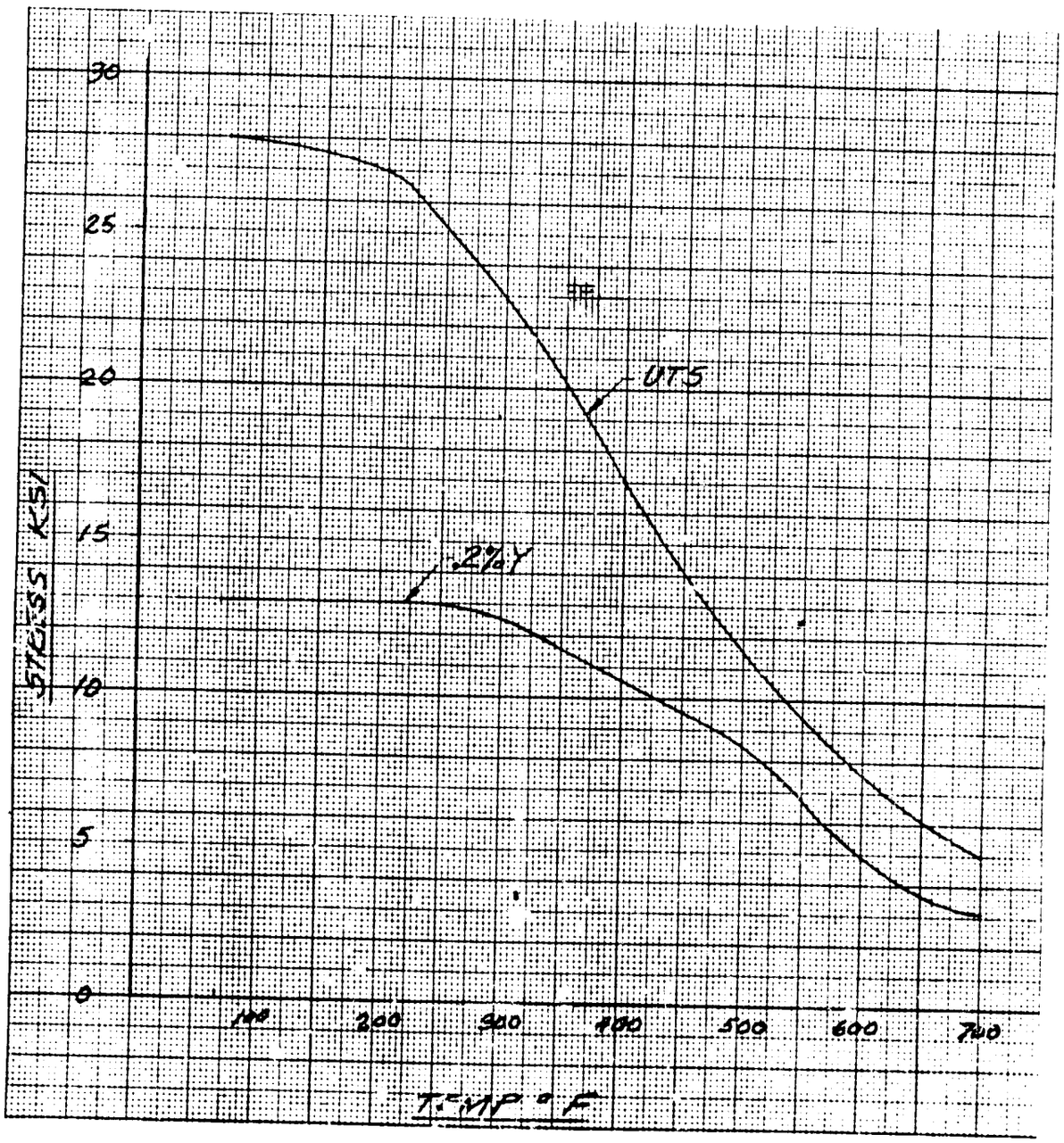

Figure 27

NICROBRAZ ALLOY (AMS 4775) BRAZE - TYPICAL TENSILE AND SHEAR PROPERTIES

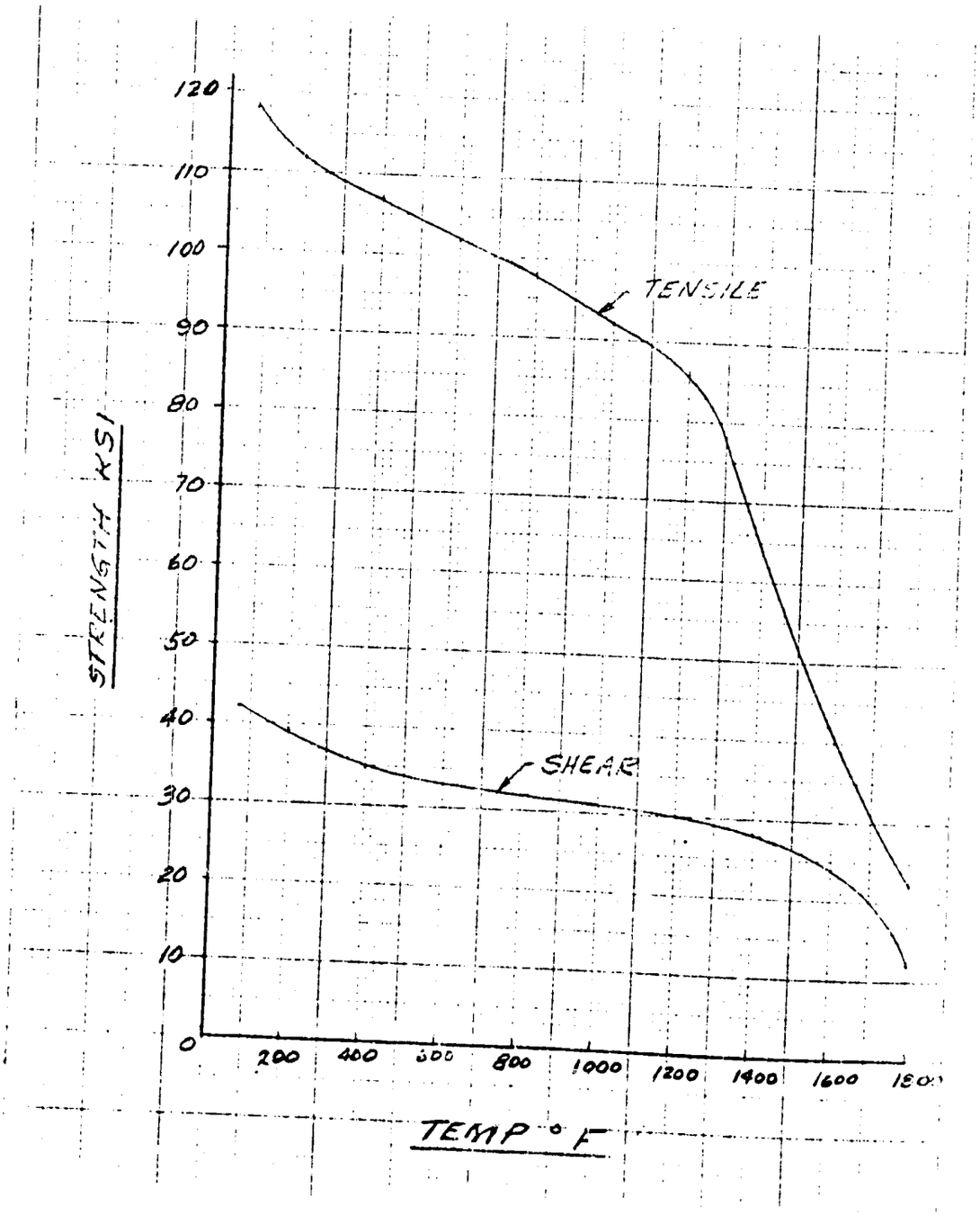

Figure 28

GENERAL STRUCTURAL DESIGN CRITERIA FOR COMPRESSOR, FAN AND TURBINE ROTOR BLADES

Condition	Engine Speed	Location	Stress Includes	Allowable Stress and/or Failure Criteria
Steady State	100%	Airfoil critical area	a) P/A	1) 80% of 0.2% yield strength 2) 0.2% creep strength for design life
			b) Combined (P/A, gas & offset bending)	1) 80% of 0.2% yield strength 2) Stress rupture strength for design life
		Airfoil root	Combined (P/A, gas & offset bending)	Material fatigue strength (at steady state) from Goodman diagram, equals 2 x gas bending stress *
		Fir tree	a) P/A	0.2% creep strength for design life
			b) Combined (P/A, gas & offset bending, & SCF)	1) 0.2% yield strength 2) Stress rupture strength for design life 3) Material fatigue strength (at steady state) from Goodman diagram, equals 2 x gas bending stress *
Transient	Transient	Airfoil critical area	Combined (P/A, gas & offset bending)	0.2% yield strength
Overspeed	115%	Airfoil & fir tree	P/A	90% of ultimate tensile strength

* For flexible blades use net gas bending stress (gas bending less centrifugal restoring).

NOTE: Spec. minimum material properties used

Figure 29

GENERAL STRUCTURAL DESIGN CRITERIA COMPRESSOR, FAN AND TURBINE ROTOR DISKS

Condition	Engine Speed	Location	Stress Includes	Allowable Stress and/or Failure Criteria
Steady State	100%	Bore*	P/A, thermal	120% of 0.2% yield strength
		Neck*	P/A, thermal	1) 0.2% yield strength 2) 0.2% creep strength for design life
		Rim*	P/A, thermal	1) 80% of 0.2% yield strength 2) 0.2% creep strength for design life
		Tenon	a) P/A	0.2% creep strength for design life
			b) Combined (P/A, gas bending & SCF)	1) 0.2% yield strength 2) Stress rupture strength for design life 3) Material fatigue strength (at steady state) from Goodman diagram, equals 2 x gas bending stress**
Transient	Transient	Bore*	P/A, thermal	Ultimate tensile strength
		Neck*	P/A, thermal	0.2% yield strength
		Rim*	P/A, thermal	0.2% yield strength
Overspeed	115%	Average Tangential	P/A	90% of ultimate tensile strength

*Structural failure results from combined principal stresses such as radial and tangential. Equivalent stress is a resultant of the two.

$$\sigma_e = \sqrt{\sigma_t^2 - \sigma_t \sigma_r + \sigma_r^2}$$

σ_e = Equivalent Stress
σ_r = Radial Stress
σ_t = Tangential Stress

** For flexible blades use net gas bending stress (gas bending less centrifugal restoring).

Figure 30

GENERAL STRUCTURAL DESIGN CRITERIA FOR COMPRESSOR, FAN AND TURBINE STATOR VANES

Condition	Engine Speed	Location	Stress Includes	Allowable Stress and/or Failure Criteria
Steady State	100%	Airfoil critical area	Gas bending	1) 80% of 0.2% yield strength 2) Stress rupture strength for design life 3) Material fatigue strength (at steady state) from Goodman diagram, equals 2 x gas bending stress
		Attachment	Combined gas bending, & SCF	1) 0.2% yield strength 2) Stress rupture strength for design life 3) Material fatigue strength (at steady state) from Goodman diagram, equals 2 x gas bending stress
Transient	Transient	Airfoil critical area	Combined gas bending	0.2% yield strength

NOTE: Spec. minimum material properties used

Figure 31

GENERAL STRUCTURAL CRITERIA FOR HOUSINGS AND SCROLLS

Condition	Stress Includes	Allowable Stress and/or Failure Criteria
Steady State	Direct	1) 0.2% yield strength 2) 0.2% creep for design life 3) Critical buckling strength
	Direct plus bending	1) 0.2% yield strength 2) Stress rupture stress for design life 3) Critical buckling strength
Transient	Combined steady state stress plus thermal stress	Low cycle fatigue life equal to or greater than design life
	Combined steady state stress plus maneuver load stress	0.2% yield strength

Figure 32

FAN ROTOR ASSEMBLY

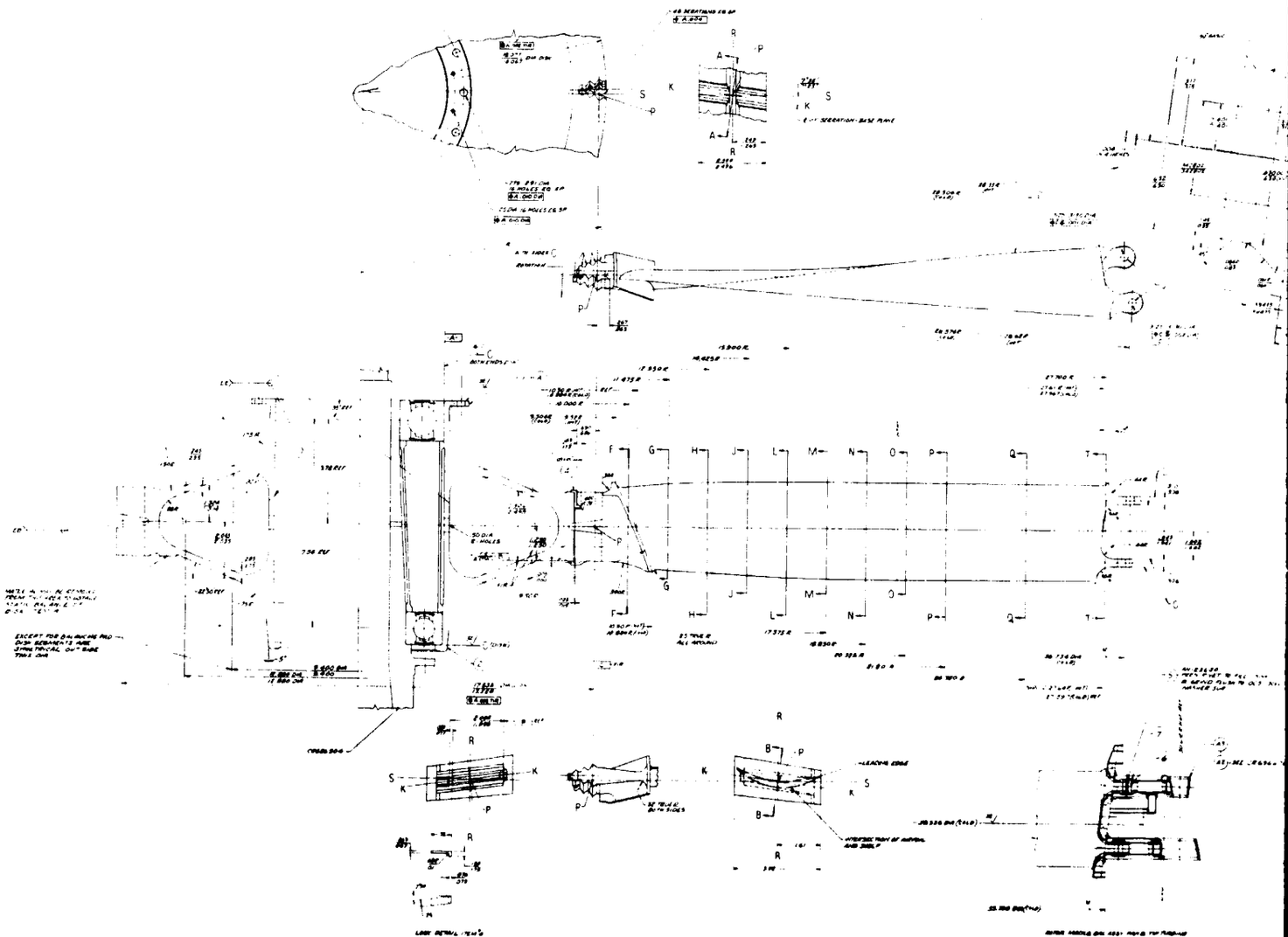

FOLDOUT FRAME 1

FAN ROTOR ASSEMBLY

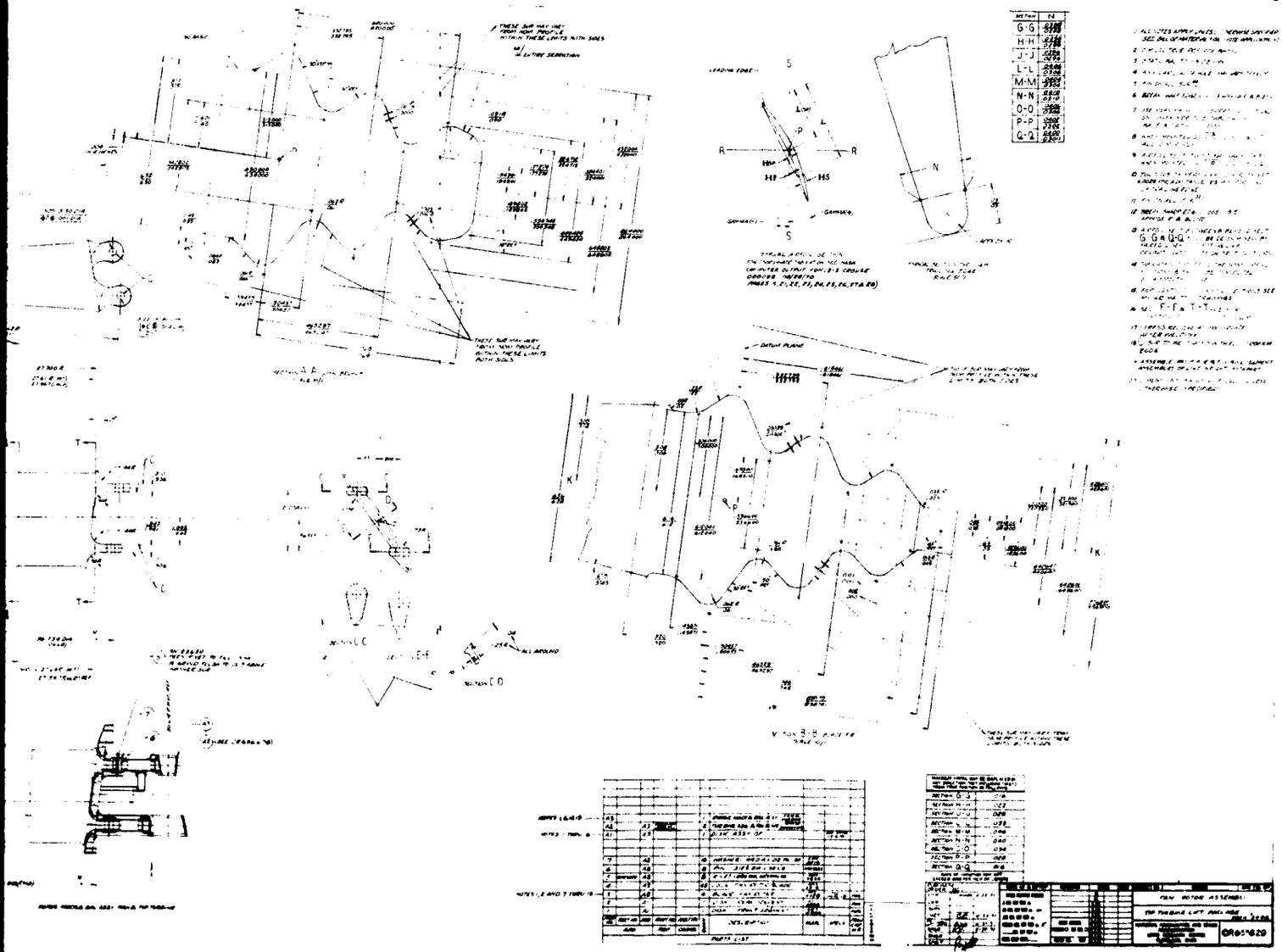

FOLDOUT FRAME 2

Figure 33

AXIAL BENDING MOMENTS AND SHEAR LOADS ON FAN RO

	CONDITION I										
	STEADY STATE										STEA
Radius in.	Aero Load On Fan Blade		Turbine Aero Load On Fan			Turbine Carrier C.F. Offset Moment in Fan Blade lb-in.	No Restoring		Centrifugal Restoring Moment lb-in.	Net Axial Moment in Fan Blade lb-in.	Axial Gyro Shear Load-lb
	Shear lbs	Moment lbs	Moment Arm (28.6R) in.	Shear lbs	Moment lb-in.		Total Shear lbs	Total Moment lb-in.			
	(1)	(2)	(3)	(4)	(5) (3)x(4)	(6)	(7) (1)+(4)	(8) (2)+(5)+(6)	(9)	(10) (8)+(9)	(10a)
27.47	0.00	0.00	1.13	8.88	10.03	810.00	8.88	820.0	-28.0	792.0	-84
26.38	-8.27	-4.52	2.22		19.71		0.53	825.2	-76.2	749.0	
25.23	-16.51	-18.80	3.37		29.93		-7.63	821.2	-117.2	704.0	
24.00	-24.69	-44.08	4.60		40.85		-15.81	806.8	-152.8	654.0	
22.68	-32.68	-81.80	5.92		52.57		-23.80	780.8	-183.8	597.0	
21.26	-40.40	-133.87	7.34		65.18		-31.52	741.3	-202.3	539.0	
19.69	-47.69	-202.82	8.91		79.12		-38.81	686.3	-219.3	467.0	
17.94	-54.35	-292.30	10.66		94.66		-45.47	612.4	-203.4	382.0	
15.92	-60.05	-407.61	12.68		112.60		-51.17	515.0	-238.0	277.0	
13.53	-64.17	-556.52	15.07		133.82		-55.29	387.3	-240.3	147.0	
10.58	-65.18	-747.31	18.02		160.02		-56.30	222.7	-237.7	-15.0	
10.28	-65.18	-766.58	18.32		162.68		-56.30	206.1	-239.1	-33.0	
8.97	-65.18	-851.97	19.63	8.88	174.31	810.0	-56.30	132.3	-239.3	-107.0	-84

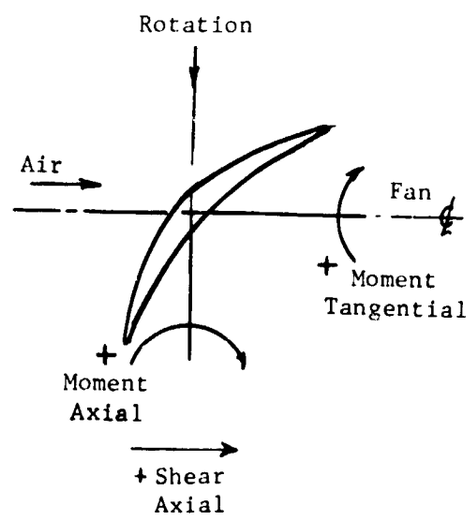

FOLDOUT FRAME 1

MOMENTS AND SHEAR LOADS ON FAN ROTOR BLADE

			CONDITION 2				CONDITION 3			
			STEADY STATE PLUS UPWARD AXIAL FORCE DUE TO GYROSCOPIC MOMENT				STEADY STATE PLUS DOWNWARD AXIAL FORCE DUE TO GYROSCOPIC MOMENT			
g tal ment -in.	Centrifugal Restoring Moment lb-in.	Net Axial Moment in Fan Blade lb-in.	Axial Gyro Shear Load-lb	Axial Gyro Moment lb-in.	Centrifugal Restoring Moment lb-in.	Net Axial Moment on Fan Blade lb-in.	Axial Gyro Shear Load-lb	Axial Gyro Moment lb-in.	Centrifugal Restoring Moment lb-in.	Net Axial Moment on Fan Blade lb-in.
(8) (5)+(6)	(9)	(10) (8)+(9)	(10a)	(11)	(12)	(13) (8)+(11)+(12)	(13a)	(14) See (11)	(15)	(16) (8)+(14)+(15)
0.0	-28.0	792.0	-84	-94.9	4.9	730	84	94.9	-84.9	830
5.2	-76.2	749.0	↑	-186.5	-8.7	630	↑	186.5	-161.7	850
1.2	-117.2	704.0		-283.1	-16.1	522		283.1	-239.3	865
6.8	-152.8	654.0		-386.4	-15.4	405		386.4	-308.2	885
0.8	-183.8	597.0		-497.3	-5.5	278		497.3	-368.1	910
1.3	-202.3	539.0		-616.6	10.3	135		616.6	-427.9	930
6.3	-219.3	467.0		-749.3	33.0	-30		749.3	-475.6	960
2.4	-203.4	382.0		-895.4	61.0	-222		895.4	-527.8	980
5.0	-238.0	277.0		-1065.1	85.1	-465		1065.1	-565.1	1015
7.3	-240.3	147.0		-1274.3	47.0	-840		1274.3	-601.6	1060
2.7	-237.7	-15.0		-1513,7	141.0	-1150		1513.7	-621.4	1115
6.1	-239.1	-33.0		-1538.9	142.8	-1190		1538.9	-625.0	1120
.3	-239.3	-107.0	-84	-1648.9	134.6	-1382	84	1648.9	-625.2	1156

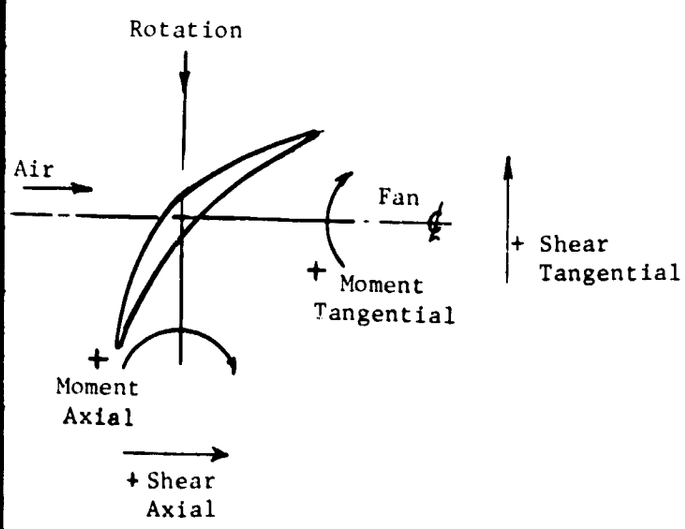

FOLDOUT FRAME 2

Figure 34

TANGENTIAL BENDING MOMENTS AND S

Radius in.	CONDITION I — STEADY STATE								
	Aero Load on Fan Blade		Turbine Aero Load on Fan			Turbine Carrier CF Offset Moment in Fan Blade lb-in.	No Restoring		Centrifugal Restoring Moment lb-in.
	Shear lbs	Moment lb-in.	Moment Arm (28.4-R) in.	Shear lbs	Moment lb-in.		Total Shear lbs.	Total Moment lb-in.	
	(1)	(2)	(3)	(4)	(5) (3) X (4)	(6)	(7) (1) + (4)	(8) (2)+(5)+(6)	(9)
27.47	0.00	0.00	0.93	-104	- 96.72	530.0	-104.0	433.3	43.7
26.38	12.12	6.63	2.02	-104	- 210.08	530.0	- 91.9	326.5	95.5
25.23	24.29	27.62	3.17	-104	- 329.68	530.0	- 79.7	227.9	139.1
24.00	36.71	65.04	4.40	-104	- 457.60	530.0	- 67.3	137.4	172.6
22.68	49.50	121.73	5.72	-104	- 594.88	530.0	- 54.5	56.8	196.2
21.26	62.82	201.75	7.14	-104	- 742.56	530.0	- 41.2	-10.8	205.8
19.69	76.85	311.08	8.71	-104	- 905.84	530.0	- 27.2	-64.8	204.8
17.94	91.89	459.05	10.46	-104	-1087.84	530.0	- 21.1	-98.8	183.8
15.92	108.17	660.71	12.48	-104	-1297.92	530.0	4.2	-107.2	147.2
13.53	126.08	941.53	14.87	-104	-1546.48	530.0	22.1	- 75.0	100.0
10.58	147.11	1344.51	17.82	-104	-1853.28	530.0	43.1	22.0	51.0
10.28	147.11	1387.99	18.12	-104	-1884.48	530.0	43.1	33.5	49.5
8.97	147.11	1580.70	19.43	-104	-2020.72	530.0	43.1	90.0	45.0

Ro

Air

FOLDOUT FRAME 1

71-342

NDING MOMENTS AND SHEAR LOADS ON FAN ROTOR BLADE

			CONDITION 2 STEADY STATE PLUS UPWARD AXIAL FORCE DUE TO GYROSCOPIC MOMENT			CONDITION 3 STEADY STATE PLUS DOWNWARD AXIAL FORCE DUE TO GYROSCOPIC MOMENT		
ing Total Moment lb-in.	Centrifugal Restoring Moment lb-in.	Net Tangential Moment in Fan Blade lb-in.	Tangential Gyro Moment lb-in.	Centrifugal Restoring Moment lb-in.	Net Tangential Moment in Fan Blade lb-in.	Tangential Gyro Moment lb-in.	Centrifugal Restoring Moment lb-in.	Net Tangential Moment in Fan Blade lb-in.
(8))+(5)+(6)	(9)	(10) (8) + (9)	(11)	(12)	(13) (8)+(11)+(12)	(14)	(15)	(16) (8)+(14)+(15)
433.3	43.7	477.0	0	26.7	460	0	66.7	500
326.5	95.5	422.0	0	48.5	375	0	148.5	475
227.9	139.1	367.0	0	62.1	290	0	212.1	440
137.4	172.6	310.0	0	70.6	208	0	277.6	415
56.8	196.2	253.0	0	65.2	122	0	318.2	375
-10.8	205.8	195.0	0	70.8	60	0	345.8	335
-64.8	204.8	140.0	0	54.8	-10	0	344.8	280
-98.8	183.8	85.0	0	38.8	-60	0	318.8	220
-107.2	147.2	40.0	0	27.2	-80	0	249.2	142
75.0	100.0	25.0	0	33.0	-42	0	159.0	84
22.0	51.0	73.0	0	33.0	55	0	68.0	90
33.5	49.5	83.0	0	31.5	65	0	66.5	100
90.0	45.0	135.0	0	31.0	121	0	58.0	148

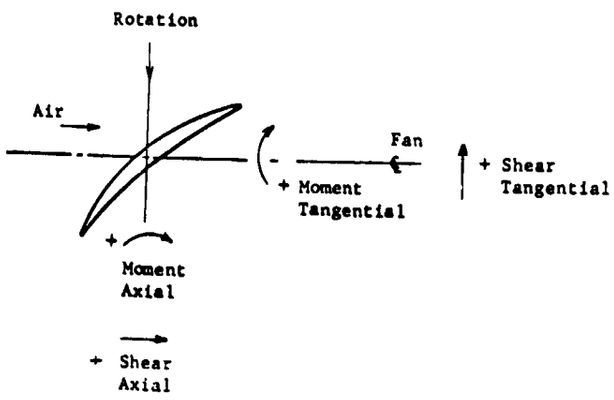

FOLDOUT FRAME 2

Figure 35

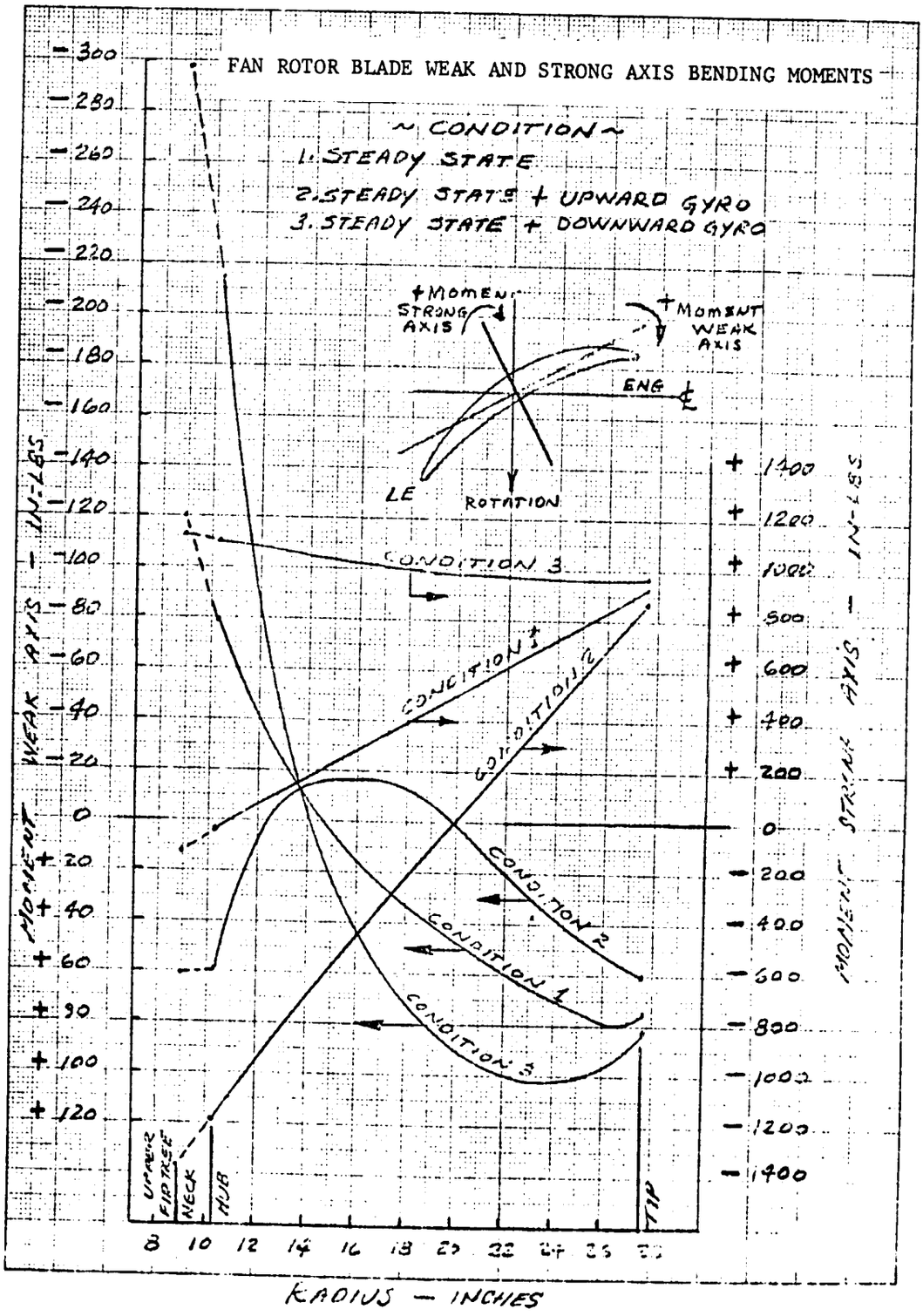
FAN ROTOR BLADE WEAK AND STRONG AXIS BENDING MOMENTS
~ CONDITION ~
1. STEADY STATE
2. STEADY STATE + UPWARD GYRO
3. STEADY STATE + DOWNWARD GYRO
+ MOMENT STRONG AXIS
+ MOMENT WEAK AXIS
ENG ℄
LE
ROTATION
CONDITION 3
CONDITION 1
CONDITION 2
CONDITION 2
CONDITION 1
CONDITION 3
WEAK AXIS MOMENT - IN-LBS
STRONG AXIS MOMENT - IN-LBS
- 300
- 280
- 260
- 240
- 220
- 200
- 180
- 160
- 140
- 120
- 100
- 80
- 60
- 40
- 20
0
+ 20
+ 40
+ 60
+ 90
+ 100
+ 120
+ 1400
+ 1200
+ 1000
+ 800
+ 600
+ 400
+ 200
0
- 200
- 400
- 600
- 800
- 1000
- 1200
- 1400
UPPER FIR TREE
NECK
HUB
TIP
8 10 12 14 16 18 20 22 24 26 28
RADIUS - INCHES

Figure 36

FAN ROTOR BLADE SECTION PROPERTIES

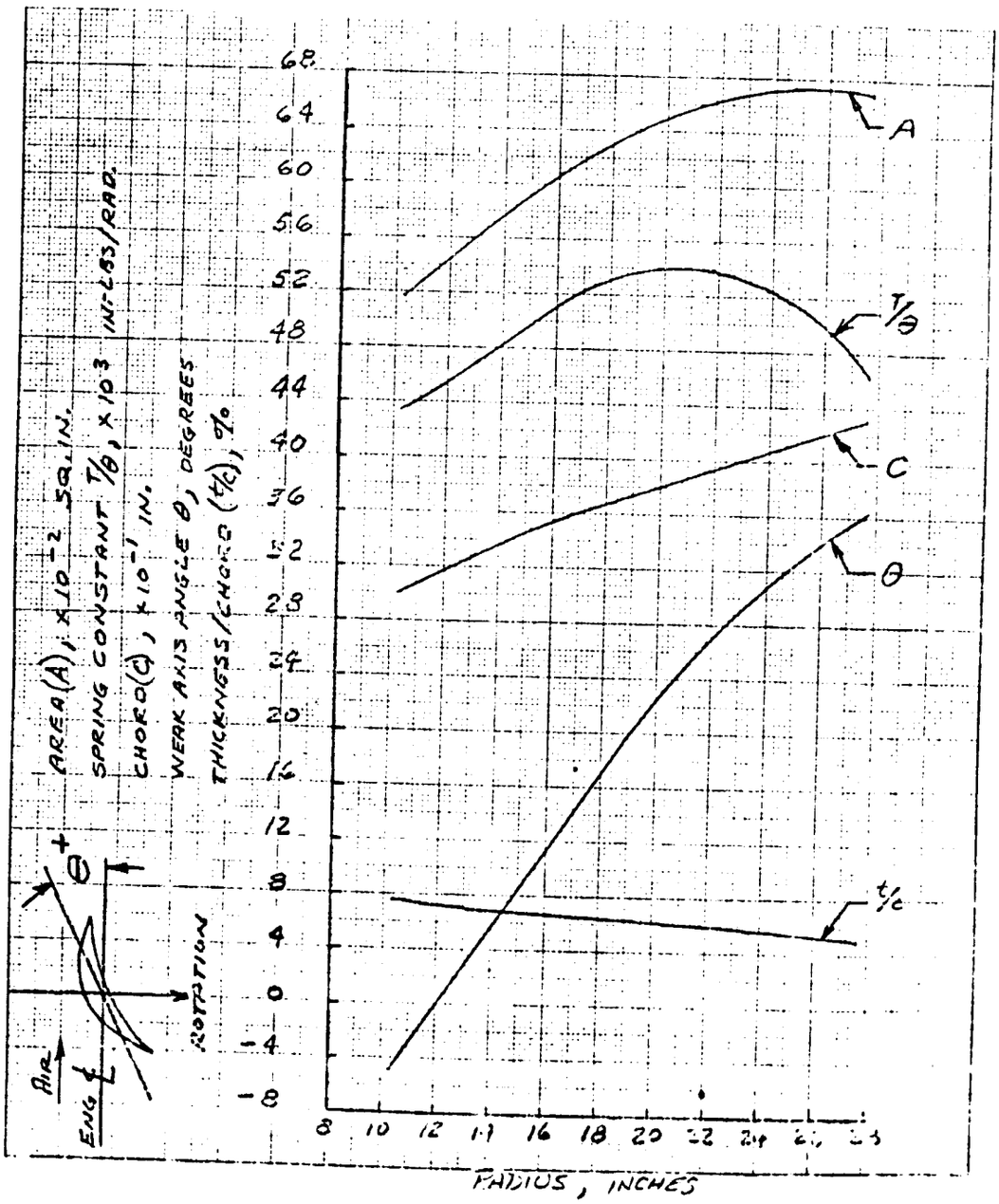

Figure 37

FAN ROTOR BLADE SECTION MODULUS

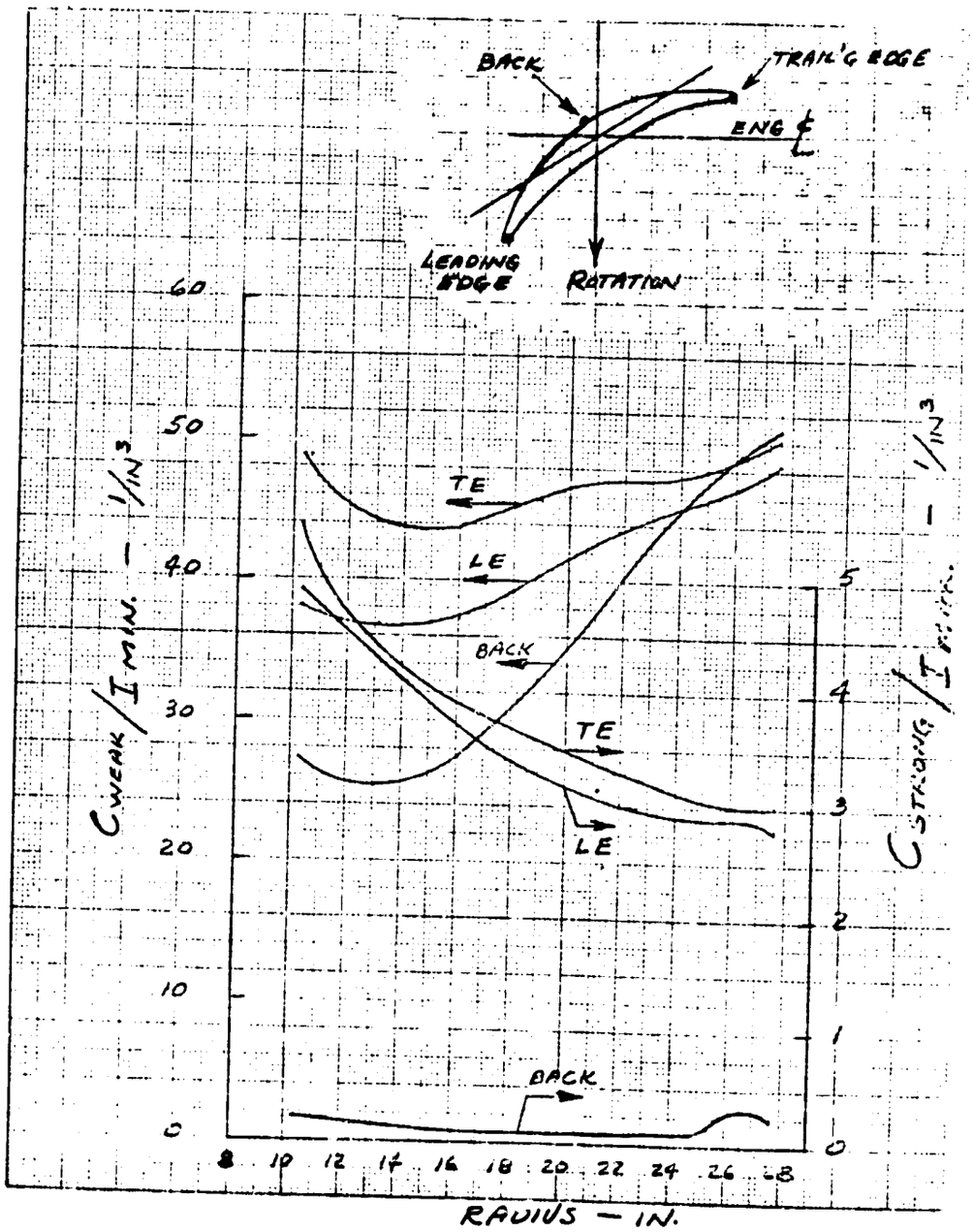

Figure 38

FAN ROTOR BLADE STRESS - STEADY-STATE

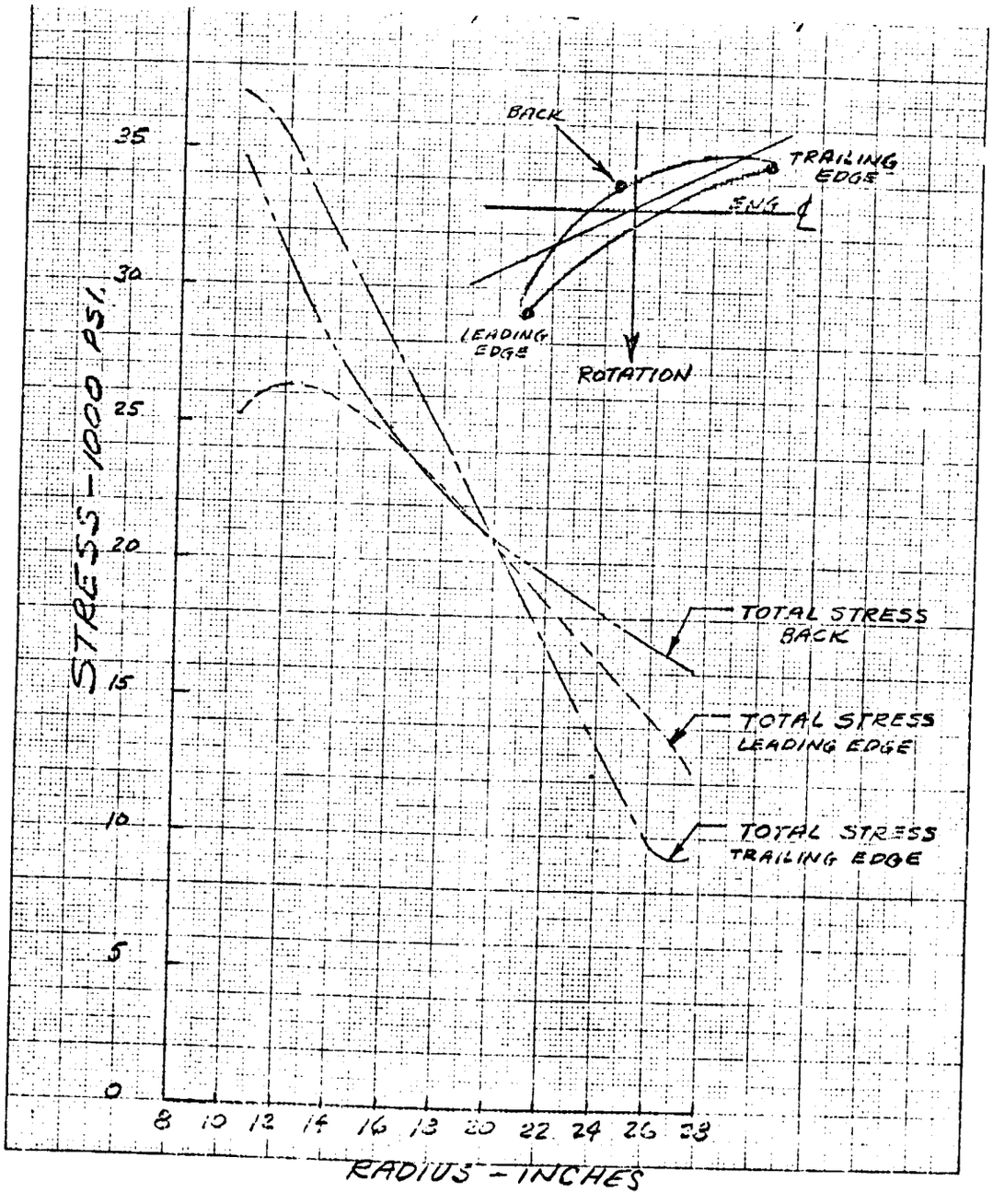

Figure 39

FAN ROTOR BLADE STRESS - STEADY-STATE PLUS UPWARD GYRO FORCE

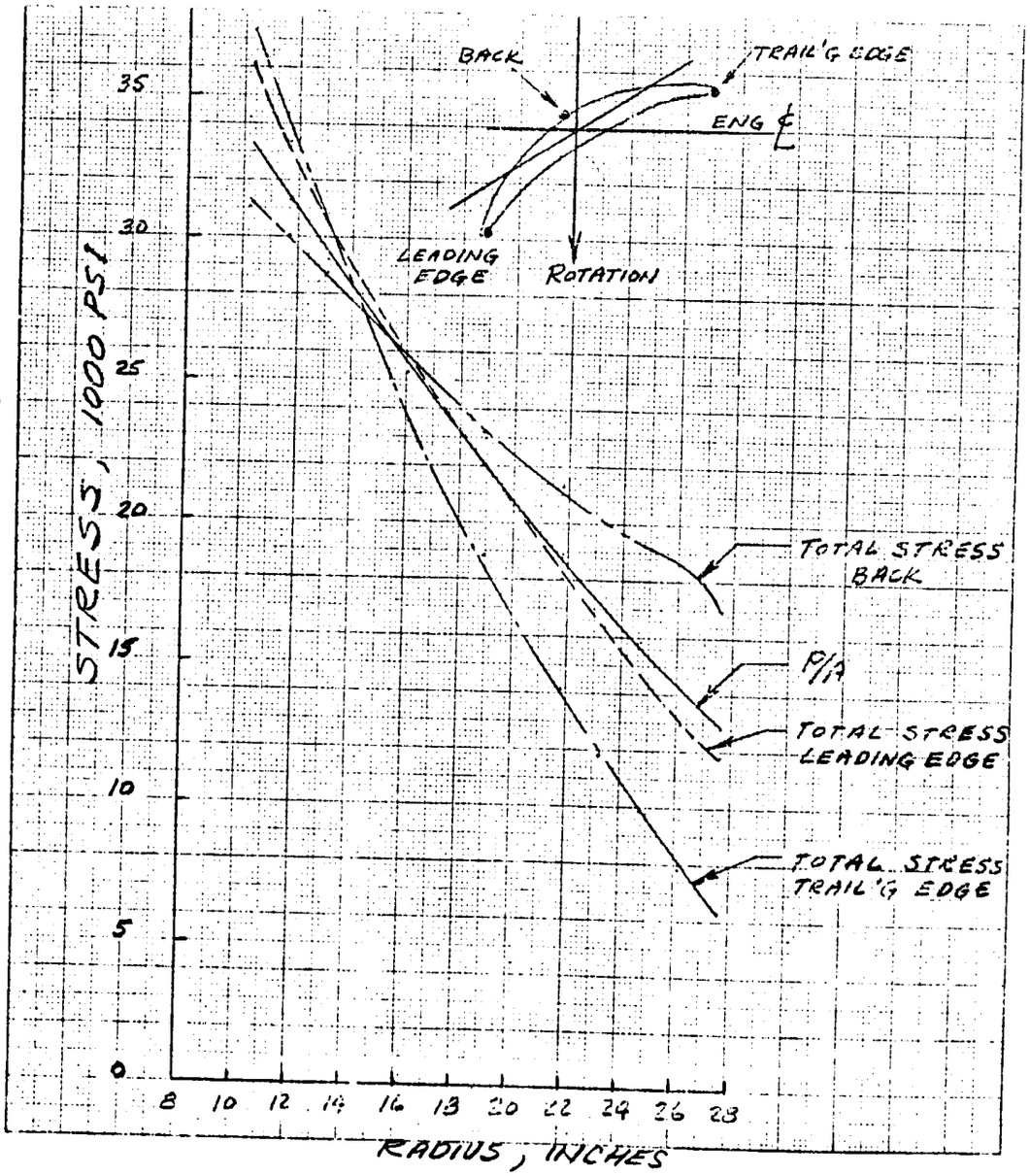

Figure 40

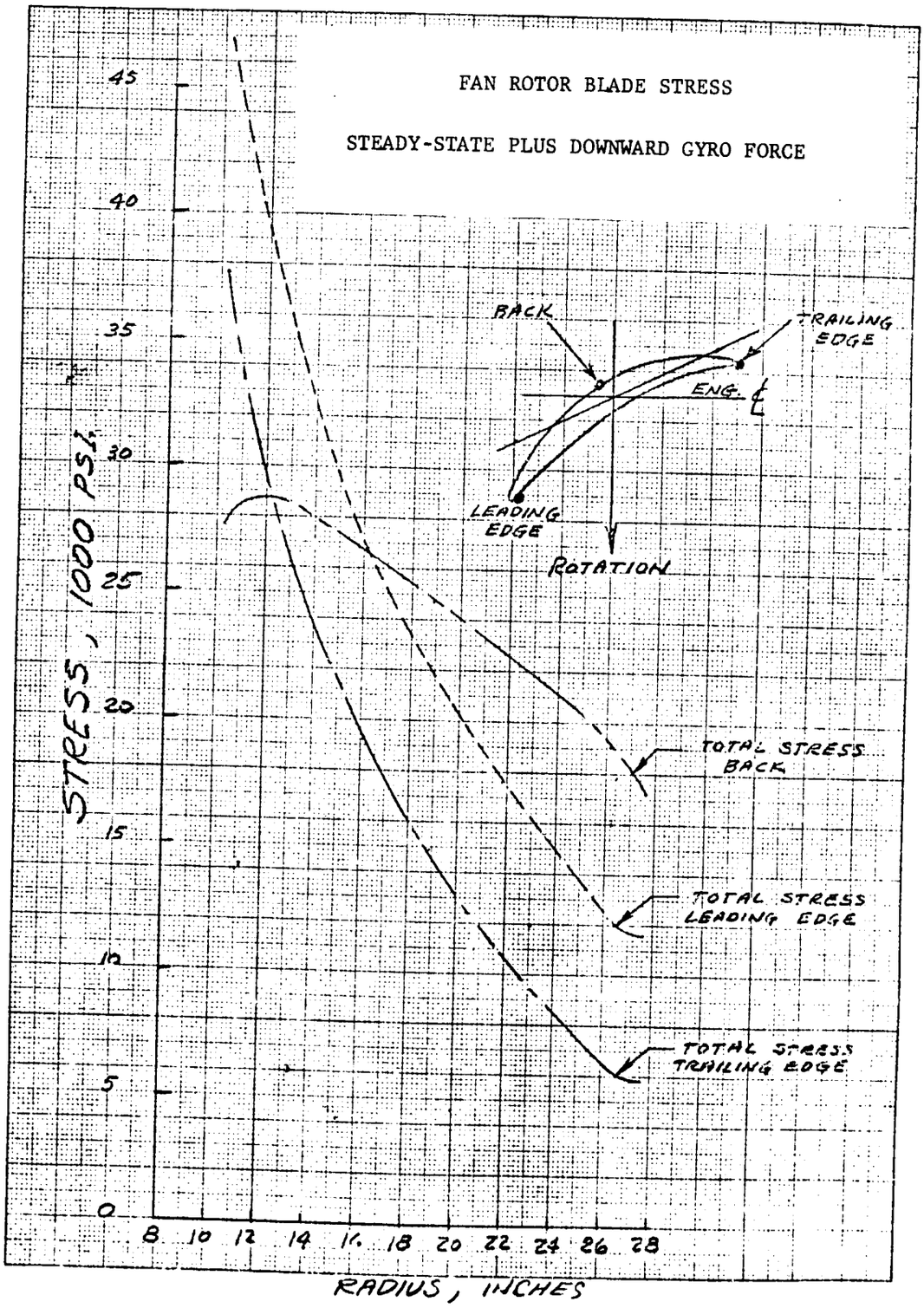
FAN ROTOR BLADE STRESS
STEADY-STATE PLUS DOWNWARD GYRO FORCE
STRESS, 1000 PSI
45
40
35
30
25
20
15
10
5
0
8
10
12
14
16
18
20
22
24
26
28
RADIUS, INCHES
BACK
TRAILING EDGE
ENG.
LEADING EDGE
ROTATION
TOTAL STRESS BACK
TOTAL STRESS LEADING EDGE
TOTAL STRESS TRAILING EDGE

Figure 41

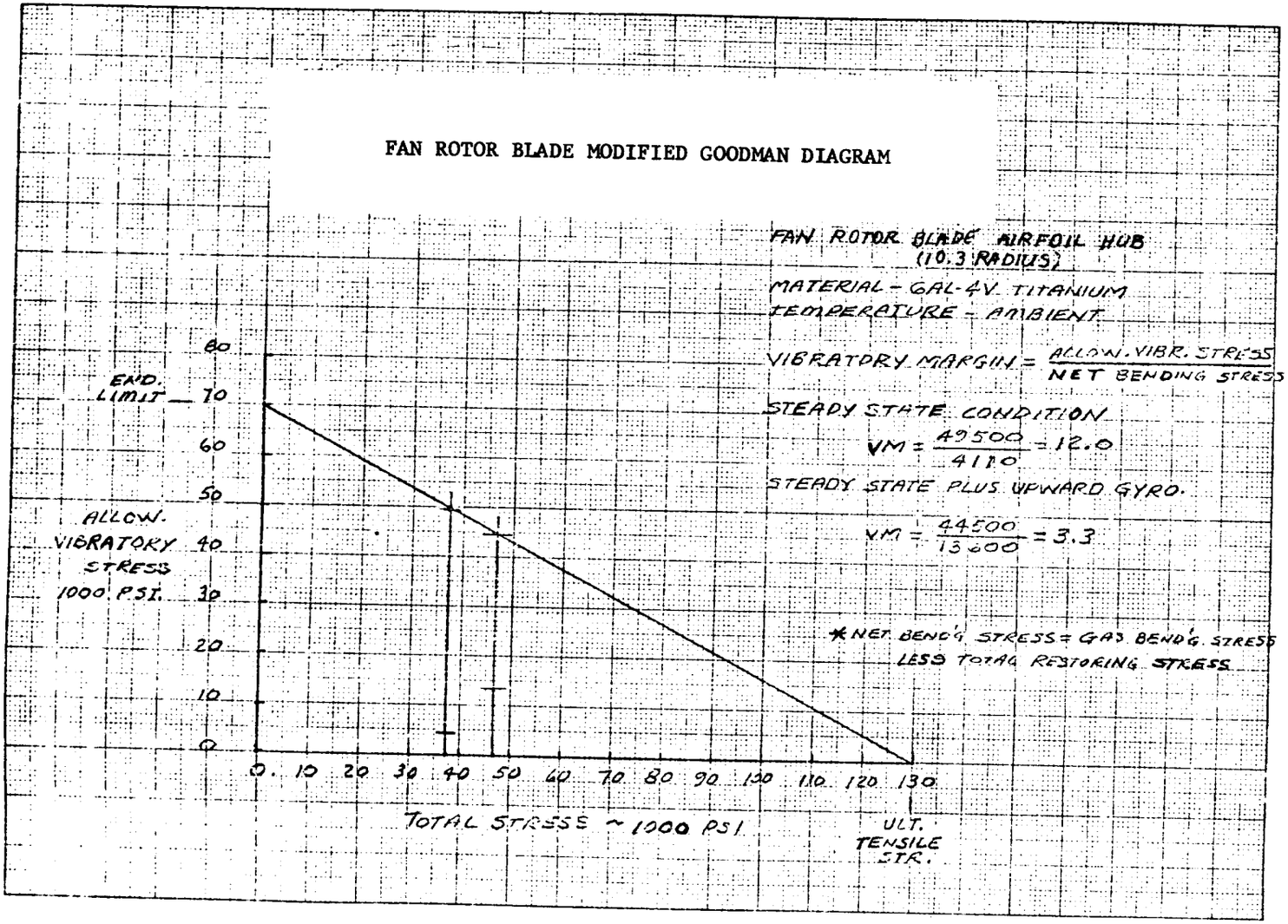
FAN ROTOR BLADE MODIFIED GOODMAN DIAGRAM
FAN ROTOR BLADE AIRFOIL HUB (10.3 RADIUS)
MATERIAL - 6AL-4V. TITANIUM
TEMPERATURE - AMBIENT
VIBRATORY MARGIN = ALLOW. VIBR. STRESS / NET BENDING STRESS *
STEADY STATE CONDITION
VM = 49500 / 4110 = 12.0
STEADY STATE PLUS UPWARD GYRO.
VM = 44500 / 13600 = 3.3
* NET BEND'G STRESS = GAS BEND'G STRESS LESS TOTAL RESTORING STRESS
END. LIMIT
ALLOW. VIBRATORY STRESS 1000 P.S.I.
80
70
60
50
40
30
20
10
0
0 10 20 30 40 50 60 70 80 90 100 110 120 130
TOTAL STRESS ~ 1000 PSI
ULT. TENSILE STR.

Figure 42

			Total Stress	Net Bending Stress	Allowable Vibratory Stress	Vibratory Margin
CONDITION 1 STEADY-STATE						
Obtuse Corner	Firtree Upper Neck	Forward	23684.	1294.	61336.	47.409
		Aft	22074.	-1294.	62265.	48.126
	Firtree Lower Neck	Forward	23119.	1510.	61662.	40.826
		Aft	21210.	-1510.	62764.	41.555
	Tenon Upper Neck	Forward	22204.	-2232.	62190.	27.868
		Aft	24972.	2232.	60593.	27.152
	Tenon Lower Neck	Forward	20443.	-3234.	63206.	19.543
		Aft	24688.	3234.	60757.	18.786
Acute Corner	Firtree Upper Neck	Forward	21273.	-1882.	62727.	33.333
		Aft	23765.	1882.	61290.	32.570
	Firtree Lower Neck	Forward	20606.	-2160.	63112.	29.213
		Aft	23439.	2160.	61477.	28.456
	Tenon Upper Neck	Forward	24856.	1511.	60660.	40.156
		Aft	23073.	-1511.	61688.	40.837
	Tenon Lower Neck	Forward	24269.	2480.	60999.	24.597
		Aft	21154.	-2480.	62796.	25.322
CONDITION 2 STEADY-STATE PLUS UPWARD AXIAL FORCE DUE TO GYROSCOPIC MOMENT						
Obtuse Corner	Firtree Upper Neck	Forward	19498.	-4703.	63751.	13.554
		Aft	26260.	4703.	59850.	12.725
	Firtree Lower Neck	Forward	18734.	-4976.	64192.	12.901
		Aft	25595.	4976.	60234.	12.105
	Tenon Upper Neck	Forward	21370.	-3120.	62671.	20.089
		Aft	25806.	3120.	60112.	19.269
	Tenon Lower Neck	Forward	20935.	-1958.	62922.	32.133
		Aft	24197.	1958.	61040.	31.172
Acute Corner	Firtree Upper Neck	Forward	20241.	-2983.	63322.	21.225
		Aft	24797.	2983.	60694.	20.344
	Firtree Lower Neck	Forward	19989.	-2818.	63468.	22.526
		Aft	24056.	2818.	61121.	21.693
	Tenon Upper Neck	Forward	20382.	-5340.	63241.	11.842
		Aft	27548.	5340.	59107.	11.068
	Tenon Lower Neck	Forward	18874.	-5311.	64111.	12.072
		Aft	26548.	5311.	59684.	11.239

FOLDOUT FRAME 1

FAN ROTOR BLADE FIR TREE AND TENON STRESSES

C.F. Load at Uppper Fir Tree Neck = 18,272 1b.

Net Bending Moment (Lb. In.)	Axial	Tan.
Steady State Condition	-107	135
Steady State + Up. Gyro	-1382	121

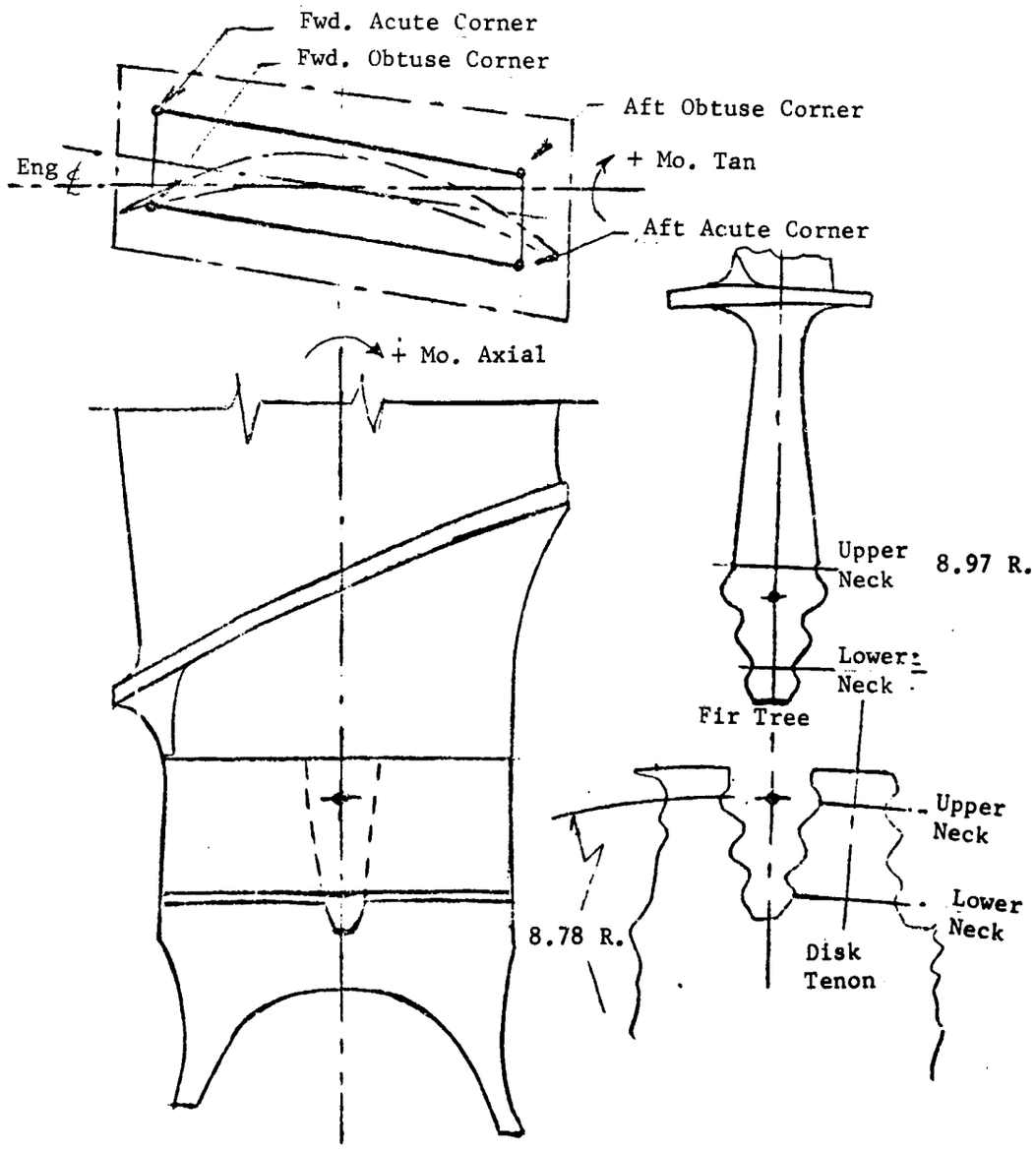

FOLDOUT FRAME 2

Figure 43

FAN ROTOR BLADE FORWARD TANG STRESSES

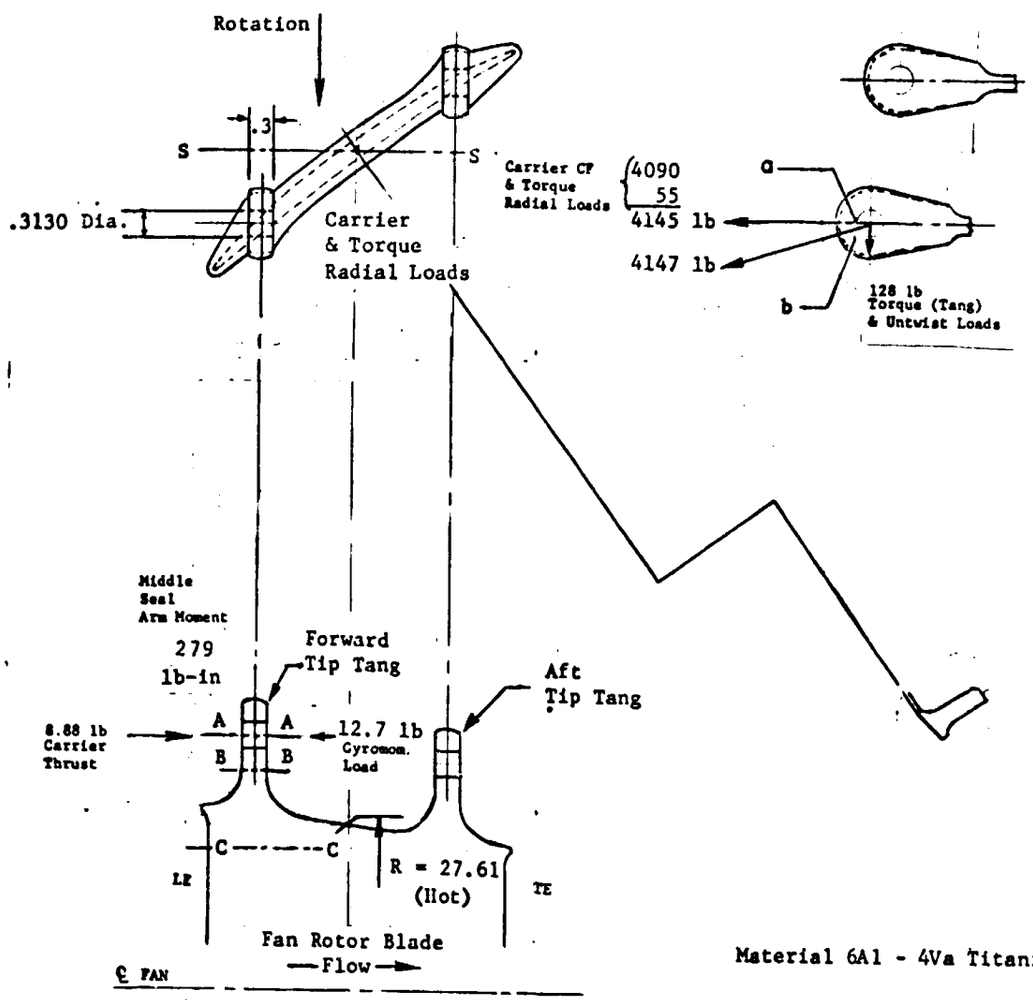

Material 6A1 - 4Va Titanium

Location	Type of Load	T - °F	Stress-Psi	Allowable Strength-Psi	M. S.
a	Bearing (Steady State)	578	88,700	123,500	+ .39
b	Tearout (Steady State)	578	31,800	49,500	+ .56
A-A	Tension + Bending (Steady State)	578	53,500	82,500	+ .54
B-B	Tension + Bending				
	1) Steady State	578	64,836	82,500	+ .27
	2) S. S. + Gyro	578	66,386	82,500	+ .24
C-C	Tension + Bending				
	1) Steady State	300	40,890	96,000	+1.35
	2) S. S. + Gyro	300	45,960	96,000	+1.08

Figure 44

FAN ROTOR DISK RIM LOADS

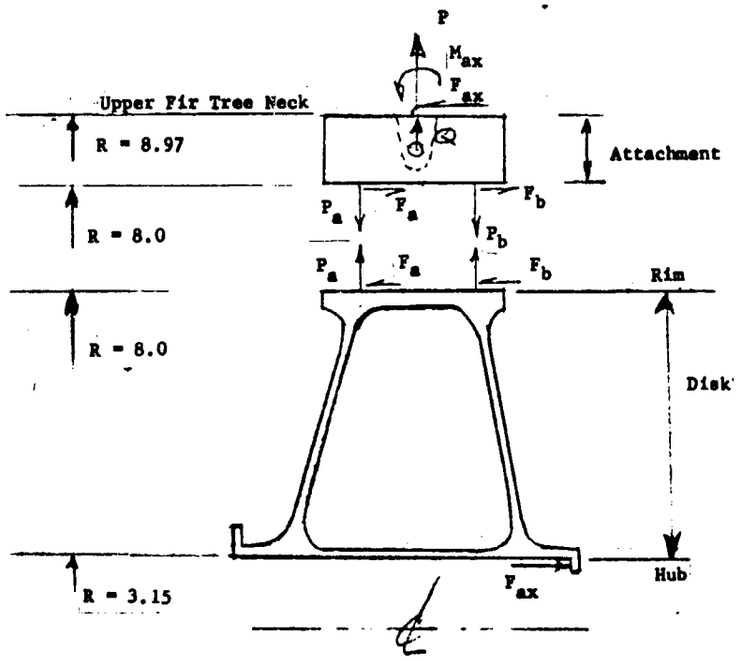

Condition	P lbs/Bl	M_{ax} lb-in/Bl	F_{ax} lbs/Bl	Q lb/in cir.	Disk Rim Loads - lbs/in of cir.			
					P_a	P_b	F_a	F_b
Steady State	18,283	107	56.3	1060	9,190	9,397	26.90	26.90
Gyro. + Steady State	18,283	1156	140	1060	8,471	10,116	66.85	66.85

Figure 45

FAN ROTOR DISC STRESSES

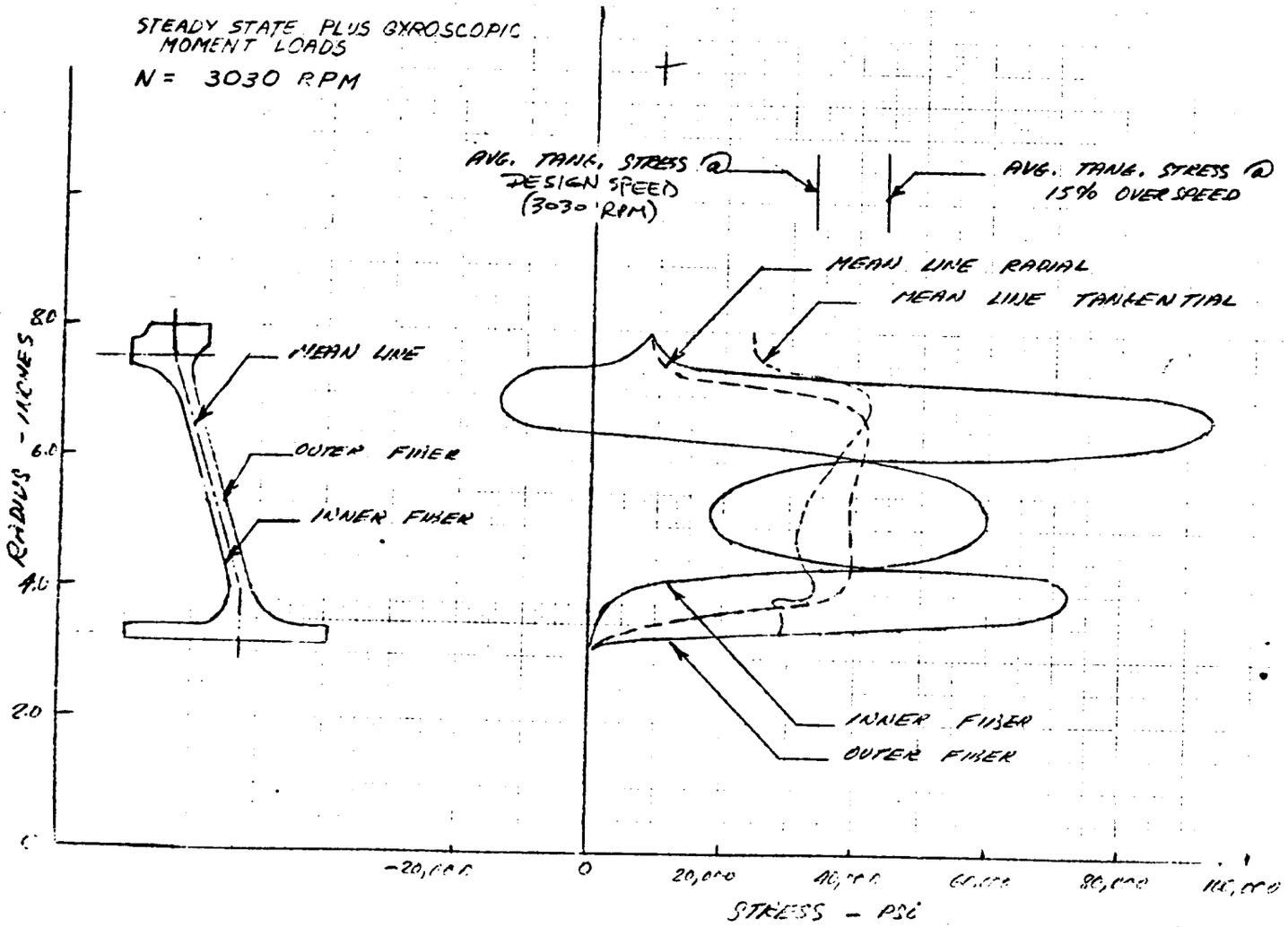

Figure 46

FAN ROTOR BLADE INTERFERENCE DIAGRAM — SECOND MODE (FIXED-FIXED)

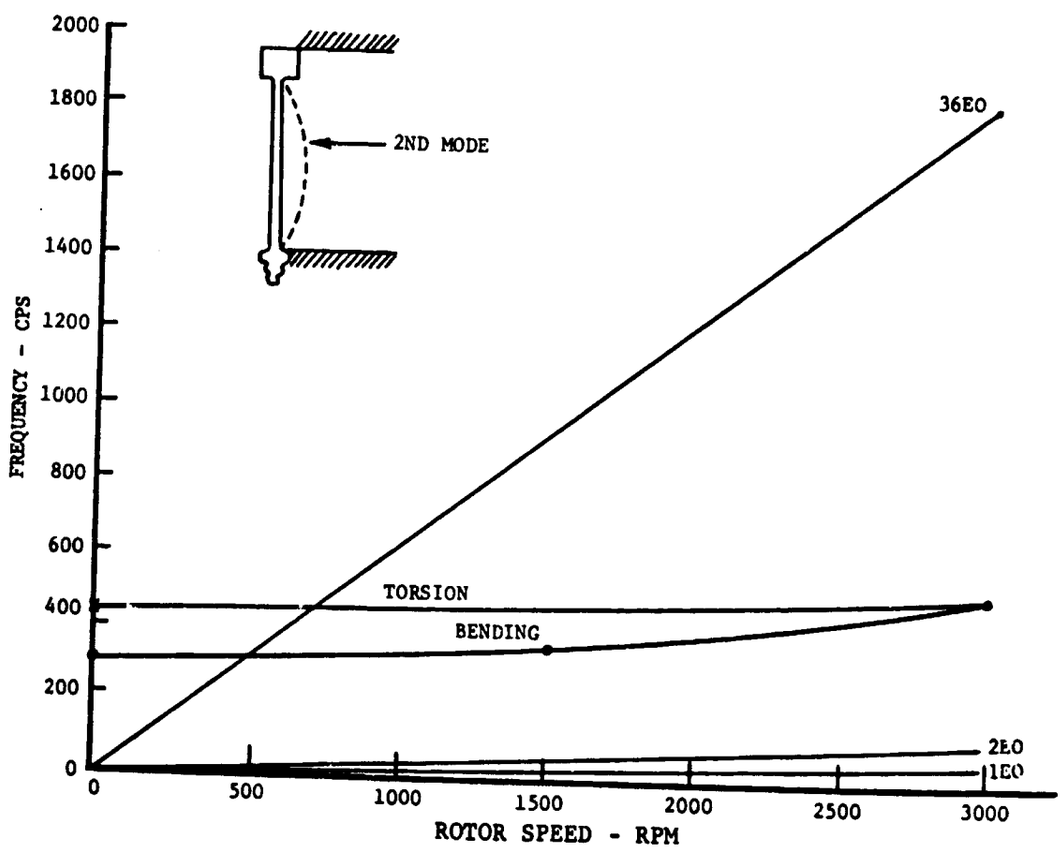

Figure 47

FAN ROTOR BLADE INTERFERENCE DIAGRAM – FIRST MODE (FIXED-FREE)

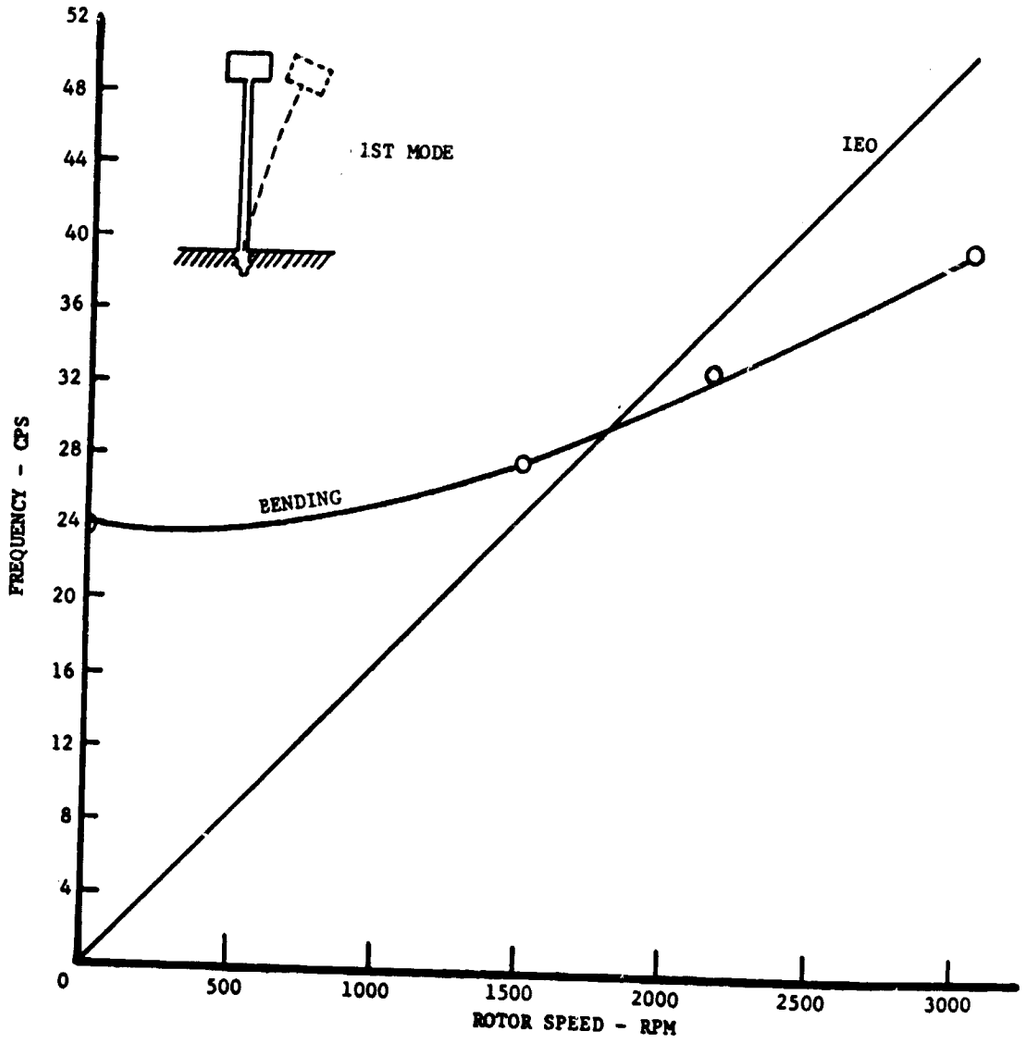

Figure 48

TURBINE ROTOR BLADE AND CARRIE

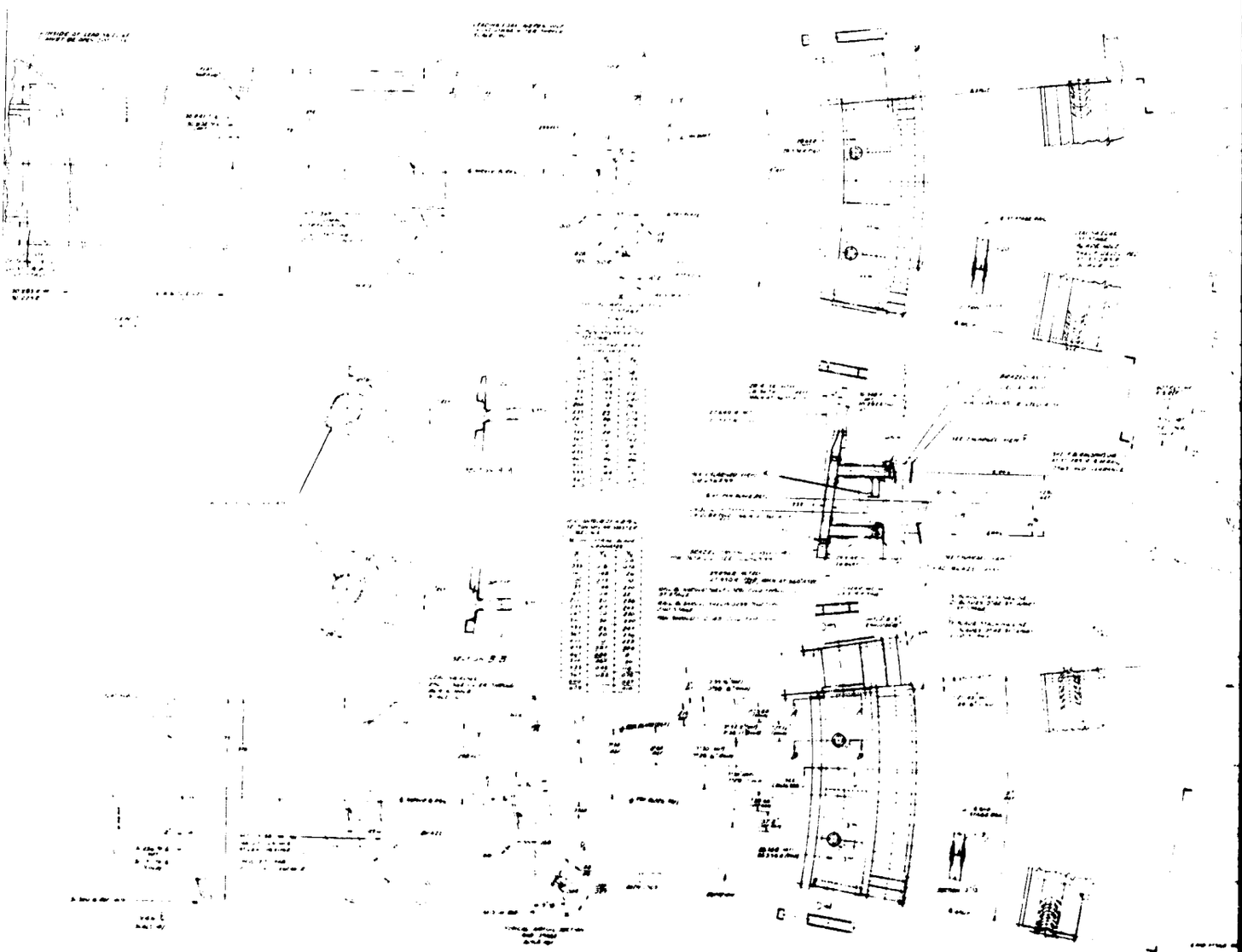

FOLDOUT FRAME 1

R BLADE AND CARRIER ASSEMBLY

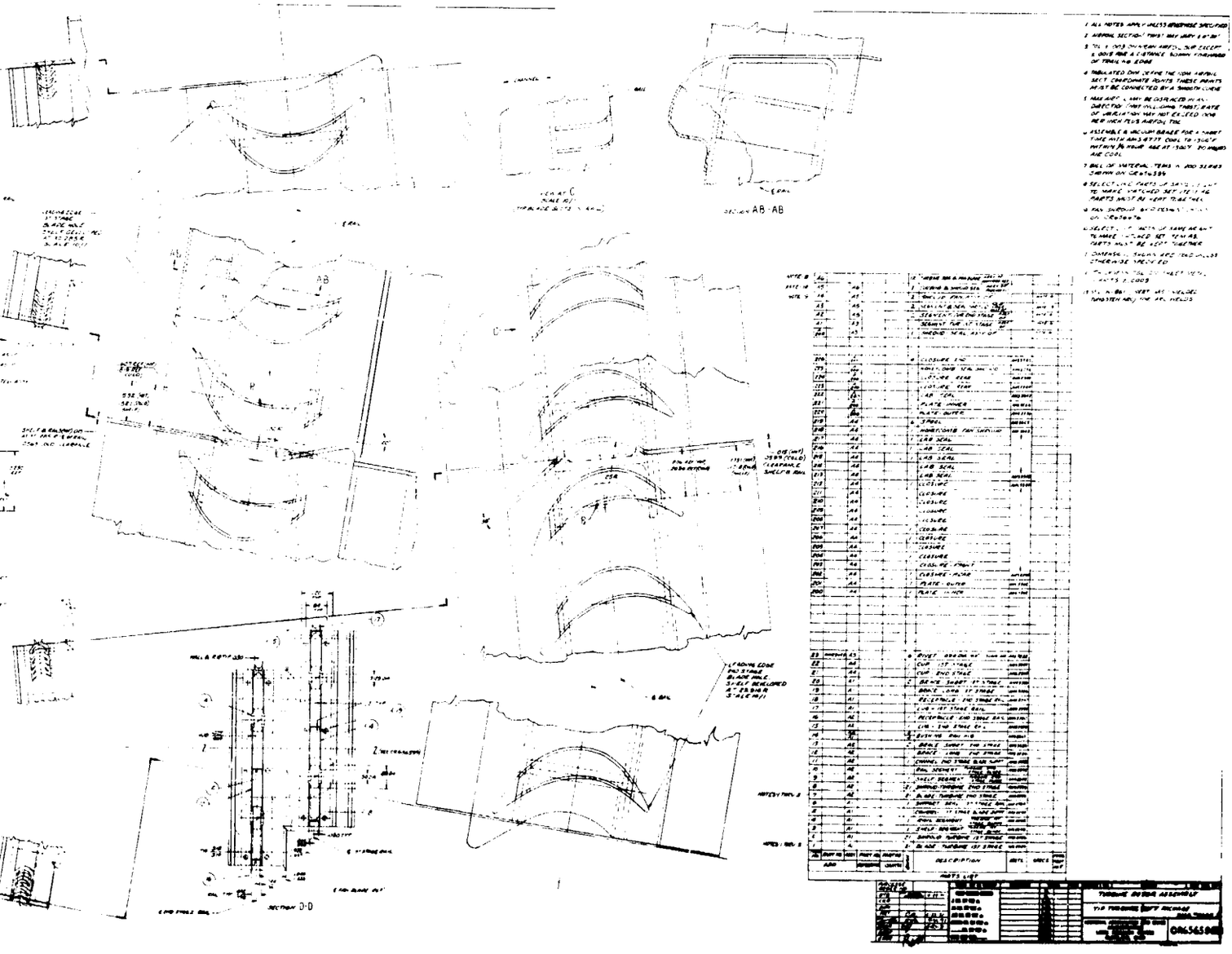

FOLDOUT FRAME 2

Figure 49

FAN AIR SHROUD

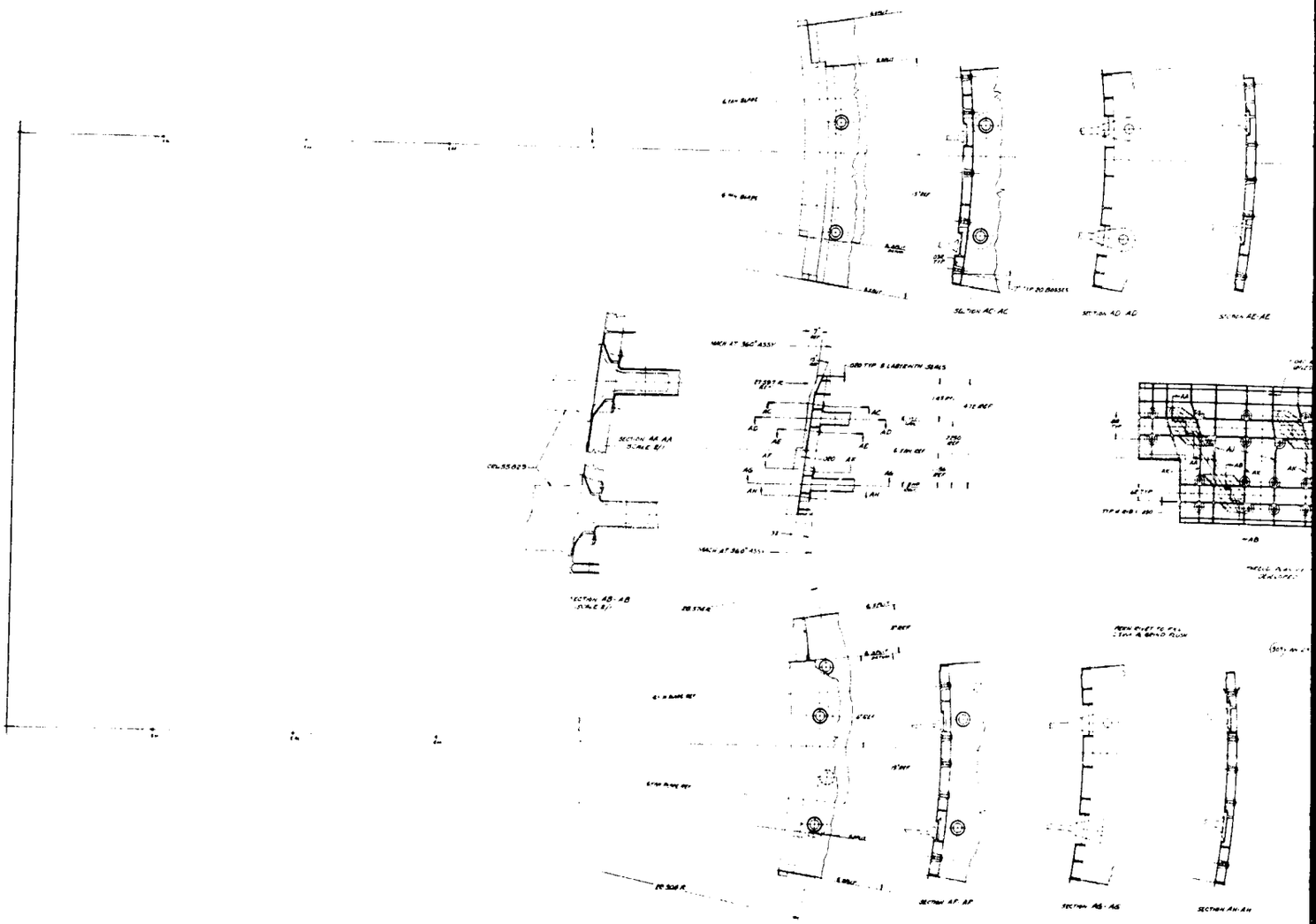

FOLDOUT FRAME 1

FAN AIR SHROUD

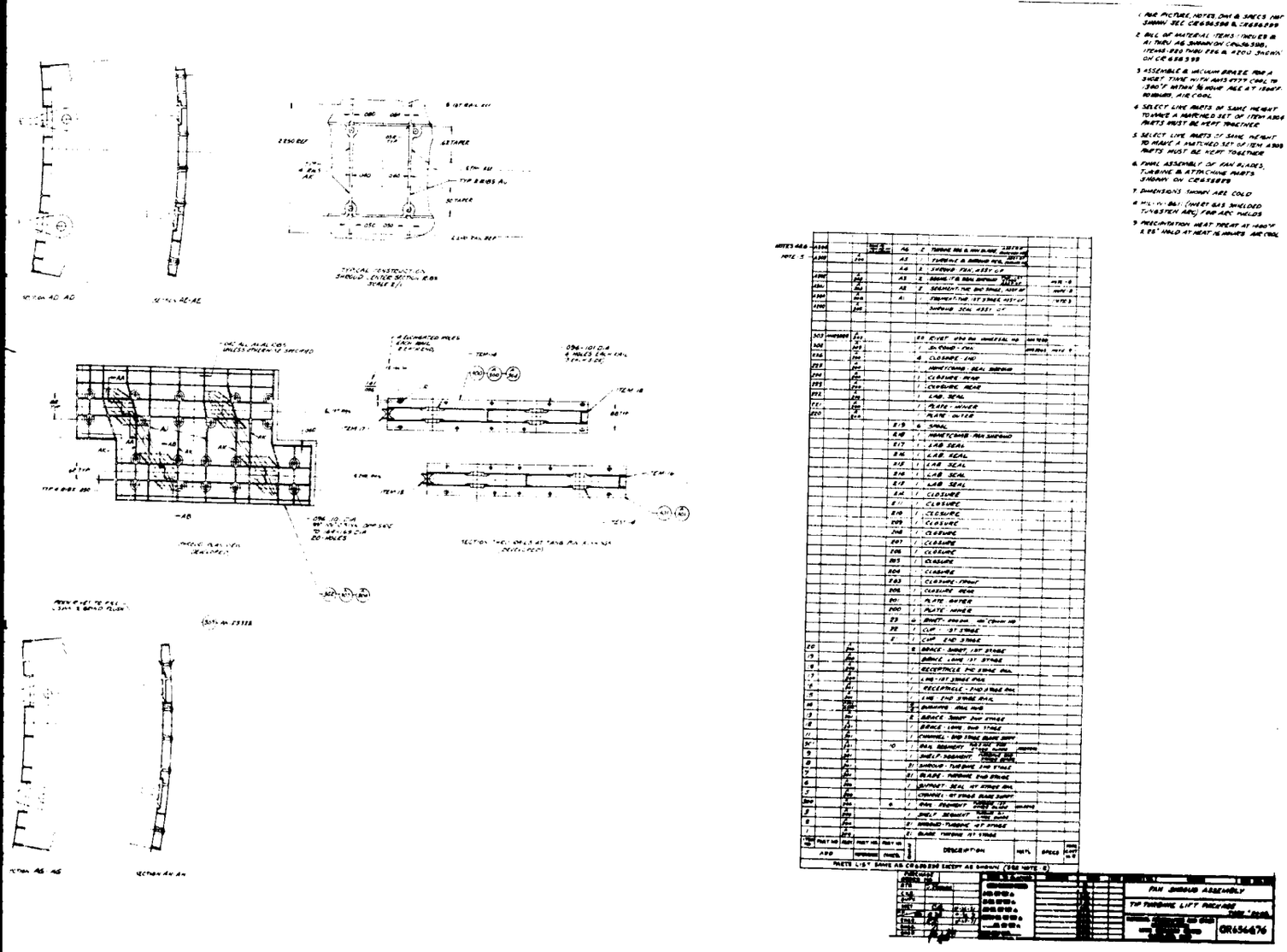

FOLDOUT FRAME 2

Figure 50

MIDDLE SEAL SUPPORT A

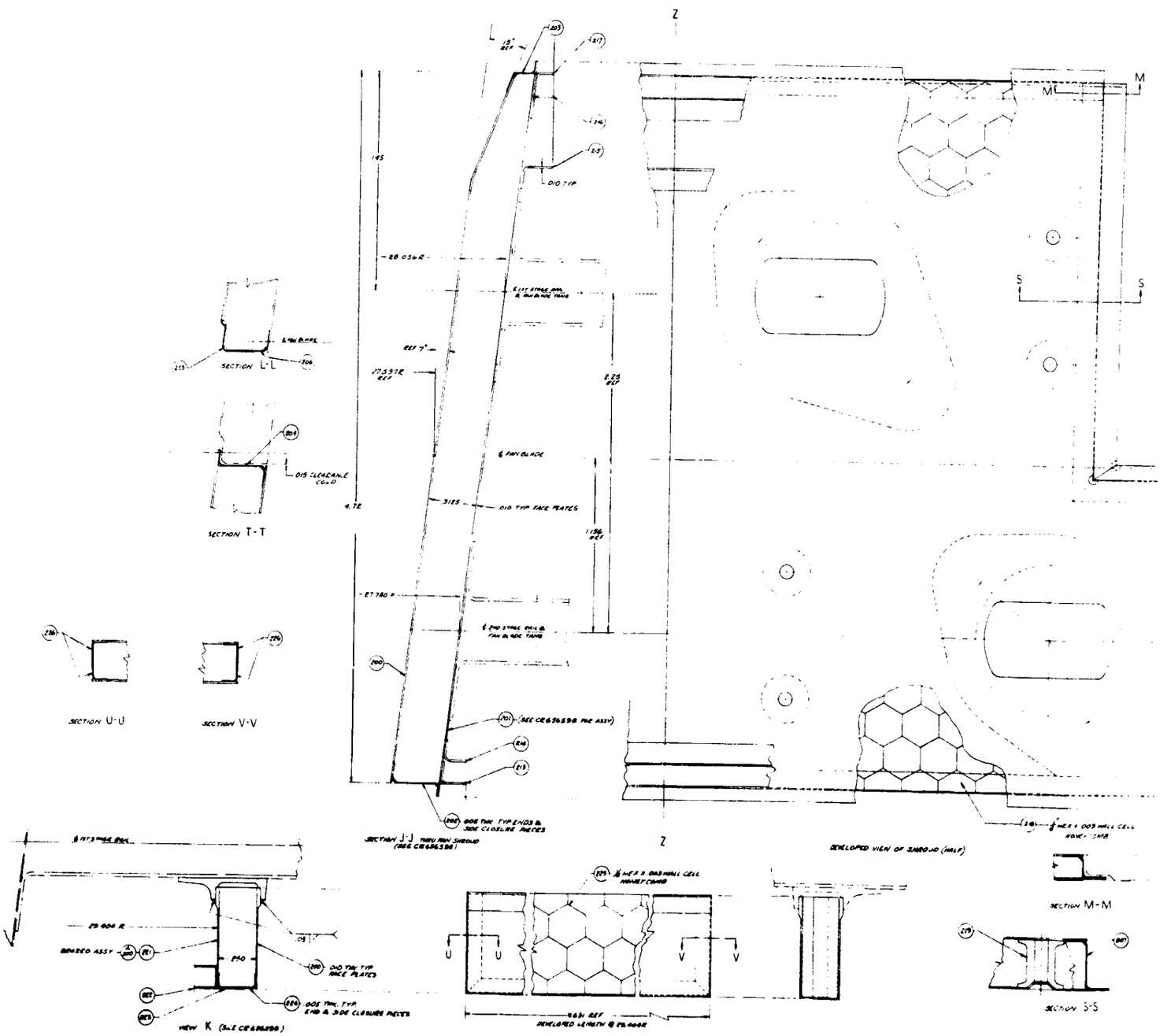

FOLDOUT FRAME 1

71-0246

DDLE SEAL SUPPORT ARM

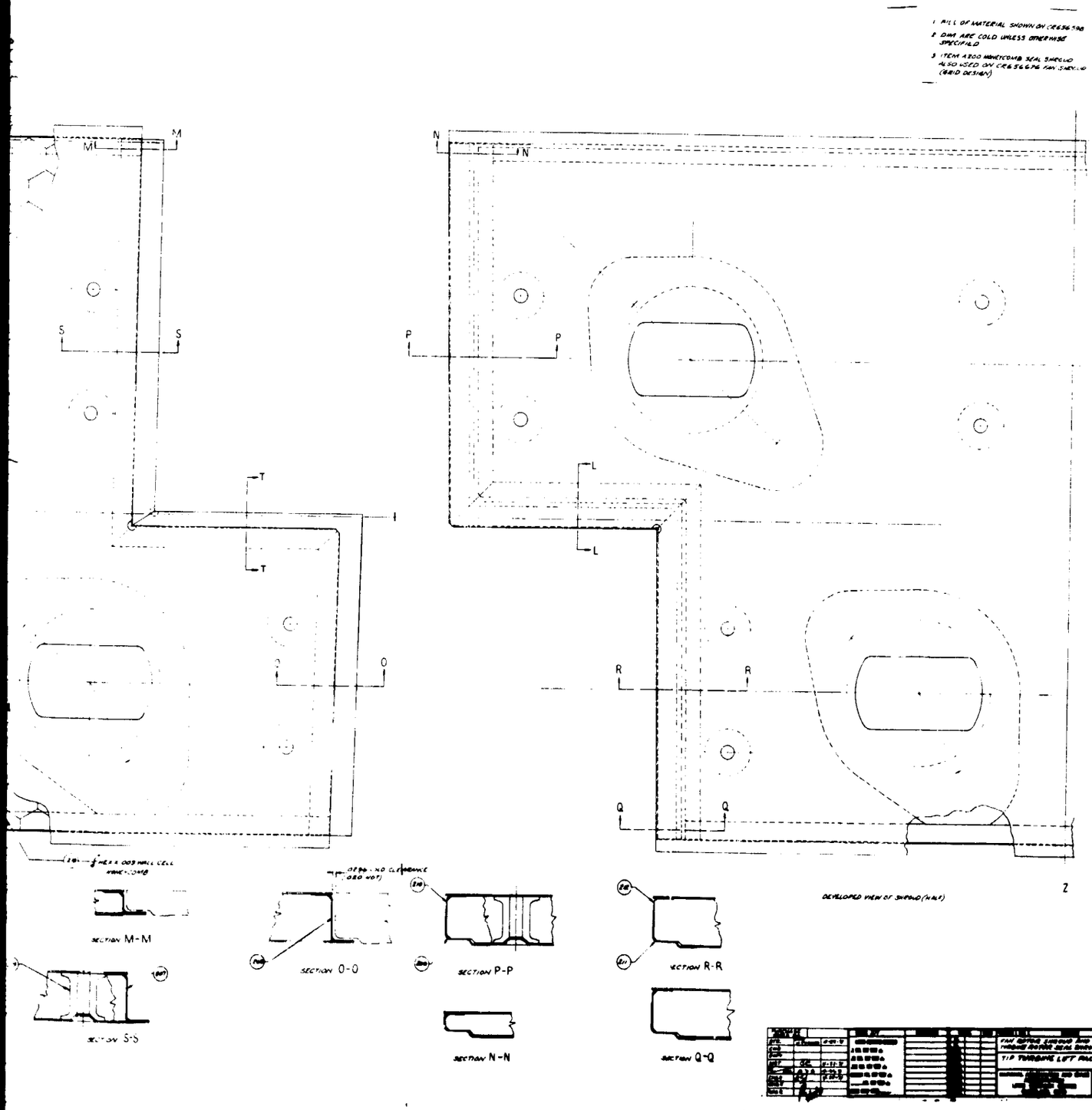

FOLDOUT FRAME 2

Figure 51

A. AIRFOIL @ SECT. A-A

Material Data

Temp.	-	1167°F
Matl.	-	Hastelloy X
U.T.S.	-	72,000 psi
.2%Y.	-	30,000 psi
.2% Creep (1000 Hrs.)	-	11,000 psi
Rupture (1000 Hrs.)	-	33,500 psi
Endurance Limit	-	35,000 psi

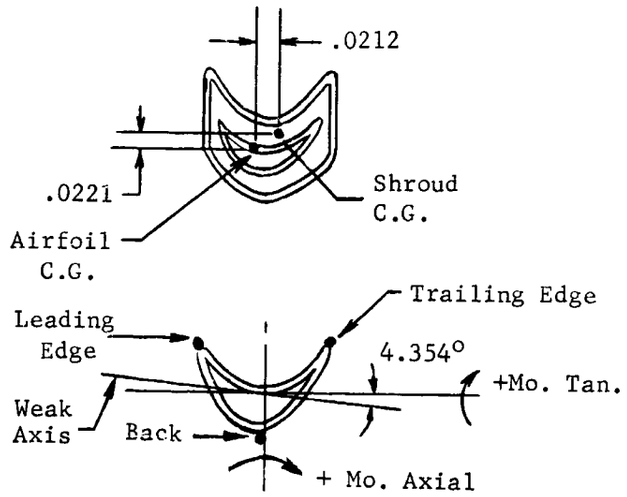

Section A - A

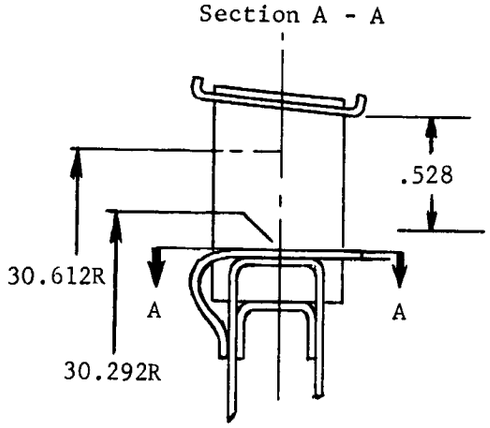

Loads (Centrifugal), lbs/blade

Shroud	6.746
Airfoil	24.699
Total	31.445

Cross-Section Area - .01534 sq. in.

Bending Moments, lb-in/blade

	Weak	Strong
Shroud Offset	- .160	-.1313
Gas	-1.761	+.1293
Total	-1.921	-.002

Section Properties (C/I), i/m^3

	Weak	Strong
Leading Edge (LE)	-1393	+550
Trailing Edge (TE)	-1409	-576
Back	+1505	-

Sign Convention

\+ Tensile Stress
\- Compressive Stress

Stresses, Psi

Leading Edge (LE)

P/A	+2050
Gas Bending	+2531
Total Bending	+2674
P/A + Total Bending	+4724

Trailing Edge (TE)

P/A	+2050
Gas Bending	+2407
Total Bending	+2707
P/A + Total Bending	+4757

Back

P/A	+2050
Gas Bending	-2650
Total Bending	-2891
P/A + Total Bending	-841

B. BRAZ

1.
2.
3.
4.
5.
6.

C. SHELF

1. M
2. L
3. B
4. N

D. SHROU

1. M
2. L
3. T
4. S
5. M

AGE TURBINE ROTOR BLADE LOADS AND STRESSES

Edge

. Tan.

B. BRAZED ATTACHMENT

1. Material Data

temperature - 1017°F
material - Braze Alloy
allowable shear - 31,000 psi

	a	b	c	d
2. Location				
3. Loads (Radial), lbs	7.673	17.373	4.138	17.338
4. Shear Area				
h, in	.12	.12	.19	.19
t, in	.02	.02	.02	.02
Area (50% Coverage), in^2	.0012	.0012	.0019	.0019
5. Shear Stress, Psi	6400	14450	2180	9140
6. Margin of Safety	+3.85	+1.14	+13.20	+2.40

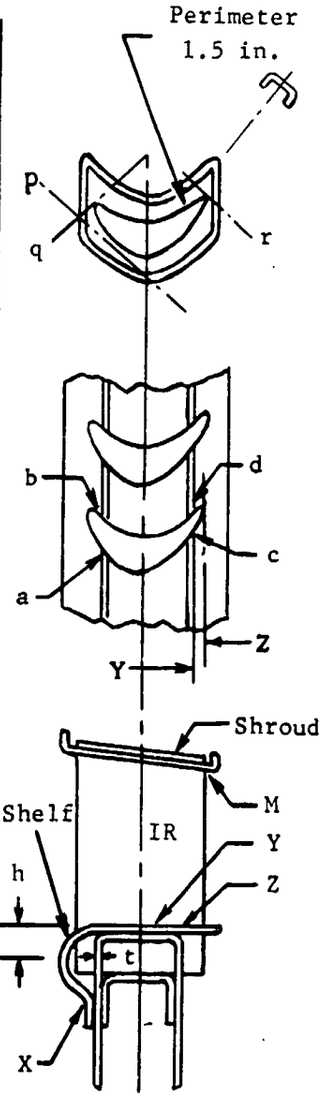

C. SHELF

1. Material Data

temperature - 1017°F
material - Inconel X
1000 Hr. Rupture - 78,500 psi

	x	y	z
2. Location			
3. Bending Stress, psi	32,600	23,000	4,300
4. Margin of Safety	+1.41	+2.40	+17.2

D. SHROUD

1. Material Data

temperature - 1200°F
material - Hastelloy X
1000 Hr. Rupture - 28,000 psi
Allowable Shear - 31,000 psi (Braze)

	p	q	r	m
2. Location				
3. Type of Stress	Bend.	Bend.	Bend.	Shear
4. Stress, psi	5,540	10,400	5,540	1,035
5. Margin of Safety	+4.00	+1.70	+4.00	+29.

Figure 52

FOLDOUT FRAME 2

SECOND STAGE

A. AIRFOIL @ SECT. B-B

Material Data

Temp - 928°F
Matl. - Hastelloy X
U.T.S. - 92,000 psi
.2%Y - 36,600 psi
.2% Creep (1000 Hrs) -
Rupture (1000 Hrs.) -
Endurance Limit - 35,000 psi

Loads (Centrifugal), lbs/bl

Shroud	7.843
Airfoil	52.196
Total	60.039

Cross-Section Area - .01576 sq. in.

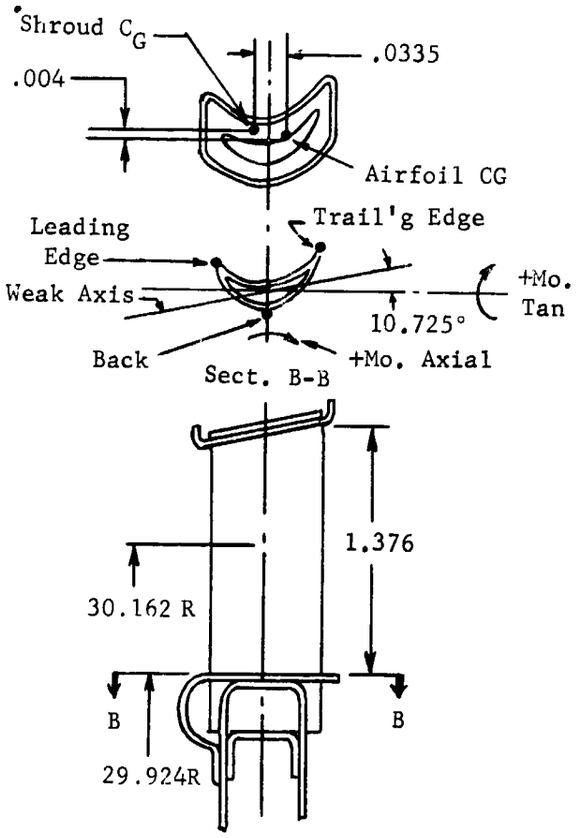

Bending Moments lb-in/bl

	Weak	Strong
Shroud Offset	- .078	+.2528
Gas	-2.068	-.0264
Total	-2.146	+.2264

Section Properties (C/I), $1/in^3$

	Weak	Strong
Leading Edge (LE)	-1752	+534
Trailing Edge (TE)	-1642	-514
Back	+1751	-

Sign Convention

\+ Tensile Stress
\- Compressive Stress

STRESSES, Psi

Leading Edge (LE)

P/A	+3810
Gas Bending	+3609
Total Bending	+3890
P/A + Total Bending	+7700

Trailing Edge (TE)

P/A	+3810
Gas Bending	+3410
Total Bending	+3414
P/A + Total Bending	+7224

Back

P/A	+3810
Gas Bending	-3621
Total Bending	-3770
P/A + Total Bending	+40

B. BRAZED AT

1. Ma'er
   te
   ma
   al
2. Locati
3. Loads
4. Shear
   h,
   t,
   Are
5. Shear
6. Margi

C. SHELF

1. Materi
   tem
   mat
   .2%
2. Locati
3. Bendi
4. Margi

D. SHROUD

1. Materi
   tem
   mat
   .2
   All
2. Locati
3. Type
4. Stress
5. Margi

FOLDOUT FRAME 1

71-345

SECOND STAGE TURBINE ROTOR BLADE LOADS AND STRESSES

B. BRAZED ATTACHMENT

1. Material Data

temperature - 928°F
material - Braze Alloy
allowable shear - 31,000 psi

	a	b	c	d
2. Location				
3. Loads (Radial), lbs	6.299	26.799	14.544	28.344
4. Shear Area				
h, in	.2	.2	.2	.2
t, in	.02	.02	.02	.02
Area (50% Coverage), in^2	.002	.002	.002	.002
5. Shear Stress, Psi	3,150	13,400	7,270	14,160
6. Margin of Safety	+8.83	+1.31	+3.27	+1.19

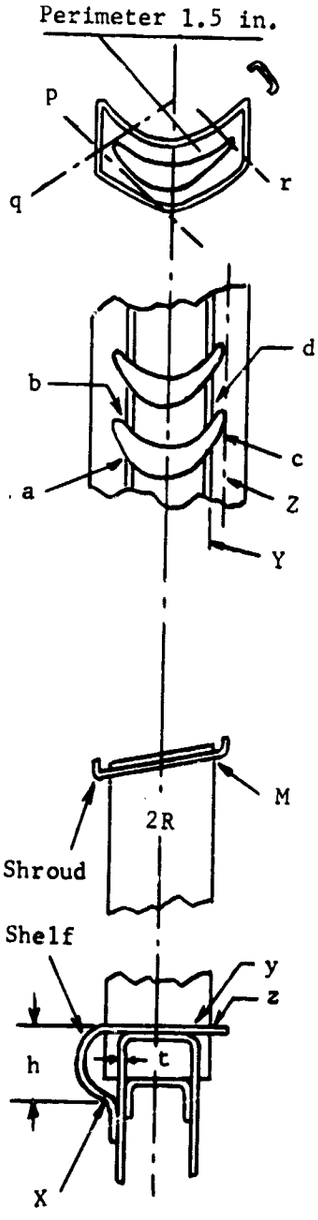

C. SHELF

1. Material Data

temperature - 928°F
material - Inconel X
.2% Yield Strength - 88,000 psi

	x	y	z
2. Location			
3. Bending Stress, psi	32,200	22,700	4,250
4. Margin of Safety	+1.74	+2.88	+19.7

D. SHROUD

1. Material Data

temperature - 915°F
material - Hastelloy X
.2% yield strength - 42,000 psi
Allowable Shear - 31,000 psi (Braze)

	p	q	r	m
2. Location				
3. Type of Stress	Bend.	Bend.	Bend.	Shear
4. Stress, psi	5,600	10,500	5,600	1,044
5. Margin of Safety	+6.5	+3.0	+6.5	+28.7

Figure 53

FOLDOUT FRAME 2

FIRST AND SECOND STAGE TURBINE ROTOR BLADE MODIFIED GOODMAN DIAGRAMS

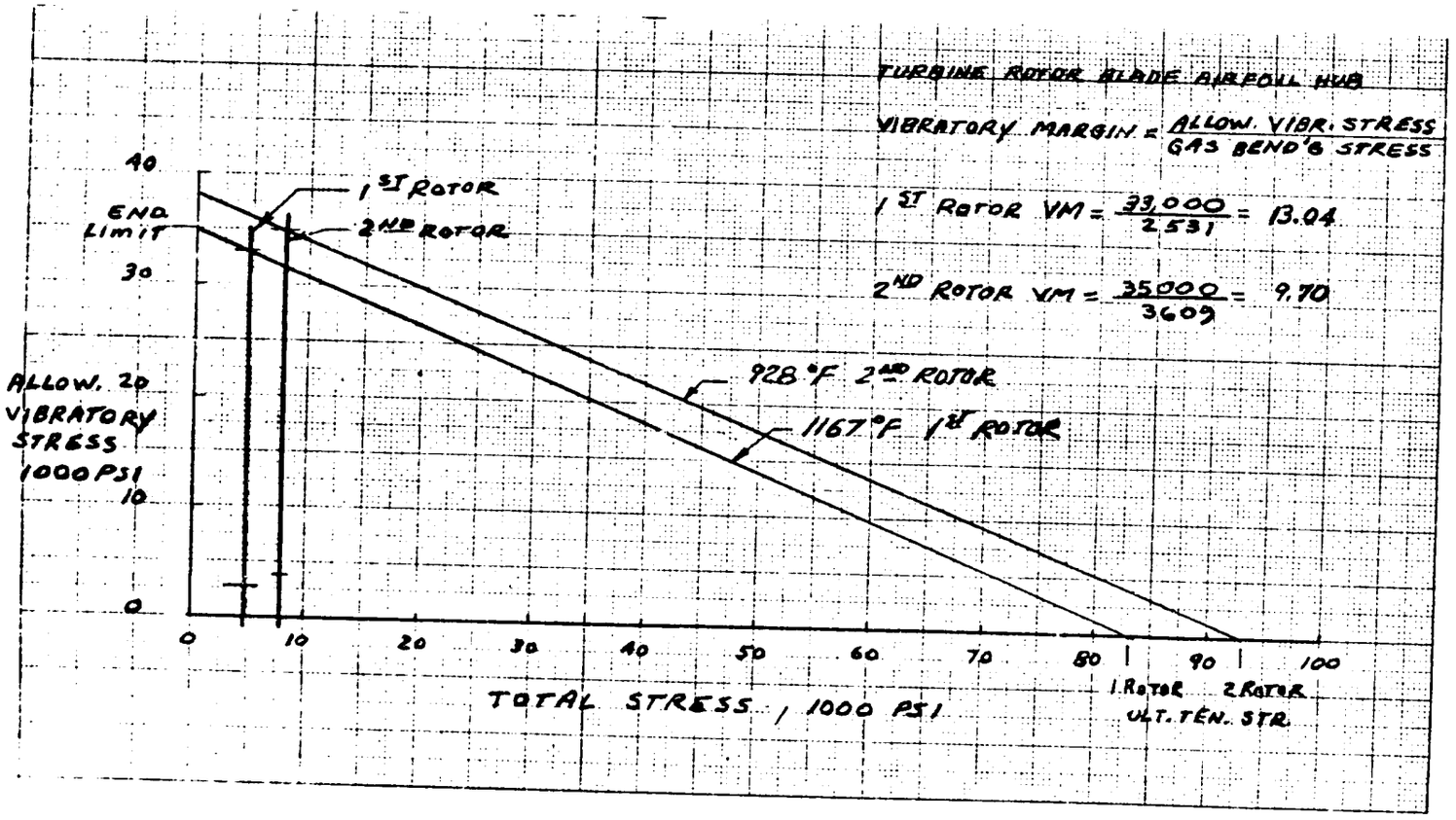

Figure 54

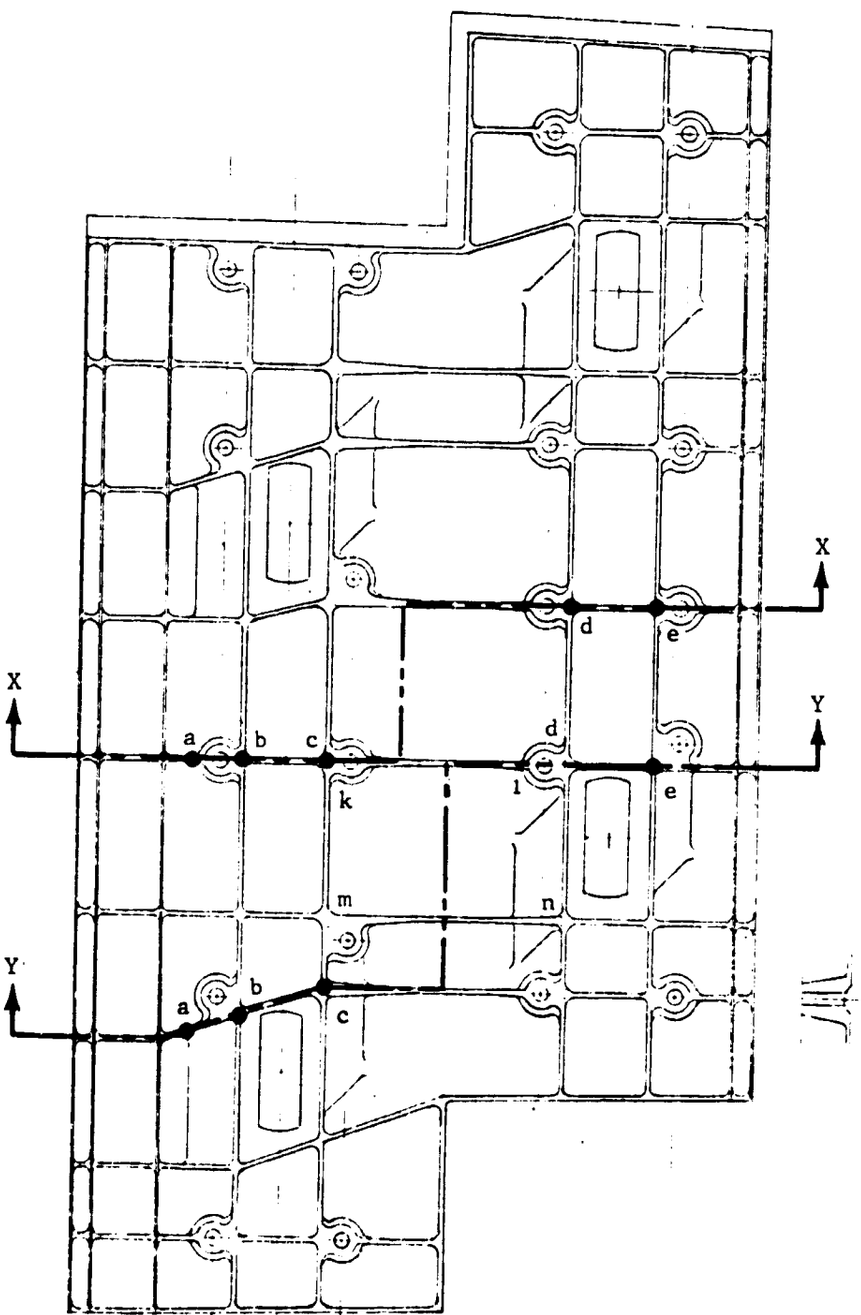

.005 in Steady State Deflection

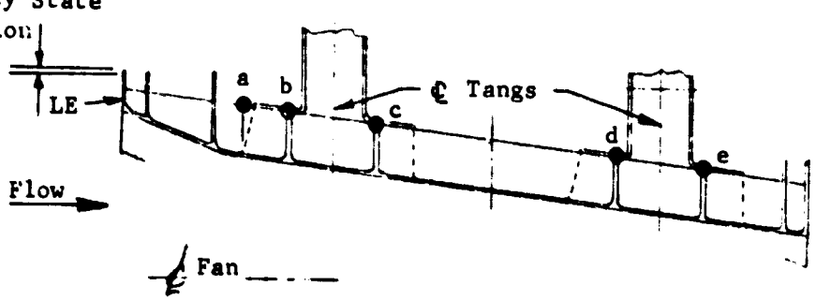

FOLDOUT FRAME 1

Flow

Fan

71-346

FAN AIR SHROUD STRESSES

A. Rib Structure

Material Rene 41

Location	a	b	c	d	e
Temperatures °F	372	372	1200*	1200*	925
Allowable Stress, Psi					
.2% Yield	126,000	126,000	114,000	114,000	119,000
1000 Hr. Rupture	-	-	74,000	74,000	-
1. Bending Stress @ Sect X-X					
Compressive Stress, Psi	65,900	112,100	59,900	-	-
M.S.	+0.91	+0.13	+0.23	-	-
2. Bending Stress @ Sect Y-Y					
Compressive Stress, Psi	50,900	99,500	54,000	58,900	77,000
M.S.	+1.48	+0.27	+0.37	+0.27	+0.54

B. Skin Panel (k, l, m, n)

Type of stress	:	Combined membrane and bending stress (all sides held)
Stress Location	:	Center of Panel
Temperature, °F	:	675
Skin Thickness, in.	:	.020
Allowable Stress Psi	:	122,500 Psi .2% yield
Stress Psi	:	42,500
M.S.	:	+1.88
Max Defiection, in.	:	0.013

* Heat transfer analysis indicate temp of 1081°F
1200°F assumed due to gas leakage.

FOLDOUT FRAME 2

Figure 55

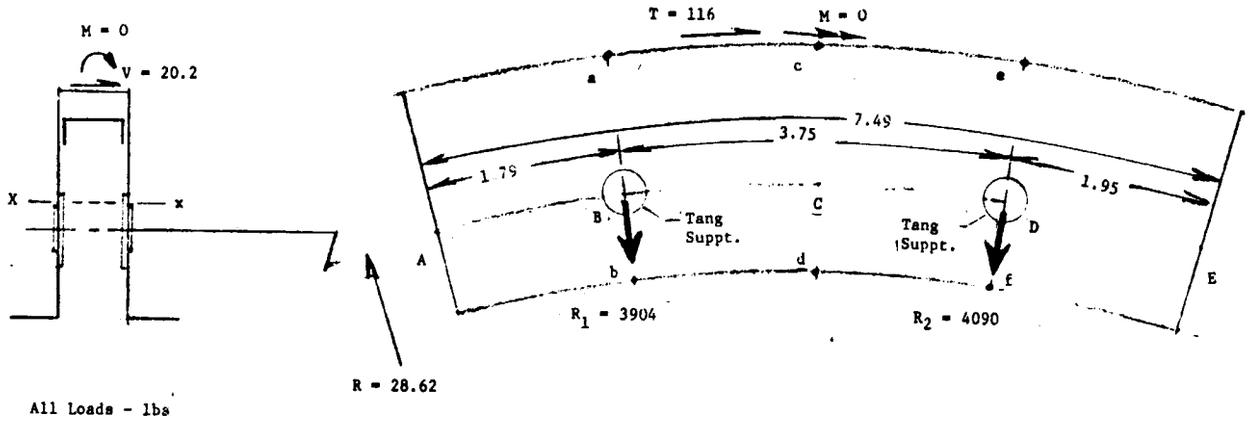

All Loads - lbs

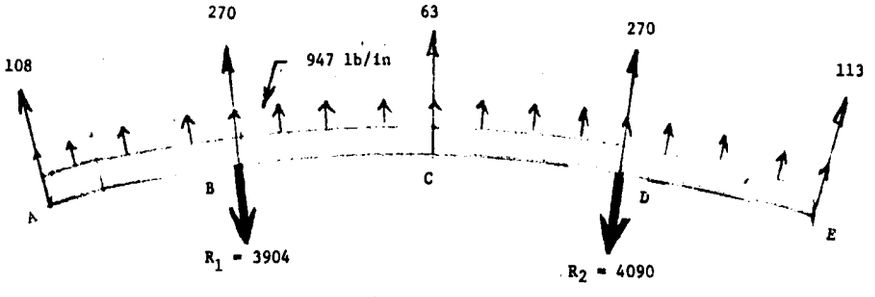

Carrier Loads - lbs

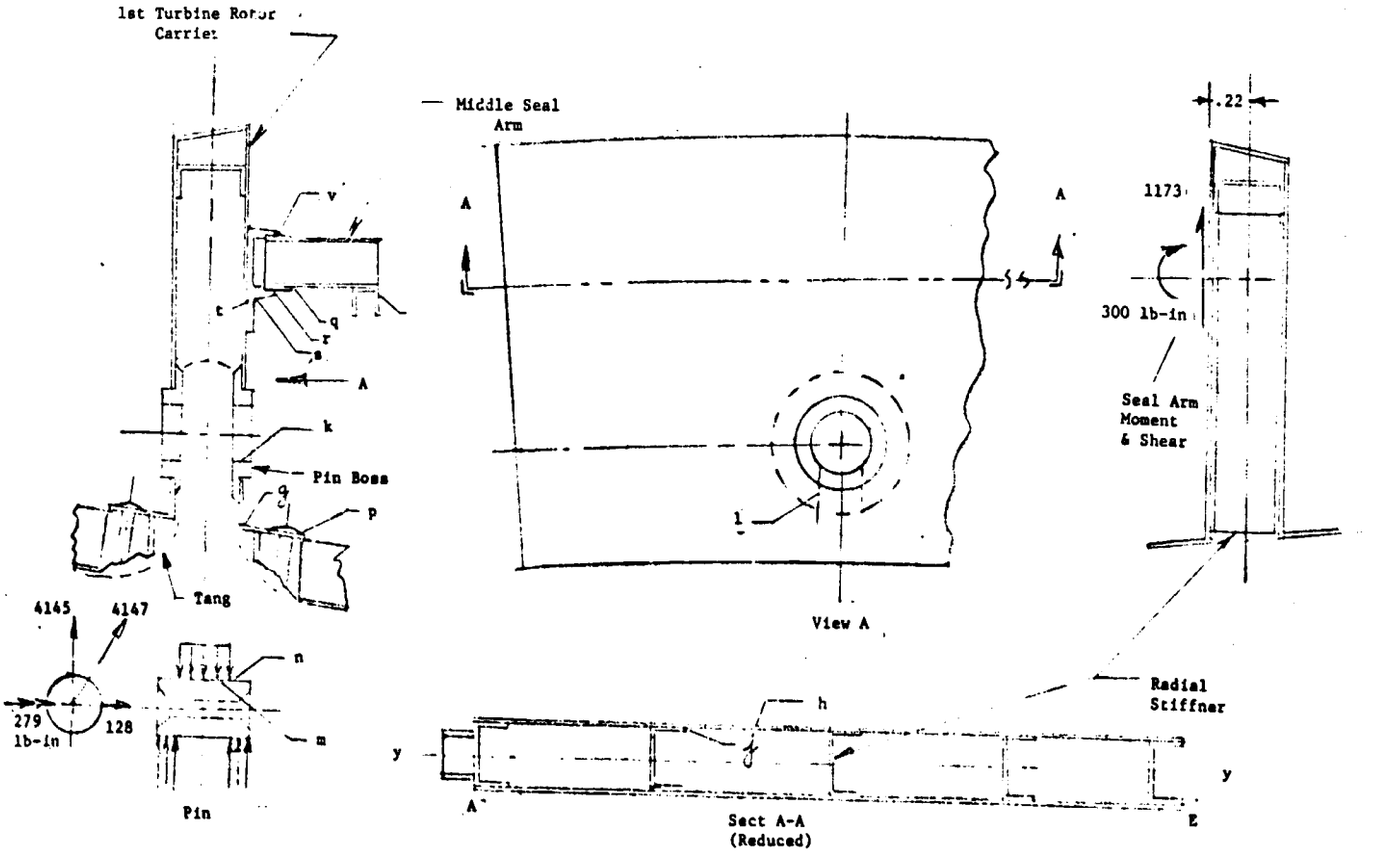

71-347

FOLDOUT FRAME 1

FIRST STAGE TURBINE CARRIER LOADS AND STRESSES

Item	Location	Type Stress	Stress-Psi	Temp °F	Mat'l	Allow. Strength-Psi	Property	M.S.
Carrier Rail	a	Bending (x-x), o	-42,300	1017	Inco X-750	82,500	1000 Hr Rupture	+.95
	b	Bending (x-x), i	+42,300	1200	Inco X-750	53,000	1000 Hr Rupture	+.25
	c	Bending (x-x), o	- 4,650	1017	Inco X-750	82,500	1000 Hr Rupture	>1.0
	d	Bending (x-x), i	+ 4,650	1200	Inco X-750	53,000	1000 Hr Rupture	>1.0
	e	Bending (x-x), o	-46,600	1017	Inco X-750	82,500	1000 Hr Rupture	+.76
	f	Bending (x-x), i	+46,600	1200	Inco X-750	53,000	1000 Hr Rupture	+.14
	g	Bending	12,910	1200	Inco X-750	53,000	1000 Hr Rupture	>1.0
Stiffners & Side Walls	h	Bending (y-y)	8,900	1200	Inco X-750	53,000	1000 Hr Rupture	>1.0
	j	Shear	1,450	1200	Braze	31,000	Shear	>1.0
Pin Boss	k	Bearing	45,000	1200	Inco 718	201,000	1.5 (.2% Y)	>1.0
	l	Tearout	73,400	1200	Inco 718	80,500	.6 (.2% Y)	+.10
Support Pin	m	Bending	92,200	700	Inco 718	150,000	.2% Y	+.63
	n	Shear	35,700	700	Inco 718	90,000	.6 (.2% Y)	>1.0
Rivet	p	Shear.	5,000	1200	Inco 600	12,000	.6 (.2% Y)	>1.0
Seal Arm	q	Tension (Bend.)	5,960	1200	Hast X	9,000	1000 Hr-.2% Creep	+.50
	r	Tension (Bend.)	4,040	1200	Hast X	9,000	1000 Hr-.2% Creep	>1.0
	s	Tension (Bend.)	3,370	1200	Hast X	9,000	1000 Hr-.2% Creep	>1.0
	t	1) Tension	205	1117	Braze	85,000	Tensile Str.	>1.0
		2) Shear	245	1117	Braze	31,000	Shear	>1.0
	u	Bending	414	1200	Hast X	28,000	1000 Hr Rupture	>1.0
	v	Shear	4,720	1200	Hast WAD	18,000	.6 (.2% Y)	>1.0

CARRIER DEFLECTION @ E = .005 IN. RADIAL

FOLDOUT FRAME 2

Figure 56

FIRST STAGE TURBINE ROTOR BLADE INTERFERENCE DIAGRAM

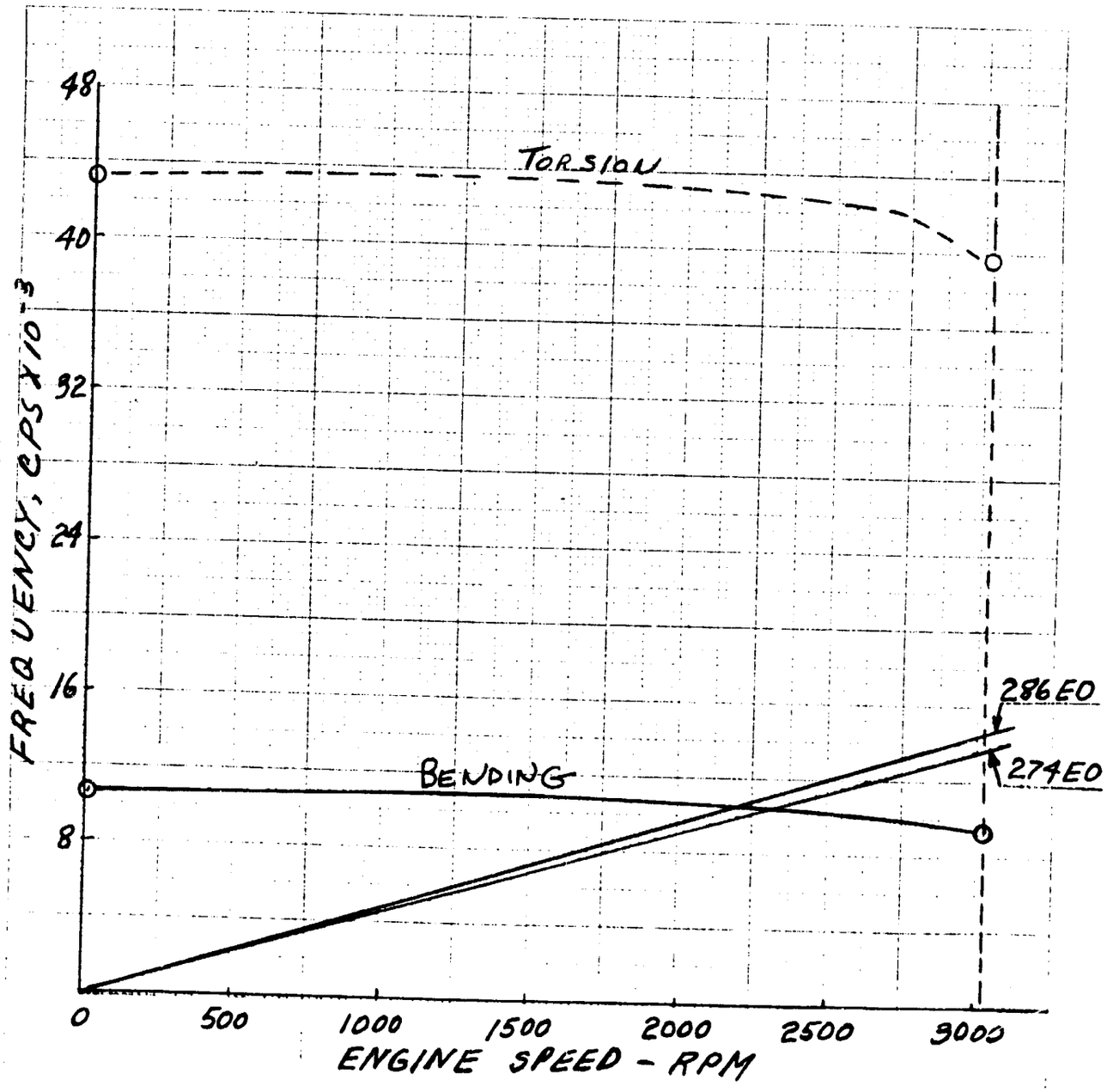

Figure 57

SECOND STAGE TURBINE ROTOR BLADE INTERFERENCE DIAGRAM

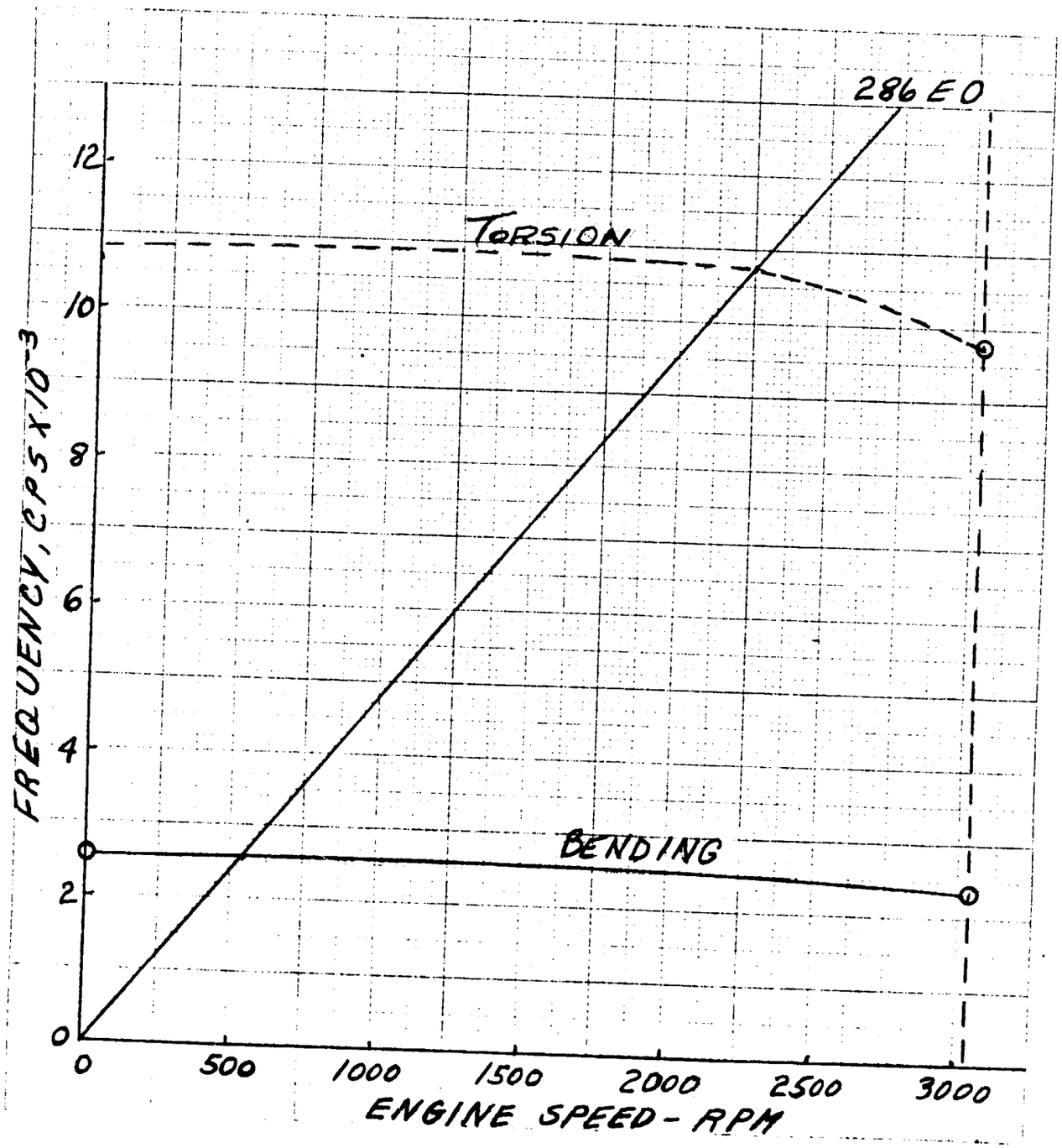

Figure 58

FAN STATOR VANE AND SUPPORT ASSEMB

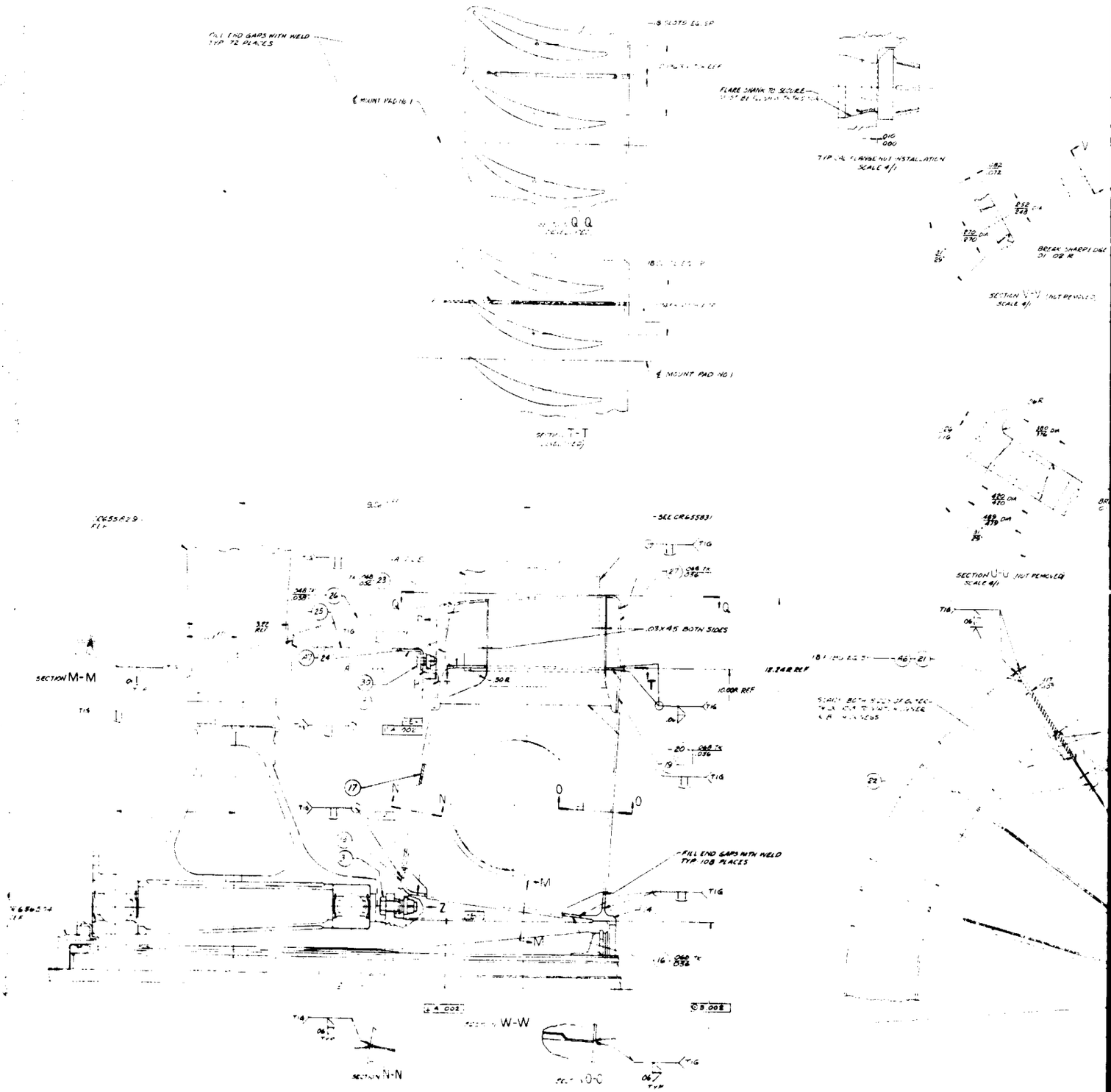

FOLDOUT FRAME 1

71-0246

SUPPORT ASSEMBLY (INNER)

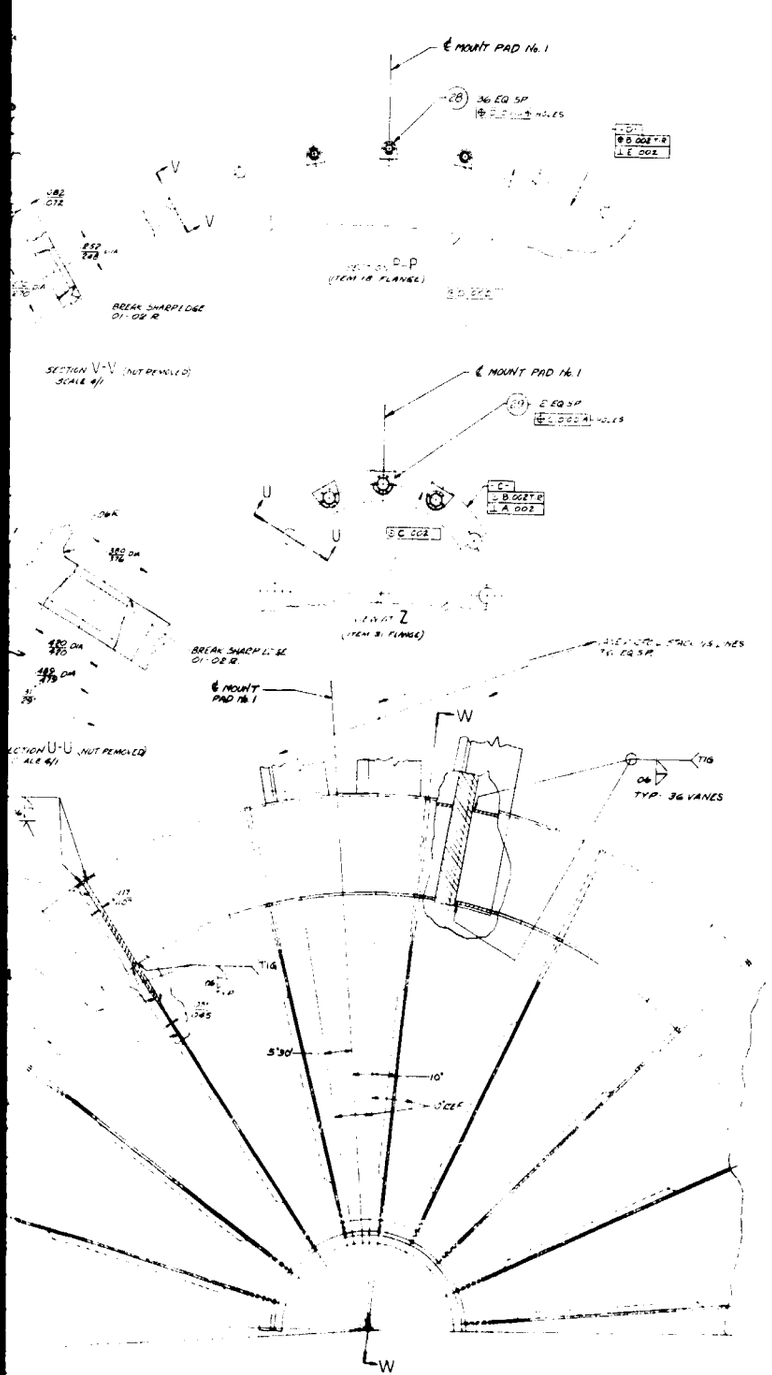

FOLDOUT FRAME 2

Figure 59

FAN STATOR VANE AND SUPPORT ASSE

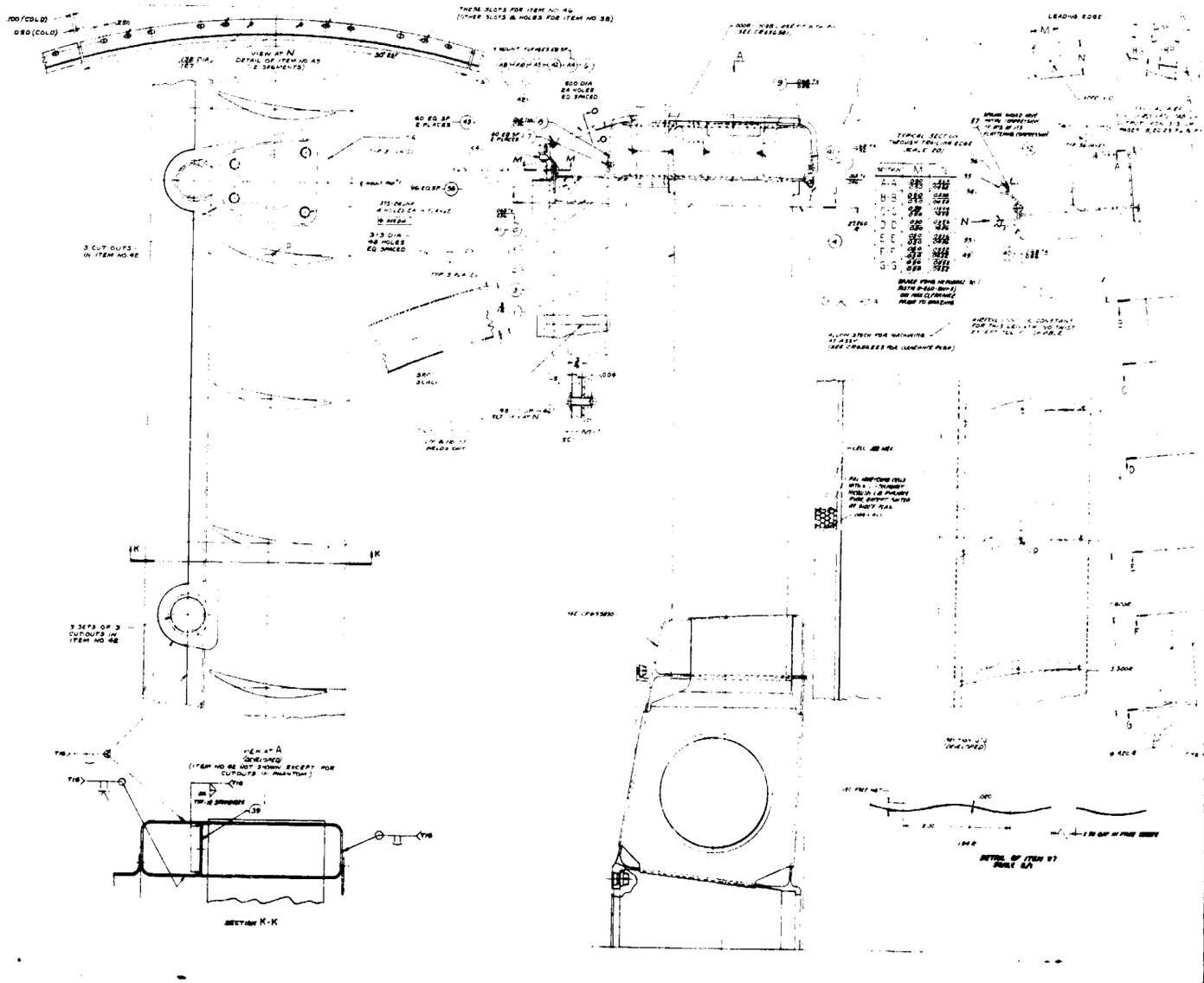

FOLDOUT FRAME 1

VANE AND SUPPORT ASSEMBLY (OUTER)

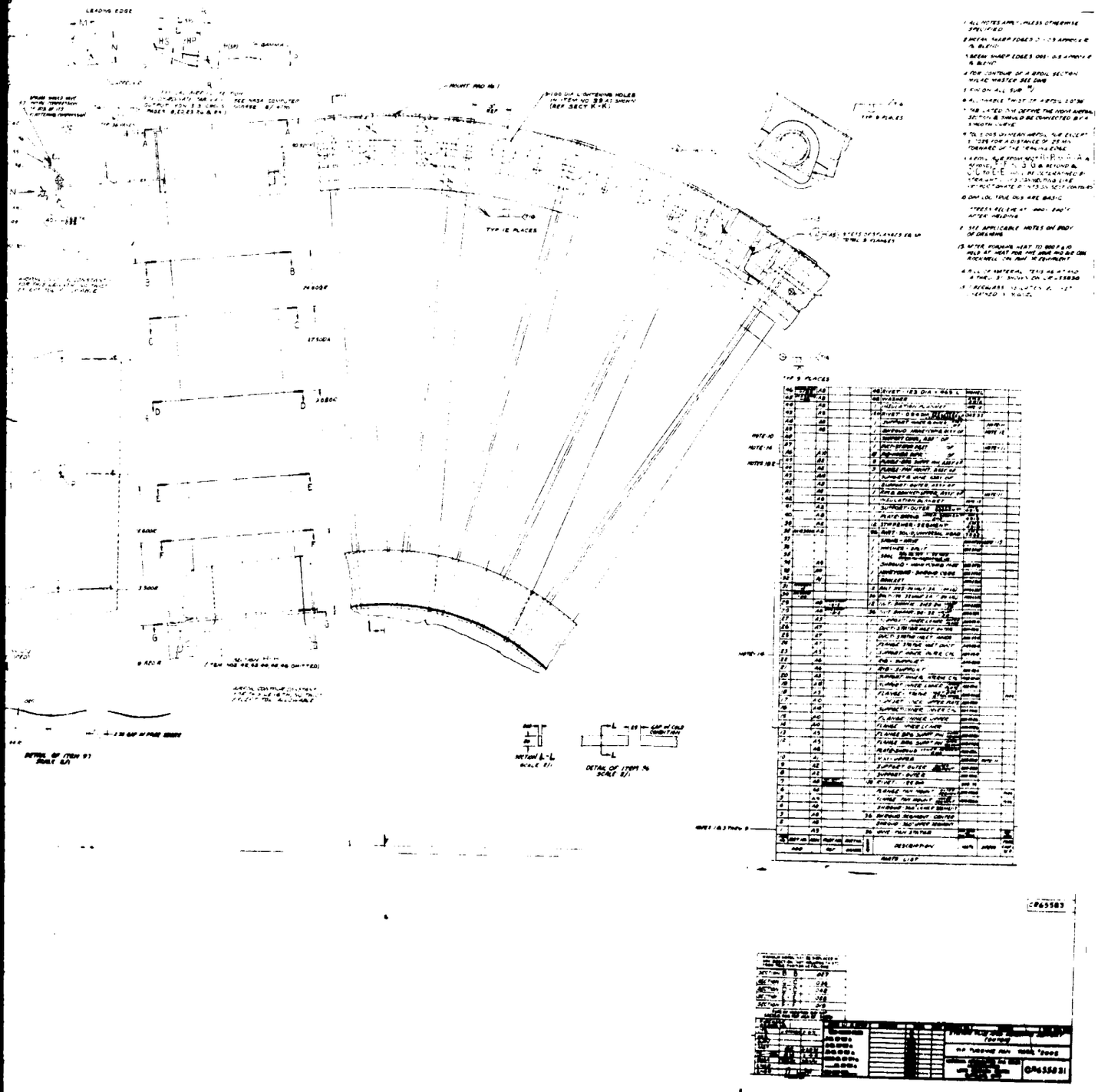

FOLDOUT FRAME 2

Figure 60

FAN STATOR SUPPORT AXIAL MOUNT LOADS

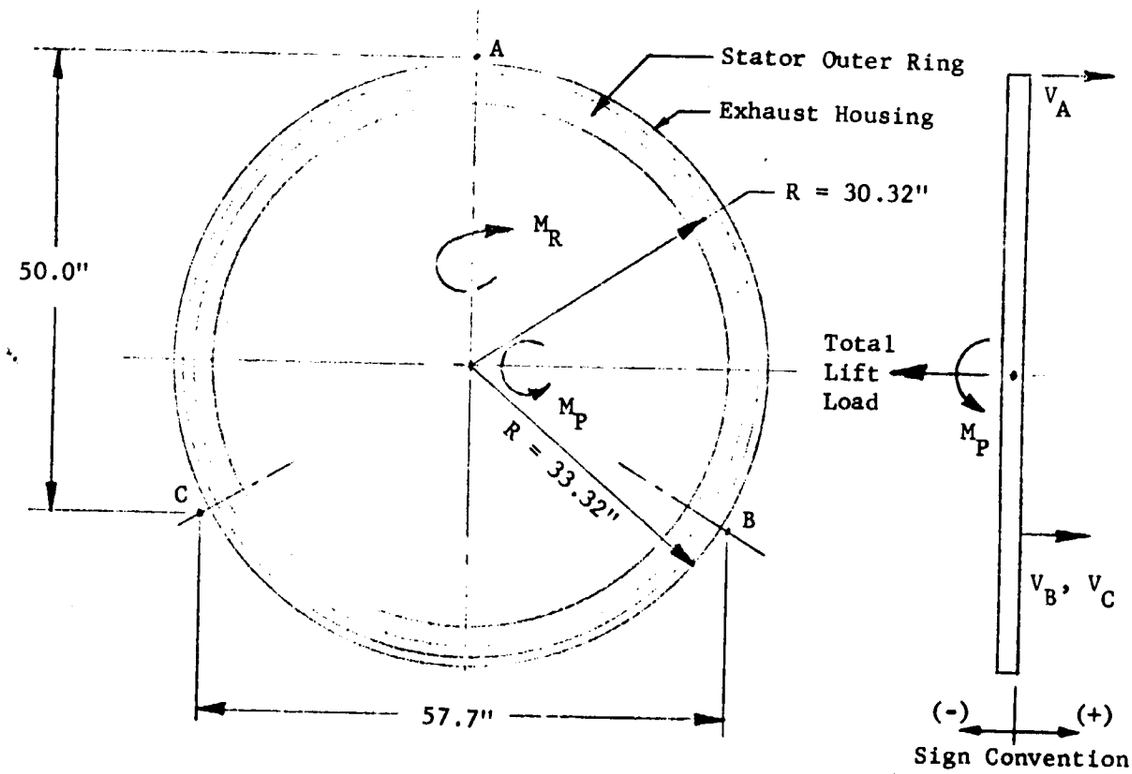

Condition	Total Lift lb	Gyroscopic Couple M_R lb-in	Gyroscopic Couple M_P lb-in	Axial Loads		
				V_A lb	V_B lb	V_C lb
1	10,758	72,000	-	3,600	2,340	4,830
2	10,758	-72,000	-	3,600	4,830	2,340
3	10,758	-	72,000	5,030	2,900	2,900
4	10,758	-	-72,000	2,150	4,310	4,310

Figure 61

TYPICAL STATOR VANE SUPPORT LOADING (CONDITION 3)

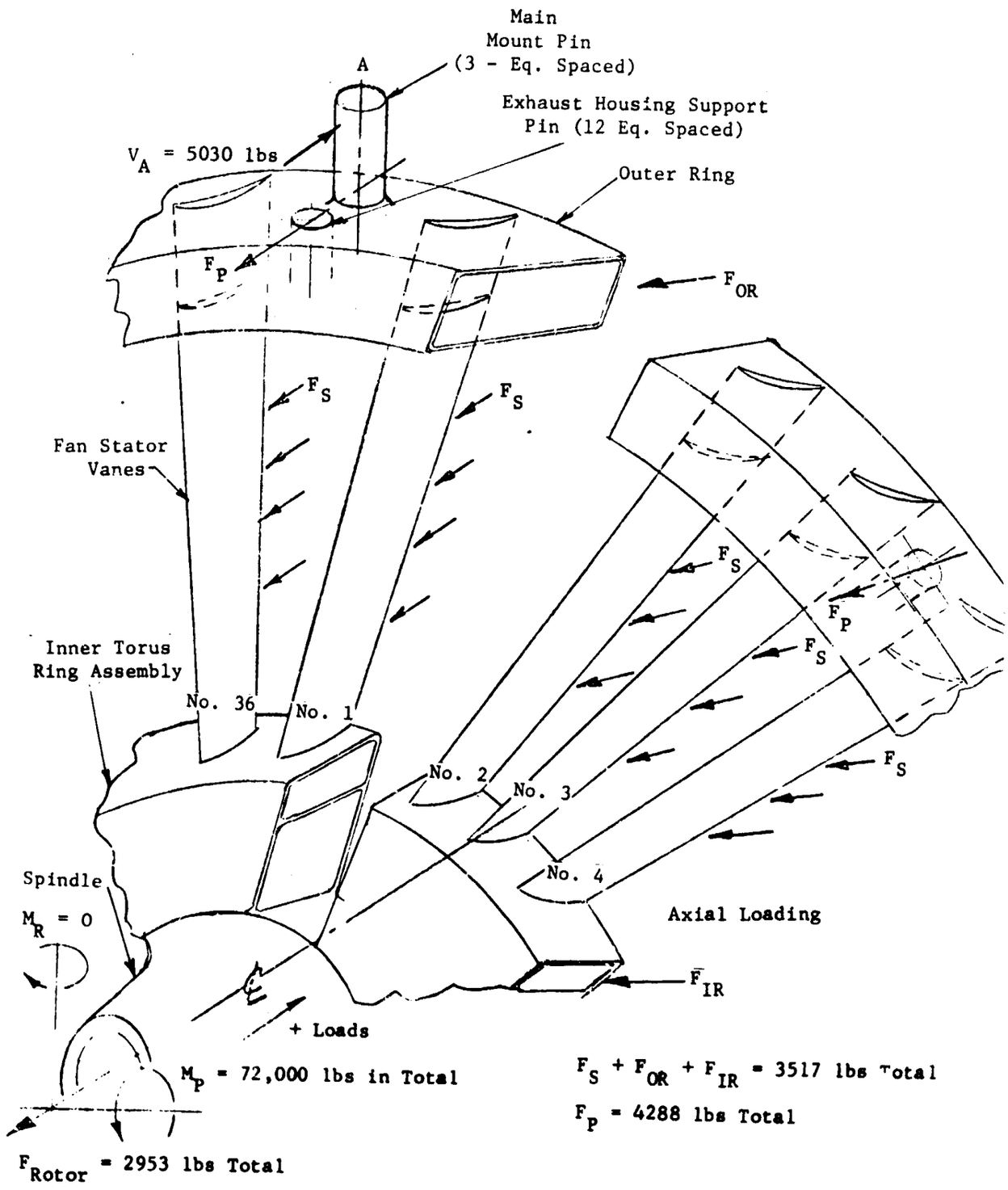

Figure 62

AXIAL BENDING MOMENTS AND SHEAR LOADS ON FAN STATOR VANE

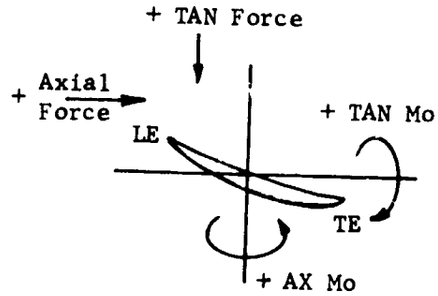

Loading Condition:

Inner Ring Guided (Zero Slope)

Outer Ring Simply Supported

Vanes	Radius in.	Steady State Aero Loads on Vanes		Gyro Load Plus Hub Load From Fan Rotor		Net Axial	
		Shear #	Moment in-lb	Shear #	Moment in-lb	Shear #	Moment in-lb
1 & 36	29.2	-53	0	300	-10,145	247	-10,145
	28.16	-53	- 55	300	- 9,833	247	- 9,888
	25.97	-49	-169	300	- 9,176	251	- 9,345
	23.72	-42	-271	300	- 8,501	258	- 8,772
	21.22	-33	-364	300	- 7,751	267	- 8,115
	18.32	-22	-443	300	- 6,881	278	- 7,324
	14.79	- 8	-497	300	- 5,822	292	- 6,319
	12.16	0	-506	300	- 5,033	300	- 5,539
	11.0	0	-506	300	- 4,685	300	- 5,191
2 & 35	29.2	-53	0	-440	- 0	-493	0
	28.46	-53	- 55	-440	- 458	-493	- 513
	25.97	-49	-169	-440	- 1,421	-489	- 1,590
	23.72	-42	-271	-440	- 2,411	-488	- 2,682
	21.22	-33	-364	-440	- 3,511	-473	- 3,875
	18.32	-22	-443	-440	- 4,787	-462	- 5,230
	14.79	- 8	-497	-440	- 6,340	-448	- 6,837
	12.16	0	-506	-440	- 7,498	-440	- 8,004
	11.00	0	-506	-440	- 8,008	-440	- 8,514

Figure 63

TANGENTIAL BENDING MOMENTS AND SHEAR LOADS ON FAN STATOR VANE

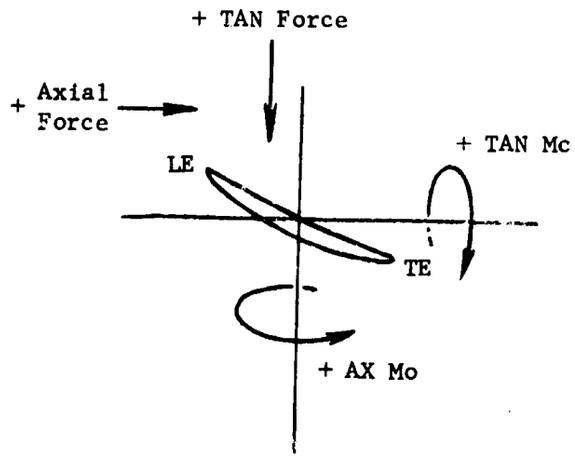

Vanes	Radius in.	Steady State Load on Vanes		Gyro Load Plus Hub Load From Fan Rotor		Net Tangential	
		Shear #	Moment in-lb	Shear #	Moment in-lb	Shear #	Moment in-lb
	29.2	186.8	1215.6	28.9	0	215.7	1215.6
	28.16	186.8	1021.3	28.9	30.1	215.7	1051.4
	25.97	171.4	620.4	28.9	93.3	200.3	713.7
1 & 36	23.72	139.5	271.5	28.9	158.4	168.4	429.9
2 & 35	21.22	105.1	- 34.8	28.9	230.6	134.0	195.8
	18.32	67.2	-283.9	28.9	314.4	96.1	30.5
	14.79	24 0	-444.6	28.9	416.4	52.9	-28.2
	12.16	0.0	-471.2	28.9	492.5	28.9	21.3
	11.0	0.0	-471.2	28.9	526.0	28.9	54.8

Figure 64

FAN STATOR VANE SECTION PROPERTIES (SOLID AIRFOILS

Radius in	Area in^2	I_{WK} in^4	I_{STRG} in^4	C_{WK} - in			C_{STR} - in		t_{max} in	Chord in	T/C	$T/\theta \times 10^6$ $\frac{lb\text{-}in}{rad\text{-}sec}$	γ Deg
				LE	TE	B	LE	TE					
30.32	1.412	.0243	1.575	.281	.281	.294	2.14	2.26	.445	4.45	.10	.405	8.76
29.20	1.412	.0243	1.575	.281	.281	.294	2.14	2.26	.445	4.45	.10	.405	8.76
28.16	1.412	.0243	1.575	.281	.281	.294	2.14	2.26	.445	4.45	.10	.405	8.76
27.10	1.412	.0243	1.575	.281	.281	.294	2.14	2.26	.445	4.45	.10	.405	8.76
24.80	1.408	.0239	1.562	.277	.277	.292	2.20	2.25	.445	4.45	.10	.405	9.00
19.05	1.404	.0258	1.548	.279	.279	.328	2.20	2.26	.445	4.45	.10	.405	11.03
13.30	1.399	.0282	1.526	.342	.342	.310	2.21	2.17	.445	4.45	.10	.405	13.88
12.15	1.398	.0294	1.524	.357	.357	.319	2.21	2.22	.445	4.45	.10	.405	14.84
11.00	1.398	.0294	1.524	.357	.357	.319	2.21	2.22	.445	4.45	.10	.405	14.84
9.82	1.398	.0294	1.524	.357	.357	.319	2.21	2.22	.445	4.45	.10	.405	14.84

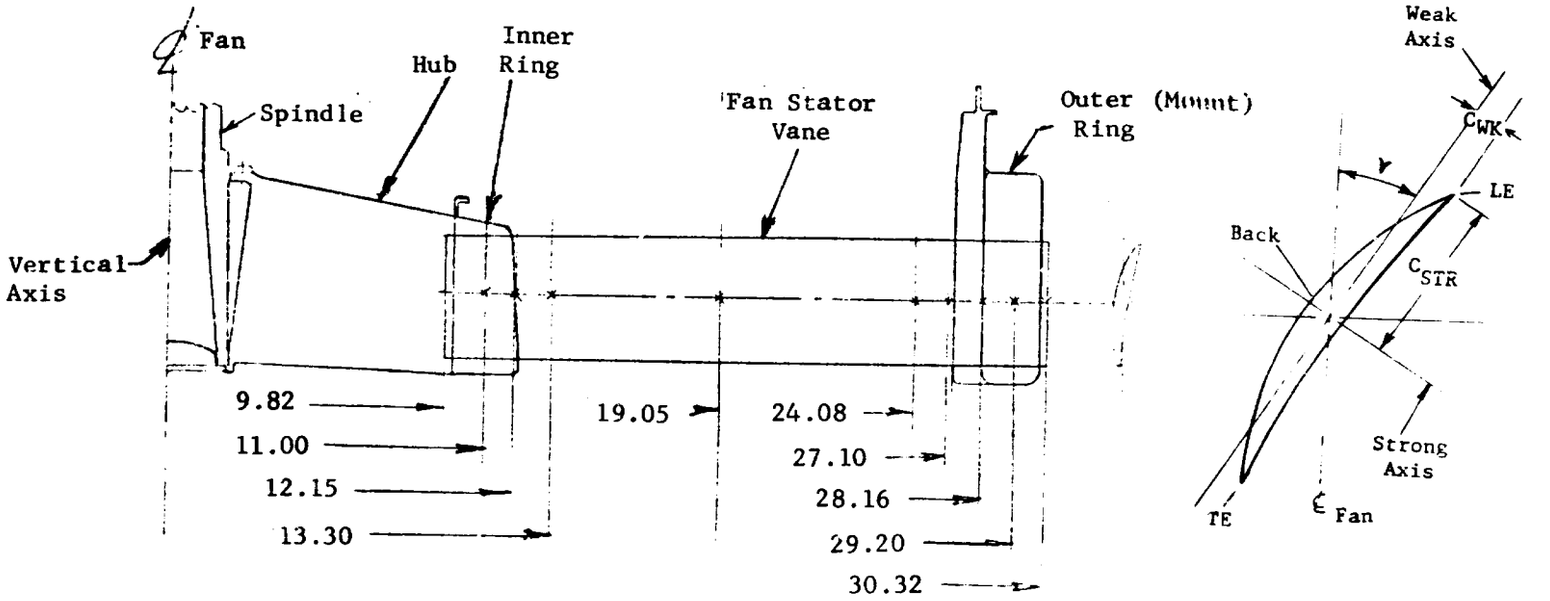

Figure 65

FAN SUPPORT OUTER RING AXIAL LOAD DISTRIBUTION

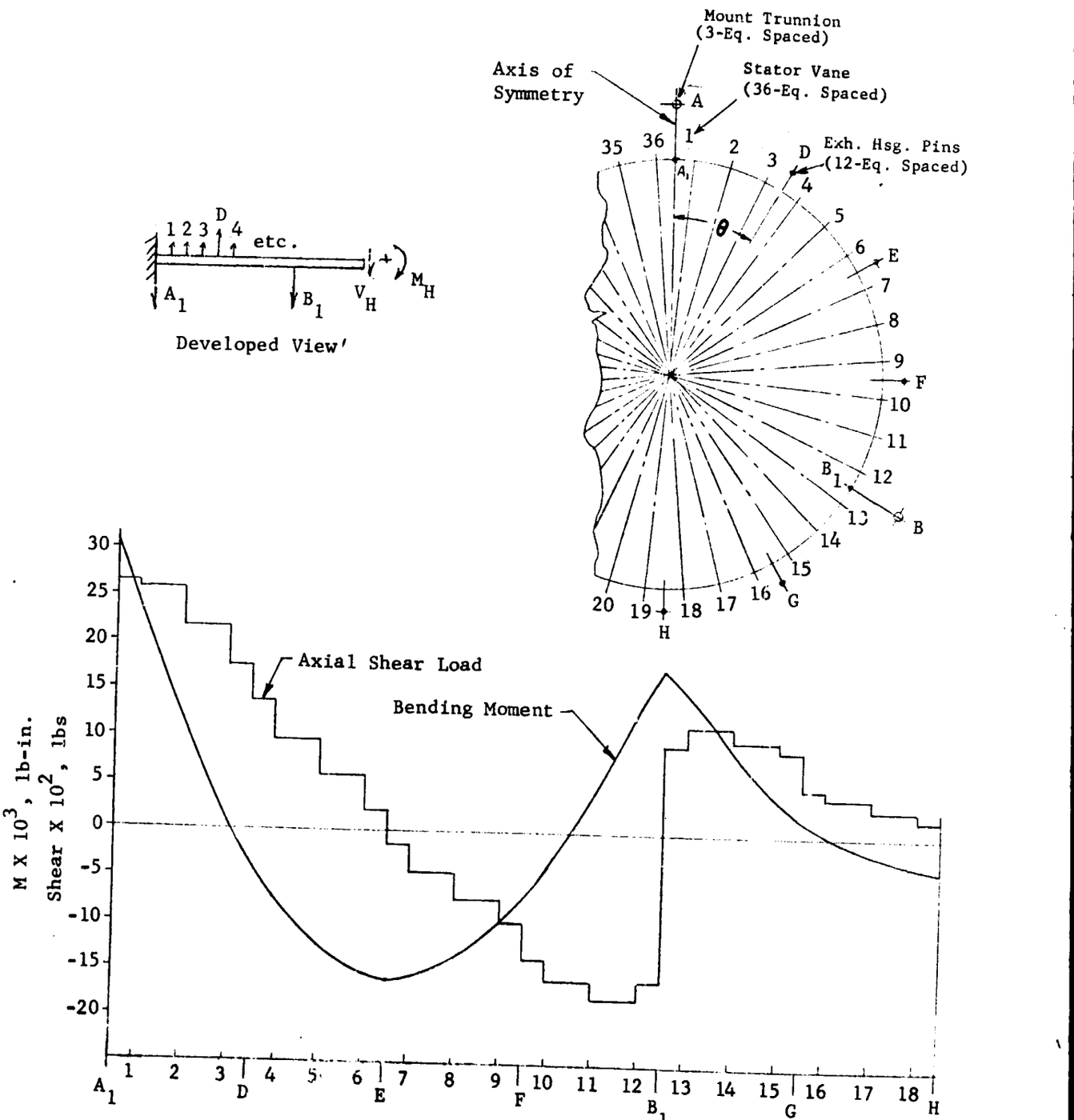

Figure 66

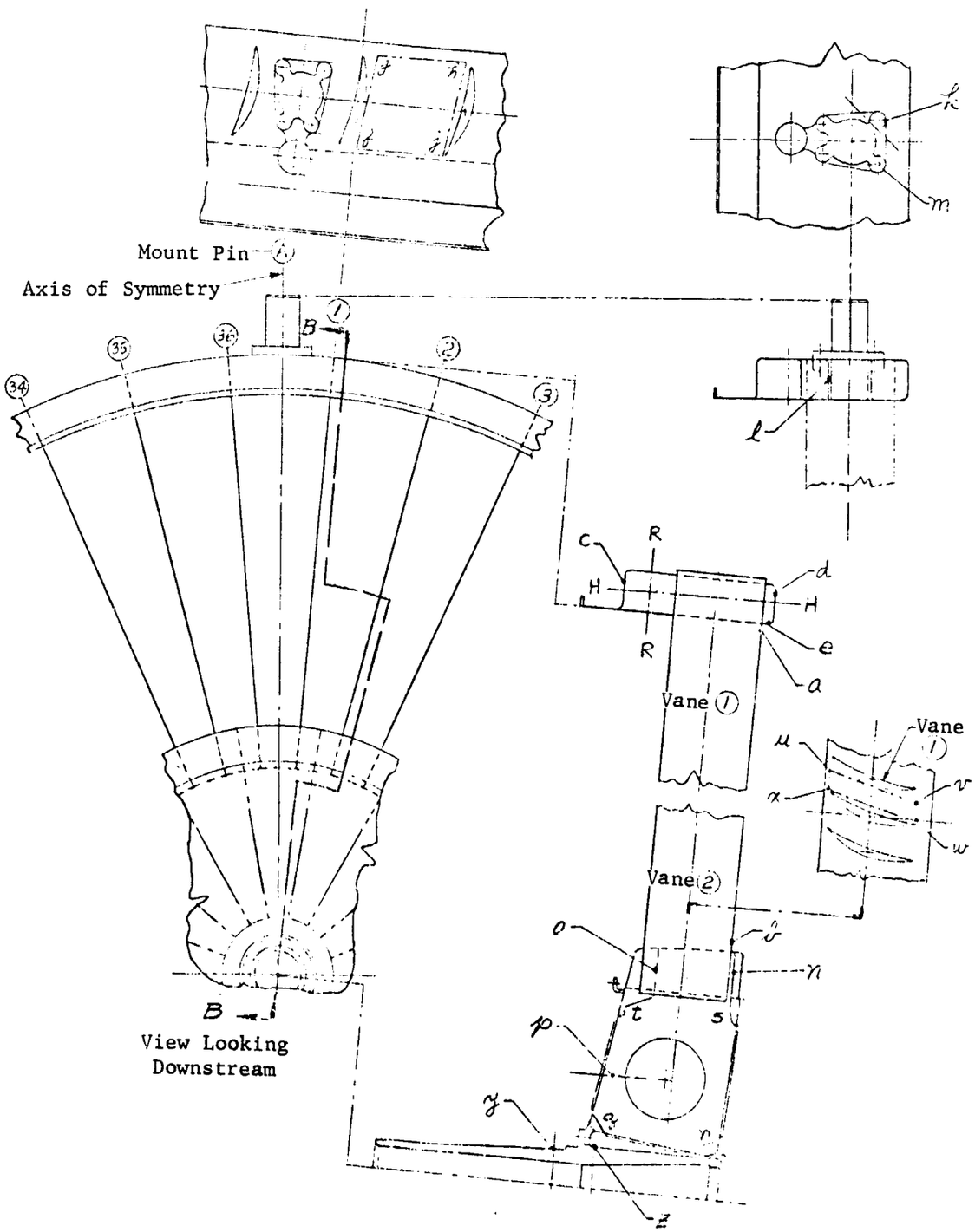

FOLDOUT FRAME 1

71-348

FAN STATOR VANE & SUPPORT ASSEMBLY STRESSES

Location	Type Loading	Stress psi	Allowable Stress psi	Load lbs	Allowable Load lbs	M.S.
a	Bending, Airfoil TE	-20,000	110,000			> 1.0
b	Bending, Airfoil TE	-36,000	110,000			> 1.0
c, d	Bending, R-R axis	±14,600	110,000			>1.0
d	Compression Buckling	-14,600	45,000			>1.0
e	Bending, R-R & H-H axis	-14,700	110,000			> 1.0
f, g	Shear, Axial	5,150	66,000			>1.0
f, g, h, j	Shear Buckling	5,150	99,200			>1.0
k	Bending, Bolt Boss	27,200	110,000			>1.0
l	Bending, Mount Pad	17,200	110,000			>1.0
m	Bolt Tension	-	-	2880	4430	+.54
n, o	Bending	±66,000	110,000			+.67
o	Compression Buckling	-	-	724	900	+.24
p	Compression	-21,500	110,000			>1.0
p	Buckling	-21,000	113,000			>1.0
q, r, s, t	Shear Buckling			880	930	+.06
u, v	Shear, Axial	18,200	66,000			>1.0
u, v, w, x	Shear, Buckling	18,200	181,000			>1.0
y	Bending, Spindle	19,900	110,000			> 1.0
z	Bending, Spindle	11,200	110,000			> 1.0

Operating Temperature - Ambient

Material:

Fan Stator Support - Titanium, 5Al-2.5Sn

Spindle - Titanium, 6Al-4Va

FOLDOUT FRAME 2

Figure 67

FAN STATOR VANE INTERFERENCE DIAGRAM

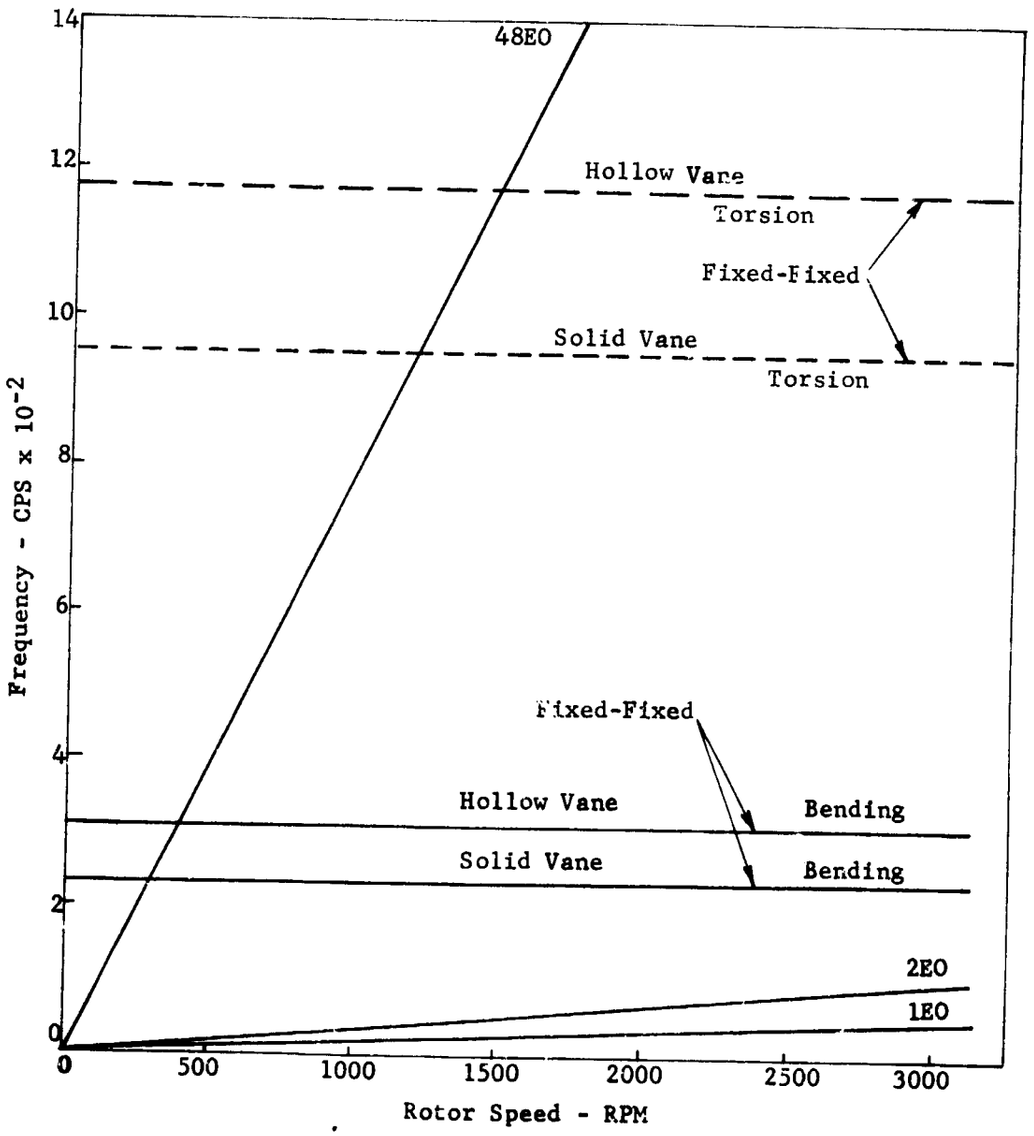

Figure 68

HOT GAS SCROLL ASSEMB

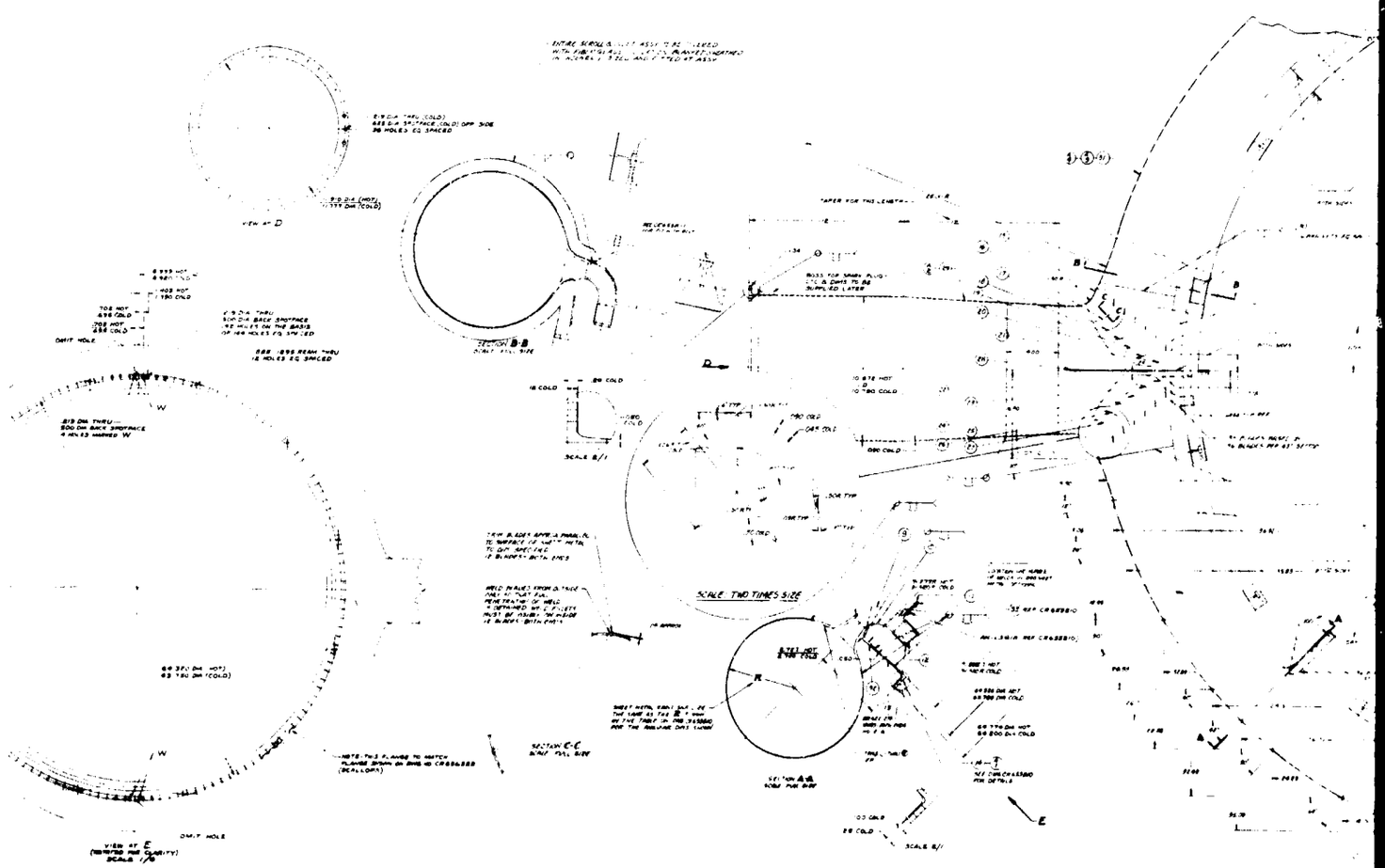

FOLDOUT FRAME 1

SCROLL ASSEMBLY

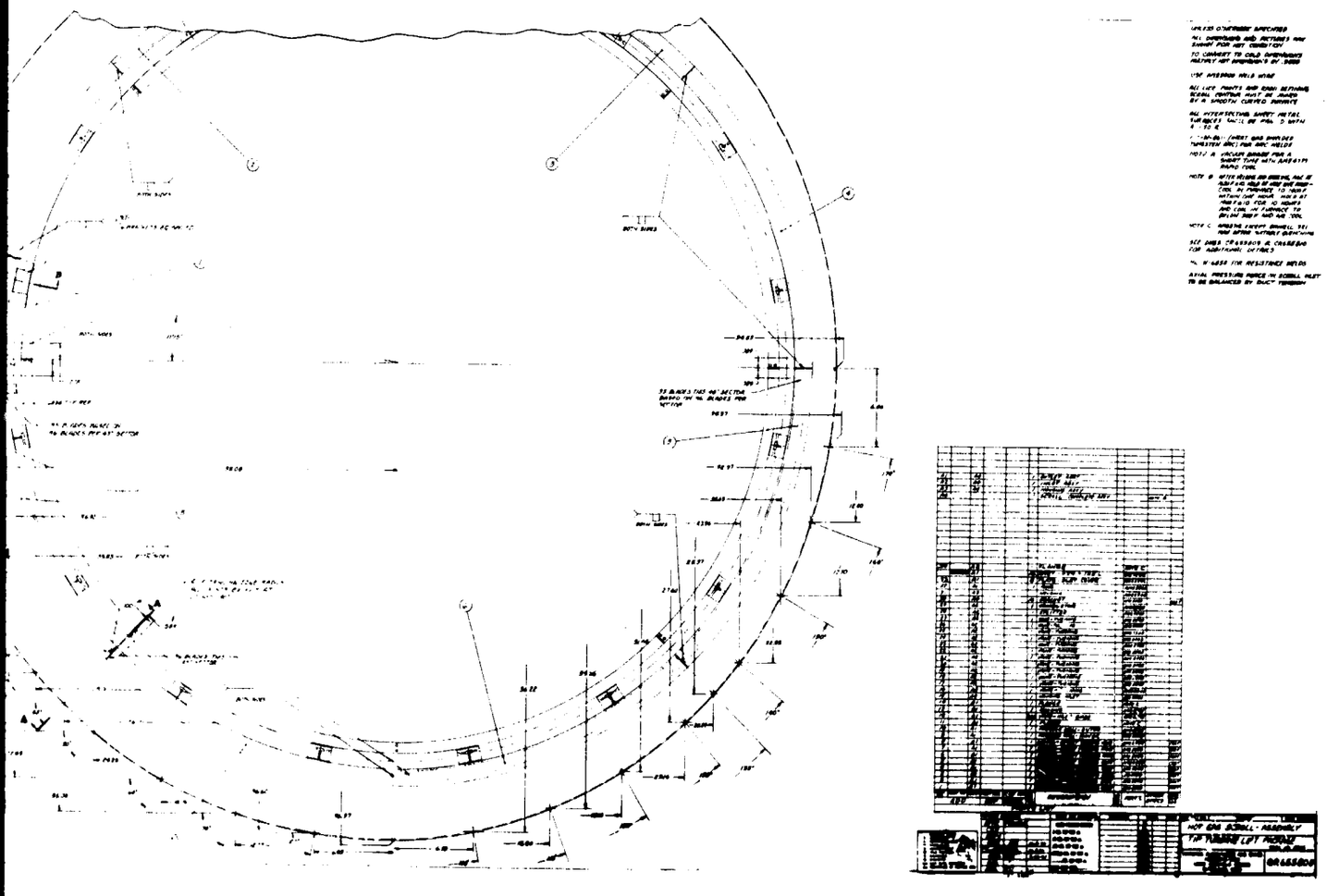

FOLDOUT FRAME 2

Figure 69

HOT GAS SCROLL FABRICATED

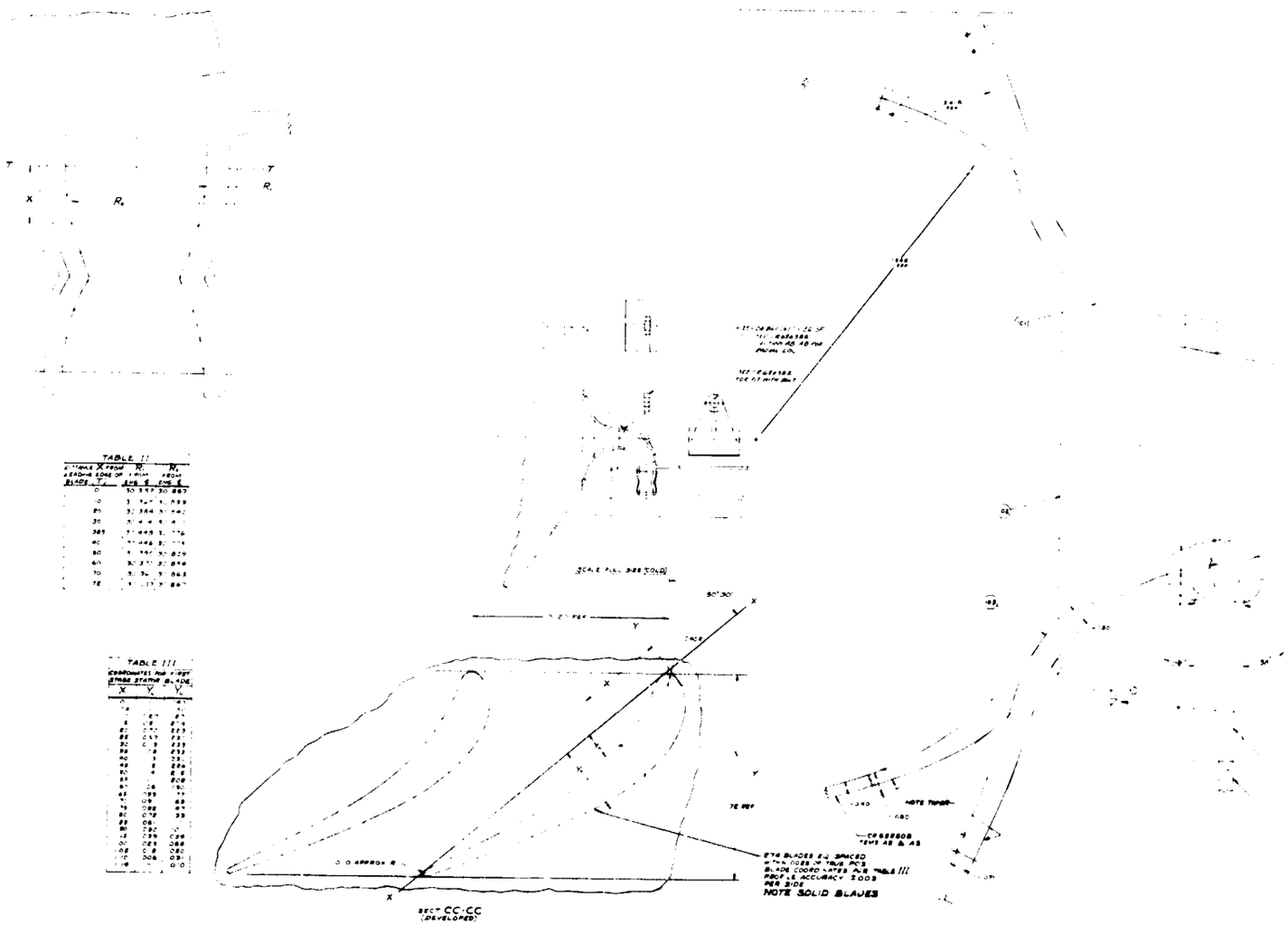

FOLDOUT FRAME 1

SCROLL FABRICATED EXIT

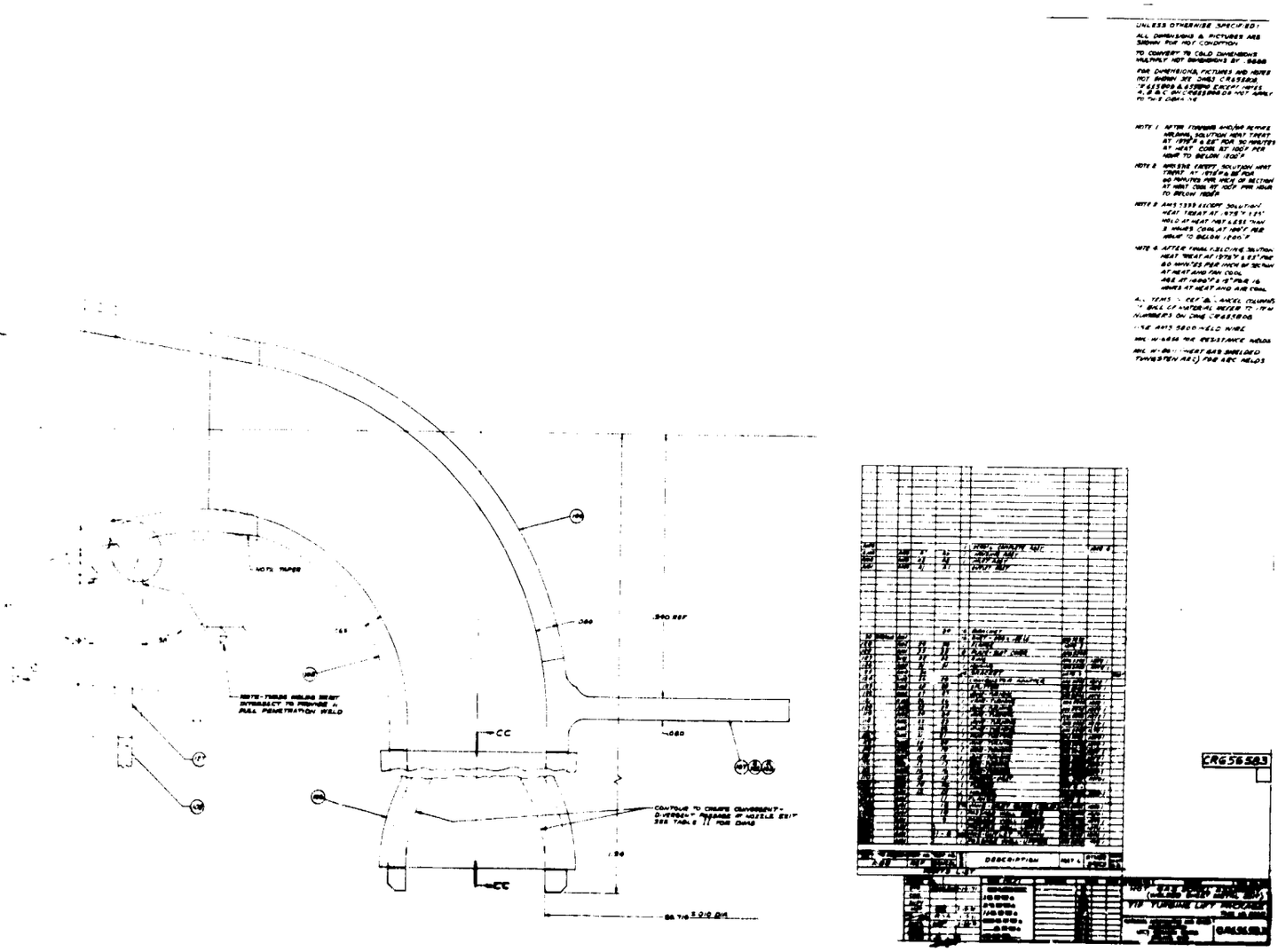

FOLDOUT FRAME 2

Figure 70

HOT GAS SCROLL CAST EX

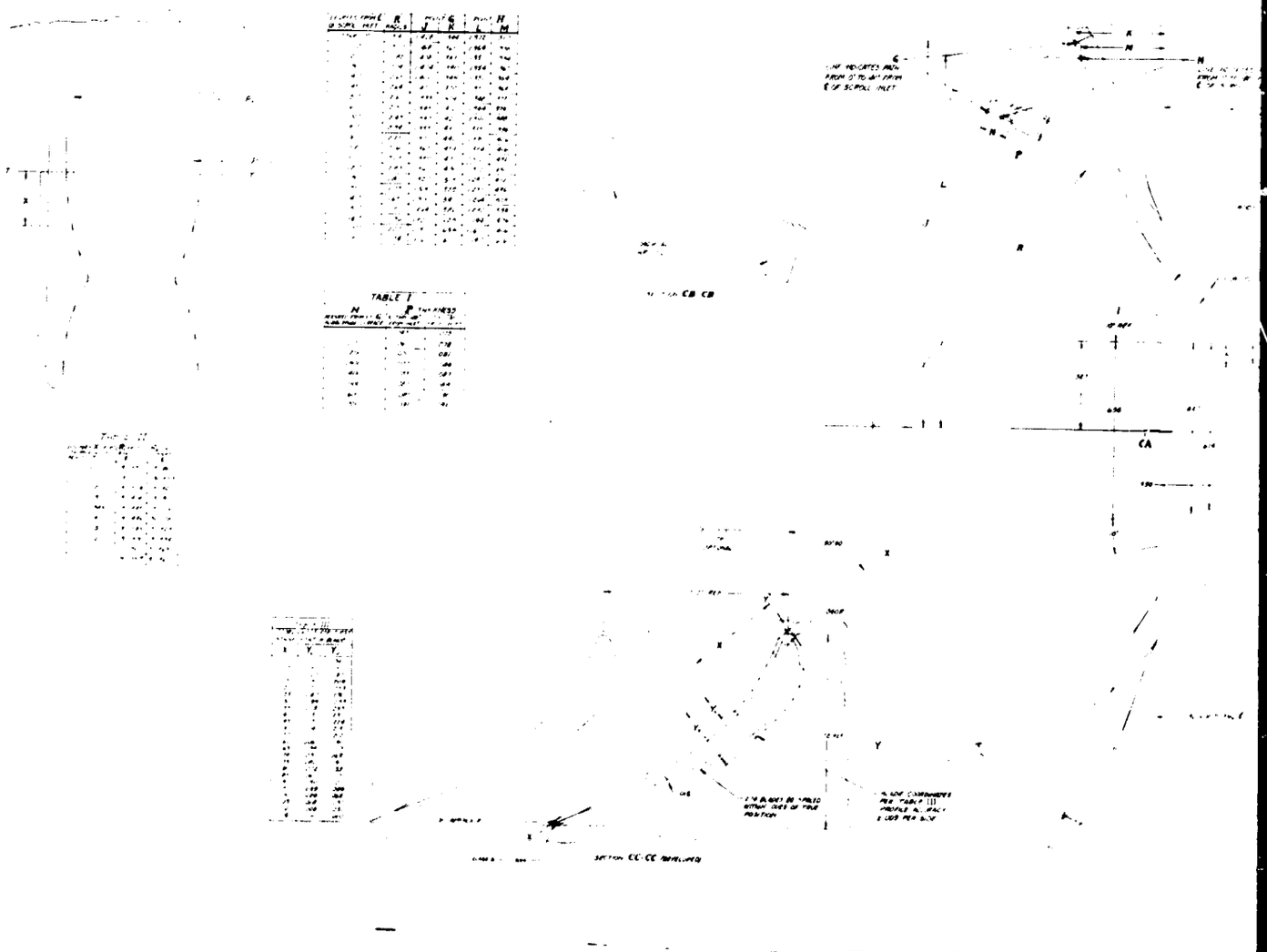

FOLDOUT FRAME 1

OT GAS SCROLL CAST EXIT

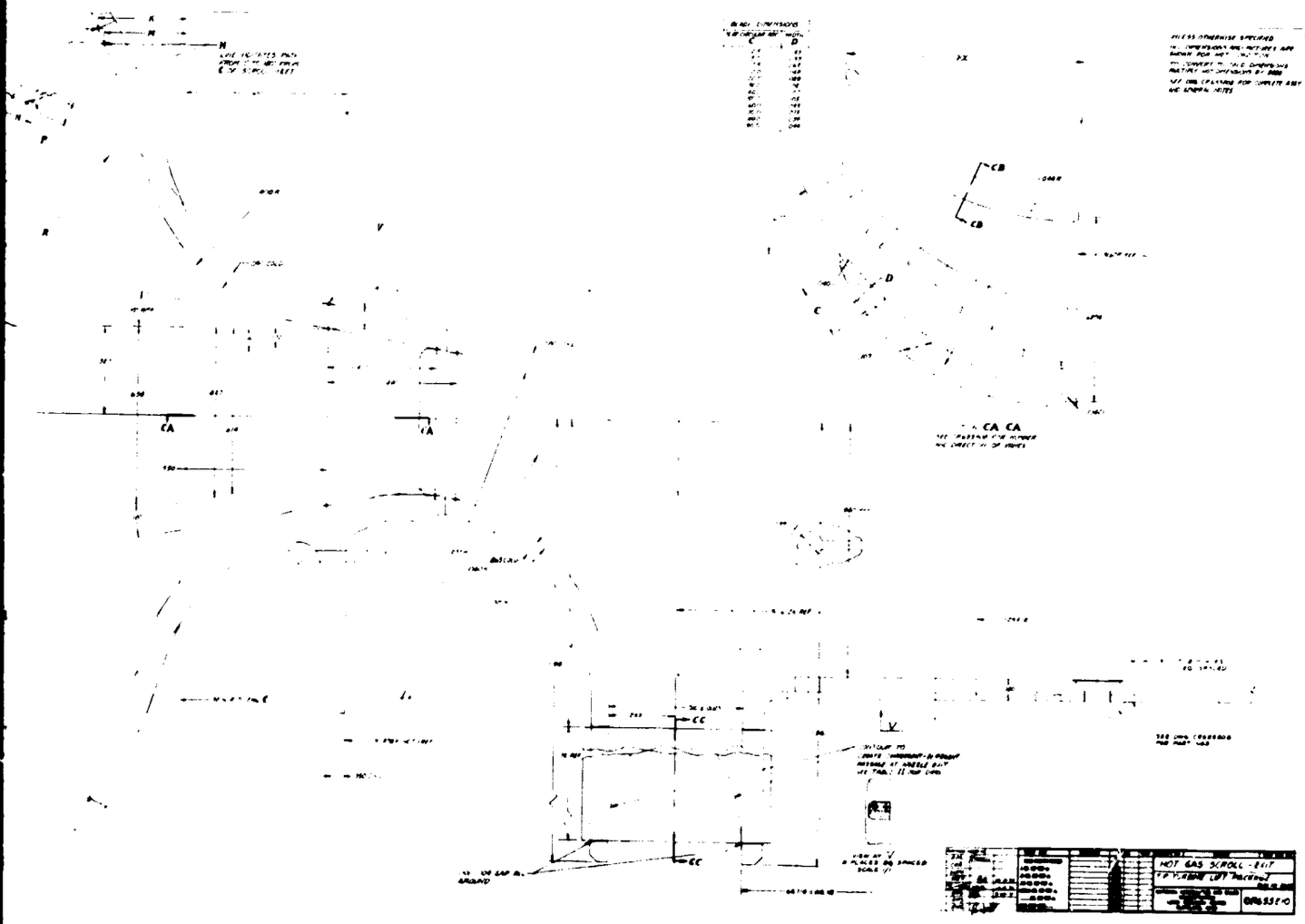

FOLDOUT FRAME 2

Figure 71

HOT GAS SCROLL INLET

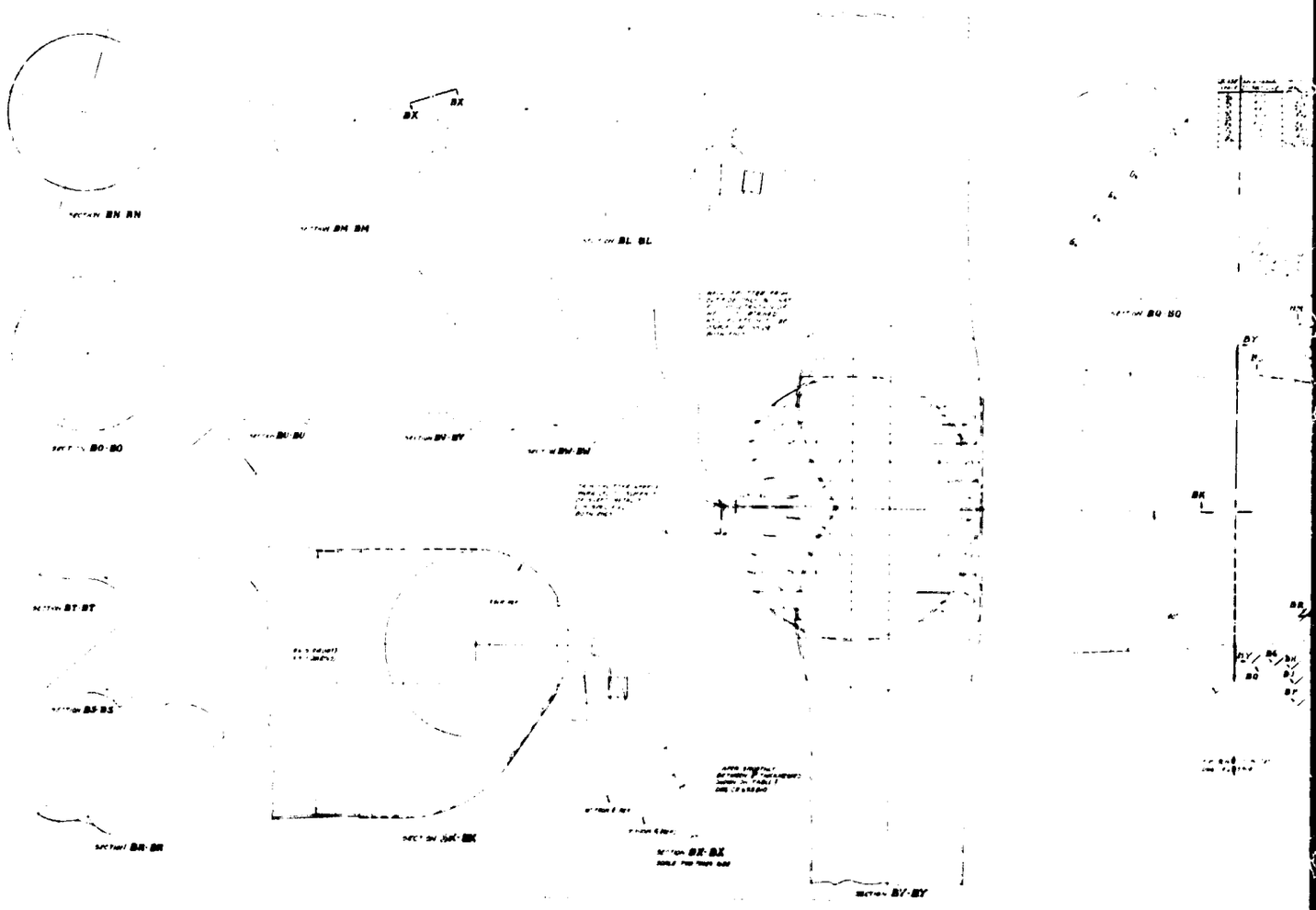

FOLDOUT FRAME 1

GAS SCROLL INLET EXIT

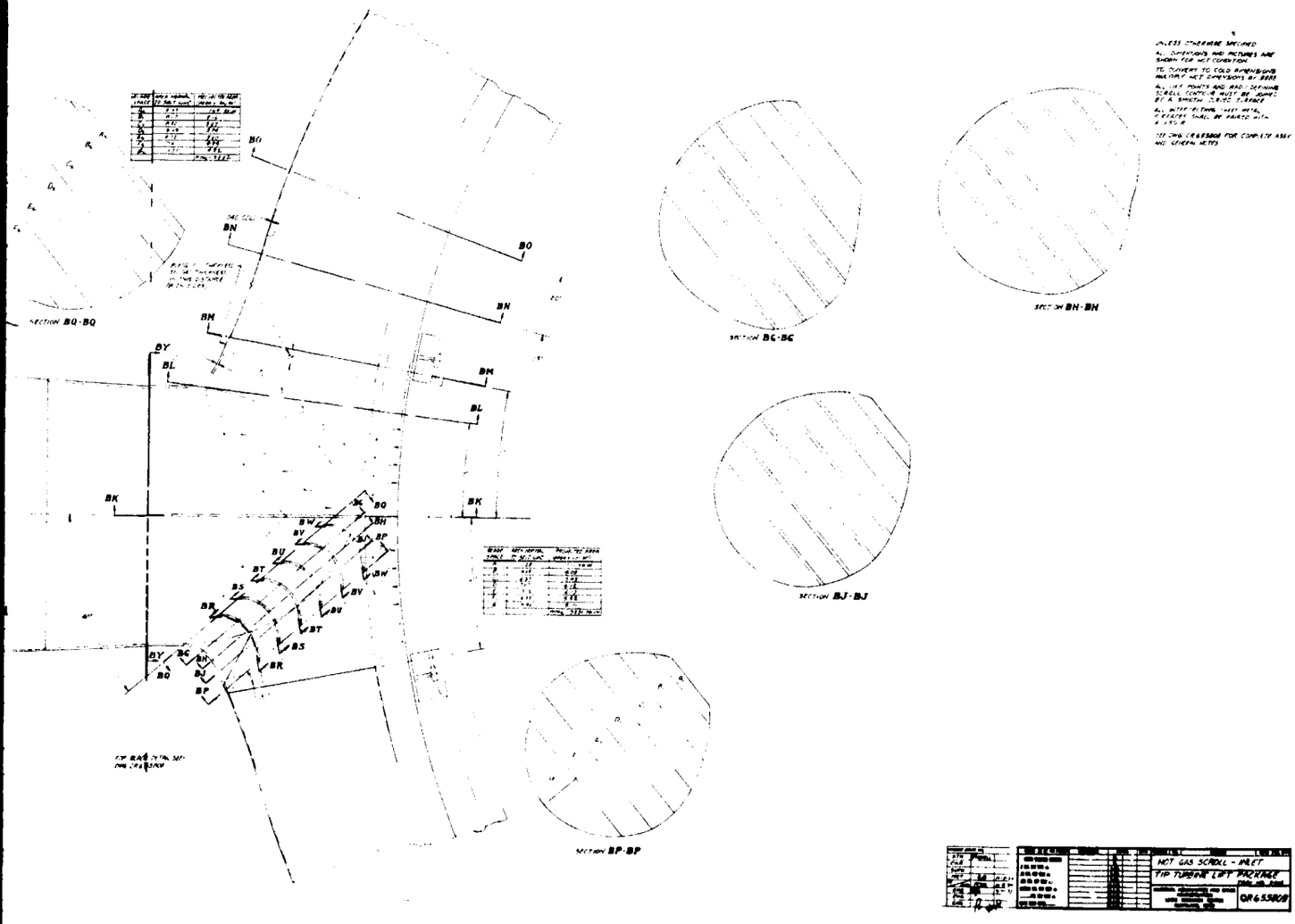

FOLDOUT FRAME 2

Figure 72

HOT GAS SCROLL NECK & TURNING VANES

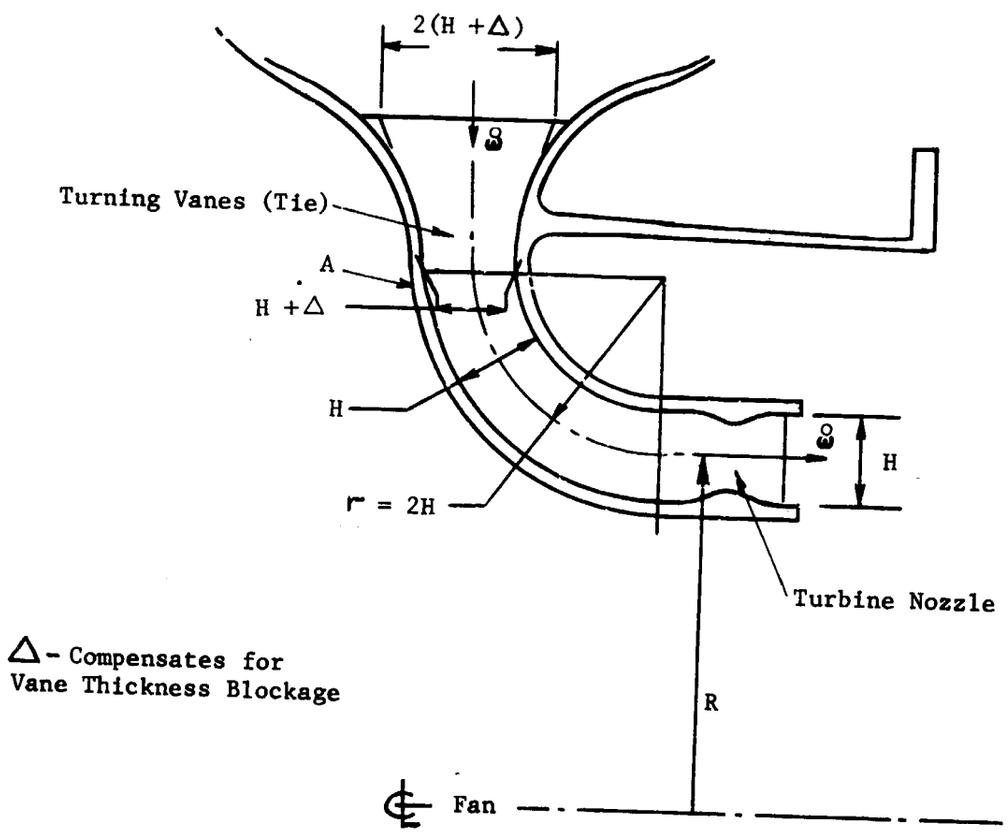

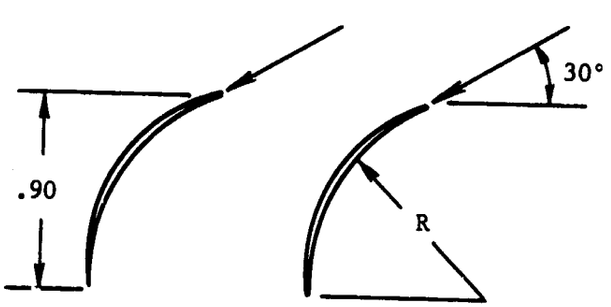

t/c = 8%
NACA 65 Series
σ = 1.5

View A

Figure 73

HOT GAS SCROLL AERODYNAMIC DATA

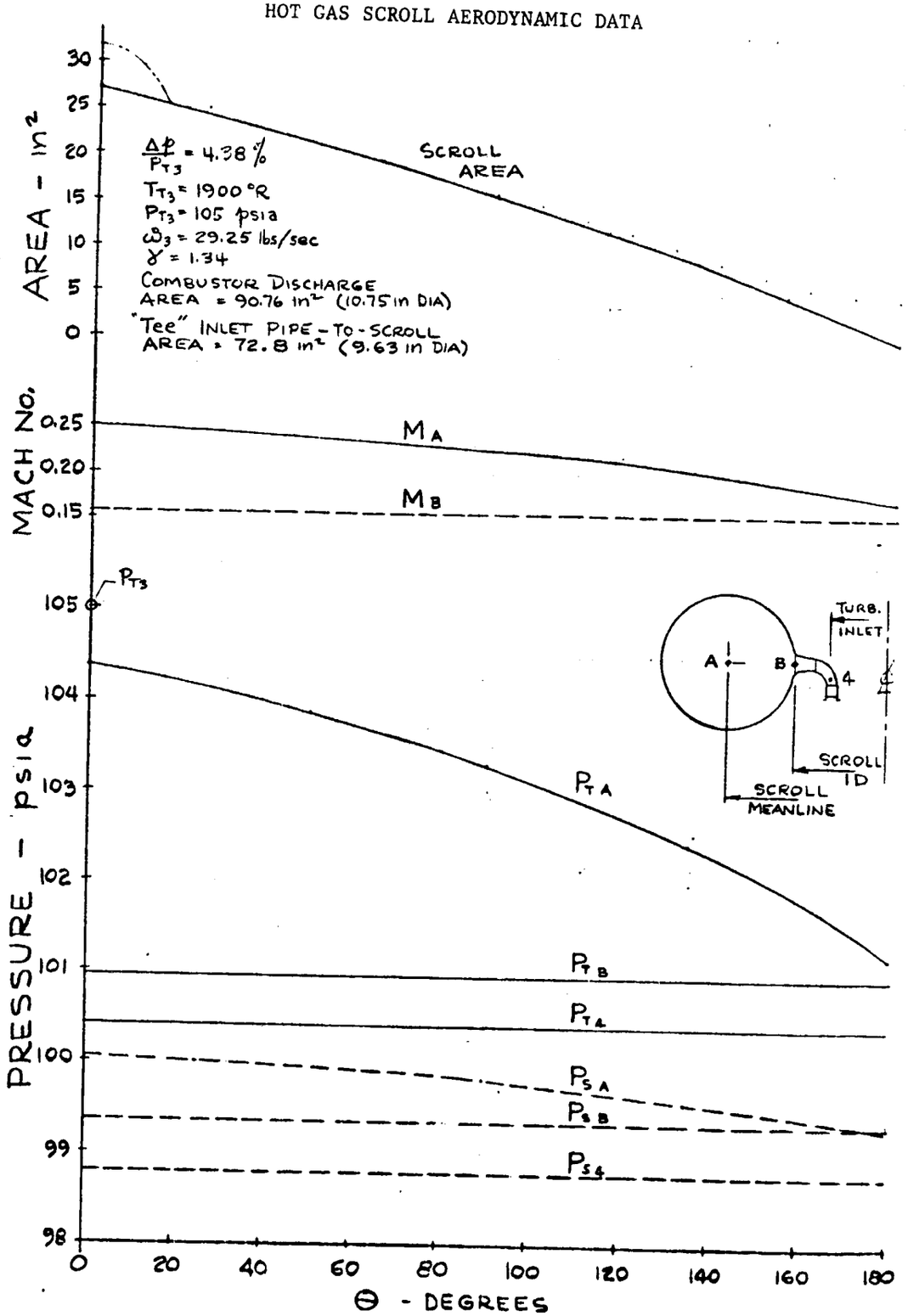

Figure 74

Material - Rene 41
Temperature - 1440°F
Pressure - 90 psi
Condition - Design Point

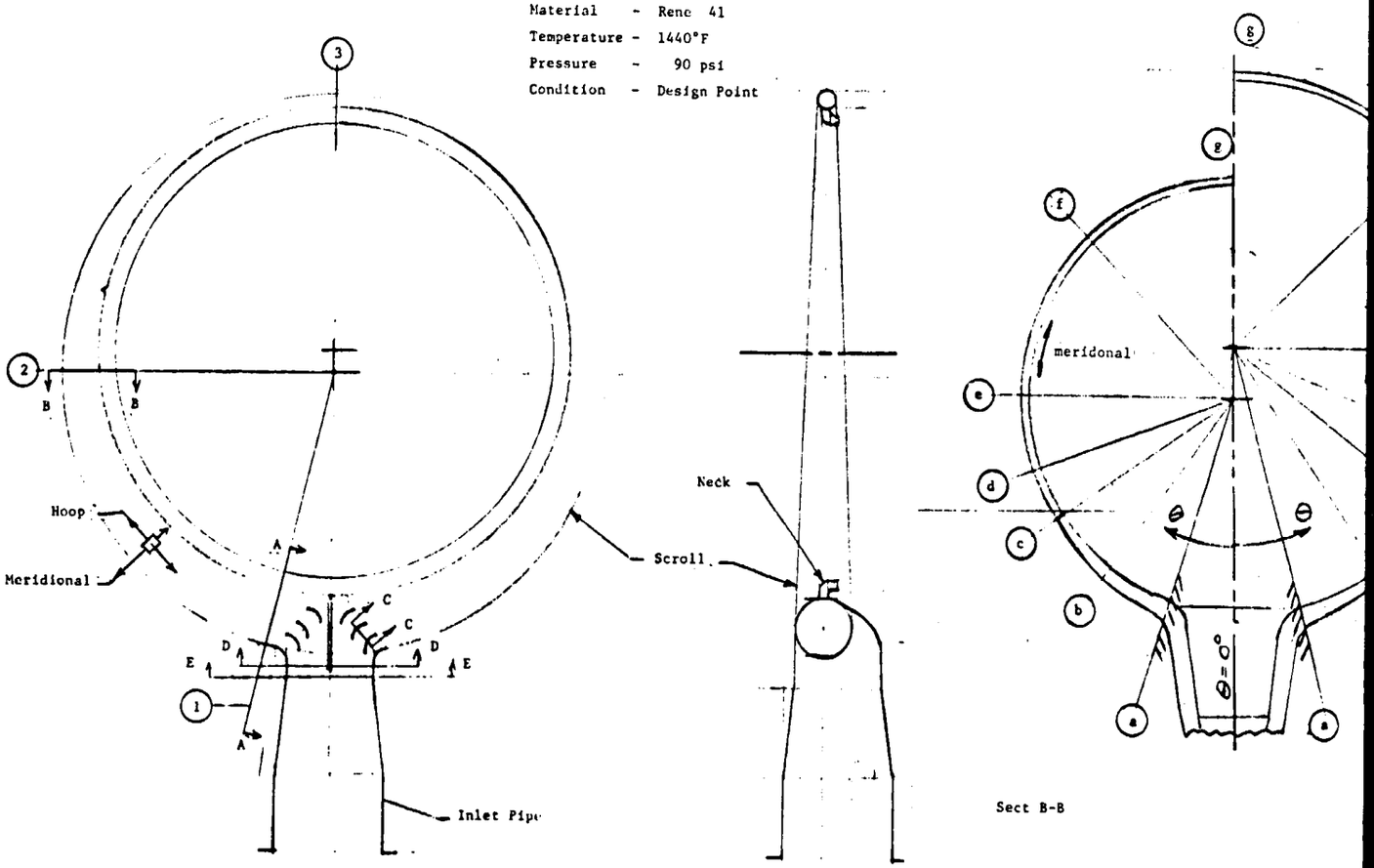

A. INLET

SECT.	THICKNESS IN.	TYPE OF STRESS	STRESS-psi	Allowable STRENGTH-psi	M.S.
CC	.065	Bending	24,200	28,000	+0.15
DD	.065	Hoop & Bending	17,409	28,000	+0.61
	.065	Hoop	17,000	19,000	+0.12
EE	.065	Hoop	10,200	19,000	+0.86

FOLDOUT FRAME 1

HOT GAS SCROLL AND INLET STRESSES

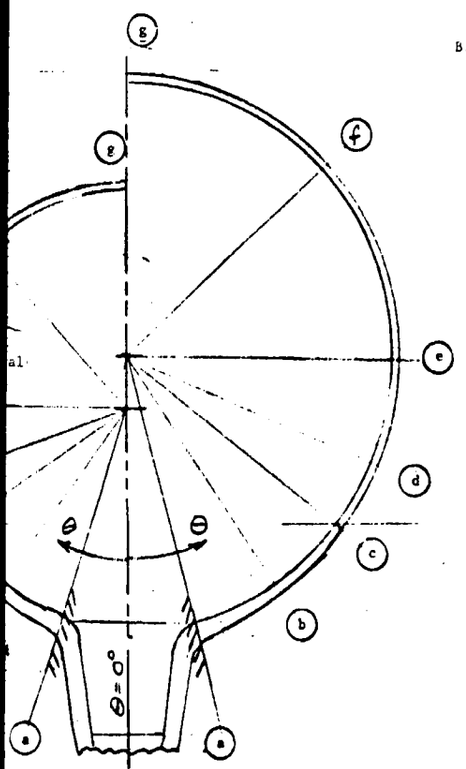

Sect A-A

B. SCROLL

1. Section A-A

location	a	b	c	d	e	f	g
angular pos. (degrees)	10.0	16.8	23.3	50.0	90.0	135.0	180.0
shell thickness, in.	0.08	0.06	0.04	0.04	0.04	0.04	0.04
stresses (incl. thermal), psi							
meridional membrane	-	-	12,200	-	-	-	-
meridional bending	-	-	7,600	-	-	-	-
meridional total	19,350	19,800	19,800	12,600	12,600	19,800	19,800
tangential total (membrane & bend)	13,200	11,000	6,450	6,300	6,300	6,300	11,000
allowable stresses, psi							
membrane allow. (.2% creep)	-	-	19,000	-	-	-	-
M.S. (meridional membrane)	-	-	+0.56	-	-	-	-
total allow. (1000 hr. rupture)	-	-	28,000	-	-	-	-
M.S. (meridional total)	-	-	+0.41	-	-	-	-
stresses (no thermal) psi							
meridional total (membrane & bend)	9,750	13,350	13,350	11,850	11,700	13,350	13,350
tangential total (membrane & bend)	2,700	4,500	5,850	6,000	6,000	5,850	3,750

2. Section B-B

location	a	b	c	d	e	f	g
angular pos. (degrees)	15.6	25.4	35.2	50.0	90.0	135.0	180.0
shell thickness, in.	0.08	0.06	0.04	0.04	0.04	0.04	0.04
stresses (incl. thermal), psi							
meridional membrane	4,200	-	-	-	-	-	-
meridional bending	13,500	-	-	-	-	-	-
meridional total	17,700	16,350	16,350	10,800	8,250	15,750	16,400
tangential total (membrane & bend)	13,200	11,100	7,200	5,100	5,100	7,200	11,100
allowable stresses, psi							
membrane allow. (.2% creep)	19,000	-	-	-	-	-	-
M.S. (meridional membrane)	+3.53	-	-	-	-	-	-
total allow. (1000 hr. rupture)	28,000	-	-	-	-	-	-
M.S. (meridional total)	+0.58	-	-	-	-	-	-
stresses (no thermal) psi							
meridional total (membr. & bend.)	6,750	9,000	9,000	8,100	8,100	9,000	9,000
tangential total (membr. & bend.)	2,100	3,000	3,900	4,200	4,200	3,900	3,000

FOLDOUT FRAME 2

Figure 75

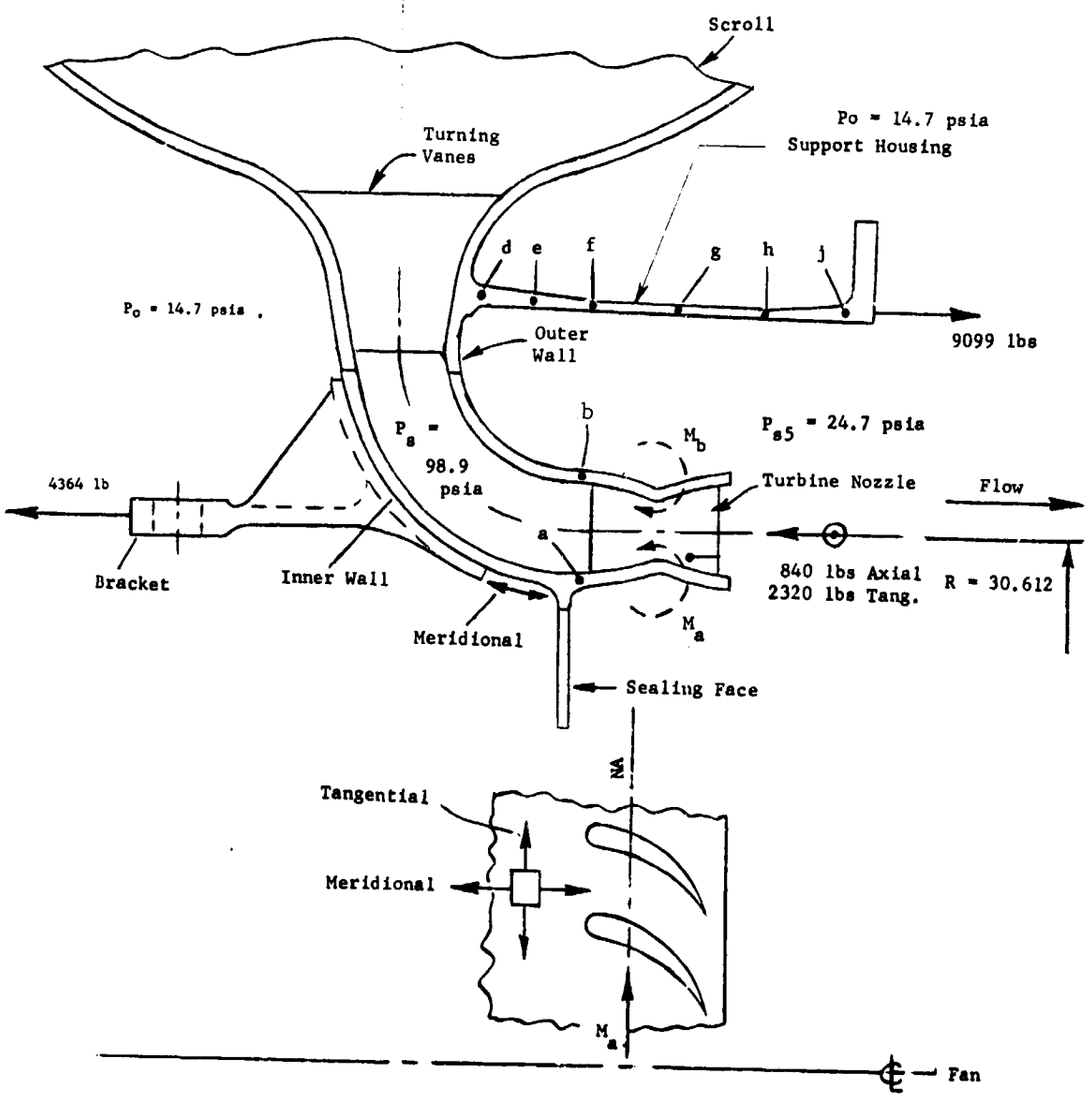

Material - René 41	
Location	
Thickness - In.	
A. Steady State Stres	
(Thermal + Mechani t = 340 sec)	
Temperature-°F	
1. Direct Stress Direction Allowable Stre (.2% Creep - 1	
Margin of Safe	
2) Direct & Bendi Direction Allowable Stre (1000 Hr Ruptu	
Margin of Safe	
B. Transient Stresses	
(Thermal + Mechanic t = 100 sec)	
Temperature - °F	
Stress Direction	
1. Direct Stress -	
2. Direct + Bendin	
Equivalent Stress -	
No. of Cycles	
Min. Allowable Cycl	

*This analysis was perf vanes for fabrication

FOLDOUT FRAME 1

T GAS SCROLL NECK LOADS & STRESSES

Material - René 41 Location	a	b	c	d	e	f	g	h	j
Thickness - In.	.080	.065	.010*	.110	.080	.050	.050	.050	.080
A. Steady State Stress (Thermal + Mechanical t = 340 sec)									
Temperature-°F	1378	1400	1378	1440	1400	1350	1310	1240	1200
1. Direct Stress Direction Allowable Stress - psi (.2% Creep - 1000 Hrs)	22,600 Merid. 29,000	15,600 Merid. 26,000	15,200 Merid. 30,000	500 Tang. 19,000	10,750 Tang. 26,000	17,450 Tang. 32,500	16,100 Tang. 40,000	16,600 Tang. 52,500	12,850 Tang. 61,000
Margin of Safety	+.28	+.67	+.97	>1.0	>1.0	+.86		>1.0	>1.0
2) Direct & Bending Stress - psi Direction Allowable Stress - psi (1000 Hr Rupture & Buckling*)	34,700 Merid. 38,000	32,000 Merid. 34,000	- Merid. 24,900*	19,400 Merid. 28,000	25,900 Merid. 33,000	36,500 Merid. 41,000	17,600 Tang. 49,000	24,600 Merid. 63,500	17,700 Tang. 74,000
Margin of Safety	+.10	+.06	+.64	+.44	+.2	+.12	>1.0	>1.0	>1.0
B. Transient Stresses (Thermal + Mechanical t = 100 sec)									
Temperature - °F	1240	1240	-	1364	1290	1190	1110	975	850
Stress Direction	Merid.	Merid.	-	Merid.	Merid.	Merid.	Merid.	Merid.	Merid.
1. Direct Stress - Psi	-	-	-	-1000	-13,000	-2000	-2000	-2000	15,000
2. Direct + Bending Stress - Psi	95,400	103,000	-	-51,800	-69,500	-102,000	-24,600	-57,600	48,000
Equivalent Stress - Psi	72,000	81,000	-	31,800	46,400	75,800	13,300	35,000	28,100
No. of Cycles	> 50,000	> 50,000	-	> 50,000	> 50,000	>50,000	> 50,000	>50,000	>50,000
Min. Allowable Cycles	24,000	24,000	-	24,000	24,000	24,000	24,000	24,000	24,000

*This analysis was performed for the flight design hollow sheet metal vanes. The prototype design incorporates stronger solid vanes for fabrication purposes only.

FOLDOUT FRAME 2

Figure 76

SECOND STAGE TURBINE STATOR VANI

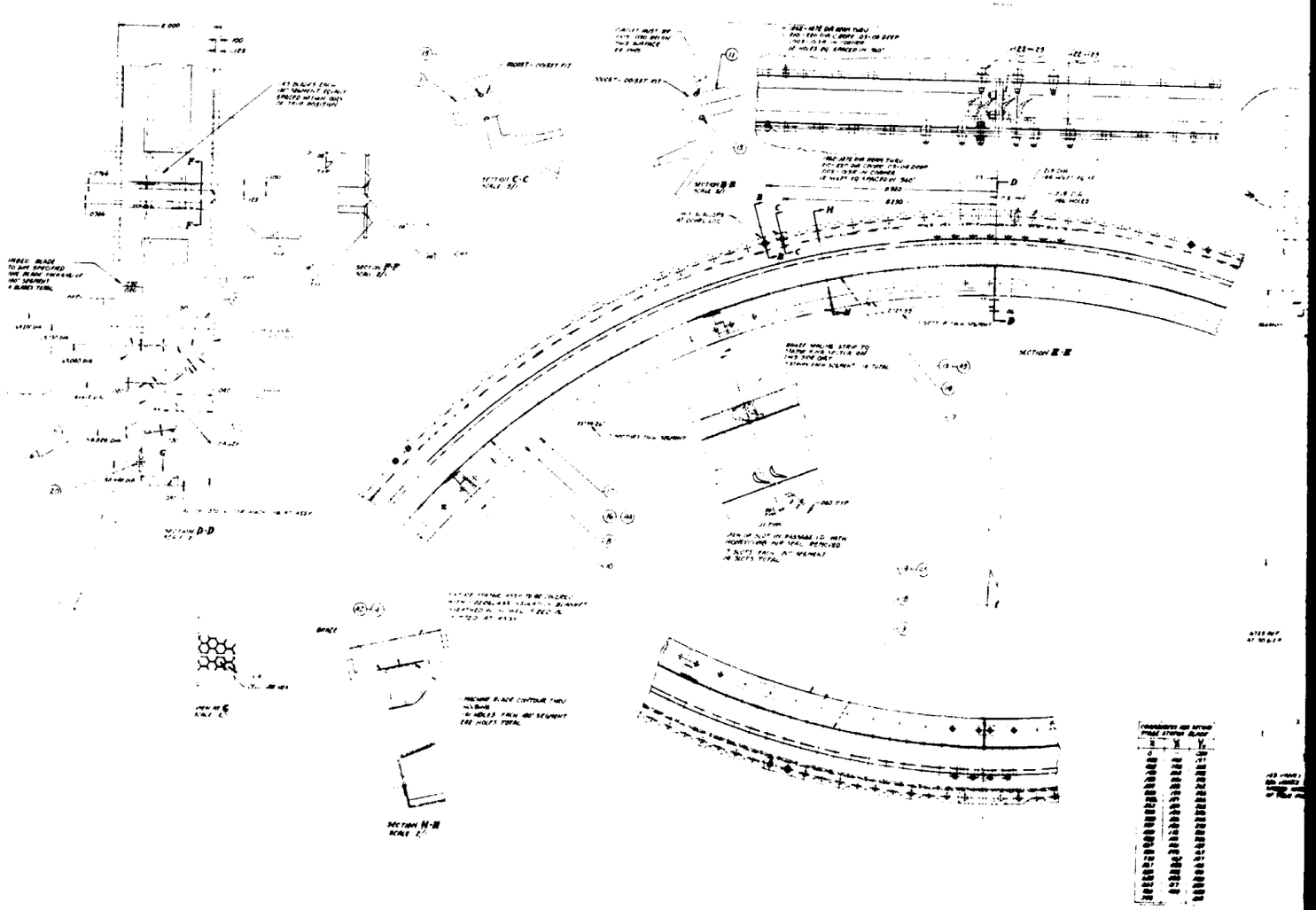

FOLDOUT FRAME 1

TURBINE STATOR VANE ASSEMBLY

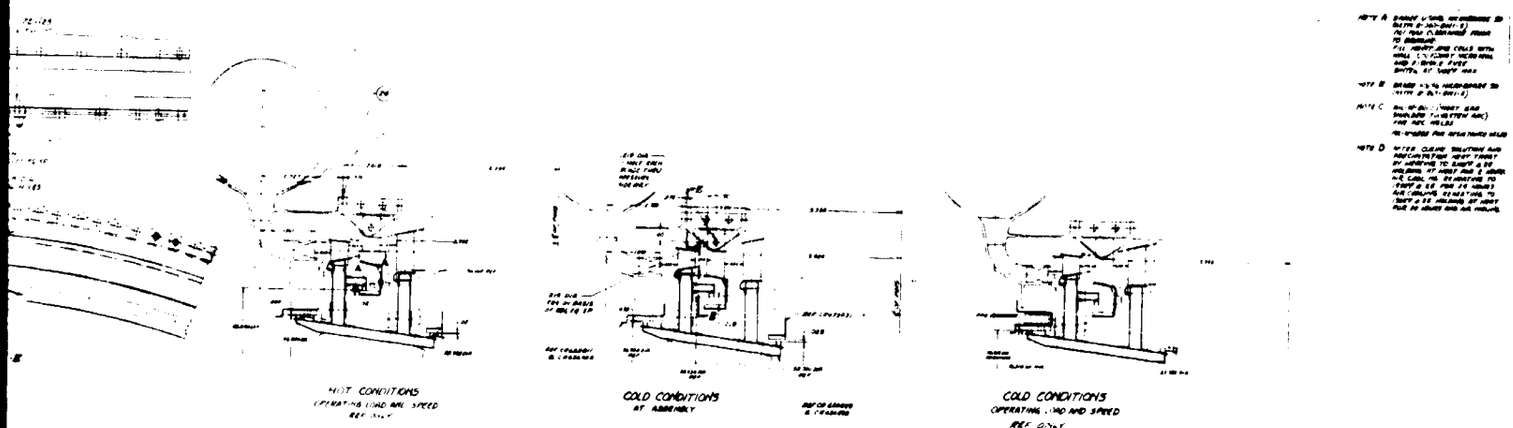

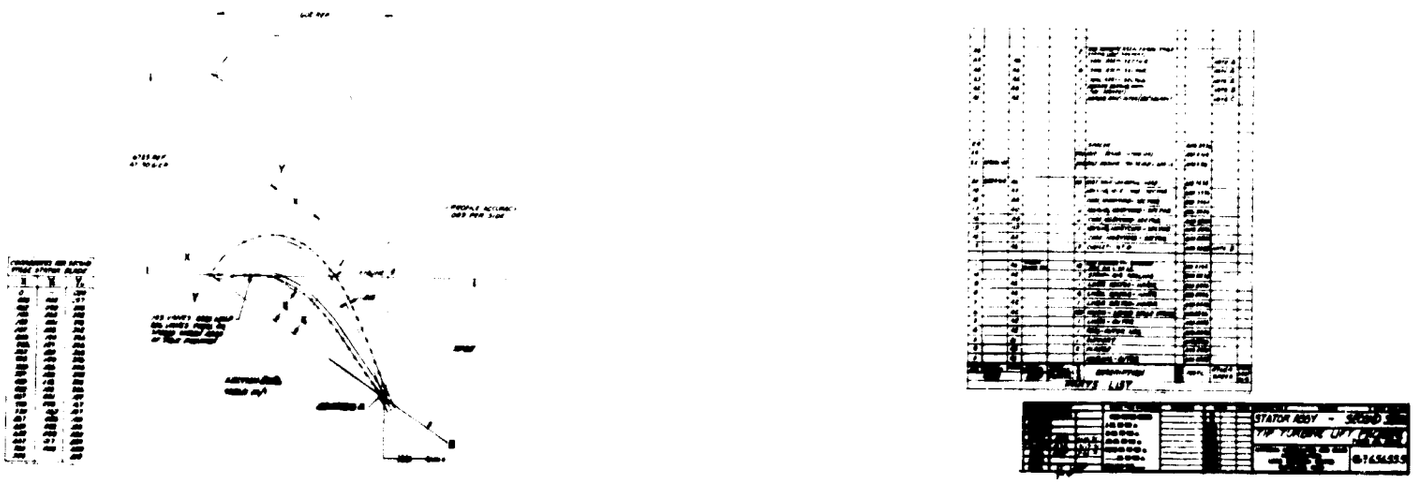

FOLDOUT FRAME 2

Figure 77

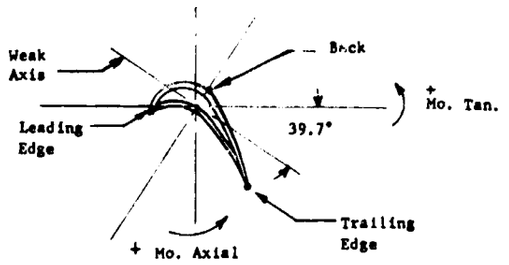

SECTION A -A

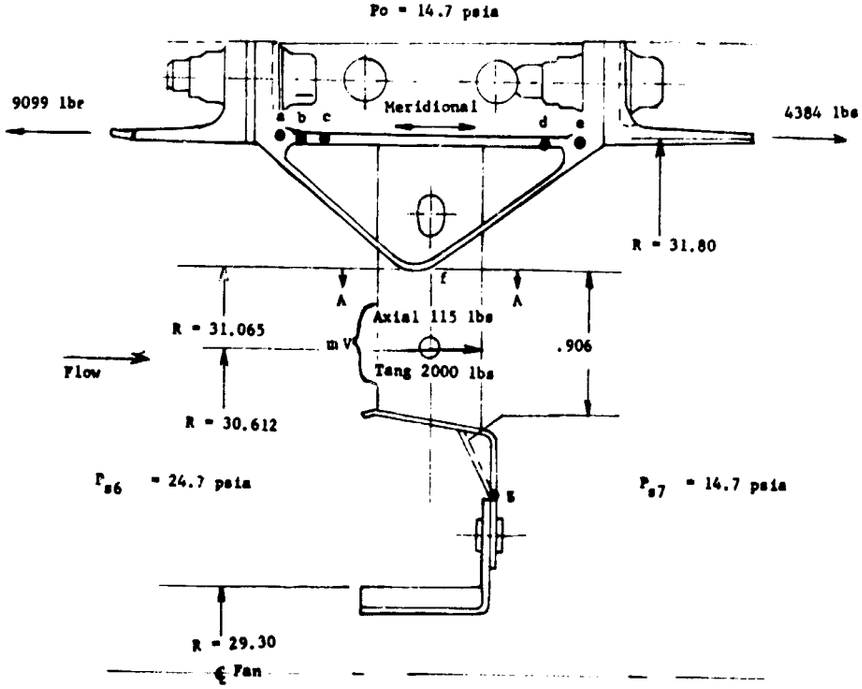

Modified Goodman Diagram

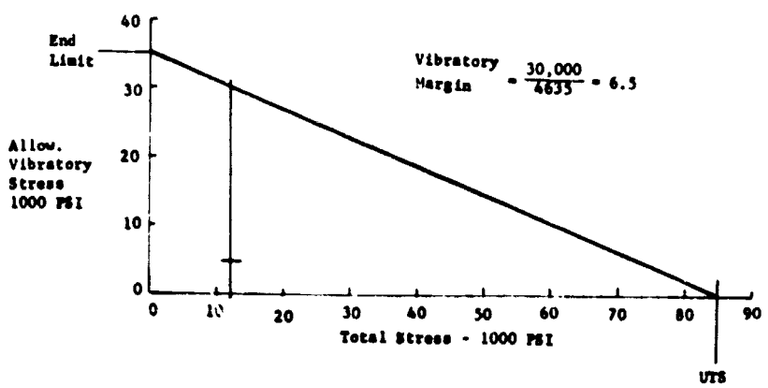

A. Airfoil at Sec

1. Shear Load

Axial	Ta
12.10	6.

2. Gas Bending

Shroud Load
Airfoil Lo
Total

3. Section Pr

Leading Ed
Trailing E
Back

B. Stator Assembly

Material - Hast

Location

Thickness

1. Steady Stat

(Thermal +

t = 340 s

Tempera

Direct

Di

Allowab
(.2% Cr

Margin

Direct

Di

Allowab
(1000 H
& .2%

Margin

2. Transient St

(Thermal +
t = 100 se

Tempera

Stress

Direct Stre

Direct + Be
psi

Equivalent

No. of Cycl

Min. Allow

FOLDOUT FRAME 1

STATOR VANE ASSEMBLY LOADS & STRESSES

A. Airfoil at Section A-A, T = 1089°F (Hastelloy X Material)

1. Shear Loads, Lbs/Ft

Axial	Tang.
12.10	6.94

2. Gas Bending Moments, Lb-In/Bl

	Axial	Tang	Weak	Strong
Shroud Load	8.07	0	5.16	6.21
Airfoil Load	2.35	3.13	3.91	-0.19
Total	10.42	3.13	9.07	6.02

3. Section Properties (C/I), $1/in^3$

	Weak	Strong
Leading Edge (LE)	1198	237
Trailing Edge (TE)	673	309
Back	942	91

4. Stress, Psi

	Leading Edge (LE)	Trailing Edge (TE)	Back
Gas Bending due to Shroud Load	7,655	1,541	5,435
Gas Bending due to Airfoil Load	4,635	2,699	3,663
Gas Bending due to Total Load	12,290	4,240	9,098

5. Sign Convention:

+ Tensile Stress
- Compressive Stress

B. Stator Assembly

Material - Hastelloy X

Location	a	b	c	d	e	f	g
Thickness	0.100	0.075	0.050	0.050	0.100	0.015	0.030
1. Steady State Stresses (Thermal + Mechanical) t = 340 sec							
Temperature, °F	1200	1200	1190	1100	1070	1089	1050
Direct Stress - psi	-10,800	-14,450	-11,900	1,300	1,450	12,290	-
Direction	Tang.	Tang.	Tang.	Tang.	Tang.	Merid.	Merid.
Allowable Stress - psi (.2% Creep - 1000 Hrs)	9500	9500	10,000	15,900	19,000	20,000	-
Margin of Safety	-.12	-.34	-.16	>1.0	>1.0	+0.63	-
Direct + Bending Stress	-13,300	-24,500	-13,300	16,000	3,500	12,290	27,000
Direction	Tang.	Merid.	Tang.	Merid.	Merid.	Merid.	Merid.
Allowable Stress, psi (1000 Hr Rupture & .2% Yield*)	28,000	28,000	29,500	*31,000	*31,500	34,000	34,000
Margin of Safety	>1.0	+.14	>1.0	>1.0	>1.0	>1.0	+0.86
2. Transient Stresses (Thermal + Mechanical) t = 100 sec							
Temperature	750	750	750	650	620	1020	-
Stress Direction	Merid.	Merid.	Merid.	Tang.	Tang.	-	-
Direct Stress - psi	500	1500	1300	2000	-3500	-	-
Direct + Bending Stress, psi	15,000	52,400	17,800	8200	-4100	-	-
Equivalent Stress - psi	8100	35,600	9800	4300	2100	68,000	-
No of Cycles	>50,000	>50,000	>50,000	>50,000	>50,000	25,000	-
Min. Allow Cycles	24,000	24,000	24,000	24,000	24,000	24,000	-

FOLDOUT FRAME 2

Figure 78

TURBINE EXHAUST HOUSING AS

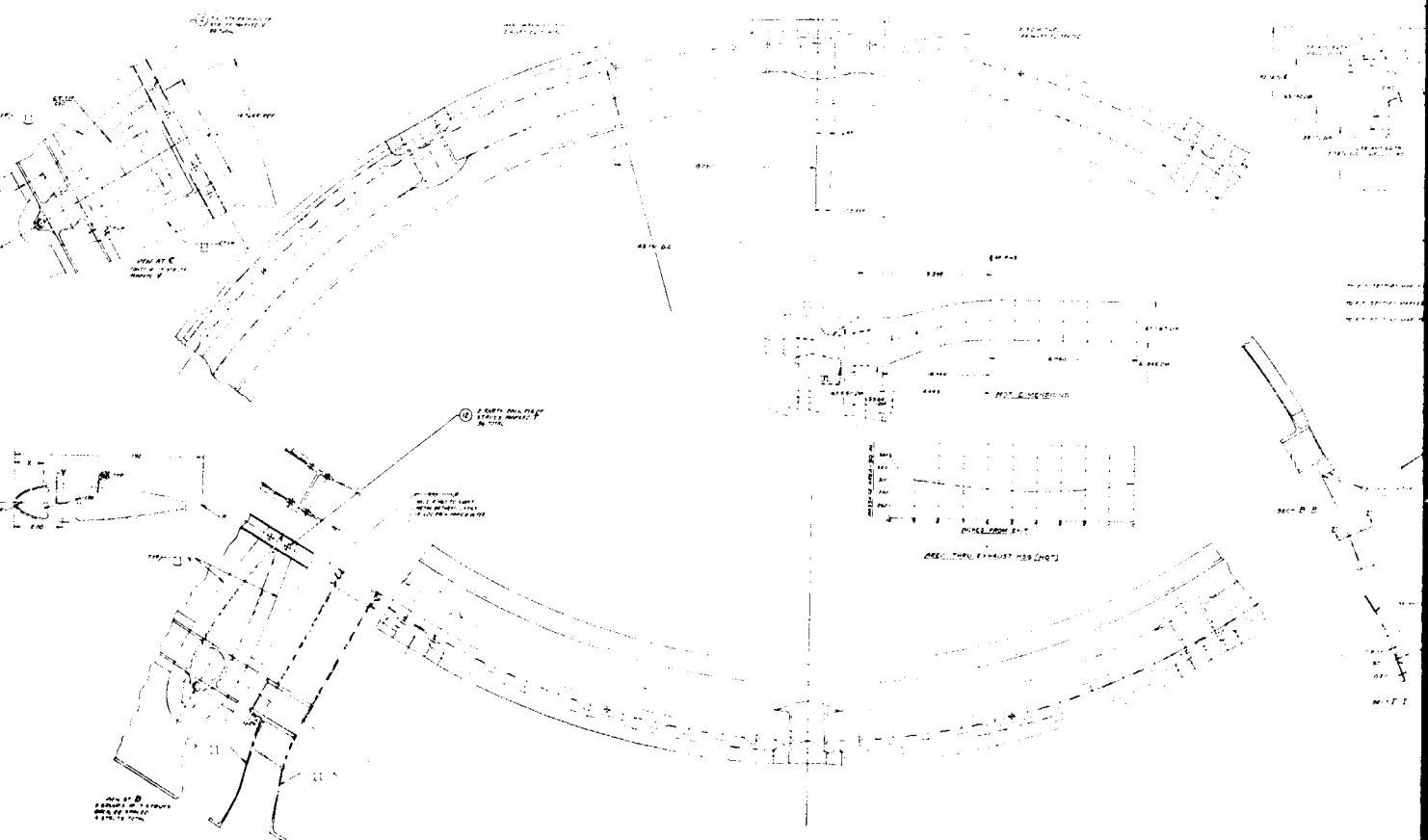

FOLDOUT FRAME 1

EXHAUST HOUSING ASSEMBLY

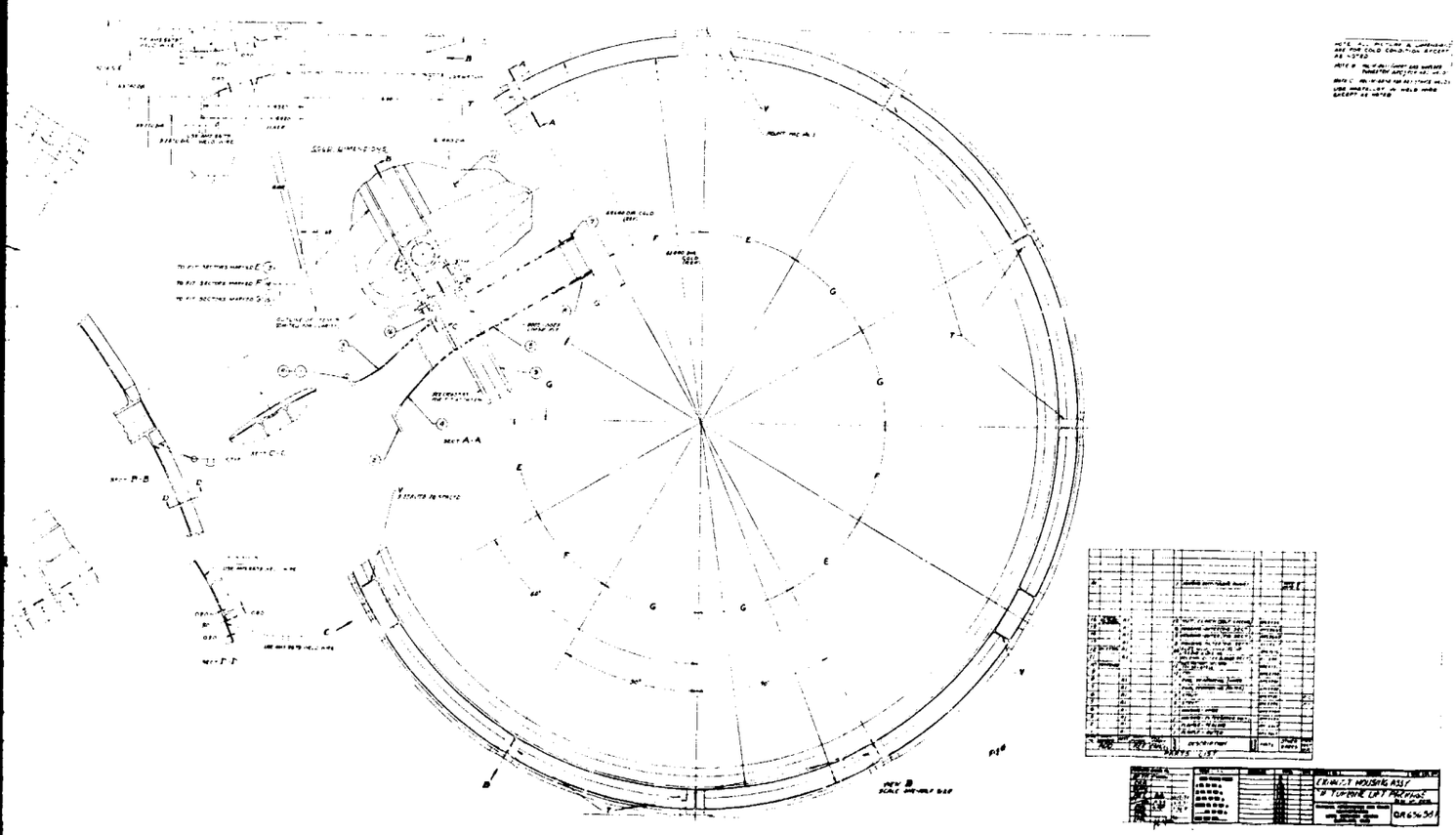

FOLDOUT FRAME 2

Figure 79

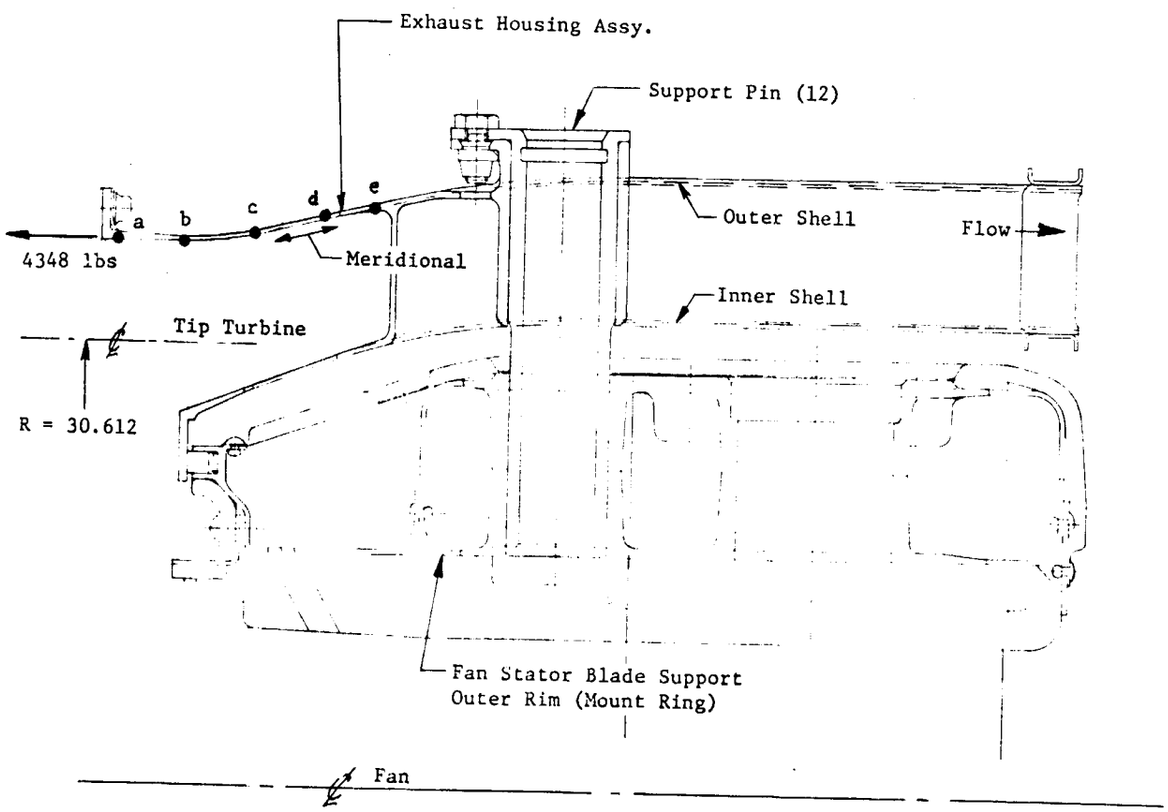

1. EXHAUS
A. Ste
(TH
t =
1)
2)
B. Tra
(Th
t =
1)
2)
2. EXHAUST
Iter
Outer Sh
Inner Sh
Ring - C

FOLDOUT FRAME 1

TURBINE EXHAUST HOUSING LOADS AND STRESSES

1. EXHAUST HOUSING DUCT STRESSES

Material Inconel 600

Location	a	b	c	d	e
Thickness - in.	.06	.04	.04	.04	.04
A. Steady State Stress					
(Thermal and Mechanical) t = 340 Sec					
Temperature - °F	1030	920	900	900	900
1) Direct Stress - psi	2,700	8,000	-650	600	582
Direction	Tang.	Tang.	Tang.	Merid.	Merid.
2) Direct & Bending Stress-psi	5,100	10,100	9,500	3,200	1,300
Direction	Merid.	Tang.	Merid.	Merid.	Merid.
Allowable Stress - psi (.2% Yield)	21,500	22,400	22,600	22,600	22,600
M.S.	>1.0	>1.0	>1.0	>1.0	>1.0
B. Transient Stress					
(Thermal and Mechanical) t = 100 Sec					
Temperature - °F	620	700	720	750	750
Stress Direction	Tangential	Tangential	Meridional	Meridional	Meridional
1) Direct Stress - psi	12,400	5,400	3,200	590	2,500
2) Direct & Bending Stress-psi	13,200	7,400	3,700	600	3,200
Equivalent Stress	7,000	3,800	1,900	300	1,600
No. of Cycles	>50,000	>50,000	>50,000	>50,000	>50,000
Min. Allow. Cycles	24,000	24,000	24,000	24,000	24,000

2. EXHAUST HOUSING BUCKLING

Item	T - °F	ΔP_{max} - psia	$\Delta P_{critical}$ - psia	Ring Moment of Inertia - in^4	Reqd Ring Moment of Inertia - in^4	M.S.
Outer Shell	900	1	1.58	-	-	+ .58
Inner Shell	900	1	1.54	-	-	+ .54
Ring - Outer	900	1	-	.005	.0026	+ .92

FOLDOUT FRAME 2

Figure 80

TURBINE EXHAUST HOUSING PIN LOADS AND STRESS

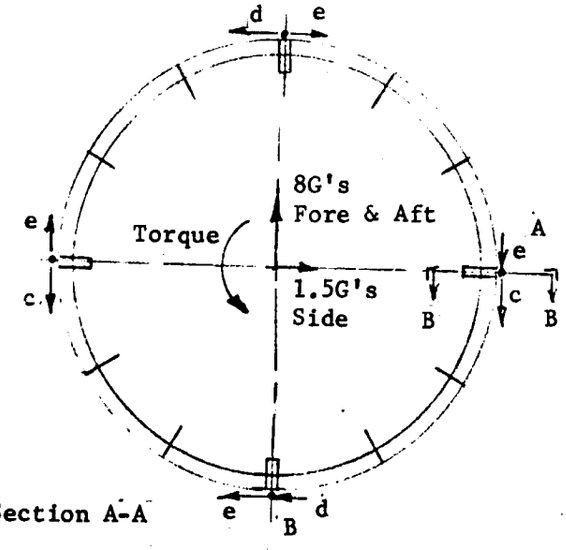

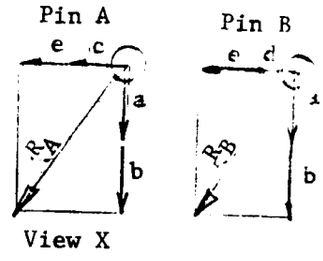

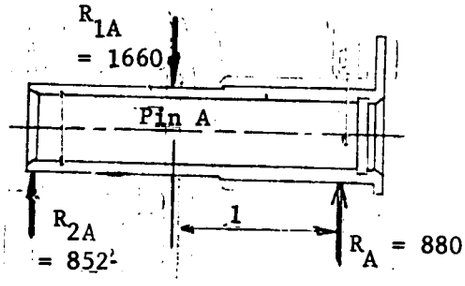

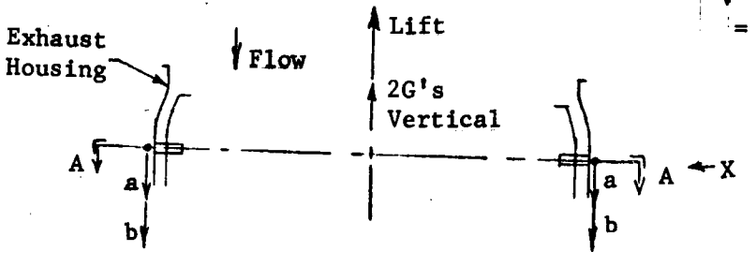

Matl: Hast. X
Temp. 900°F
.2% Yield - 33,000 psi

Shear Allow
(.6) (.2%y) - 19,600 psi

		Total Load	Load per Pin - Lbs A	B
a)	Lift	4,348 lbs	362	362
b)	2G's Vertical	524 lbs	44	44
c)	8G's Fore & Aft	2,096 lbs	349	0
d)	1.5G's Side	393 lbs	0	66
e)	Torque (Tangential)	132,100 lb-in	349	349
f)	Resultant Load - Lbs		807	581
g)	Shear Stress - Psi		17,900	-
	M.S.		+.10	-
h)	Bending Stress - Psi		11,900	-
	M.S.		+1.77	-

Figure 81

AXIAL & RADIAL TURBINE LABYRINTH SEAL DISPLACEMENTS

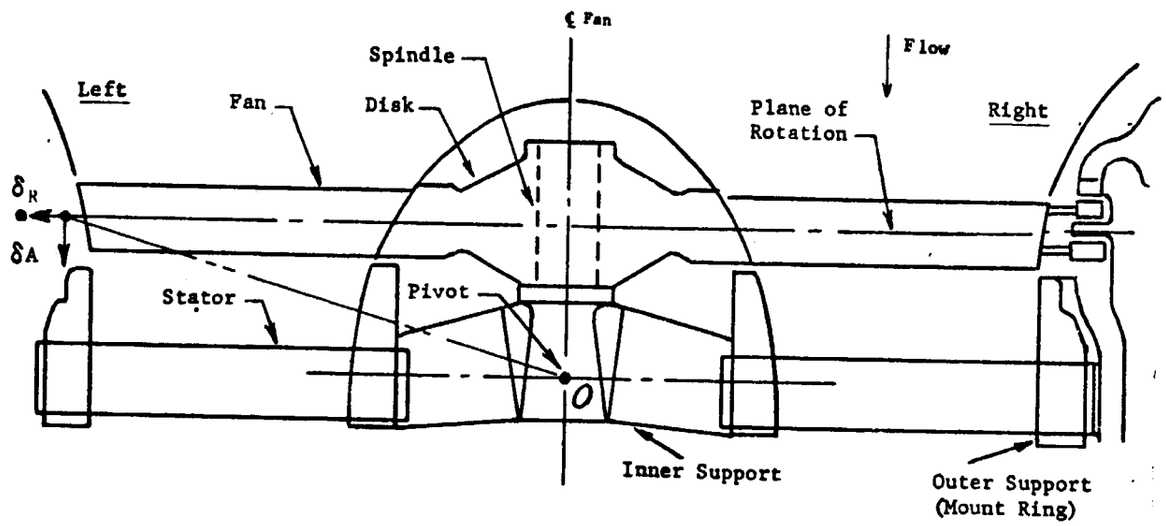

Sign Convention

Radial Outward +
Radial Inward -
Axial Downward +
Axial Upward -

Condition	Steady State Loading				Steady State Plus Gyroscopic Moment From 1 Rad/Sec			
Fan Rotor Blade Tip Displacement -ins. / Due To:	Right		Left		Right		Left	
	δ_R	δ_A	δ_R	δ_A	δ_R	δ_A	δ_R	δ_A
1) Loading on Rotor Blade	.046	-.028	.046	-.028	.046	.006	.046	-.061
2) Rotation About Point "O"	0	0	0	0	-.042	.142	.042	-.142
3) Translation of Point "O"	0	.166	0	.166	0	.166	0	.166
4) Bending of Spindle	0	0	0	0	-.021	.108	.021	-.108
Total Displacements	.046	.138	.046	.138	-.017	.422	.10_	-.145

Figure 82

Fig 223

LABYRINTH SEAL GOUGE FROM GYROSCOPIC MOMENT

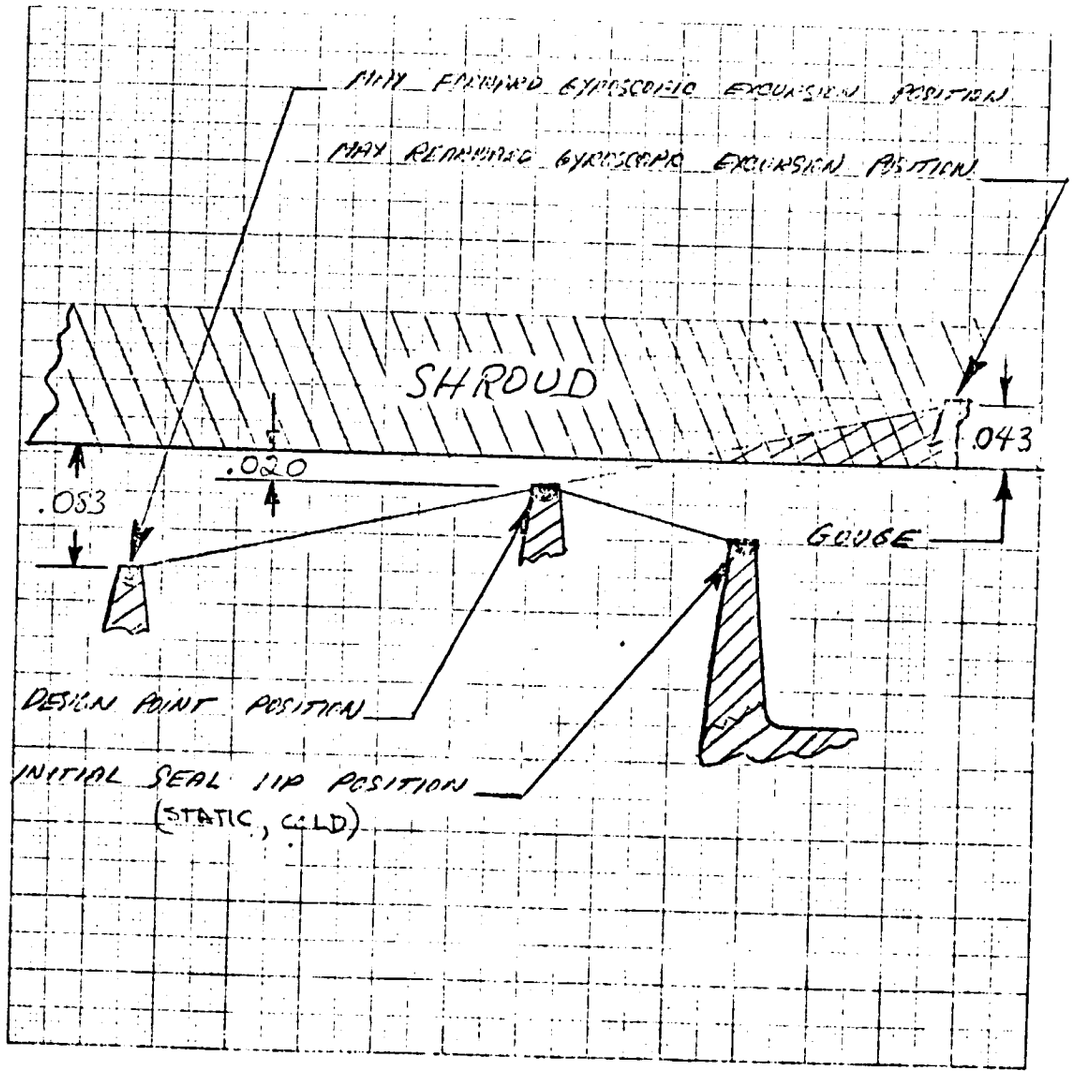

Figure 83

FRONT LABYRINTH SEAL GAP CHARACTERISTICS

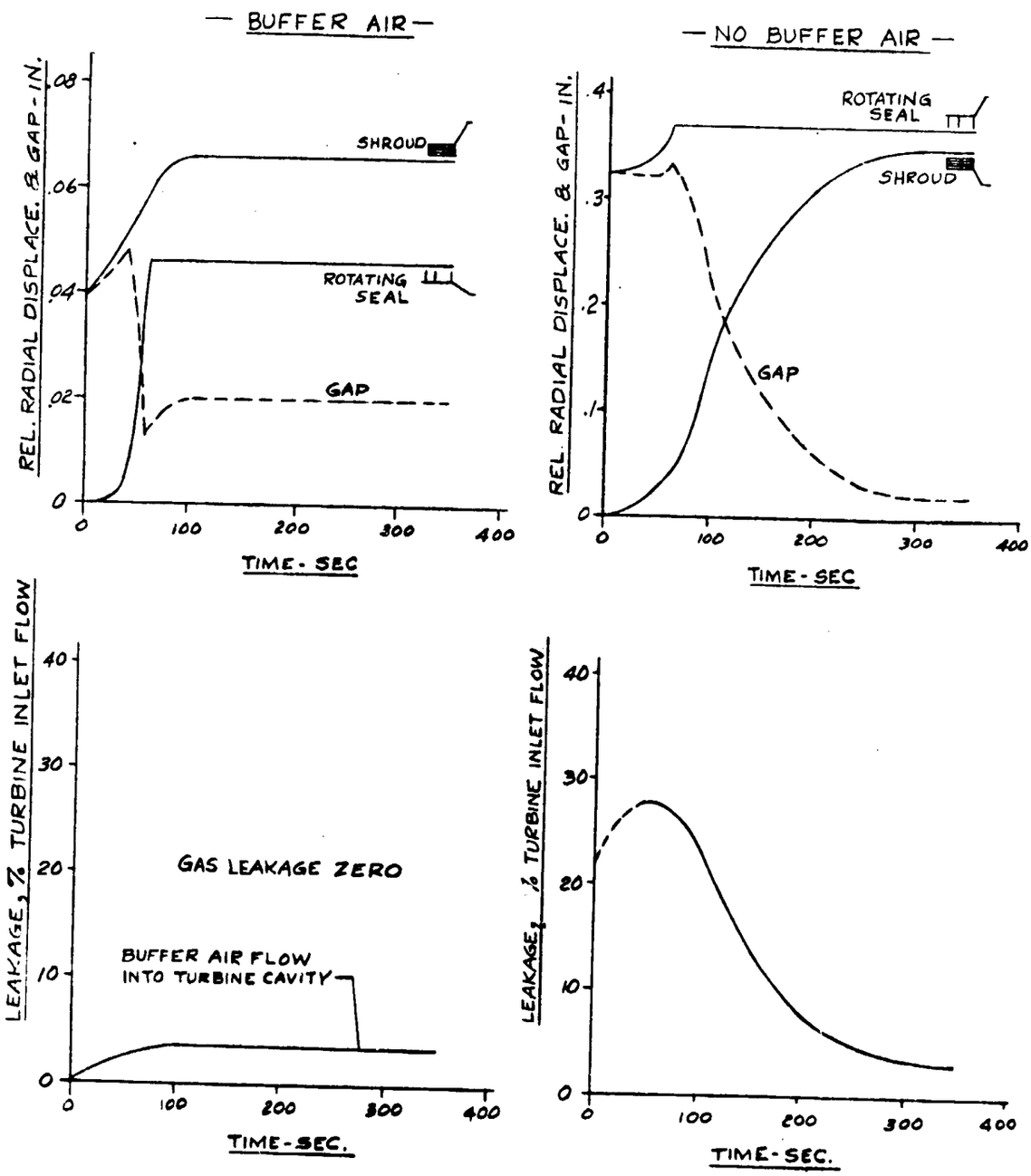

Figure 84

MIDDLE LABYRINTH SEAL GAP CHARACTERISTICS

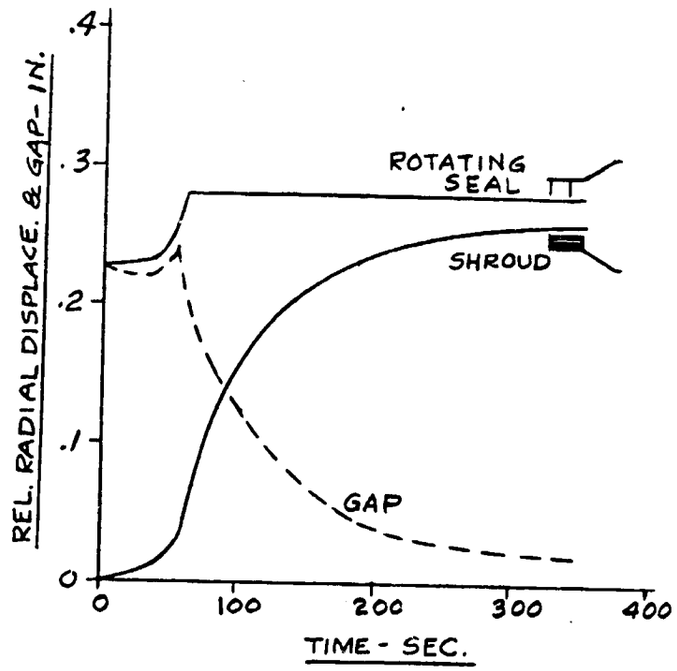

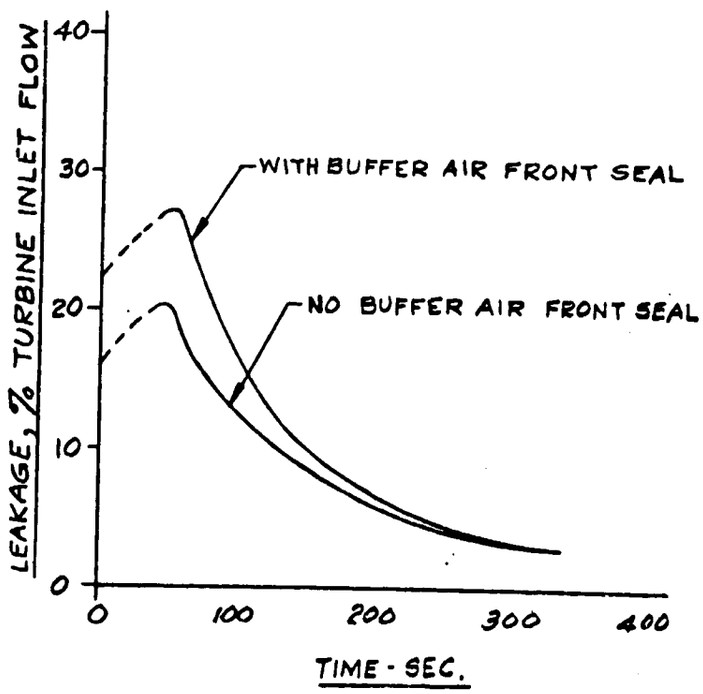

Figure 85

REAR LABYRINTH SEAL GAP CHARACTERISTICS

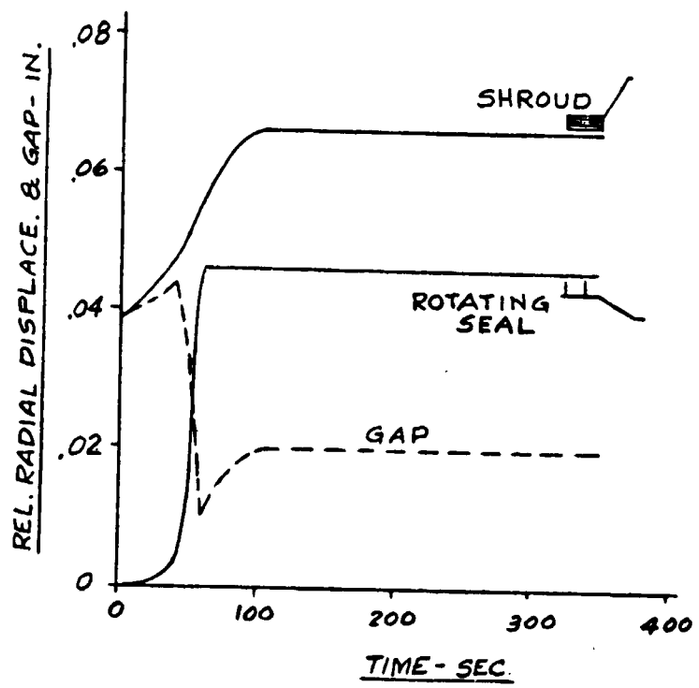

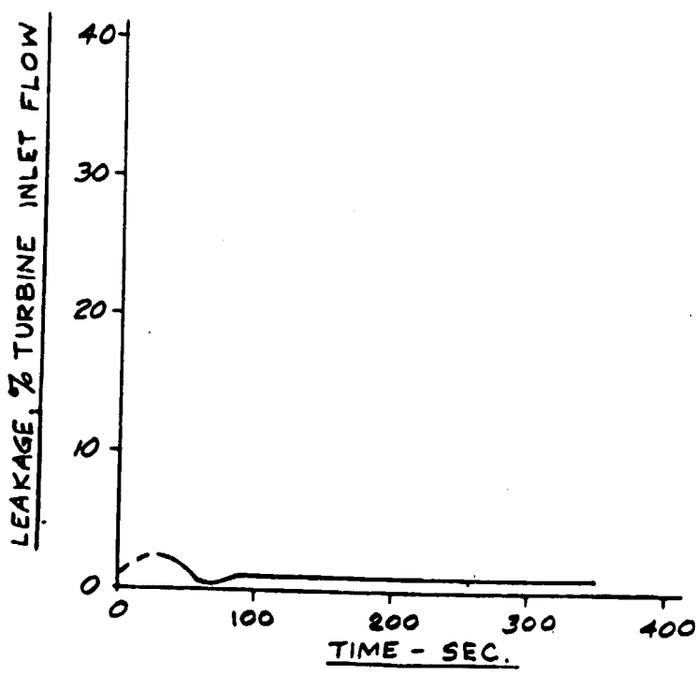

Figure 86

TURBINE GAS PASSAGE MISMATCH FROM THERMAL EFFECTS

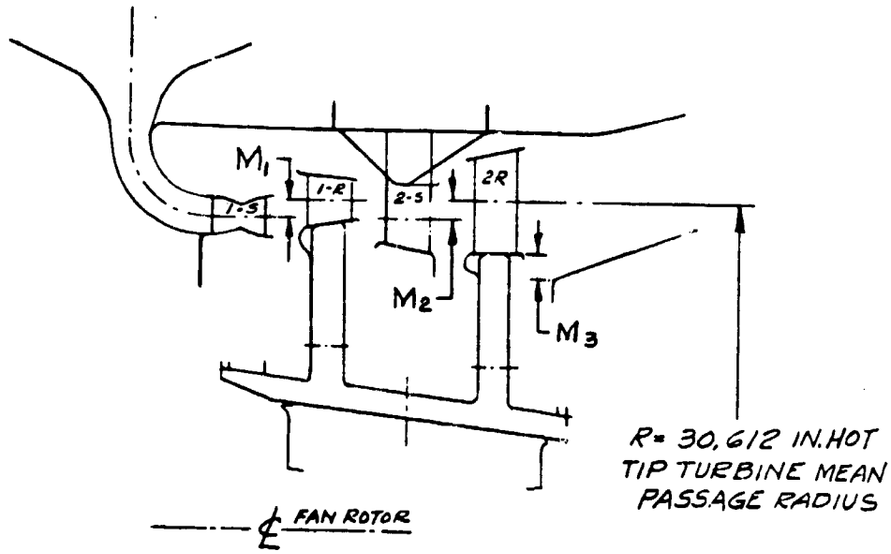

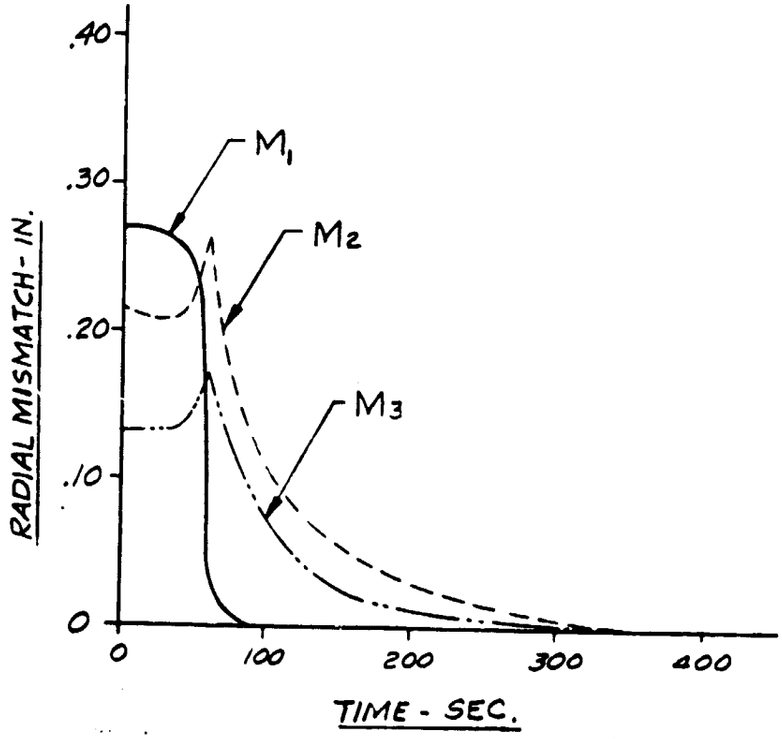

Figure 87

BUFFER AIR FLOW S

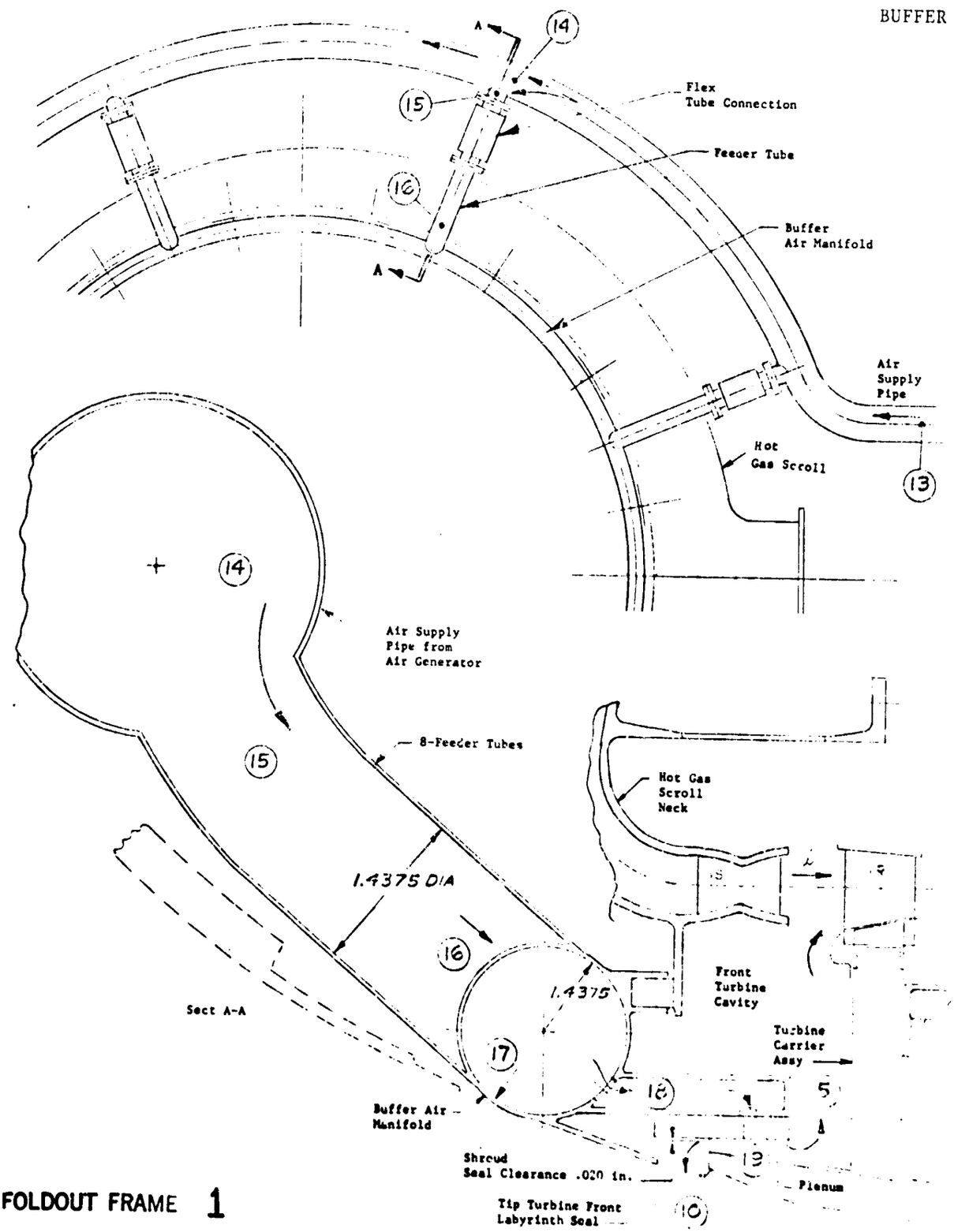

FOLDOUT FRAME 1

71-353

	DESCRIPTION	K*	W lb/sec	A Sq. In.	P_T Psia	V ft/sec	Mach. No.	q $\%P_T$
13 - 14	6.5" ID Pipe ≈ 40 Ft. long	1.3	2.63	33.2	P_{T13}=33.8 P_{T14}=33.6	92	0.07	0.34
14 - 15	90° Branch with a 2.55 Contraction	1.1	2.63	13.0	P_{T15}=32.8	238	0.182	2.27
15 - 16	8 1.4375" I.D. tubes L/D≈715	0.3	2.63	13.0	P_{T16}=32.6	238	0.182	2.27
16 - 17	90° Branch	1.3	2.63	-	P_{T17}=31.8	238	0.182	2.27
17 - 18	Holes Assumed sufficiently Large to insure negligible Loss	0	2.63	-	P_{18} = 31.8	-	-	-
18 - 19	Series of Holes D/L Approx. 1.0 Total Area in 11.3 Sq.in.	1.0	2.63	11.3	P_{19}=29.8	393	0.30	5.92
19 - 5	Single Tooth Seal	-	1.05	-	P_5 =25.0	-	-	-
19 - 10	Double Tooth Seal	-	1.58	-	P_6 = 11.4	-	-	-

* K = Loss Coefficient Defined as $\frac{\Delta P}{q}$

FOLDOUT FRAME 2

Figure 88

BUFFER AIR FLOW & PLENUM PRESSURE

(33.8 psia & 250°F AIR GENERATOR)

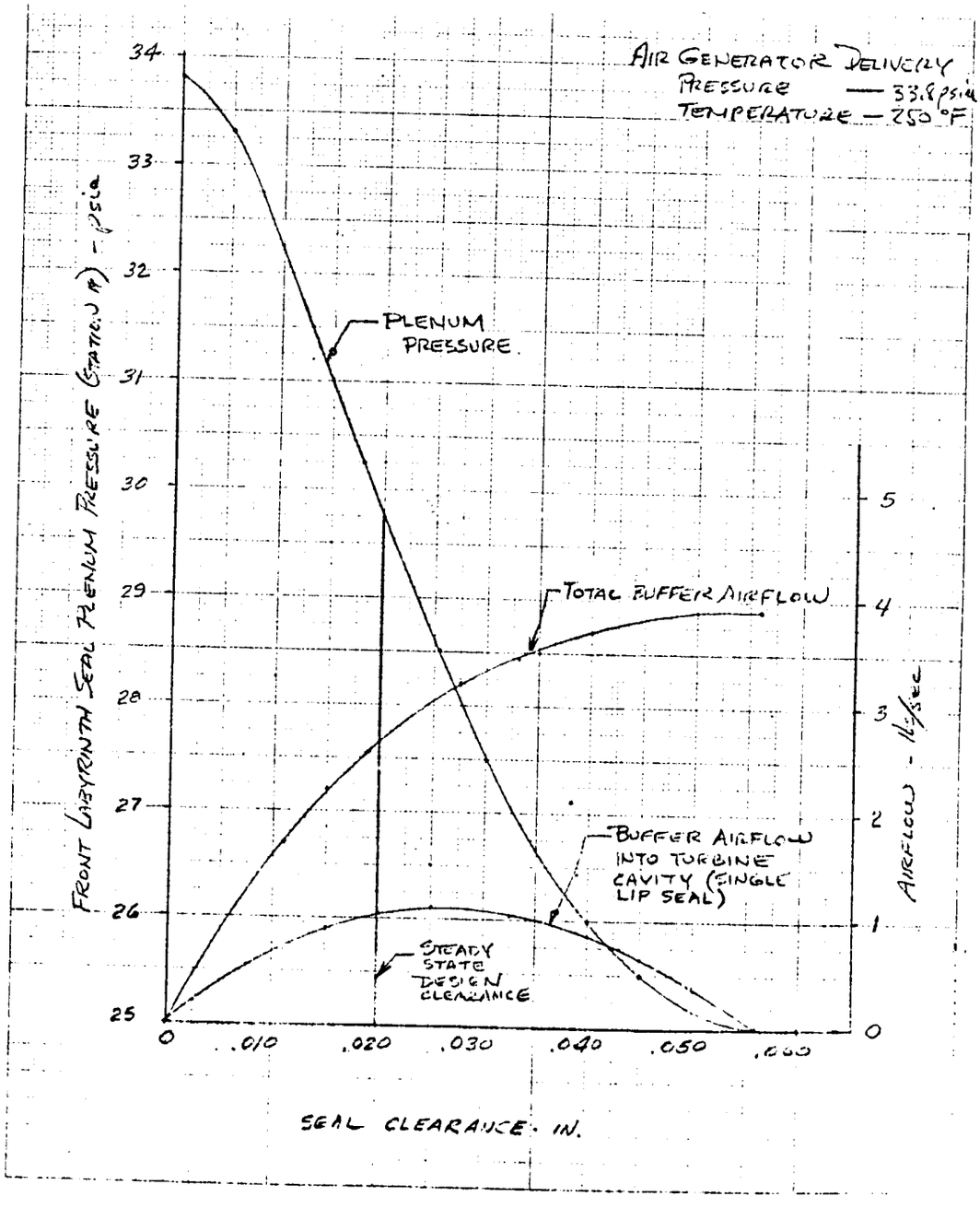

Figure 89

BUFFER AIR FLOW & PLENUM PRESSURE
(47.3 psia & 300°F AIR GENERATOR)

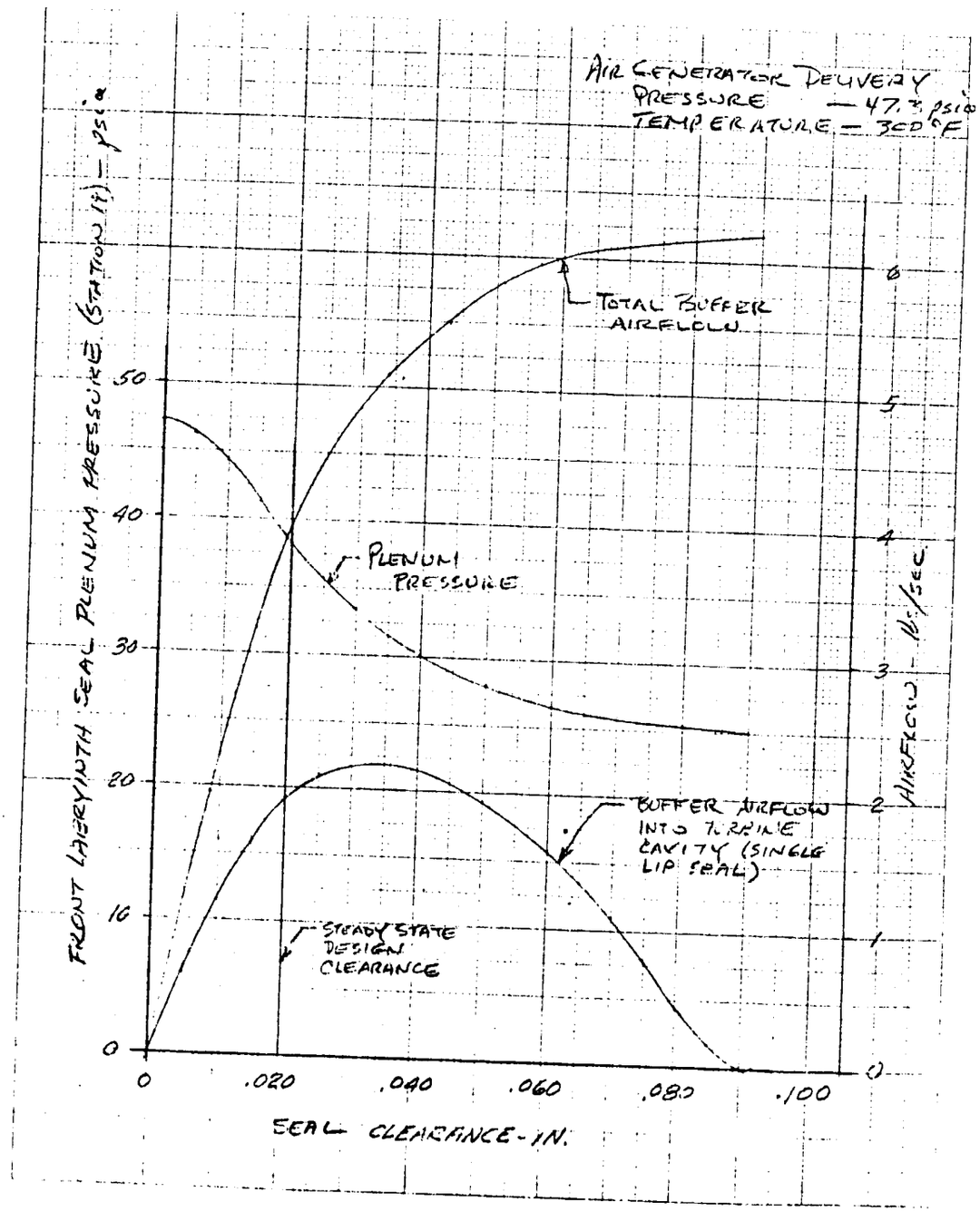

Figure 90

BUFFER AIR MANIFOLD ASSEMBLY (DIRECT C

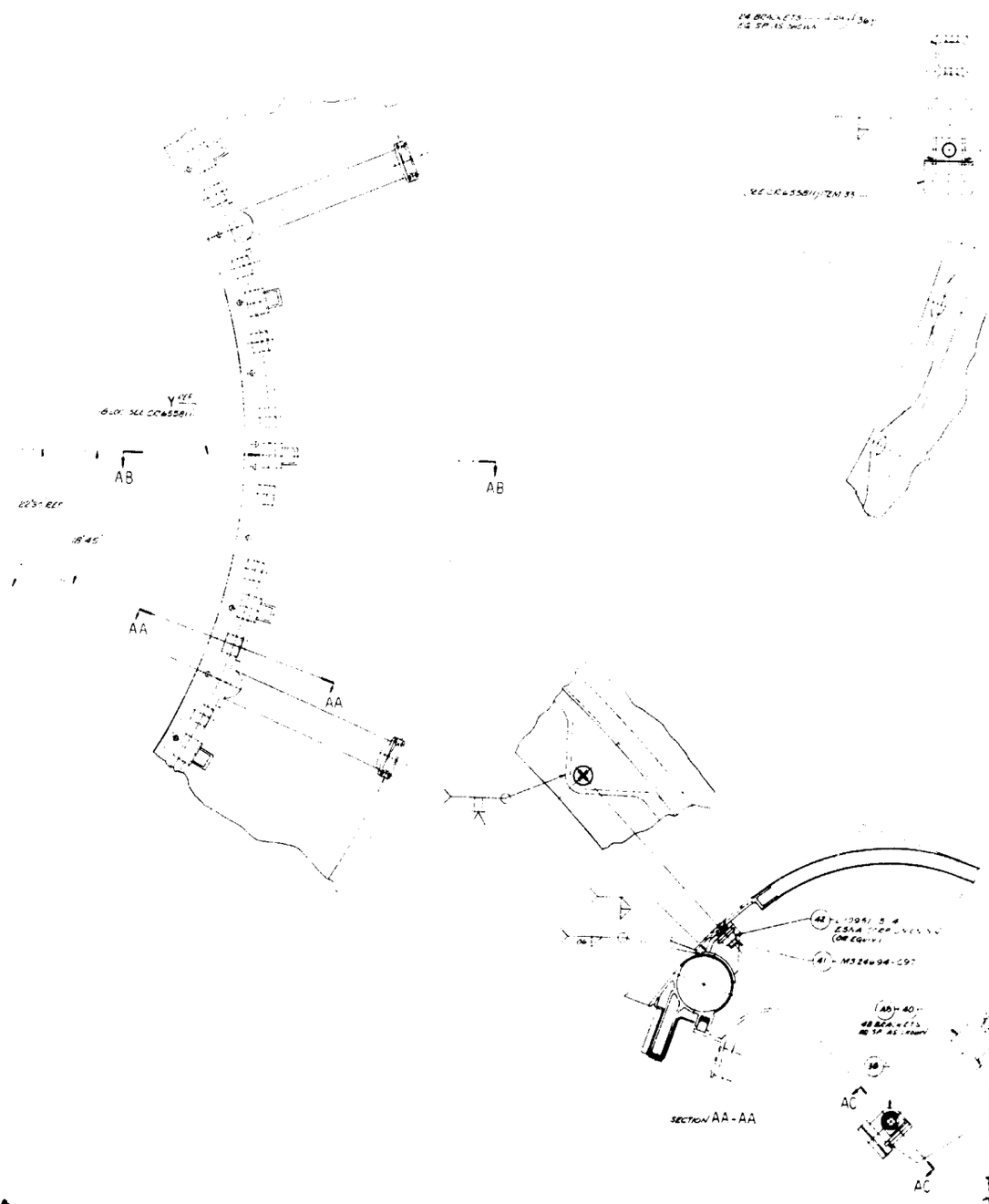

FOLDOUT FRAME 1

EMBLY (DIRECT CONNECTED BELLMOUTH)

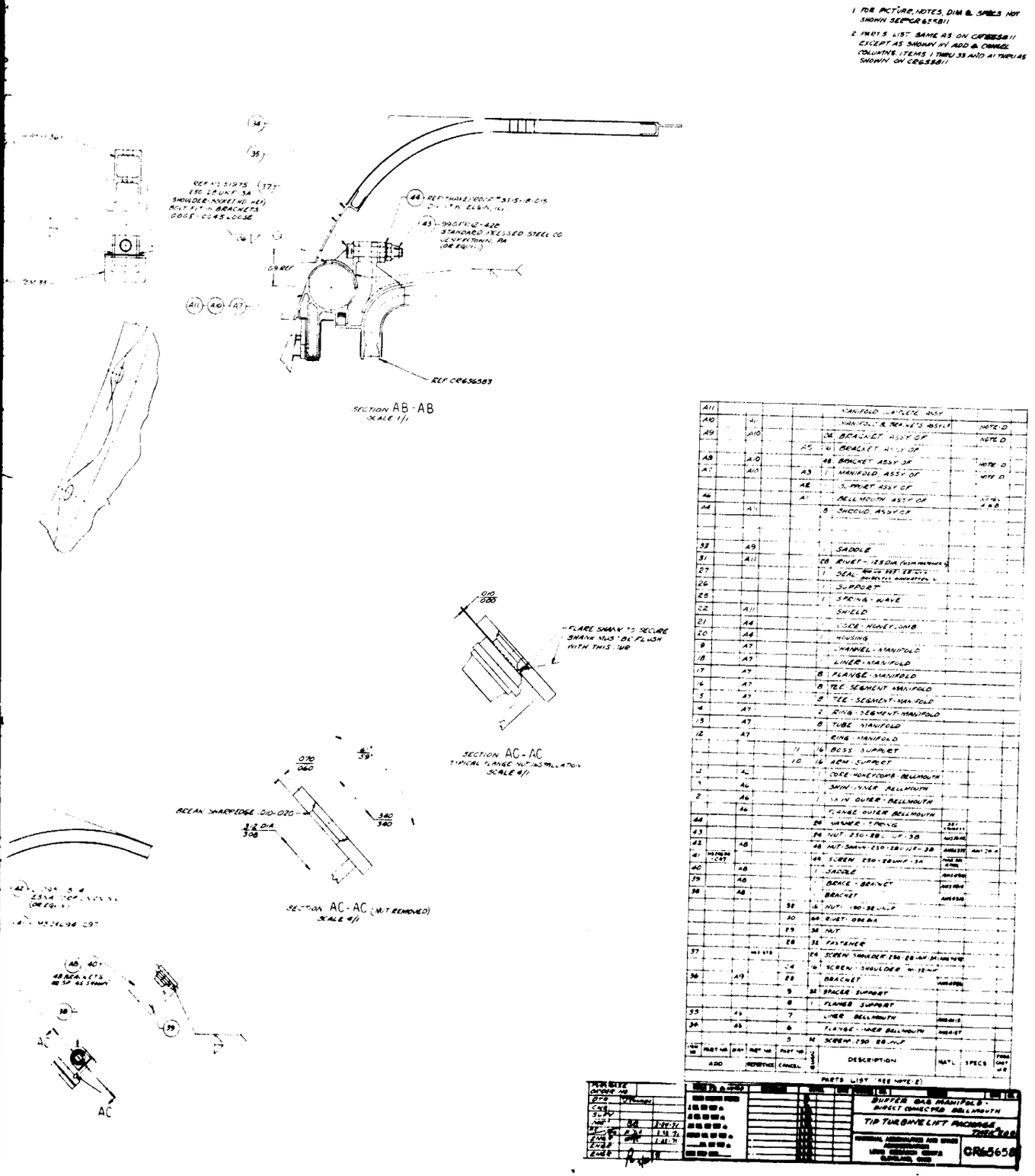

FOLDOUT FRAME 2

FOLDOUT FRAME

Figure 91

BUFFER AIR MANIFOLD ASSEMBLY (PINNED CO

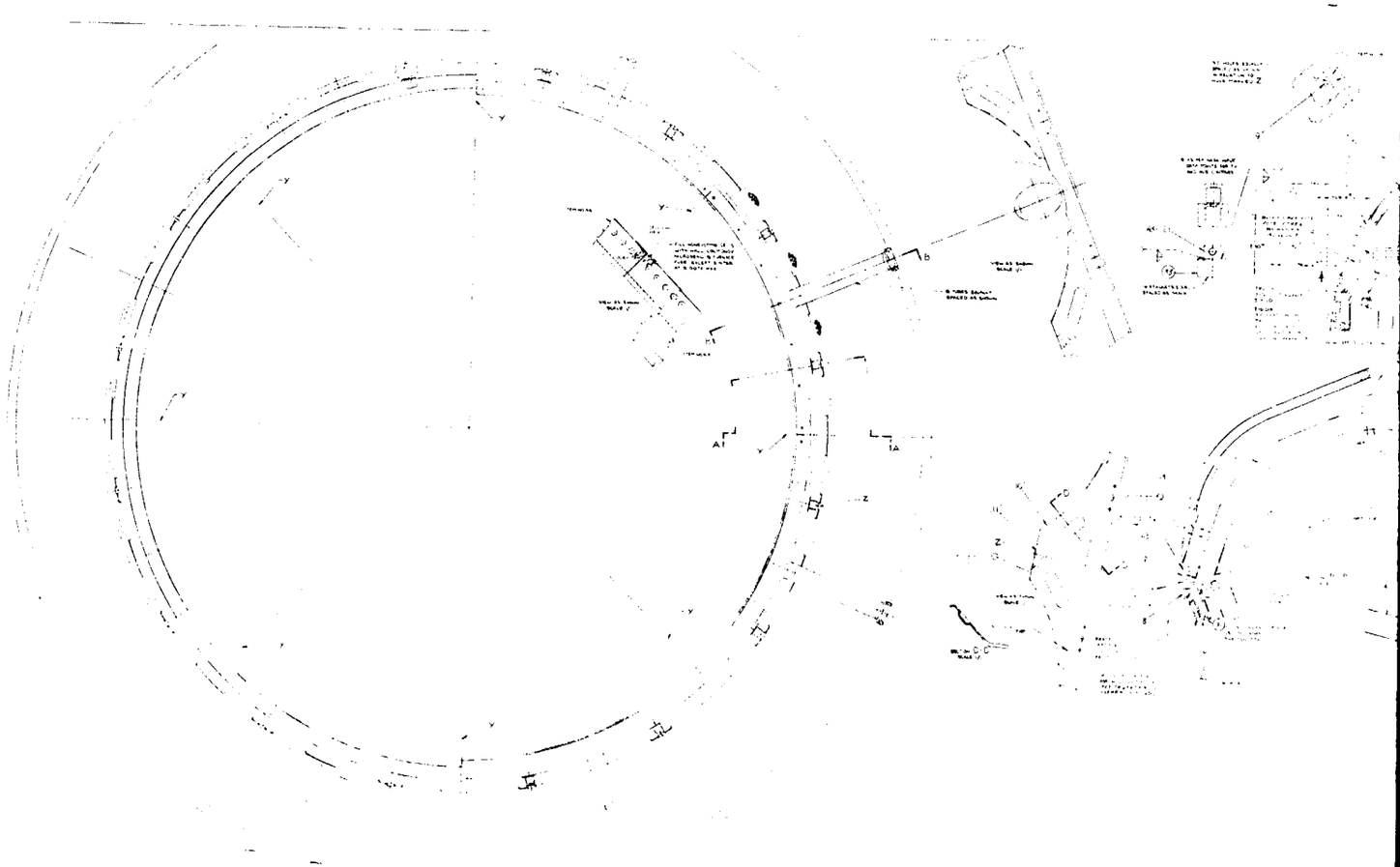

FOLDOUT FRAME 1

D ASSEMBLY (PINNED CONNECTED BELLMOUTH)

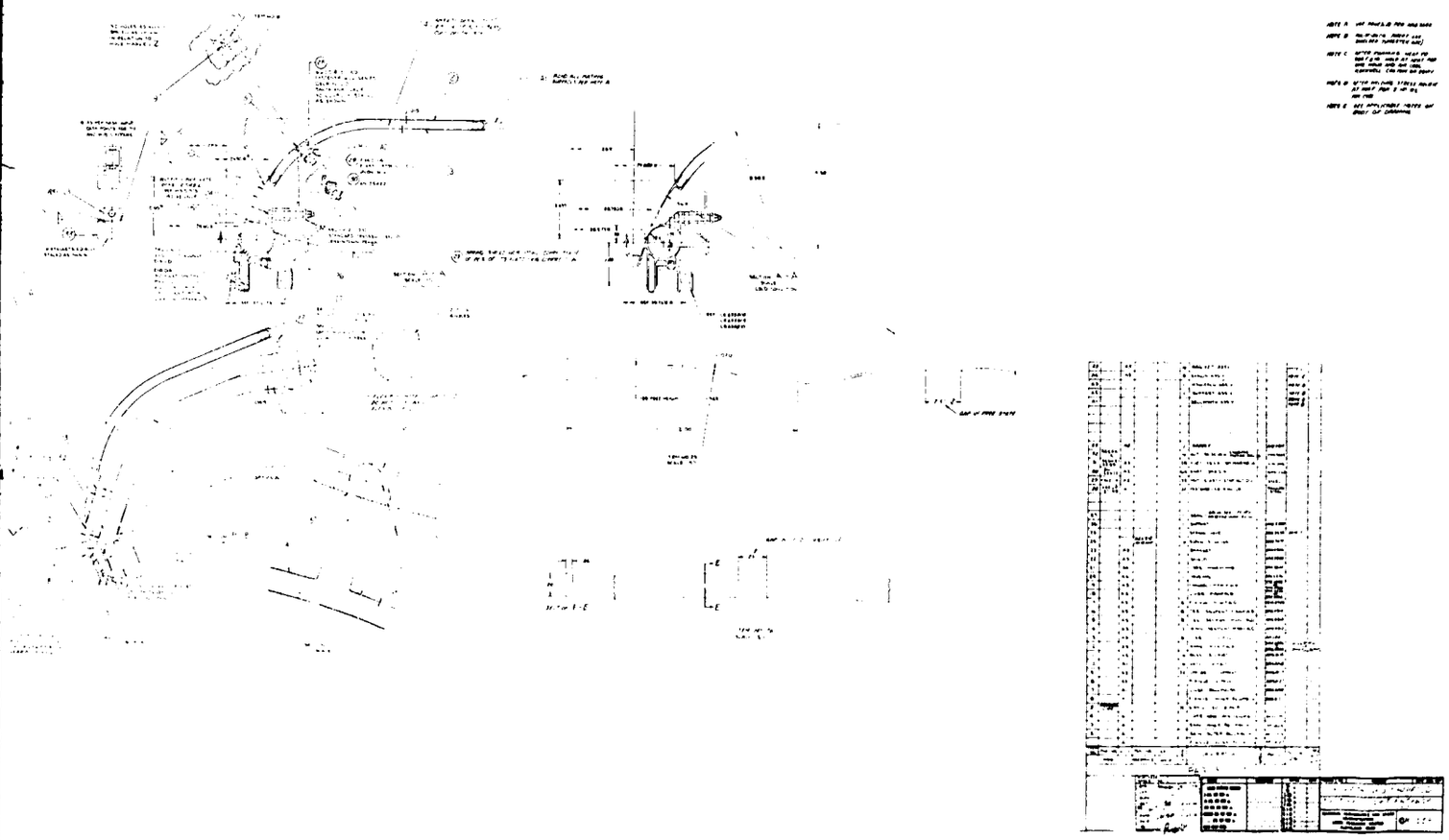

FOLDOUT FRAME 2

Figure 92

BUFFER AIR MANIFOLD AND BELLMOUTH INLET LOADS AND STRESSES

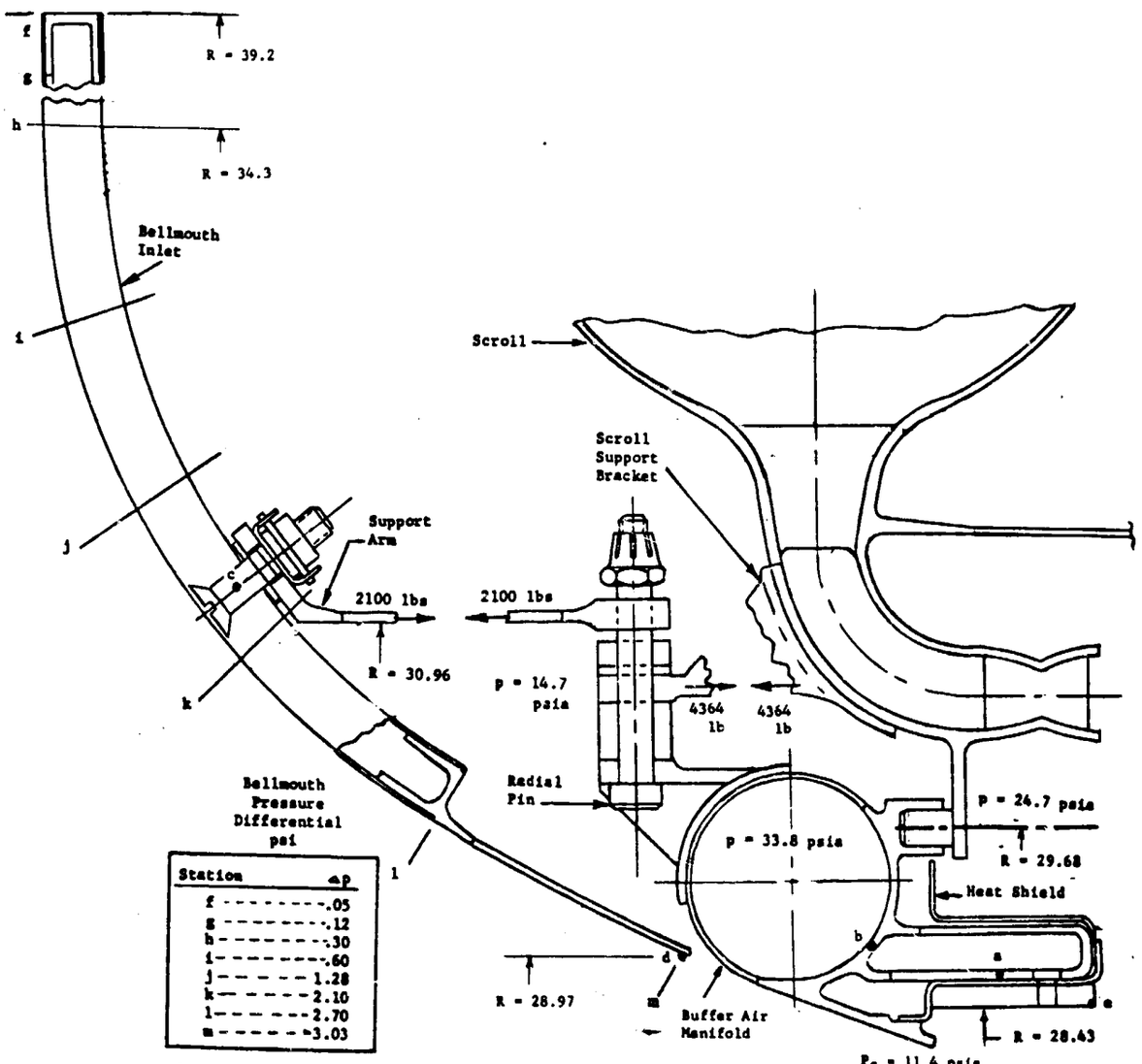

Location	a	b	c	c	d	e
Temp. °F	400	400	90	90	-	-
Mat'l	Titanium	Titanium	Aluminum	Aluminum	Aluminum	Titanium
Allowable Strength, psi	79,900	79,000	13,000	13,000.	-	-
Type of Load	Bend	Bend	Direct + Bend	Shear	Bend	Bend
Stress - psi	15,900	30,700	1,450	13.4	-	-
M.S.	>1.0	>1.0	>1.0	>1.0	-	-
Deflection - in.					.004	.008

Figure 93

TURBINE INTERSTAGE AERODY

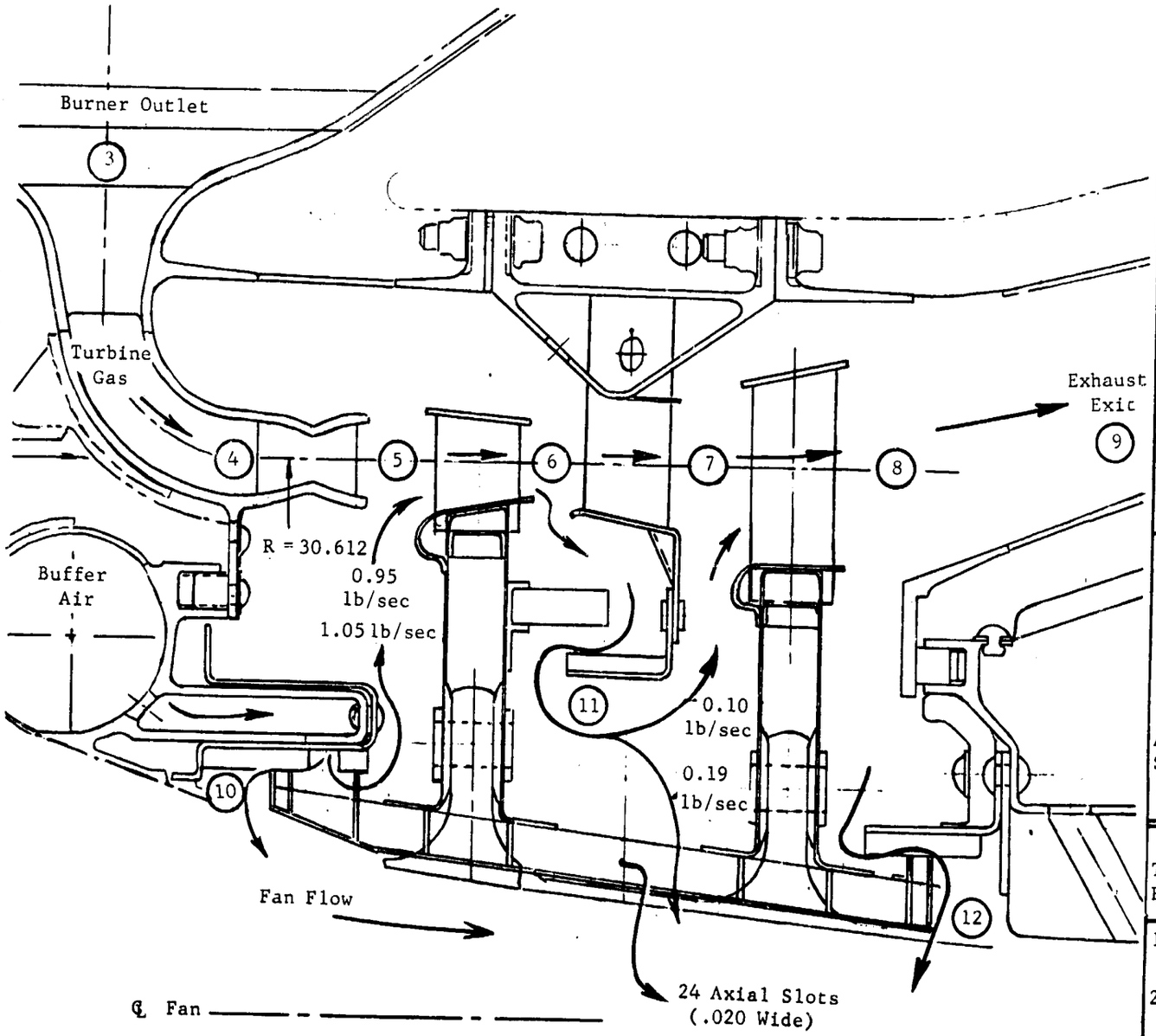

DESIGN P
1st Roto
2nd Roto
TRANSIENT FAN AT 2
1st Roto
2nd Roto
Before Li
Air Gener Speed
TRANSIENT FAN AT 82
1st Roto
2nd Roto
Air Gener

FOLDOUT FRAME 1

71-354

TERSTAGE AERODYNAMIC DATA

DESIGN POINT AT 3030 RPM		3	4	5	6	7	8	9	10	11	12
1st Rotor T_{rel} = 1650°R	T_t °R	1900	1900	1900	1534	1534	1338	1338	-	-	-
2nd Rotor T_{rel} = 1390°R	T_s °R	1887	1893	1380	1449	1290	1316	-	-	-	-
	P_t Psia	105.0	100.4	84.79	30.79	28.64	15.67	14.7	11.40	14.70	13.78
	P_s Psia	-	98.9	24.70	24.70	14.70	14.70	14.7	11.40	14.70	13.78
	W lb/sec	29.25	29.25	30.20	29.90	30.00	29.90	29.90	1.58	0.29	0.23
TRANSIENT CONDITION FAN AT 2600 RPM											
1st Rotor T_{rel} = 870°R	T_t °R	965	965	965	765	765	660	-	-	-	-
2nd Rotor T_{rel} = 687°R	T_s °R	-	-	687	727	646	650	-	-	-	-
Before Light-Off	P_t Psia	98.50	94.80	80.80	29.80	28.10	15.45	-	12.5	14.7	14.1
Air Generator at Full Speed	P_s Psia	-	-	24.8	24.8	14.70	14.70	-	12.5	14.1	14.1
	W lb/sec	38.0	38.0	-	-	-	-	-	-	-	-
TRANSIENT CONDITION FAN AT 825 RPM											
1st Rotor T_{rel} = 588°R	T_t °R	605	605	605	572	572	555	-	-	-	-
2nd Rotor T_{rel} = 560°R	T_s °R	-	-	565	510	552	554.7	-	-	-	-
Air Generator at Idle	P_t Psia	22.0	21.80	21.10	16.74	16.64	14.72	-	14.6	14.7	14.7
	P_s Psia	-	-	16.53	16.53	14.7	14.7	-	14.6	14.1	14.7
	W lb/sec	7.5	7.5	-	-	-	-	-	-	-	-

haust
Exit
9

Figure 94

FOLDOUT FRAME 2

TURBINE INLET OPERATING CONDITIONS

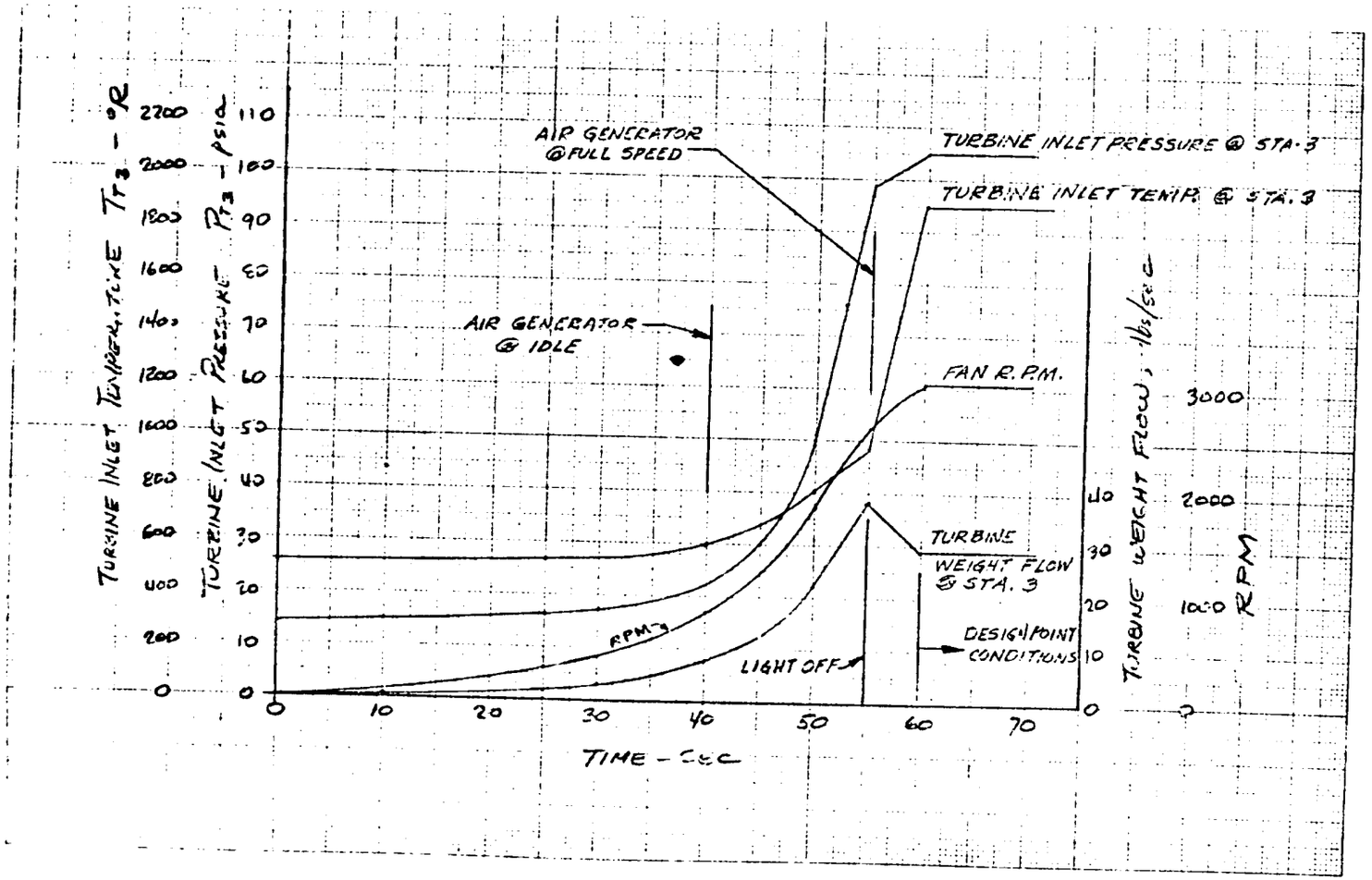

Figure 95

TURBINE SECTION TEMPERATURES (t = 40 SECONDS)

Temperature Stabilized at Air Generator Idle Conditions
N_{fan} = 825 RPM

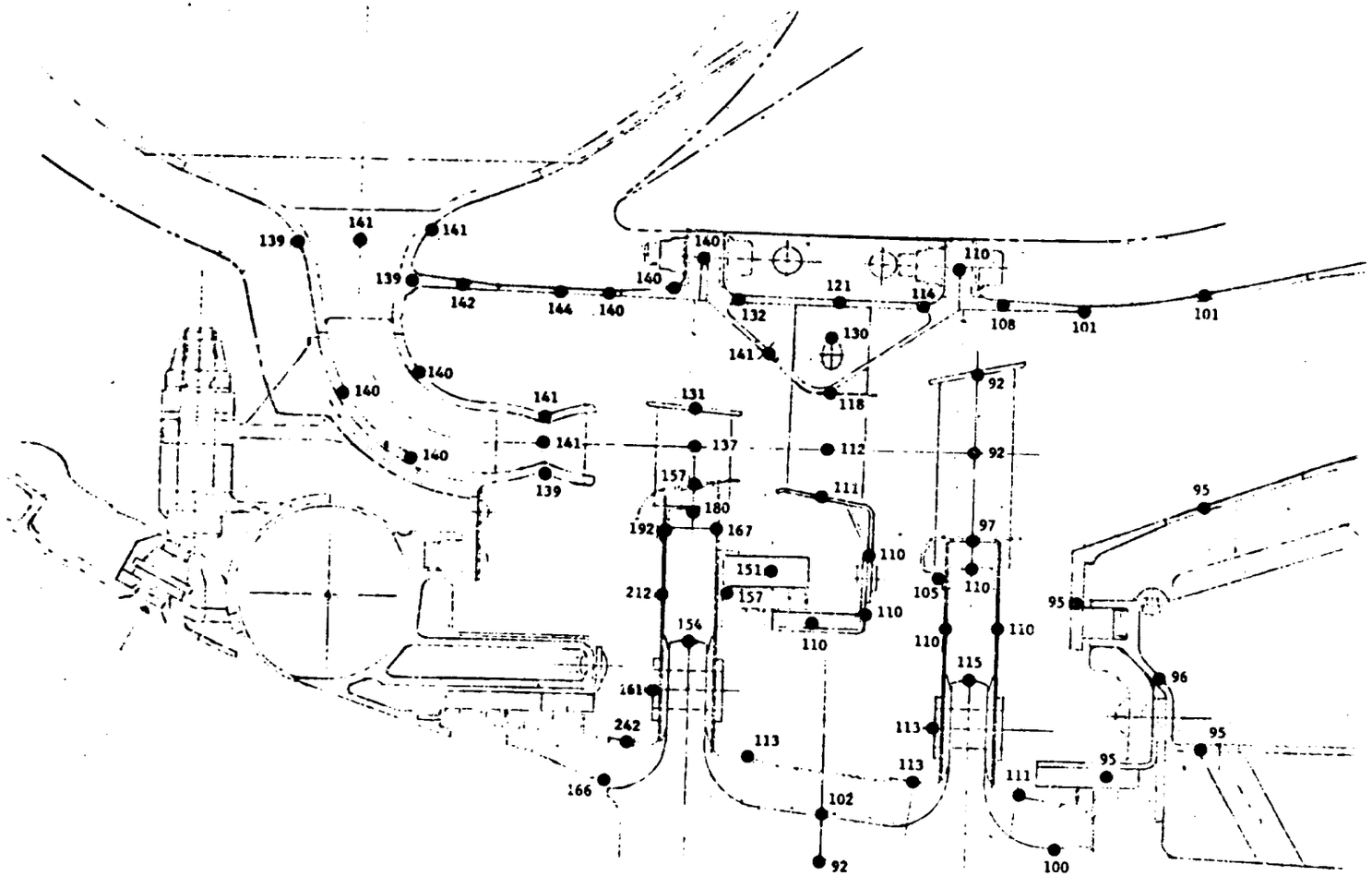

Figure 96

TURBINE SECTION TEMPERATURES (t = 50 SECONDS)

N_{fan} = 1820 RPM

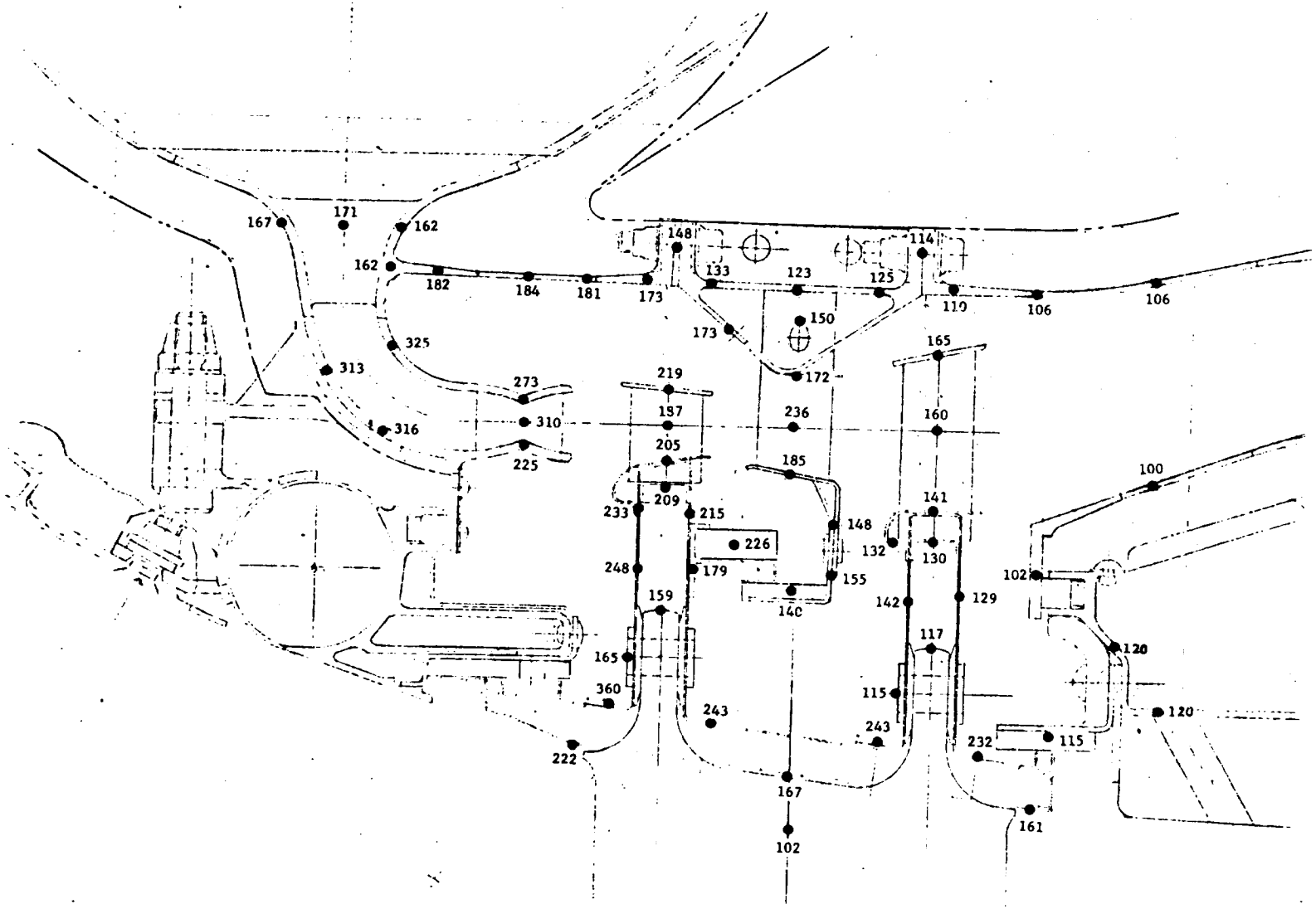

Figure 97

TURBINE SECTION TEMPERATURES (t = 55 SECONDS)

Light-Off, Air Generator at Full Power
N_{fan} = 2600 RPM

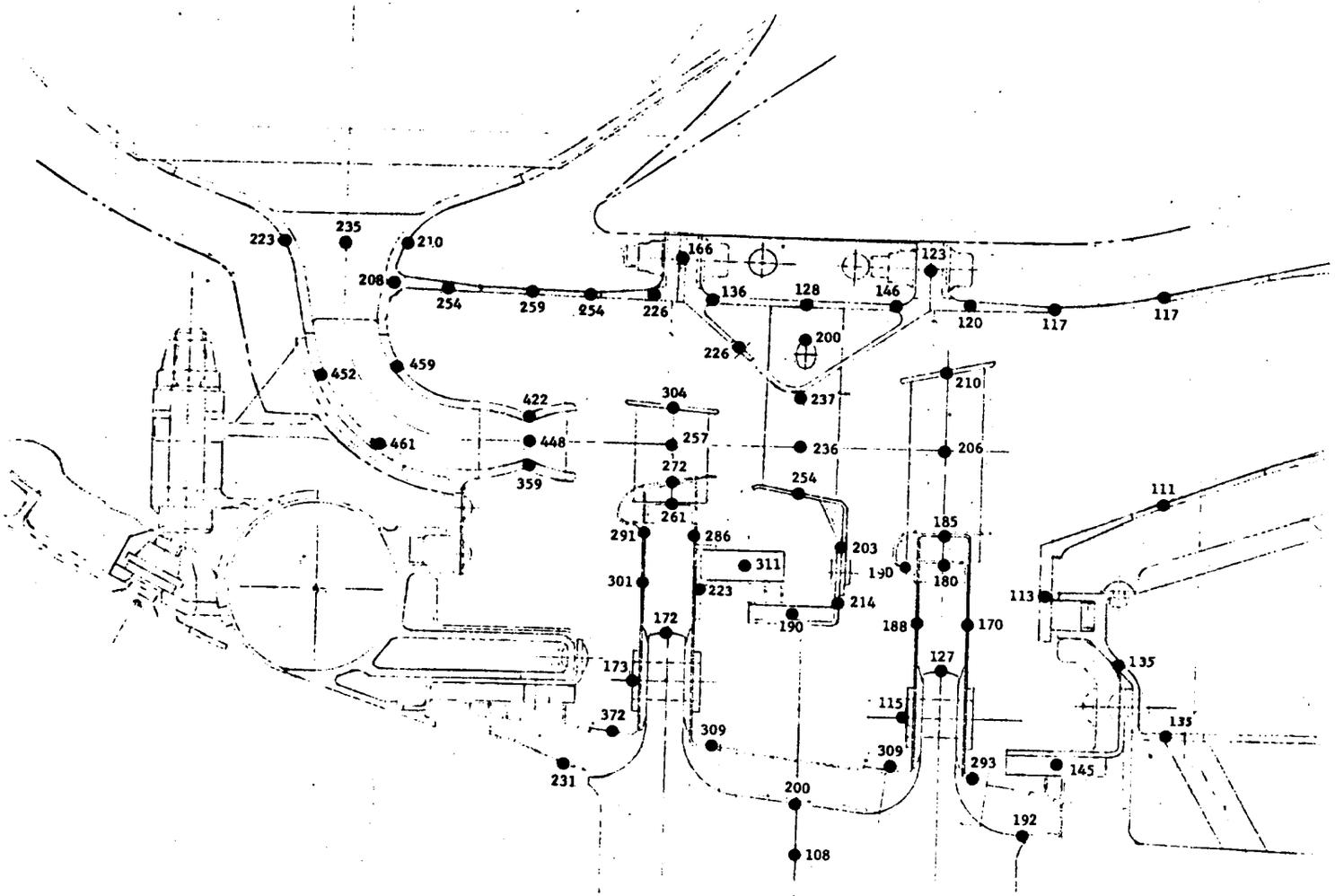

Figure 98

TURBINE SECTION TEMPERATURES (t = 60 SECONDS)
5 Sec After Light-Off
N_{fan} = 3030 RPM

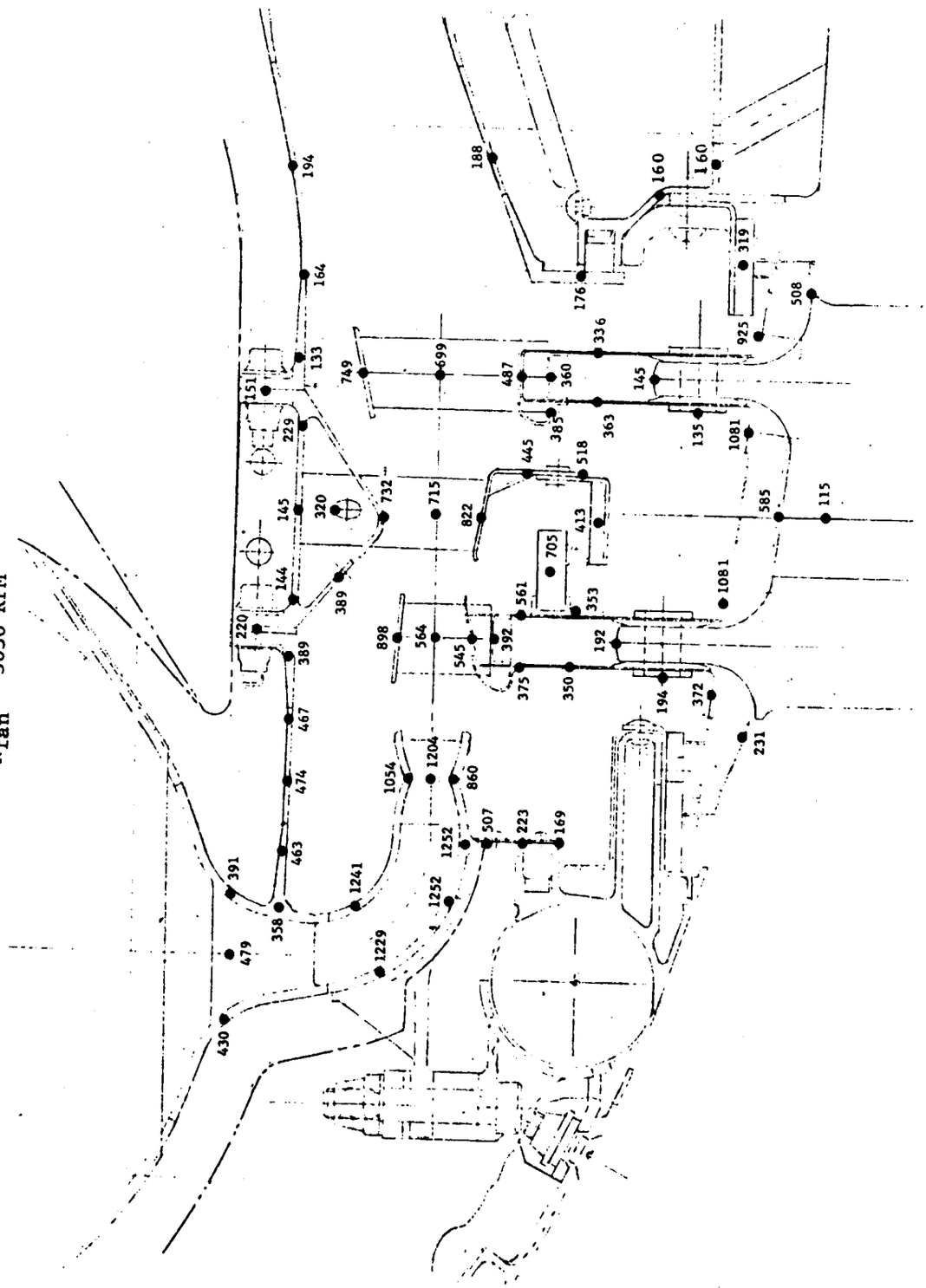

Figure 99

TURBINE SECTION TEMPERATURES (t = 100 SECONDS)
45 Sec After Light-Off
N_{fan} = 3030 RPM

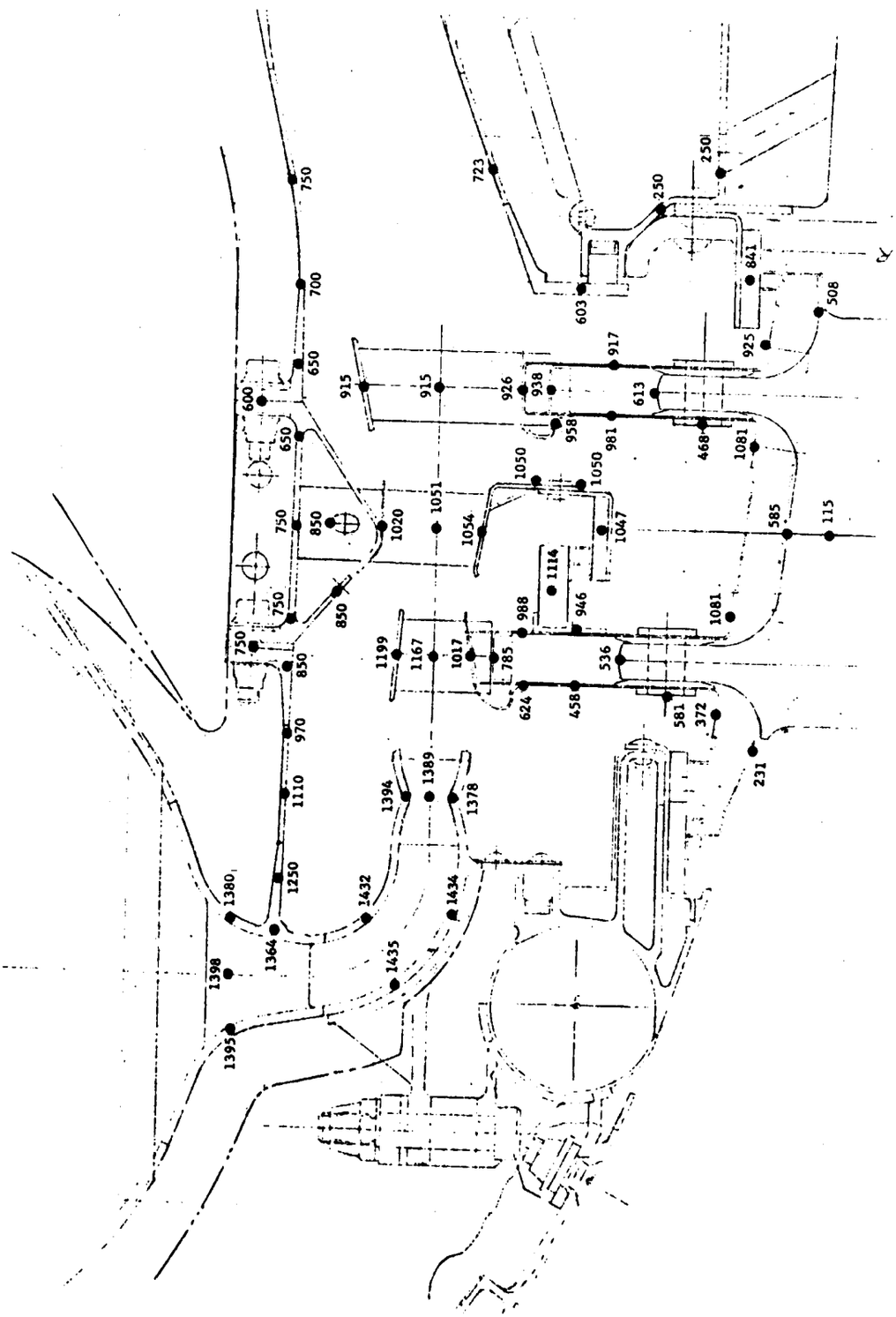

Figure 100

TURBINE SECTION TEMPERATURES - (t = 140 SECONDS)

85 Sec After Light-Off
N_{fan} = 3030 RPM

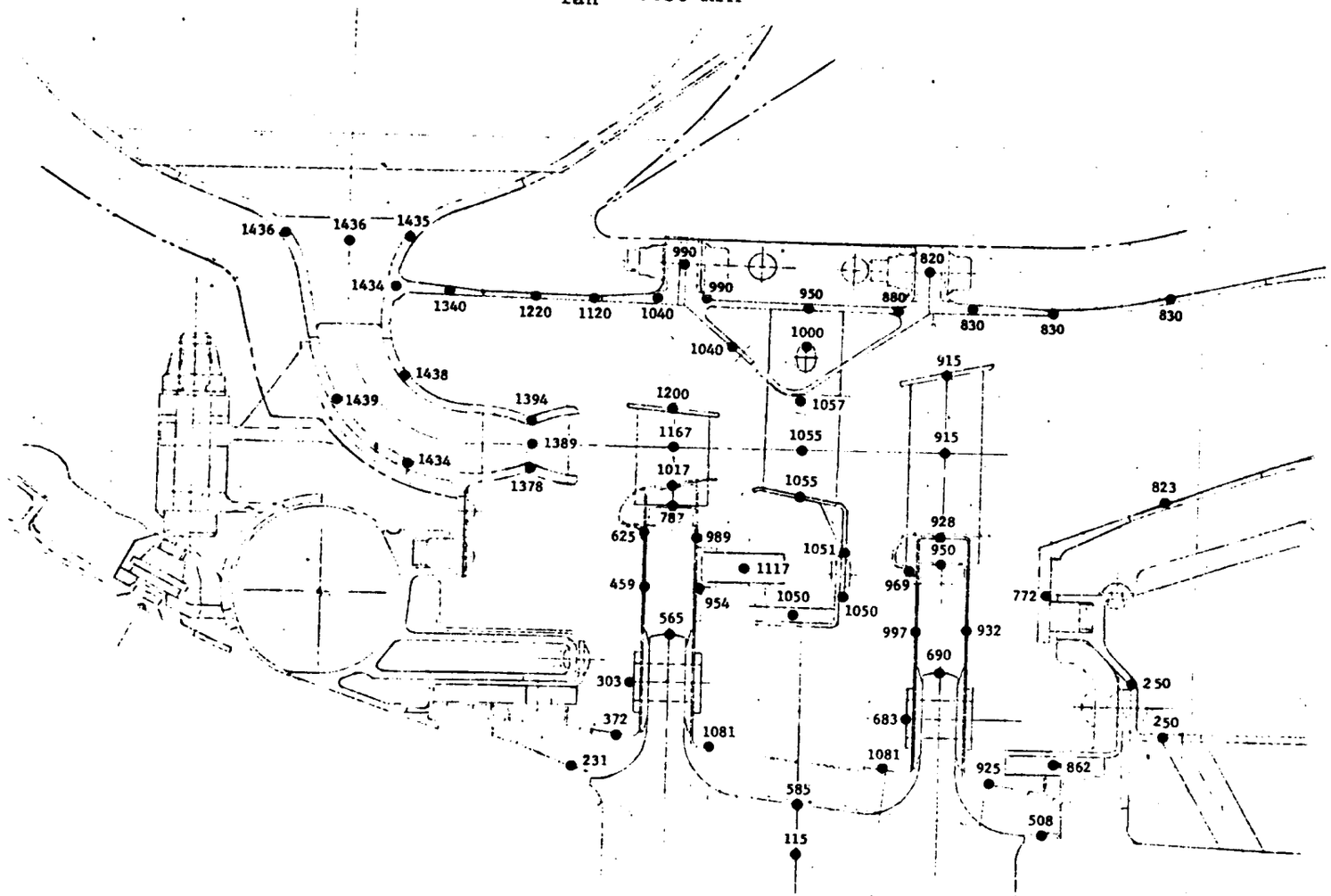

Figure 101

TURBINE SECTION TEMPERATURES - (t = 240 SECONDS)

185 Sec After Light-Off

N_{fan} = 3030 RPM

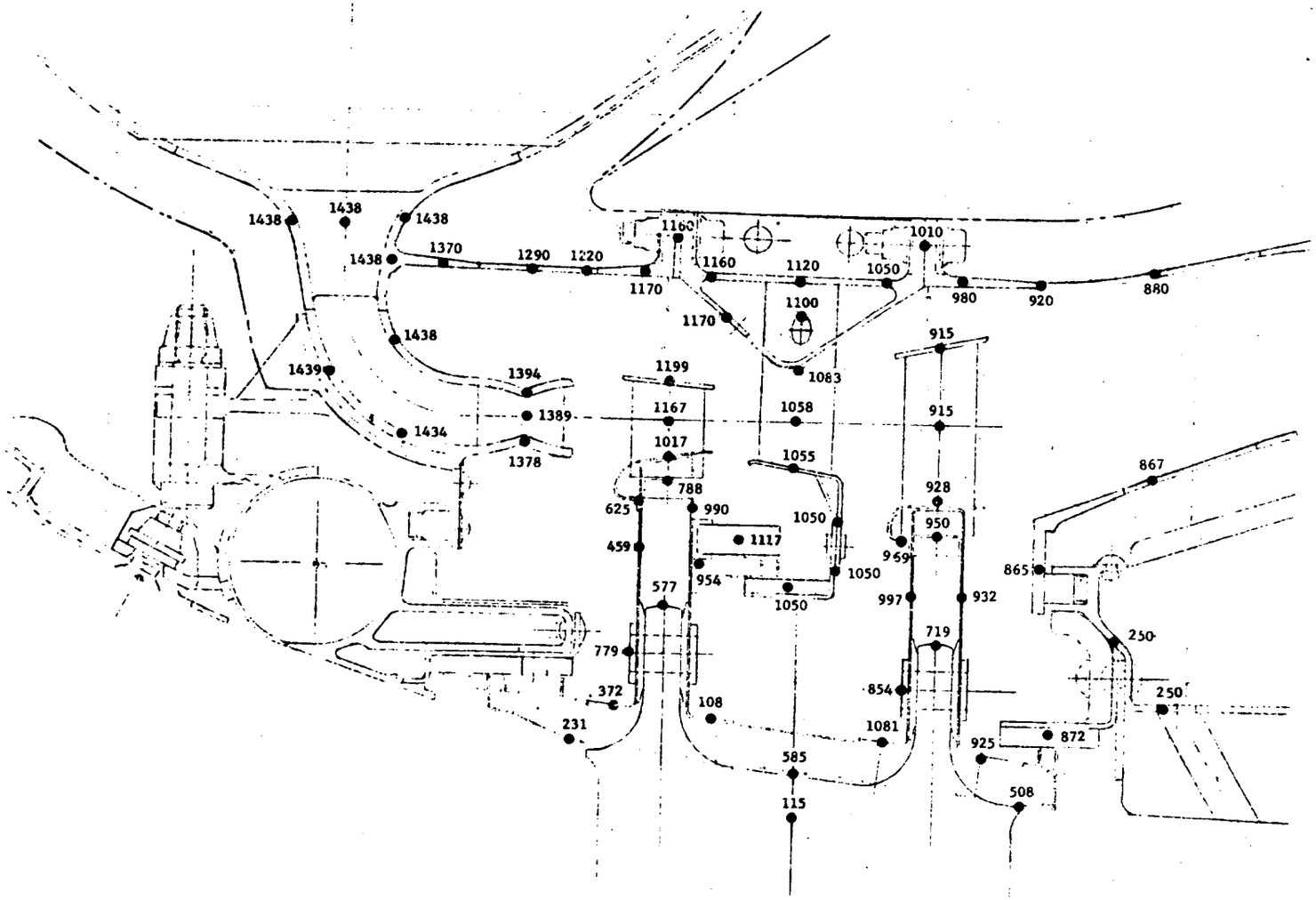

Figure 102

TURBINE SECTION TEMPERATURES - (t = 340 SECONDS)

285 Sec After Light-Off
N_{fan} = 3030 RPM

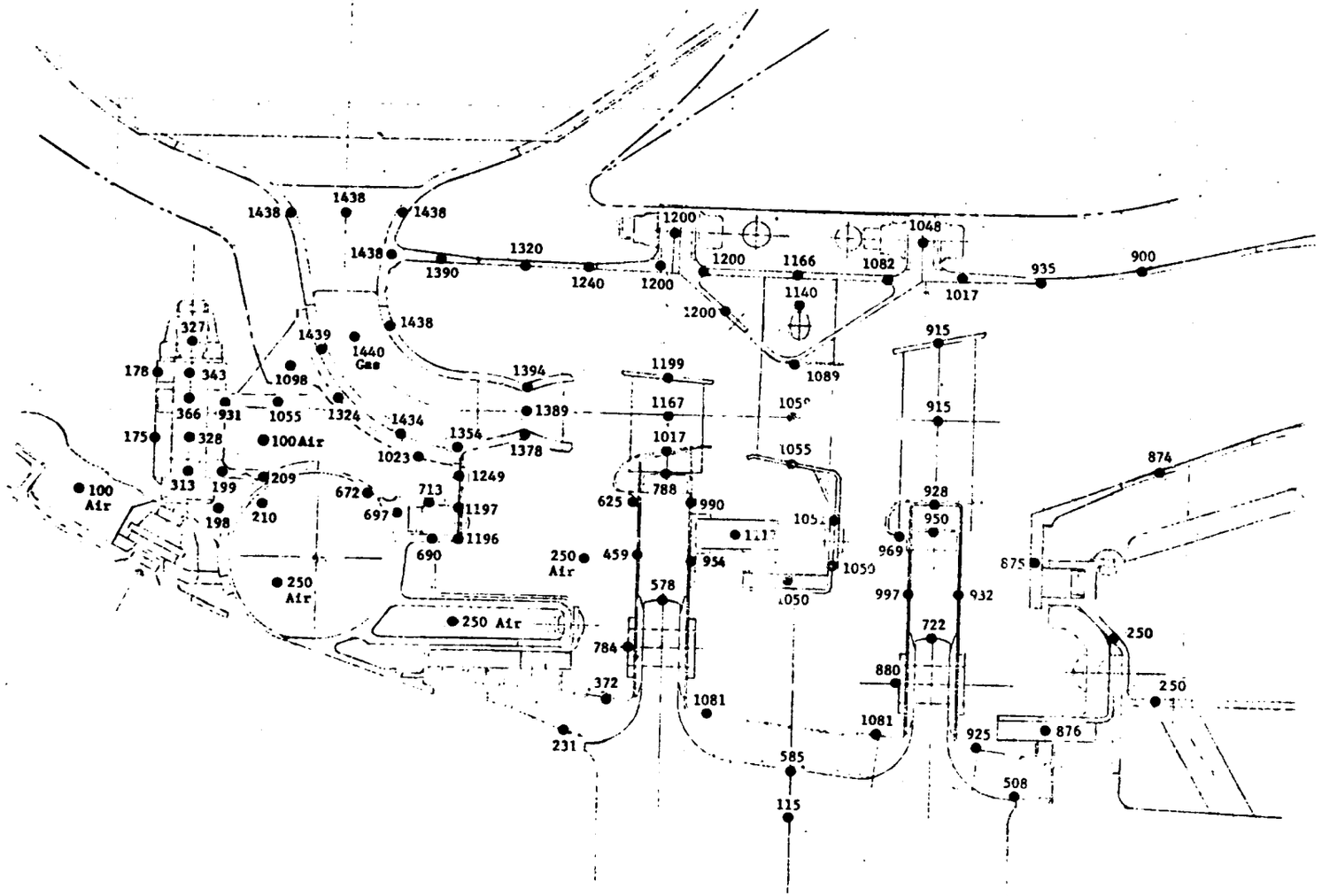

Figure 103

BEARING DESCRIPTION AND DESIGN INPUT LOADS

BEARING DESCRIPTIONS

Type	Single row, deep groove ball, two seals	
Bearing Location	Upper (thrust)	Lower
Basic No.	315	218
Dimensions:		
Bore x O.D. x width, mm.	75 x 160 x 37	90 x 160 x 30
No. and dia. of balls, in.	8 - 1.125	11 - .8125
Radial internal clearance, in.	.0015	.00175
Operating DN Value	0.23×10^6	0.27×10^6
Lubrication	Grease	Grease
Rotation		
(a) Shaft	Stationary	
(b) Housing	3030 RPM	
Bearing Spacing, in.	7.50	

DESIGN INPUT LOADS

	Steady-State	Steady-State Plus Gyro Moment
Axial Preload, lb.	800	800
Axial Lift Load, lbs.	2953	2953
Gyromoment, lb-in.	0	72,000
Time Gyromoment Applied, %	99	1

Figure 104

BEARING LOADS - STEADY STATE

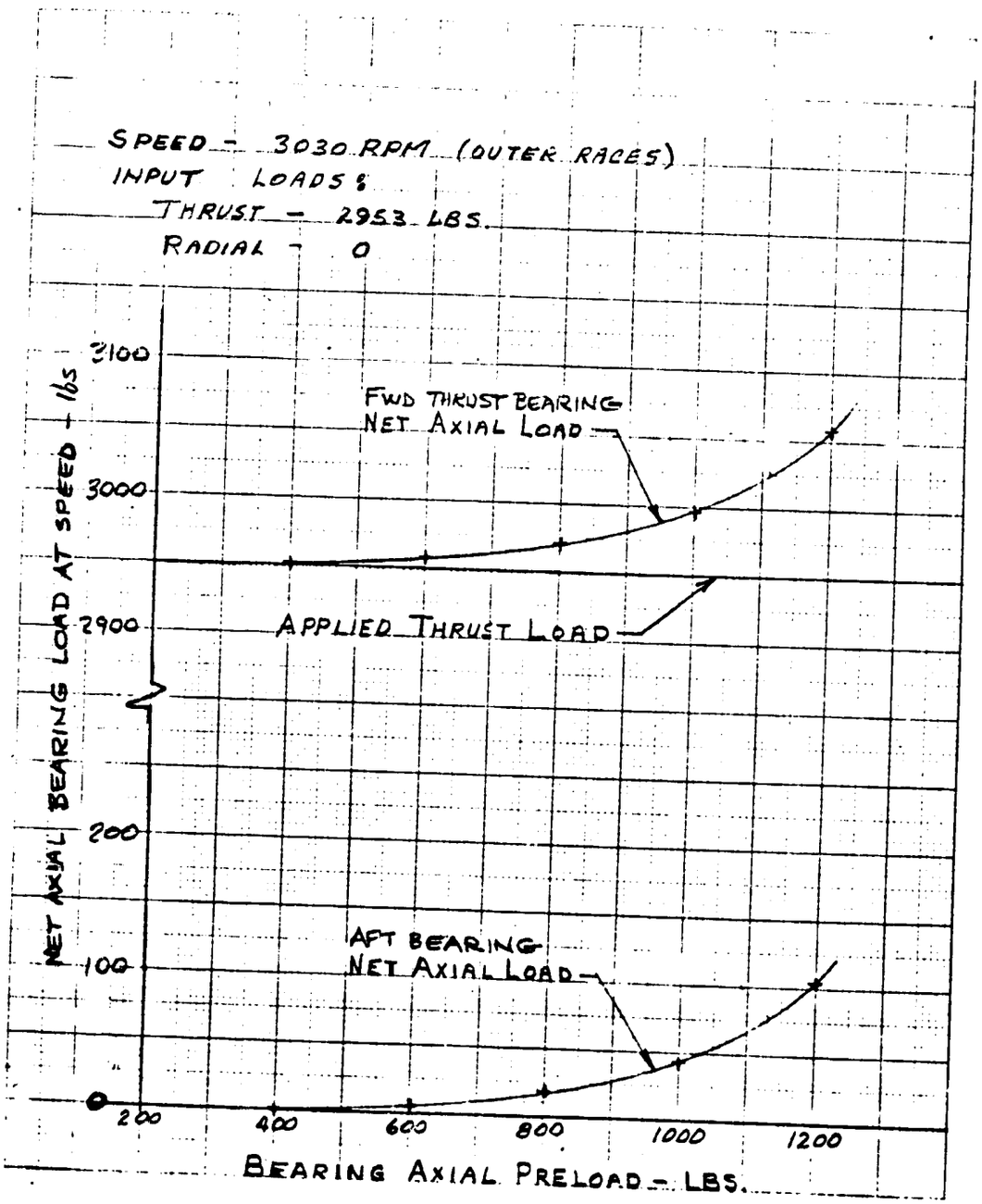

Figure 105

BEARING LOADS - STEADY STATE PLUS GYROMOMENT

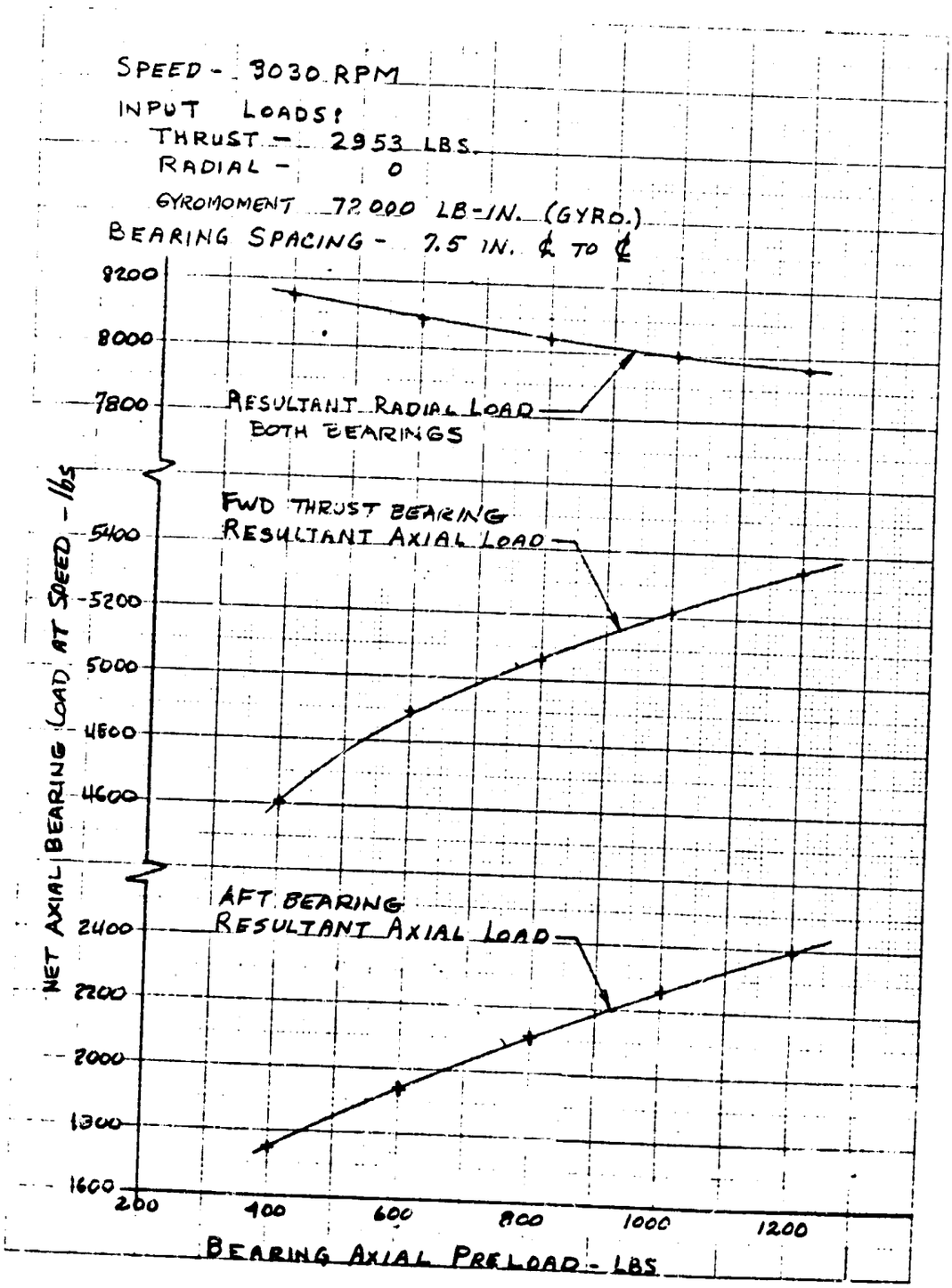

Figure 106

WEIGHT SUMMARY

	Material	Estimated Weight - lb.	Final Weight lb.
Inlet Bellmouth Assy		51.0	59.9
(a) bellmouth	Alum	25.0	18.2
(b) buffer air manifold	Ti	26.0	41.7
Scroll Housing Assy		120.0	110.2
(a) neck, support & vane assy	Ni	70.0	66.0
(b) scroll	Ni	50.0	44.2
Fan Rotor Assy		154.0	154.0
(a) fan blades	Ti	101.0	101.0
(b) disk	Ti	53.0	53.0
Fan Stator Vane & Support Assy		115.0	190.6
(a) spindle, bearings & misc.	Ti + St'l	27.0	34.3
(b) stator vanes	Ti	35.0(2)	63.3(1)
(c) outer ring assy	Ti	32.0	59.1
(d) inner ring assy	Ti	21.0	33.9
Turbine Second Stator Assy	Ni	15.0	32.2
Exhaust Housing Assembly	Ni	76.0	83.1
Turbine Rotor Assy	Ni	100.0	50.0
Total Weight		631.0	680.0(3)

(1) - 30 hollow, 6 solid

(2) - All hollow

(3) - Fan Rotor Assembly Mass Moment of Inertia, 228 lb-in-sec^2

Figure 107